

SANDIA REPORT

SAND85-0598 • UC-70

Unlimited Release

Printed January 1989

8524

RS-8232-2/68653

cy1

Yucca Mountain Project

Selected Analyses to Evaluate the Effect of the Exploratory Shafts on Repository Performance at Yucca Mountain

Joseph A. Fernandez, Thomas E. Hinkebein, John B. Case

Prepared by
Sandia National Laboratories
Albuquerque, New Mexico 87185 and Livermore, California 94550
for the United States Department of Energy
under Contract DE-AC04-76DP00789



8232-2/068653



0000001 -



“Prepared by Yucca Mountain Project (YMP) participants as part of the Civilian Radioactive Waste Management Program (CRWM). The YMP is managed by the Yucca Mountain Project Office of the U.S. Department of Energy, Nevada Operations Office (DOE/NV). YMP work is sponsored by the Office of Geologic Repositories (OGR) of the DOE Office of Civilian Radioactive Waste Management (OCRWM).”

Issued by Sandia National Laboratories, operated for the United States Department of Energy by Sandia Corporation.

NOTICE: This report was prepared as an account of work sponsored by an agency of the United States Government. Neither the United States Government nor any agency thereof, nor any of their employees, nor any of their contractors, subcontractors, or their employees, makes any warranty, express or implied, or assumes any legal liability or responsibility for the accuracy, completeness, or usefulness of any information, apparatus, product or process disclosed, or represents that its use would not infringe privately owned rights. Reference herein to any specific commercial product, process, or service by trade name, trademark, manufacturer, or otherwise, does not necessarily constitute or imply its endorsement, recommendation, or favoring by the United States Government, any agency thereof or any of their contractors or subcontractors. The views and opinions expressed herein do not necessarily state or reflect those of the United States Government, any agency thereof or any of their contractors.

Printed in the United States of America
Available from
National Technical Information Service
U.S. Department of Commerce
5285 Port Royal Road
Springfield, VA22161

NTIS price codes
Printed copy: A12
Microfiche copy: A01

**SELECTED ANALYSES TO EVALUATE THE EFFECT OF THE EXPLORATORY SHAFTS ON
REPOSITORY PERFORMANCE AT YUCCA MOUNTAIN**

Joseph A. Fernandez
Thomas E. Hinkebein
Geotechnical Design Division
Sandia National Laboratories
Albuquerque, NM 87185

John B. Case
IT Corporation
5301 Central Avenue, N.E.
Suite 700
Albuquerque, NM 87108

ABSTRACT

This report presents a number of analyses to determine whether the construction of two shafts associated with the exploratory shaft facility can significantly influence the long-term isolation capabilities of a high-level nuclear waste repository at Yucca Mountain, on and adjacent to the Nevada Test Site. Both shafts are planned to be located predominantly in fractured, welded tuff within the unsaturated zone. The calculational effort, using analytical solutions, focuses primarily on the potential influence of the shaft liner and the zone of increased rock damage around the shaft (termed in this paper the modified permeability zone, MPZ). Two mechanisms are considered in determining whether the MPZ can significantly enhance radionuclide releases. These mechanisms include water flow entering the exploratory shafts from both realistic and improbable scenarios and airflow exiting the shaft as a result of convective and barometric forces. The influence of the liner on the performance of the repository is determined by evaluating the potential chemical interaction between ground water and the concrete liner and the subsequent potential for precipitates to deposit within the MPZ and the shaft fill. It is concluded from these calculations and the current knowledge of the hydrology of the unsaturated zone at Yucca Mountain that the presence of the shafts and the associated MPZ and shaft liner do not significantly impact the long-term isolation capability of the repository. This conclusion is reached because both exploratory shafts will be collared in bedrock above and laterally away from the flood channel. This location makes it unlikely that significant amounts of water will enter the shaft even if a probable maximum flood occurs. Additionally, airflow out of the shaft can be controlled effectively by emplacement of shaft fill, and deposition of solids from the interaction of the shaft liner with the ground water is a localized phenomenon and should not significantly decrease the drainage capability of the rock at the base of the shaft. This report also (1) describes methods to remove the liner, to restore the MPZ, to emplace a seal, and to restore the exploratory shaft pad area in the event that future analyses suggest that further reduction of shaft inflow is necessary and (2) evaluates the impact on the sorption of the Calico Hills zeolites if the decision is made to sink the shaft into the Calico Hills unit.

ACKNOWLEDGMENTS

The authors wish to acknowledge the assistance of other individuals who contributed to this study. Mr. John G. S. Hynd, an engineering consultant, provided information on the techniques associated with seal and backfill emplacement, liner removal, and the associated costs. Messrs. Craig Givens, Joe Tyburski, and Bernard Lauctes, International Technology Corporation, performed selected calculations. Messrs. Joe Tillerson, Ralph Peters, and Andy Peterson, Sandia National Laboratories, provided review comments to the authors.

SPECIAL NOTE

A December 1988 version of this report was submitted concurrently with the Site Characterization Plan--Consultation Draft (DOE, 1988). Following submission of the December 1988 version and before submission of this report for final publication, several errors were noted. This report (January 1989 version) contains corrections associated with these errors. Substantive changes made to the December 1988 version and reflected in this report are specifically mentioned below.

p. 18, line 10--Replace "radially down the liner" with "downward."

p. 57, line 5--Replace "the surface location of a" with "an arbitrary surface location."

p. 57, line 7--Replace " $\Delta r = \dots$ " with " $\Delta r =$ radial distance increment between r_i and r_{i+1} ."

p. 87, Figure 4-3--Correct figure inserted.

p. 102, lines 15 and 16--Delete "The displaced ... conductivity."

p. 102, line 18--Replace "independent" with "less dependent on."

p. 151, lines 9 and 11--Change "mm" to " μm ."

p. 152--Change "fracture aperture (m)" to "fracture aperture (μm)."

p. 208, Figure C-9b--Correct figure inserted.

pp. 235 and 236--Text revised.

pp. 236 and 237--Delete "2" from denominator in Equations E-5, E-6, and E-8.

BACKGROUND OF REPORT

The original version of this report was prepared as a letter report in response to the question: Do the shaft liner, the shaft internals, and the increased rock damage around the shaft (resulting from shaft construction) significantly influence the release of radionuclides from the repository? The letter report was submitted to the U.S. Department of Energy, Nevada Operations Office, in July 1985. The contents of this letter report were subsequently discussed during an NRC/DOE workshop titled "NNWSI Exploratory Shaft Facility Design and Construction Workshop" in August 1985.

During the workshop, additional concerns were raised by the participants about the approach used to resolve the original question and the level of detail contained in the original letter report. To address these concerns, Sandia National Laboratories (SNL) decided to prepare three reports.

- (1) "Technical Basis for Performance Goals, Design Requirements and Material Recommendations for the NNWSI Repository Sealing Program," SAND84-1895, by J. A. Fernandez, P. C. Kelsall, J. B. Case, and D. Meyer (1987);
- (2) "Modification of Rock Mass Permeability in the Zone Surrounding a Shaft in Fractured, Welded Tuff," SAND86-7001, by J. B. Case and P. C. Kelsall (1987); and
- (3) "Selected Analyses to Evaluate the Effect of the Exploratory Shafts on Repository Performance at Yucca Mountain," SAND85-0598, by J. A. Fernandez, T. E. Hinkebein, and J. B. Case (this report).

During the preparation of this report, the designs and surface locations of the exploratory shafts changed. These changes necessitated performing additional calculations to address, among other things, the impact of flooding and erosion at the new shaft locations. The question concerning the impact of flooding and erosion at the new exploratory shaft locations was raised during another meeting between NRC and DOE in April 1987.

This report, therefore, addresses

- o the original question asked before July 1985;
- o the concerns raised during the August 1985 workshop between NRC and DOE;
- o the concerns raised during the April 1987 meeting between NRC and DOE; and
- o additional concerns raised by the authors and reviewers during the development of this report.

CONTENTS

	<u>Page</u>
ACKNOWLEDGMENTS	4
BACKGROUND OF REPORT	5
EXECUTIVE SUMMARY	15
1.0 PURPOSE OF REPORT	23
2.0 SHAFT DESIGN INFORMATION	27
2.1 Location of the Exploratory Shafts	27
2.2 Construction of the Exploratory Shafts	30
2.3 Shaft Sealing Concepts	31
2.4 Preferred Options for Shaft Seals	31
3.0 POTENTIAL FOR ENHANCING RADIONUCLIDE RELEASE RESULTING FROM SELECTED WATER FLOW SCENARIOS	35
3.1 Flooding and Erosion Potentials at the Exploratory Shaft Locations	35
3.1.1 Channel Flooding at the Exploratory Shaft Locations Resulting from a Probable Maximum Flood .	35
3.1.2 Extent of the Flood Channel	36
3.1.3 Height of Water in the Channel	39
3.1.4 Sheet Flow over the Exploratory Shaft Pad	43
3.1.5 Erosion Potential at the Exploratory Shaft Locations	48
3.2 Water Flow into the Exploratory Shafts Resulting from Fracture Flow	50
3.2.1 Description of Scenarios	50
3.2.2 Model Description	52
3.2.3 Input Parameters	57
3.2.4 Assumptions Used in the Model	58
3.2.5 Model Results	59
3.2.6 Storage and Drainage Capacity of the Exploratory Shafts and Associated Facility	63
3.2.7 Discussion of Results	64
3.3 Scenario Describing Uniform Dispersion of Surface Water at Depth	71
3.4 Scenario Describing Fully Saturated Alluvial Flow at the Old Exploratory Shaft Locations	75
3.5 Conclusions	76
4.0 POTENTIAL FOR ENHANCING RADIONUCLIDE RELEASE BY AIR MOVEMENT RESULTING FROM CONVECTIVE FORCES	79
4.1 Airflow Mechanisms	79
4.2 Method of Analysis	81
4.3 Model Description	81
4.3.1 Temperature and Pressure Distributions	82
4.3.2 Flow Path Resistances	82
4.4 Model Results	85
4.5 Conclusions	91
5.0 POTENTIAL FOR ENHANCING RADIONUCLIDE RELEASE BY AIR MOVEMENT RESULTING FROM BAROMETRIC FORCES	93
5.1 Model Description	93
5.1.1 Physical Model	94
5.1.2 Mathematical Model and Assumptions	94

CONTENTS

	<u>Page</u>
5.2 Input to the Mathematical Model	99
5.3 Model Results	102
5.4 Conclusions	110
6.0 POTENTIAL FOR CHANGING THE CONDUCTIVITY OF THE SHAFT LINER, MODIFIED PERMEABILITY ZONE, SHAFT FILL, AND SHAFT SUMP	113
6.1 Effect of Elevated Ground-Water Temperature on the Conductivity of the Liner	113
6.2 Effect of Ground-Water Chemistry on the Hydraulic Conductivity of the Exploratory Shaft Fill and Modified Permeability Zone	115
6.2.1 Leaching of Alkaline Species from the Concrete Liner	116
6.2.2 Chemical Equilibrium Model of Ground-Water Reactions	120
6.2.2.1 Migration of Precipitates	123
6.2.2.2 Model for Precipitate Deposition	125
6.2.3 Results	126
6.2.4 Conclusions	127
6.3 Effect of Fines Migration on the Hydraulic Conductivity of the Shaft Sump	129
7.0 POTENTIAL FOR IMPACTING REPOSITORY PERFORMANCE RESULTING FROM PENETRATION OF THE CALICO HILLS UNIT BY THE EXPLORATORY SHAFT	131
7.1 Changes in the Sorption of the Calico Hills Unit as a Result of Elevated Ground-Water Temperature	131
7.1.1 Temperature Elevation of Water Entering the Shaft .	131
7.1.2 Impact of Increased Ground-Water Temperature on the Sorption of the Calico Hills Unit	132
7.2 Changes in the Thickness of the Calico Hills Unit Above the Ground-Water Table	134
7.3 Conclusions	134
8.0 POSSIBLE REMEDIAL MEASURES TO MODIFY PHYSICAL FEATURES ASSOCIATED WITH THE EXPLORATORY SHAFT FACILITY	137
8.1 Remedial Measures to Remove the Liners from the Exploratory Shafts	137
8.1.1 Liner Removal	137
8.1.2 Muck Removal	145
8.1.3 Conclusions	146
8.2 Remedial Measures To Restore the Modified Permeability Zone	148
8.2.1 Restoration of the Modified Permeability Zone by Grouting	150
8.2.2 Restoration of the Modified Permeability Zone Using Expansive Concrete	151
8.2.3 Conclusions	153
8.3 Remedial Measures to Restore the Exploratory Shaft Pad Area	154
8.3.1 Excavation and Fill Required to Construct the Exploratory Shaft Pad	154

CONTENTS

	<u>Page</u>
8.3.2 Design Strategies to Control Infiltration of Precipitation	156
8.3.3 Design Strategies to Control Erosion	159
8.3.4 Conclusions	160
9.0 CONCLUSIONS	161
 APPENDICES	
A. POTENTIAL FOR RADIONUCLIDE TRANSPORT	165
B. A MODEL OF THE MODIFIED PERMEABILITY ZONE	179
C. SCENARIO DESCRIBING FULLY SATURATED ALLUVIAL FLOW AT THE OLD EXPLORATORY SHAFT LOCATIONS	189
D. EXPLANATION OF WATER INFLOW TO EXPLORATORY SHAFT 1 FROM THE SCENARIO IN APPENDIX C	225
E. THE DENSITY METHOD AS APPLIED TO FLOW THROUGH A POROUS MEDIA ...	233
F. ESTIMATED CONSTRUCTION SCHEDULE AND COSTS FOR LINER REMOVAL AND SEAL INSTALLATION	239
G. CALCULATION OF THE TEMPERATURE OF WATER REACHING THE BASE OF THE EXPLORATORY SHAFTS	245
H. COMPARISON OF DATA USED IN THIS REPORT WITH THE REFERENCE INFORMATION BASE (RIB)	255
I. DATA RECOMMENDED FOR INCLUSION IN THE SITE AND ENGINEERING PROPERTIES DATA BASE (SEPDB) AND INFORMATION PROPOSED FOR INCLUSION IN THE REFERENCE INFORMATION BASE (RIB)	269
REFERENCES	271

TABLES

	<u>Page</u>
3-1. Comparative Peak Discharges from Floods in the Yucca Mountain Area	45
3-2. Zone of Influence Based on the Rate of Rainfall	60
3-3. Total Volume of Water Entering Both Exploratory Shafts Based on the Rate of Rainfall	61
3-4. Zone of Influence for Sheet Flow over a Bare Fracture Network	62
3-5. Total Volume of Water Entering Both Exploratory Shafts for Sheet Flow over a Bare Fracture Network	62
3-6. Zone of Influence for Channel Flow	63
4-1. Summary of Areas and Lengths for Vertical Emplacement	84
4-2. Summary of Areas and Lengths for Horizontal Emplacement	84
6-1. Chemical Analyses of Water Before and After Contact with PSU 82-022 Concrete	118
8-1. Summary of Advantages, Disadvantages, and Cost of Liner Removal Methods	142
8-2. Comparison of Production Cycle Times for Various Methods Used to Remove Concrete Liners	144
8-3. Comparison of Costs for Breaking Out the Concrete Lining and Rock	145

FIGURES

		<u>Page</u>
2-1	Exploratory Shaft (ES-1) and Corresponding Geologic Stratigraphy	28
2-2	Surficial Geology of the Exploratory Shaft Area	29
2-3	General Arrangement for the Shaft Seals Showing Optional Components	32
3-1	Estimated High-Water Locations Associated with a Probable Maximum Flood in the Exploratory Shaft Area Under Thunderstorm Conditions	37
3-2	Estimated High-Water Locations Associated with a Probable Maximum Flood in the Exploratory Shaft Area Under General Storm Conditions	38
3-3	Average Height Versus Time Curves for the (a) Thunderstorm and (b) General Storm	40
3-4	Topographic Cross Sections with Probable Maximum Flood Levels Under a Thunderstorm Condition	41
3-5	Topographic Cross Sections with Probable Maximum Flood Levels Under a General Storm Condition	42
3-6	Flow Rate as a Function of Elevation for the Exploratory Shaft Locations	44
3-7	Watershed Above the Exploratory Shaft Pad	47
3-8	Height of Water over the Exploratory Shaft Pad During Sheet Flow Conditions Resulting from (a) a Thunderstorm and (b) a General Storm	49
3-9	Schematic of Near-Surface Fracture Flow	53
3-10	Schematic of Flow in a Single Fracture	54
3-11	Drainage Direction for the Exploratory Shaft Facility	65
3-12	Zones of Influence for a General Storm Probable Maximum Flood Using the Rainfall Rate Scenario and the Maximum Zone of Influence, Case 3, for Channel Flow in Coyote Wash	67
3-13	Zones of Influence for a Thunderstorm Probable Maximum Flood Using the Rainfall Rate Scenario and the Maximum Zone of Influence, Case 3, for Channel Flow in Coyote Wash	68
3-14	Zones of Influence for a General Storm Probable Maximum Flood Using the Sheet Flow Scenario and the Maximum Zone of Influence, Case 3, for Channel Flow in Coyote Wash	69

FIGURES

	<u>Page</u>
3-15 Zones of Influence for a Thunderstorm Probable Maximum Flood Using the Sheet Flow Scenario and the Maximum Zone of Influence, Case 3, for Channel Flow in Coyote Wash	70
3-16 Topography, Drainage Basin Outline, and Grid Used in Developing the Uniform Dispersion Scenario	72
3-17 Illustration of the Water Flow That Enters the Exploratory Shaft and Modified Permeability Zone from a Single Surface Element	74
4-1 Mechanisms for Convective Airflow (a) Through Shafts Only and (b) Through Shafts and Rock	80
4-2 Total Flow Rate as a Function of Shaft Fill, Air Conductivity (Vertical Emplacement and Low Conductivity MPZ Model)	86
4-3 Total Flow Rate as a Function of Shaft Fill, Air Conductivity (Vertical Emplacement and High Conductivity MPZ Model)	86
4-4 Total Flow Rate as a Function of Shaft Fill, Air Conductivity (Horizontal Emplacement and Low Conductivity MPZ Model)	87
4-5 Total Flow Rate as a Function of Shaft Fill, Air Conductivity (Horizontal Emplacement and High Conductivity MPZ Model)	87
4-6 Airflow Through ES-1 and ES-2 (Shaft Fill and MPZ Flows Included) as a Percentage of Flow Through the Rock over the Repository Area (Vertical Emplacement and Low Conductivity MPZ Model)	88
4-7 Airflow Through ES-1 and ES-2 (Shaft Fill and MPZ Flows Included) as a Percentage of Flow Through the Rock over the Repository Area (Vertical Emplacement and High Conductivity MPZ Model)	88
4-8 Airflow Through ES-1 and ES-2 (Shaft Fill and MPZ Flows Included) as a Percentage of Flow Through the Rock over the Repository Area (Horizontal Emplacement and Low Conductivity MPZ Model)	89
4-9 Airflow Through ES-1 and ES-2 (Shaft Fill and MPZ Flows Included) as a Percentage of Flow Through the Rock over the Repository Area (Horizontal Emplacement and High Conductivity MPZ Model)	89
5-1 Repository Used in Barometric Pressure Model	95
5-2 Barometric Pressure Events	100

FIGURES

	<u>Page</u>
5-3 Ratio of Displaced Air Volume to Void Volume for ES-1 for a Severe Thunderstorm Event (Vertical Emplacement and Low Conductivity MPZ Model)	103
5-4 Ratio of Displaced Air Volume to Void Volume for ES-1 for a Severe Thunderstorm Event (Vertical Emplacement and High Conductivity MPZ Model)	103
5-5 Ratio of Displaced Air Volume to Void Volume for ES-1 for a Tornado Event (Vertical Emplacement and Low Conductivity MPZ Model)	104
5-6 Ratio of Displaced Air Volume to Void Volume for ES-1 for a Tornado Event (Vertical Emplacement and High Conductivity MPZ Model)	104
5-7 Ratio of Displaced Air Volume to Void Volume for ES-1 for a Seasonal Event (Vertical Emplacement and Low Conductivity MPZ Model)	105
5-8 Ratio of Displaced Air Volume to Void Volume for ES-1 for a Seasonal Event (Vertical Emplacement and High Conductivity MPZ Model)	105
5-9 Ratio of Displaced Air Volume to Void Volume for ES-1 for a Severe Thunderstorm Event (Horizontal Emplacement and Low Conductivity MPZ Model)	106
5-10 Ratio of Displaced Air Volume to Void Volume for ES-1 for a Severe Thunderstorm Event (Horizontal Emplacement and High Conductivity MPZ Model)	106
5-11 Ratio of Displaced Air Volume to Void Volume for ES-1 for a Tornado Event (Horizontal Emplacement and Low Conductivity MPZ Model)	107
5-12 Ratio of Displaced Air Volume to Void Volume for ES-1 for a Tornado Event (Horizontal Emplacement and High Conductivity MPZ Model)	107
5-13 Ratio of Displaced Air Volume to Void Volume for ES-1 for a Seasonal Event (Horizontal Emplacement and Low Conductivity MPZ Model)	108
5-14 Ratio of Displaced Air Volume to Void Volume for ES-1 for a Seasonal Event (Horizontal Emplacement and High Conductivity MPZ Model)	108
6-1 The pH of Water from Below the Shaft Liner as a Function of the Volumetric Flow Rate Through the Shaft or MPZ	121

FIGURES

	<u>Page</u>
6-2	Deposition of Precipitate 124
6-3	Advance of the Precipitation Front in the Modified Permeability Zone 128
7-1	Contours of the Thickness of the Unsaturated Portion of the Calico Hills Unit Beneath the Repository 135
8-1	Production Cycle for Breaking and Removing the Liner and Placing the Backfill 138
8-2	Breaking the Liner with the Roadheader Unit 139
8-3	Removing the Pieces of Concrete Using the Orange-Peel-Grab Unit 147
8-4	Restoration of the Modified Permeability Zone and Emplacement of the Shaft Seal 149
8-5	Minimum Conductivity for Grouting 152
8-6	Contours of the Cut and Fill Depths Associated with the Exploratory Shaft Pad 155
8-7	Reestablishing the Original Slope in the Area of the Exploratory Shaft 157

EXECUTIVE SUMMARY

One aspect of the Yucca Mountain Project (YMP) is the development of the exploratory shaft (ES) testing program. The purpose of this program is to obtain at-depth site information on the hydrology and geology at the site. The results from these tests will be used to determine the effectiveness of the geologic setting at Yucca Mountain to isolate high-level radioactive waste. Before initiating the construction of the exploratory shafts (ES-1 and ES-2), it is necessary to determine the quality assurance levels to be applied to ES design and construction. The purpose of this report is to provide part of the technical basis for use by the U.S. Department of Energy, Nevada Operations Office, in establishing the appropriate quality assurance levels. This technical basis is developed through the use of analytical solutions that address the primary concern in this report: Do the shaft liner, the shaft internals, and the increased rock damage around the shaft (resulting from shaft construction) significantly influence the release of radionuclides from the repository? The approach taken to resolve this concern is to evaluate selected physical processes and bounding scenarios which, in our judgment, answer the most important concerns brought up by the DOE, U.S. Nuclear Regulatory Commission, and by ourselves. Therefore, this report is not intended to provide an exhaustive analysis of all possible scenarios and physical processes, which could occur and could impact the postclosure repository performance, but is considered sufficient to answer the question posed above.

The primary concern evaluated in this report is the significance of the rock-damaged zone or the modified permeability zone (MPZ)^{*} and the shaft liner on the long-term performance of the repository. A secondary concern addressed in this report is the effect of a shaft penetrating the Calico Hills unit. Penetration of this unit by the shaft has been evaluated to illustrate the potential effect of the elevated temperature of the ground water on the zeolites in the Calico Hills unit, if this unit is penetrated. The thickness of the Calico Hills unit at ES-1 is also discussed in this report. The shaft internals will be removed to accommodate

*The MPZ is the zone immediately surrounding an underground excavation in which the permeability of the rock mass has been altered because of the redistribution of stress and the effects of blast damage.

emplacement of shaft fill and, consequently, will not impact the postclosure performance of the repository.

Because release and transport of radionuclides from the underground facility can be due to several mechanisms, scoping calculations are presented in Appendix A to provide a perspective on the more important mechanisms that should be considered when assessing the significance of the MPZ. Based on these calculations, release of radionuclides resulting from water transport is considered to be the most realistic and dominant mechanism. Air transport of gases by convective and barometric forces through the drifts and/or shafts was also considered important because of the thermal energy differences within the repository and the occurrence of meteorological events at the surface. The calculations, therefore, focus primarily on conditions that would enhance the transport of radionuclides in the water and the transport of gases in the air.

In the first mechanism, it is assumed that water enters the upper portion of the shafts from fractures saturated from a probable maximum precipitation (PMP) event. The calculation presented in this report defines a broad range of inflows into the shaft. These inflows depend on the matrix and fracture properties of the densely welded Tiva Canyon Member. In computing the amount of water entering the shaft, it is assumed that both the MPZ and the shaft intercept the fracture flow.

Two additional water flow scenarios were also considered to provide a range of water flows entering the shafts. The first scenario involves infiltration of all of the precipitation from a PMP event into the stratigraphy over the drainage basin associated with the ESs. The portion of precipitation from the PMP that intercepts the shafts and their associated MPZs, regardless of depth, enters the shafts. In the second scenario, the water from a PMP event saturates the alluvium surrounding ES-1* and enters the upper portion of the shaft. The specific mechanism is flow from the saturated alluvium into the shaft fill.

*This analysis was performed as part of the original evaluation of the ESs. The scenario is applicable to the old ES locations and is presented to fully document the evaluations completed in support of the YMP.

The authors conclude that for water inflow, the presence of the shafts including the shaft fill, the shaft liner, and the MPZ is not likely to influence the release of radionuclides from the repository because (1) both ES-1 and ES-2 have been relocated to more favorable locations outside the flood plain of existing arroyos in an area where the bedrock is exposed; (2) a realistic scenario of water flow into the shafts during a PMP event indicates that the amounts potentially entering the shafts are small and range from 0 to $<50 \text{ m}^3/\text{event}$; and (3) even if a highly improbable scenario* occurs, the volume of water entering the shaft can be contained within the shaft sump and/or the exploratory shaft facility.

An additional concern about the flow of water into the MPZ and out of the base of the shaft is the potential to form mineral precipitates in the MPZ and the shaft fill. Mineral precipitation could occur because the concrete liner will cause some modifications to the chemistry of the ground water. These water chemistry changes may cause the ground water to become supersaturated with respect to some minerals, and precipitation could then occur. If precipitation occurs above the repository station, decreased water flows would be expected to enter the base of the shaft. If precipitates form at the base of the shaft, the drainage capacity in this area could be decreased.

Based on the model in this report, precipitates are predicted to form and quickly deposit at nucleation sites in void spaces. This deposition is controlled by diffusional processes where the length of the diffusional path (i.e., one-half of the pore diameter or one-half of the fracture aperture) is small, and travel times are short. Hence, forward migration of precipitates in the porous medium is expected to be limited. As this process continues, a buildup of precipitates occurs in a frontal advance. This precipitation front is projected to start at the top of the liner and progress downward in both the shaft fill and the MPZ. It has been concluded that if the anticipated volume of water (0 to $\sim 40 \text{ m}^3/\text{year}$; Fernandez et al. 1987) enters the shafts, no significant precipitation

*The scenario used to compute the unanticipated volume of water ($\sim 20,000 \text{ m}^3$) is considered highly improbable because it couples a probable maximum flood event with an obstruction in the drainage basin that can retain the flood waters above the ES locations. It also was developed for the old locations of the ES, i.e., ES-1 was located in the alluvium.

occurs. If an unanticipated and highly improbable volume ($\sim 20,000 \text{ m}^3$ /event, Appendix C) enters the shaft, precipitates could advance as much as 60 m downward in the MPZ where fracture porosity is small. However, once the front advances beyond the base of the liner, the maximum frontal advance is expected to be about 0.016 m (for the scenario described in Appendix C) because of the increased porosity of the shaft fill. Hence, the deposition of solids from the interaction of the shaft liner with ground water is expected to be a localized phenomenon. We can, therefore, conclude that the fractures in the MPZ above the repository horizon are likely to fill with precipitate as a consequence of water infiltration. As additional water inflow occurs, the permeability of the MPZ will tend to be reduced as deposition occurs. Because deposition is a localized phenomenon and water volumes are expected to be low, the projected reduction in permeability is expected to be a near-surface phenomenon. The drainage capacity of the rock at the base of the shaft, therefore, should not be detrimentally reduced.

As mentioned earlier, the MPZ may be significant if it substantially enhances the release of gaseous radionuclides because of increased airflow through the MPZ. Because the emplaced waste in the repository will release heat, temperature gradients will develop in the rock mass. The temperature differential will tend to cause air to rise in the ESs. The convective airflow analyses presented in this report consider potential airflow in and near the shafts and also consider the potential flow through the rock above the waste disposal areas.

For several combinations of air conductivity of the host rock above the repository, the percentage of flow through the shaft (including the MPZ) to the total flow (including shaft, the MPZ, and the rock mass above the waste disposal area) was plotted as a function of the air conductivity of the shaft fill. It was concluded from the analysis that shafts and ramps are not preferential pathways for gaseous radionuclide releases if the air conductivity of the shaft fill is less than about $3 \times 10^{-4} \text{ m/min}$ or has an equivalent hydraulic conductivity of 10^{-2} cm/s . Saturated hydraulic conductivities of this magnitude are believed to be easily attainable (Fernandez et al., 1987). When the air conductivity of the shaft fill is $>3 \times 10^{-4} \text{ m/min}$, the air flows predominantly through the shaft fill. It is only when the conductivity of the shaft fill is low that flow through the

MPZ is proportionally greater than flow through the shaft fill. However, when this happens, the total airflow through the MPZ and shaft fill, as compared to the flow through the rock over the repository, is low (i.e., <2.5%). Therefore, it can also be concluded that the MPZ is not likely to detrimentally influence the performance of the repository by enhancing the release of gaseous radionuclides.

A second mechanism was considered in assessing the influence of the shaft fill and the MPZ on increasing the release of gaseous radionuclides from the repository. This second mechanism involves the displacement of air from ES-1 or ES-2 as a result of barometric forces. The purpose of the analysis associated with the mechanism is to predict what volume of air contained in the shaft fill and the MPZ under unsaturated conditions can be displaced as a result of several meteorological events. If only a portion of the shaft fill and MPZ air volume is displaced when the pressure drops at the surface, the surface air will be forced into the shaft fill and MPZ when a pressure reversal occurs at the surface.

It has been concluded from these analyses that the volume of air in the ESs is not fully displaced during a broad range of meteorological conditions if the air conductivity of the shaft fill is less than about 10^{-1} m/min.

A final area of evaluation mentioned above was the penetration of the ES into the Calico Hills unit.* This calculation has been presented to illustrate what impact penetration by the shaft would have. From the evaluation presented in this report, the impact of this penetration on the sorption of the Calico Hills unit was found to be negligible. This conclusion was reached for the following reasons.

- o Water passing through the ES will be separated from waste stored in the repository. Therefore, the likelihood of water containing radionuclides reaching the ES is diminished.

*The current position of the YMP is that the ES will not penetrate the Calico Hills unit.

- o The minimum thickness (70 m) of the Calico Hills unit at the eastern edge of the repository will be preserved while allowing information to be gained by sinking the ES into the upper margin of the Calico Hills.

- o The temperature of water passing through the ES has been calculated to closely approach the global formation temperature for all considered water flow rates, including the maximum flooding event defined in this report. This calculated temperature increase will be far less than that required to significantly impact the sorption of the Calico Hills zeolites. Therefore, if any radionuclides do reach the base of ES-1, it is likely that they would still be effectively retained at the base of the shaft.

The discussion and results presented above focused on determining whether the design and construction of the ESs could significantly influence the performance of the repository. As an aid to future analyses of the effect of the shaft liner, MPZ, or the ES pad on the performance of the repository, we have described the preferred methods for restoring the MPZ, removing the liner, emplacing the seal, and restoring the ES pad. The following conclusions have been reached on the preferred methods.

- o Grouting in welded tuff is feasible and is preferred for restoring the MPZ because drilling smooth-walled, grout holes allows fractures in the MPZ to be examined through the use of a borescope. Also, at present, it is not certain how large an interface stress can be developed through the use of only an expansive concrete (one of the alternatives) or how effective the development of such stress would be in reducing the potential for flow in closing fractures. Grouting the MPZ, however, is more expensive than constructing an expansive concrete plug.

- o Evaluation of the advantages and disadvantages suggests that the hydraulic splitter is favored for removing the liner, although other approaches are technically feasible. Conventional equipment slightly modified by suspending the splitters from chains may be used. The costs are somewhat less than for other methods evaluated, and the use of the splitters does not leave potentially

undesirable chemical residue. While supplemental hand methods may be needed, this is not considered a significant disadvantage.

- o The construction sequence for emplacing a shaft plug entails making saw cuts at the top and bottom of the plug, removing the liner, excavating the keyway, backfilling to the underside of the plug, placing concrete, and contact grouting.
- o A simple rock and soil mixture over the ES pad could limit the amount of flow entering the upper portion of the shaft and could provide erosional protection.

1.0 PURPOSE OF REPORT

The Yucca Mountain Project (YMP), managed by the Nevada Operations Office of the U. S. Department of Energy (DOE), is examining the feasibility of developing a nuclear waste repository in an unsaturated tuff formation beneath Yucca Mountain. Yucca Mountain is located on and adjacent to the Nevada Test Site, Nye County, Nevada. One aspect of the YMP is to develop the exploratory shaft (ES) testing program. The purpose of the ES testing program is to obtain at-depth site information about the hydrology and geology of the unsaturated tuff at Yucca Mountain. The results from many of these tests will be used to determine the effectiveness of the geologic setting at Yucca Mountain to isolate high-level radioactive waste.

Before constructing the exploratory shafts (ES-1 and ES-2), it is necessary to determine the quality assurance levels to be applied to the design and construction of the ES. The DOE is responsible for assigning the quality assurance levels. This report provides analyses that will establish part of the technical basis for assigning the appropriate quality assurance levels. This basis has been established by evaluating whether the design and construction of ES-1 and ES-2 could compromise the long-term isolation capabilities of the repository. The concern raised was: Do the shaft liner, the shaft internals, and the increased rock damage around the shaft significantly influence the release of radionuclides from the repository? Because the shaft internals, including instrument conduits, utility piping, ventilation ducts, and conveyance hardware, will potentially be removed for repository operations (i.e., development, waste emplacement, monitoring, and, if necessary, retrieval) and will certainly be removed to accommodate emplacement of shaft fill (during decommissioning), shaft internals will have no impact on the long-term performance of the repository. Therefore, only the influence of the damaged zone or the modified permeability zone (MPZ) and the shaft liner on the long-term performance of the repository has been considered. The significance of this influence has been determined by evaluating selected physical processes and bounding scenarios that have been raised by the DOE, the Nuclear Regulatory Commission, and by ourselves. Therefore, this report is not intended to provide an exhaustive analysis of all possible scenarios

and physical processes that could occur and could impact the future repository performance but is considered sufficient, as detailed in Chapter 9, to support the construction of the ES.

An integral part of the long-term performance of the overall repository system is the closure of ES-1 and ES-2. Therefore, it is necessary to determine the desired performance of these sealed shafts and, for completeness, the entire sealing system. Additionally, a model must be developed for the MPZ. In Fernandez et al. (1987), performance goals and design requirements for the sealing system are presented. The need for sealing is also assessed by evaluating the flow of water into and out of the underground facility, shafts, and ramps for anticipated conditions. In Case and Kelsall (1987), a model of the MPZ in welded tuff is presented. Development of the MPZ is due to the blast-damage effects and stress relaxation. In this report, selected results from both Fernandez et al. (1987) and Case and Kelsall (1987) have been restated. These results are supplemented by additional analyses of the potential mechanisms of radionuclide release that are of greatest concern and analyses of the potential modification of ground-water chemistry by the liner. This report also describes contingency plans to remove the liner, restore the MPZ, emplace a seal, and restore the ES pad area. This information is presented in case future analyses suggest that removing the liner and restoring the MPZ are required. It is not the intent of this report to present a total systems analysis.

Reference conditions of the shafts considered in this report are given in Chapter 2. Chapter 3 presents selected water flow scenarios that may impact the performance of the Yucca Mountain Mined Geologic Disposal System. The analyses described in Chapter 3 establish the magnitude of water entering the ESs as a result of these selected water-flow scenarios. The impact of these volumes of water is also discussed. Chapters 4 and 5 evaluate the potential for air to flow out of the repository as a result of convective and barometric forces, respectively.

The potential airflow out of the repository is assessed by considering the convective circulation of air in response to thermal gradients and the

movement of air in response to changes in barometric pressures. The significance of this air movement has been determined by considering how much air might flow preferentially through the shafts and ramps. For the barometric analysis, the volume of air that can exit shafts and ramps as a result of several surface weather conditions has also been evaluated.

The potential for changing the conductivity of the shaft liner, the MPZ, the shaft fill, and the shaft sump is evaluated in Chapter 6. This evaluation is accomplished by analyzing the interaction of water entering the shaft through the shaft liner. Once the potential changes in water chemistry are predicted, the likelihood and location of mineral precipitation are assessed. In addition to discussing these chemical effects, the potential for fines migration in the shaft fill is discussed to determine the reduction of shaft sump conductivity. Chapter 7 addresses the potential influence of the penetration of ES-1 into the tuffaceous beds of Calico Hills. Specifically, the potential change in the sorption of the Calico Hills unit is evaluated. This potential change in sorption may result from elevating the temperature of water potentially passing through the ES. Finally, in Chapter 8 possible remedial measures to remove the liners from the ESs, restore the MPZ, and reclaim the ES pad area are presented. Also, the procedure for emplacing a shaft seal is presented in Chapter 8 together with schedule and cost estimates for removing the shaft liner, emplacing backfill, and emplacing a shaft seal, if this becomes necessary.

2.0 SHAFT DESIGN INFORMATION

This chapter contains information primarily on the design of the ESs. Limited information about the repository design is also presented to better understand how the ESs have been integrated with the repository. In general, the underground facility comprises interconnecting access and emplacement drifts and is planned to be located in the unsaturated portion of the Topopah Spring Member approximately 200 to 400 m above the groundwater table. The Topopah Spring Member is predominantly a densely welded, highly fractured tuff having a low matrix hydraulic conductivity.

Access to the underground facility is provided by ramps and shafts. The current repository design in the "Site Characterization Plan Conceptual Design Report" (SCP-CDR)(SNL, 1987, pp. 4-10 to 4-12) incorporates six openings to the underground facility, including four vertical shafts and two inclined ramps. Both types of accesses may penetrate several stratigraphic units, including the alluvium and welded and nonwelded tuff units. The ramps connect directly with the main access drifts at the northern end of the repository, and the shafts are located in the northeastern portion of the repository. The men-and-materials and emplacement exhaust shafts have shallow sumps extending 24 and 3 m below the repository. The bottoms of both of these shafts are in the Topopah Spring Member. The current design of the exploratory shaft facility (ESF) does not show penetration of ES-1 into the Calico Hills unit (DOE, 1988, Section 8.4.2.1.6.1). The sump or tailshaft (the distance from the repository level to the base of the shaft) for ES-1 is about 15 m. The bottom of ES-2 will extend about 31 m below the repository level. Figure 2-1 shows a profile of ES-1 and the corresponding geologic stratigraphy.

2.1 Location of the Exploratory Shafts

ES-1 and ES-2 are located in a wide valley through which the north and south forks of Coyote Wash flow (Figure 2-2). The valley floor is underlain by coarse alluvium and mud and debris flow deposits, with surficial fine-grained sand, probably of eolian origin. Bedrock (Tiva Canyon Member) is exposed in the steep valley walls to the north, south, and west. These locations for ES-1 and ES-2 will be approximately 105 m north of and above

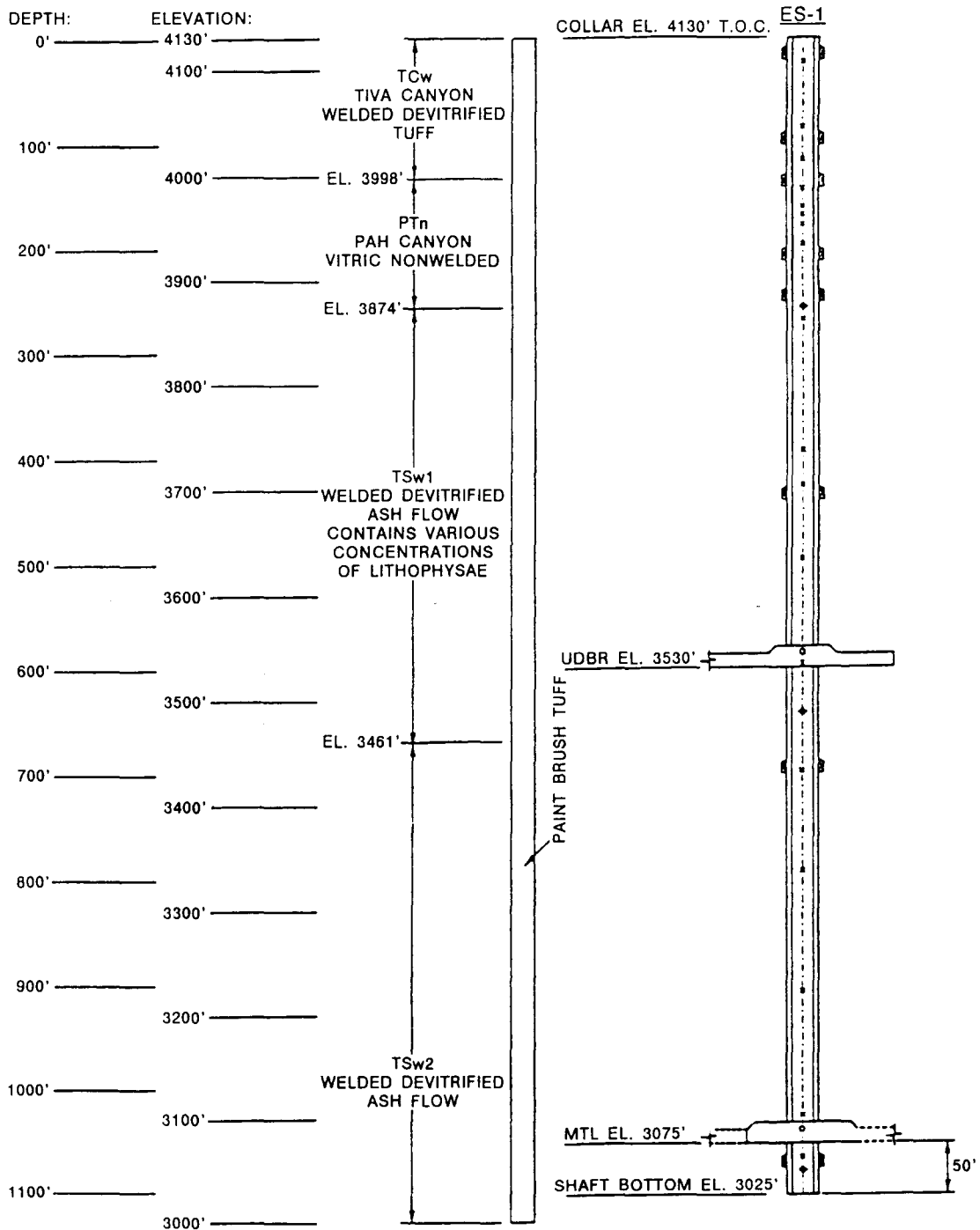


Figure 2-1. Exploratory Shaft (ES-1) and Corresponding Geologic Stratigraphy

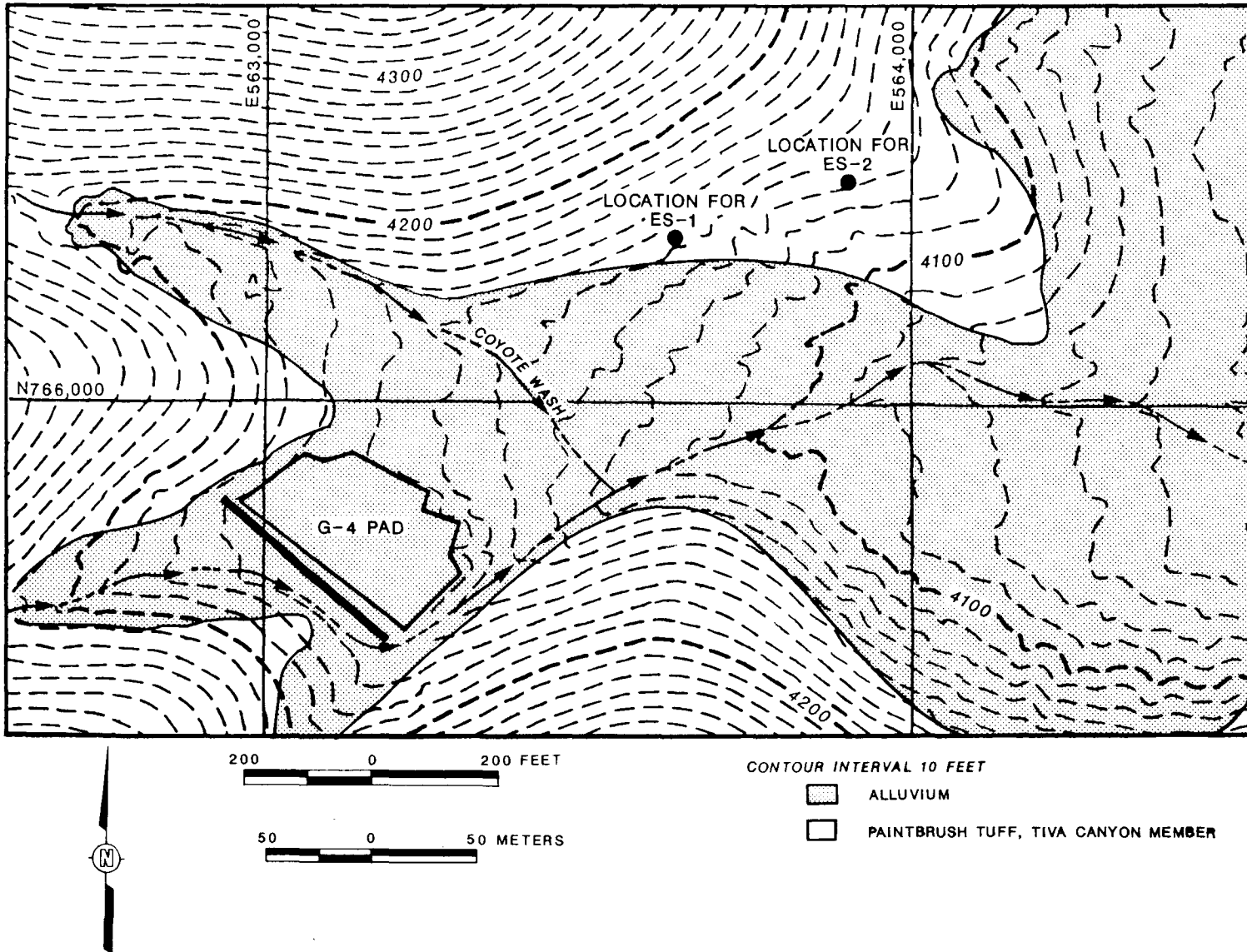


Figure 2-2. Surficial Geology of the Exploratory Shaft Area

the confluence of two small ephemeral streams, which are tributaries of the Coyote Wash drainage system.

2.2 Construction of the Exploratory Shafts

Before the repository is constructed, an ESF will be developed. The ESF primarily includes (1) the main shaft (ES-1), which will transport personnel, materials, and equipment from the surface to the subsurface test area and will provide ventilation to the ESF; (2) an underground testing area; and (3) a secondary shaft (ES-2), which will provide secondary emergency egress, transport personnel and materials, provide for muck removal, and provide additional ventilation capacity. It is the current intent of the YMP to incorporate ES-1 and ES-2 into the design of the underground facility for the repository.

The current design details for ES-1 and ES-2 follow. The excavated diameter of the shafts will be approximately 4.3 m with a finished diameter of 3.7 m. Both shafts are to be lined with an unreinforced concrete liner at least 0.3 m thick. Some reinforcement is planned in the shaft collar and in the brow* at each breakout. The collars for the new locations of ES-1 and ES-2 will be in bedrock. Most of the concrete liner will not be reinforced but will contain some steel rods to hold the forms used to construct the liner.

Both shafts will be mined using a conventional drill-blast-muck mining sequence. During the mucking operation, minimal amounts of water will be used to suppress the dust in the shaft so that tests characterizing the unsaturated zone will not be affected. Because the excavation of the shafts involves blasting, some additional fracturing of the rock mass into the shaft wall may occur. The blasting will be controlled to enhance the vertical advance*, limit damage in the rock surrounding the shaft, and produce rock fragments of an acceptable size.

*The shaft collar is that part of the shaft liner that is at the upper portion of the shaft and is generally constructed of reinforced concrete. The shaft brow refers to the roof rock in the area where the shaft opens up into the shaft station. The shaft station refers to the location where the drift intersects the shaft.

2.3 Shaft Sealing Concepts

The primary functions of shaft seals are to reduce the potential for entry of surface water or ground water into the waste emplacement areas and to reduce airflow out of the repository via the shafts.

Flow through the shaft can be reduced by backfilling or by placing one or more seals (plugs) at intervals along the shaft. Backfill alone may not be a satisfactory option if there is the potential for a significant flow of water through the MPZ adjacent to the shaft wall. In such a case, it might be necessary to form a cutoff through the damaged zone, possibly by keying a plug into the walls. Another alternative for reducing the potential flow into the waste disposal area is emplacing a repository station seal in the drift connected to the ES. Figure 2-3 illustrates the general arrangement for shaft seals.

2.4 Preferred Options for Shaft Seals

The anchor-to-bedrock plug/seal is currently the preferred option for reducing the flow of water and deterring human entry because

- o The anchor-to-bedrock plug/seal can be located in a relatively benign environment protected from surficial temperature extremes, surficial geologic processes, and heat generated by the waste. Station plugs, located at the intersection of the shafts and repository station drifts, are isolated from the waste emplacement areas by barrier pillars.* The maximum temperature at the station plug is estimated to be 40°C (Richardson, in preparation, Appendix G). The in situ stress would also be greater than that associated with a plug/seal closer to the surface.
- o The hydrologic design requirement for the anchor-to-bedrock plug/seal is potentially less stringent than that for a seal at the

*The barrier pillar refers to the rock zone, surrounding the shaft, that isolates the shaft from subsidence effects of underground rooms. For a nuclear waste repository, the barrier pillar also isolates the shaft from a high temperature environment.

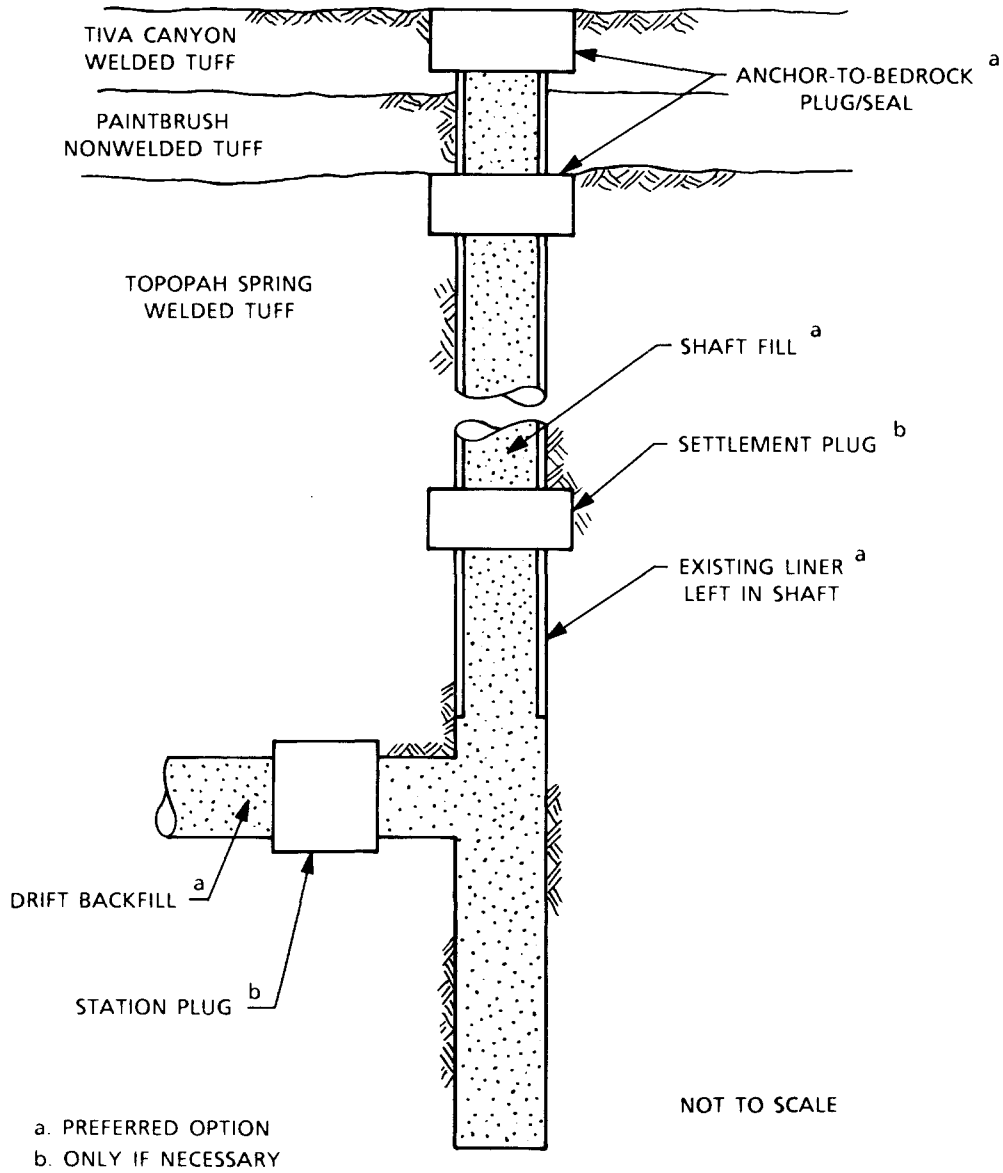


Figure 2-3. General Arrangement for the Shaft Seals Showing Optional Components

base of the shaft because of the lower hydrologic head (Fernandez et al., 1987).

- o Only one seal is required for each shaft, making a total of four, whereas eight seals might be required if they are placed in the shaft stations.
- o Constructing a seal at a shallow depth in a shaft should be easier and probably cheaper than constructing one at the base of the shaft.
- o The anchor-to-bedrock plug can be designed to reduce the potential for flow through the MPZ, whereas shaft backfill would have no influence on the MPZ. Moreover, development of the MPZ at the shallow depth of the anchor-to-bedrock plug should be less than the MPZ developed at the location of the station plug where inelastic deformation is more likely to occur (Case and Kelsall, 1987).

3.0 POTENTIAL FOR ENHANCING RADIONUCLIDE RELEASE RESULTING FROM SELECTED WATER FLOW SCENARIOS

Shafts represent potential pathways that could compromise the ability of the geologic repository to meet the performance objectives following permanent closure. As analyzed in this report, performance can be compromised in two ways. First, water could enter the underground facility through the shafts and contact waste packages in disposal areas, potentially accelerating the radionuclide release; and second, release of gaseous radionuclides could occur through the shafts.

Two zones can affect water entry into and airflow out of the repository--the shaft (the backfill and the shaft liner) and the MPZ behind the shaft liner. The intent of this chapter is to evaluate whether the presence of the MPZ and the shafts could significantly enhance radionuclide release as a result of water flow into the shaft and the MPZ. This evaluation is performed by assuming (1) the shafts are filled by a granular material, (2) an MPZ develops, and (3) water flow enters the shafts from selected scenarios. Using these assumptions, the significance of water flow into the underground facility from the shafts is evaluated. A description of the MPZ is included in Appendix B and is described in more detail elsewhere (Case and Kelsall, 1987). Three scenarios for possible water inflow are postulated. These scenarios provide a range of water flows into the ESs.

3.1 Flooding and Erosion Potentials at the Exploratory Shaft Locations

The characteristics of the flood channel during a probable maximum flood (PMF) are defined and used in the selected scenarios discussed in this chapter. In addition to a discussion on the characteristics of the PMF, the erosion potential in the vicinity of the ESs is also discussed.

3.1.1 Channel Flooding at the Exploratory Shaft Locations Resulting from a Probable Maximum Flood

The PMF is used in this report because it represents a "hypothetical" flood that attempts to define the maximum flood potential at a specific site. This PMF is defined as: "The flood that may be expected from the

most severe combination of critical meteorologic and hydrologic conditions that are reasonably possible in the region" (National Research Council, 1985, p. 256). One of the most important factors in determining the PMF is the intensity and duration of the rainfall. The rainfall producing the PMF is the probable maximum precipitation (PMP). Bullard, using the National Weather Service's Hydrometeorological Report No. 49, determines two PMPs representing two different rainfall conditions. Therefore, to be consistent with the data reported in Bullard (1986), two PMP conditions are considered in this report--a general storm and a local storm (thunderstorm). The general storm assumes a total rainfall of 8.1 in. in 14 hours. The thunderstorm assumes a total rainfall of 13.9 in. in 6 hours. Using the assumptions cited above, the PMFs have been computed by the U.S. Bureau of Reclamation (Bullard, 1986). The results of these computations are used in Section 3.1 to estimate (1) the extent of the flooding channel resulting from the PMF and (2) the height of water in the channel as a function of time. The approaches used to compute the extent of flooding and the height of water in the channel are discussed below.

3.1.2 Extent of the Flood Channel

The as-built topography* and the Manning equation (Trefethen, 1959) for open channel flow were used to develop a map defining the maximum extent of the PMF. The PMF high-water marks shown on Figures 3-1 and 3-2 were developed from eight cross sections. In applying the Manning equation, the assumptions used were similar to those used by Squires and Young (1984, p. 24). Specifically, the values for slope of the energy-grade line used in Manning's equation were assumed to be equivalent to the slope of the water surface and the channel bottom. The value for the roughness coefficient, n , in Manning's equation was assumed to be 0.060. Roughness coefficients used by Squires and Young ranged from 0.030 to 0.055. Because it is our intent to estimate the highest water elevation (or cross-sectional area of water flow in the channel) during a PMF at selected locations, it is necessary to reduce the velocity of channel flow as

*The cross sections used in developing the extent of the PMF channel assumed the current topography with the exception of the modifications made to develop the ES pad.

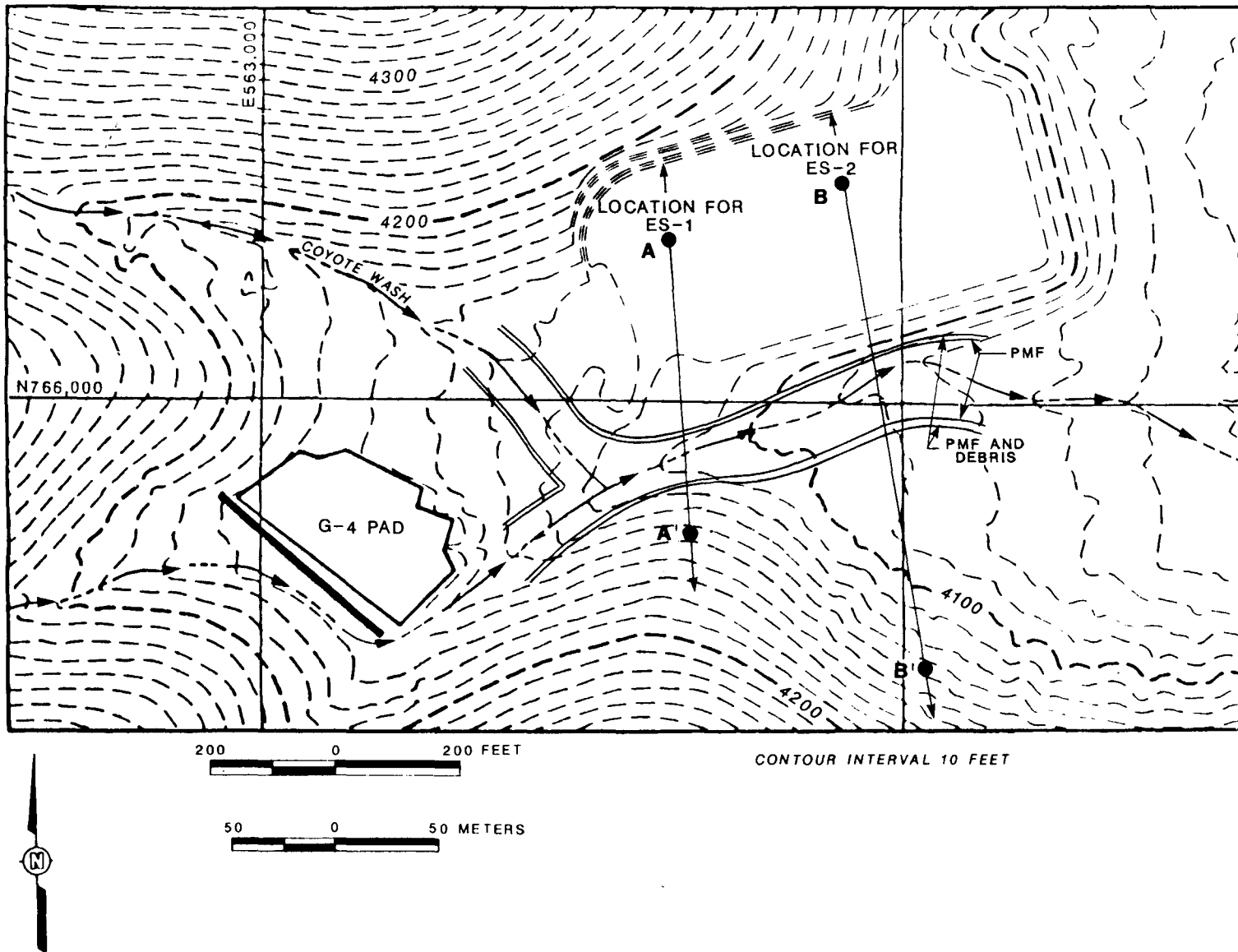


Figure 3-1. Estimated High-Water Locations Associated with a Probable Maximum Flood in the Exploratory Shaft Area Under Thunderstorm Conditions

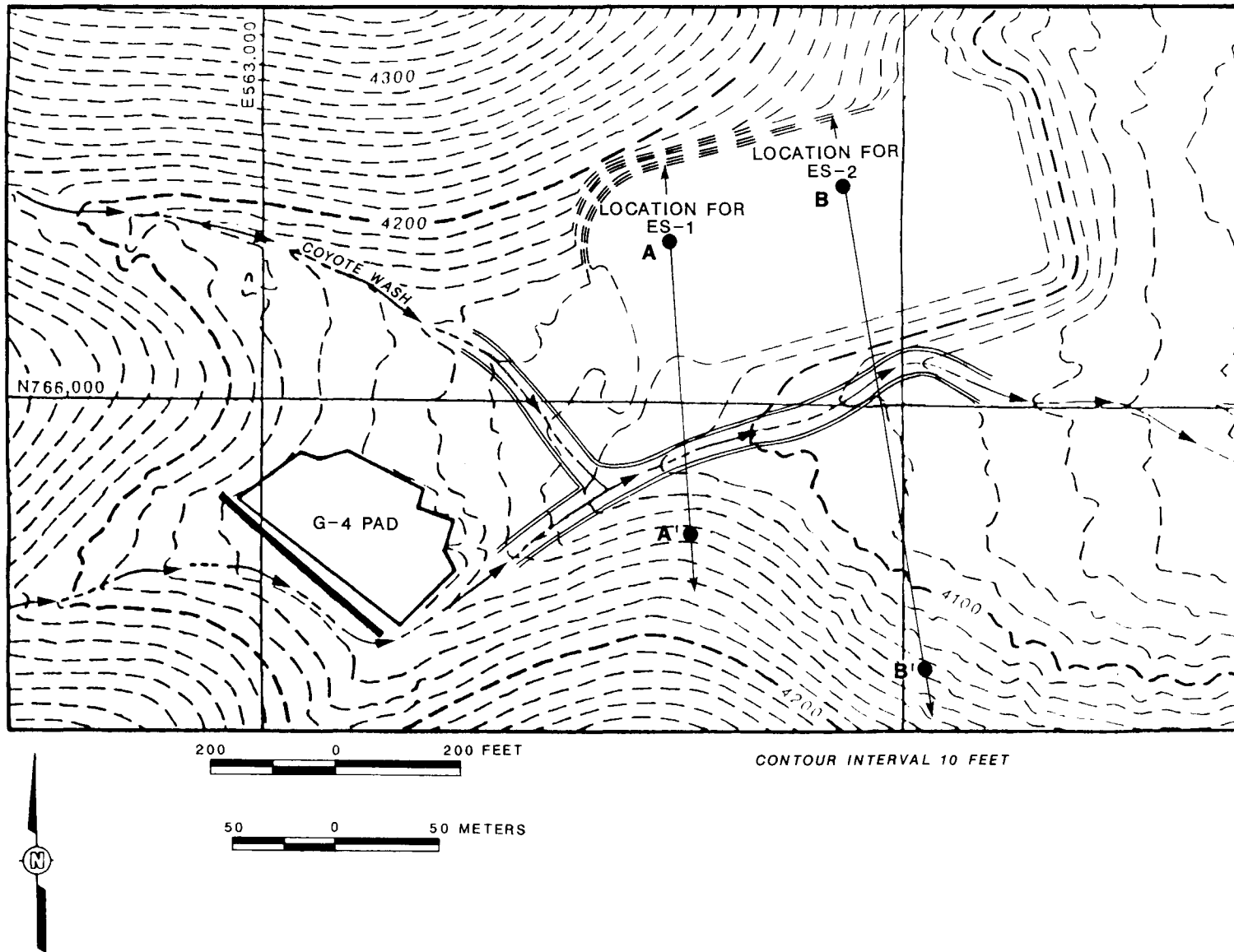


Figure 3-2. Estimated High-Water Locations Associated with a Probable Maximum Flood in the Exploratory Shaft Area Under General Storm Conditions

presented in the Manning equation. This reduction of velocity can be achieved by selecting a greater "n" value (as used in this analysis), which conservatively predicts a higher water-level rise.

Figures 3-1 and 3-2 show the maximum high-water locations for the PMF relative to the location of the ESs assuming two peak discharges. The inner lines represent the clear water flow only and the outer lines represent the clear water and debris flows. The peak discharge for the clear water flow is $95 \text{ m}^3/\text{s}$ for the thunderstorm event and $8.6 \text{ m}^3/\text{s}$ for the general storm event (Bullard, 1986). To arrive at the peak discharge for the clear water plus debris flow, the debris flow is assumed to be 50% of the clear water flow. The horizontal distances of the high-water mark from the ES-1 and ES-2 locations are 84 and 82 m, respectively, for the thunderstorm event and 92 and 83 m, respectively, for the general storm event.

3.1.3 Height of Water in the Channel

To develop realistic flow conditions (height versus time) in the channel, five cross sections were selected for evaluation. These were cross sections at the ES locations, the area between the ESs, and the areas upgrade and downgrade from the ESs. The flow rate, Q, versus height, h, relationships were developed at specific times using (1) "Q versus time, t," hydrographs given by the U.S.B.R. (Bullard, 1986, Tables 11 and 26), (2) the topographic profiles at these five cross sections, and (3) the Manning equation. The "Q versus h" curve is termed the conveyance curve. By combining the conveyance and the hydrograph curves, the "h versus t" curves were developed at each of these five cross sections. By taking each corresponding time for each "h versus t" curve and averaging the h values for each curve, an average "h versus t" curve was obtained. The results from this analysis are depicted in Figure 3-3 for both a thunderstorm and a general storm.

Figures 3-4 and 3-5 present cross sections of the topography and the maximum water elevations of the PMF at the ES-1 and ES-2 locations. These cross sections are presented primarily to illustrate the difference between the elevations of the ES collars and the elevation of the PMF. Based on

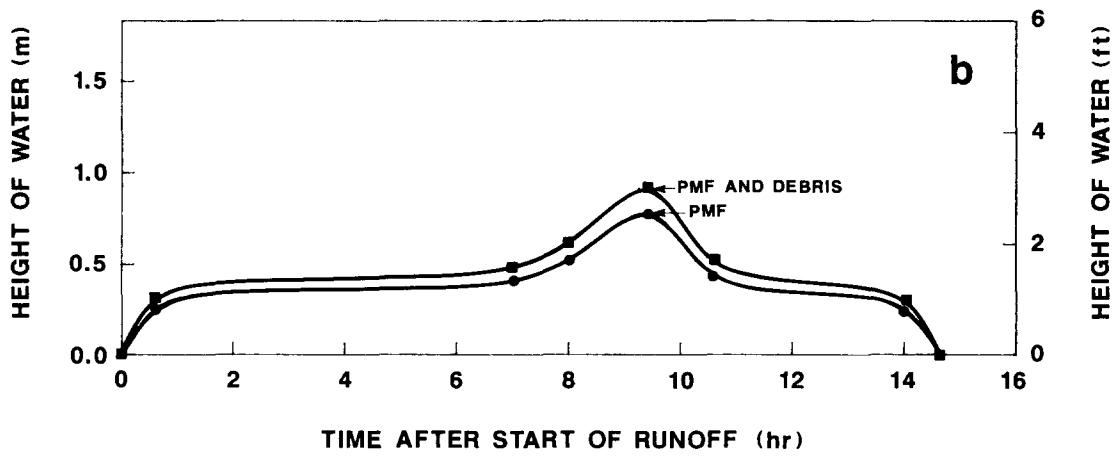
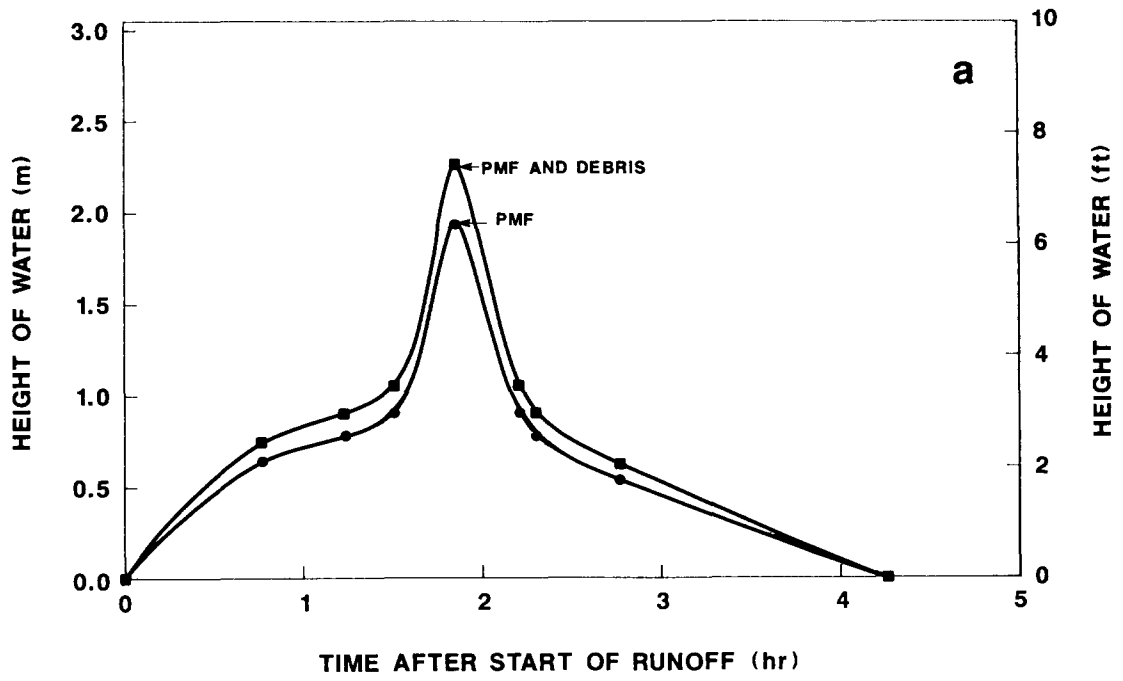
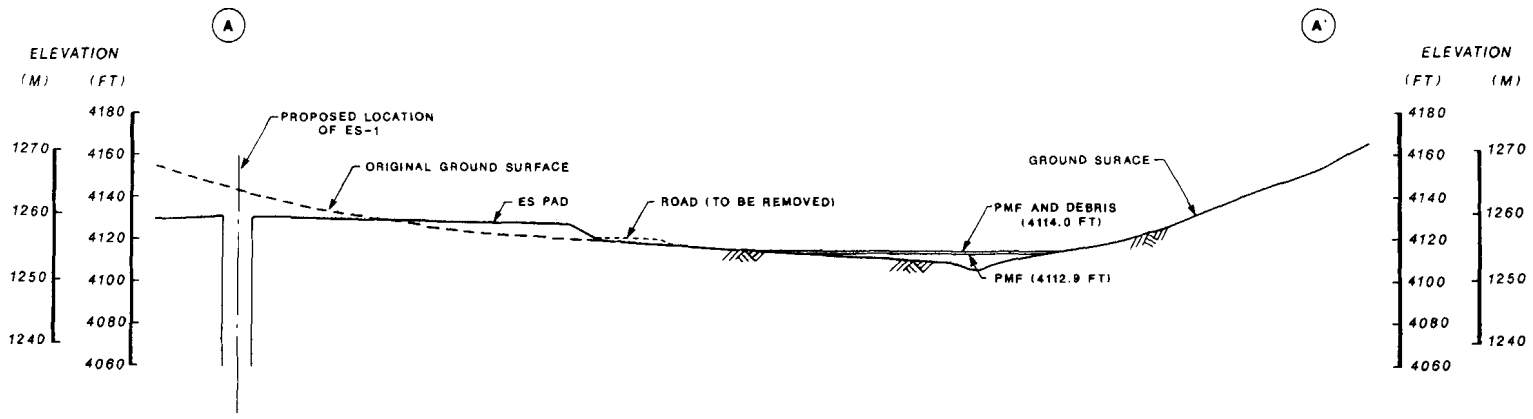


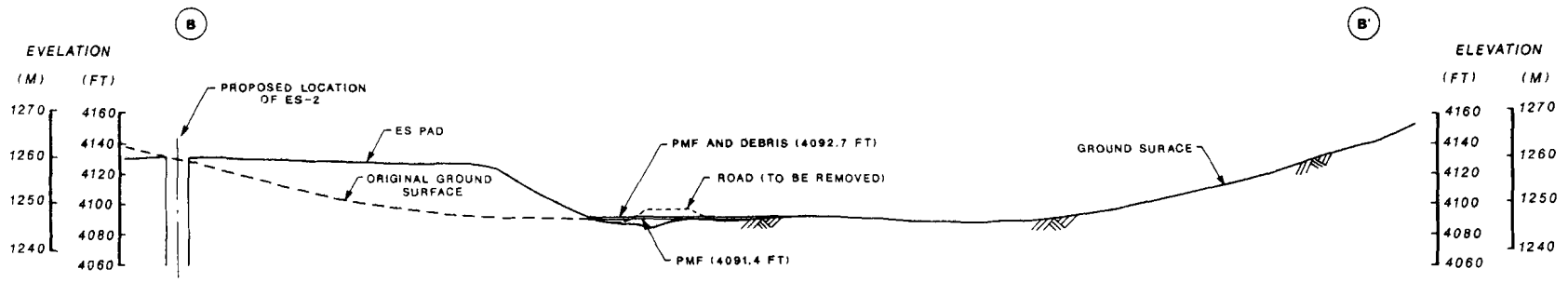
Figure 3-3. Average Height Versus Time Curves for the (a) Thunderstorm and (b) General Storm



SECTION A-A' CHANNEL CROSS SECTION LOOKING DOWNSTREAM
THUNDERSTORM PMF LEVELS

50 0 50 FEET

25 0 25 METERS

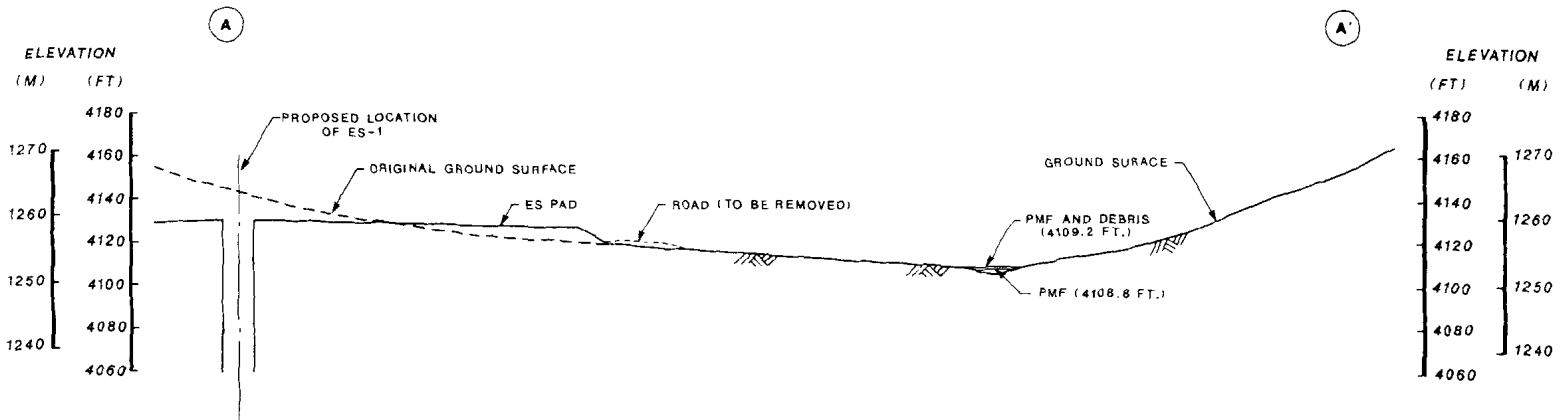


SECTION B-B' CHANNEL CROSS SECTION LOOKING DOWNSTREAM
THUNDERSTORM PMF LEVELS

50 0 50 FEET

25 0 25 METERS

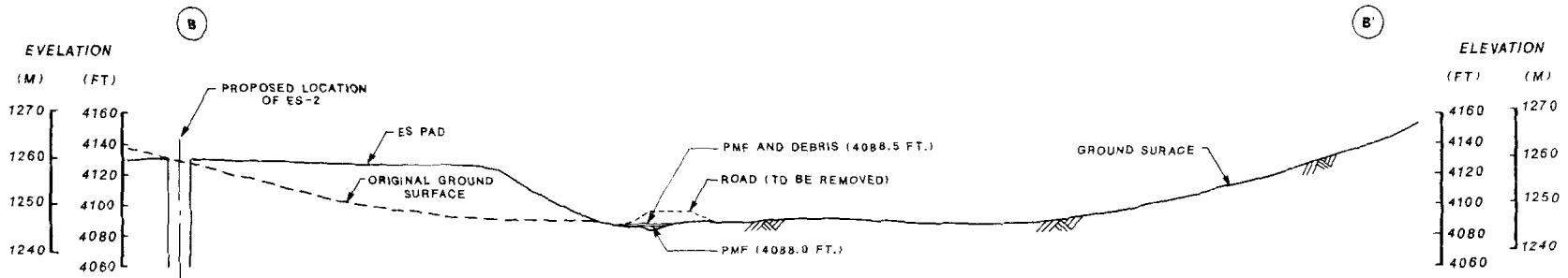
Figure 3-4. Topographic Cross Sections with Probable Maximum Flood Levels Under a Thunderstorm Condition



SECTION A-A' CHANNEL CROSS SECTION LOOKING DOWNSTREAM
GENERAL STORM PMF LEVELS

50 0 50 FEET

25 0 25 METERS



SECTION B-B' CHANNEL CROSS SECTION LOOKING DOWNSTREAM
GENERAL STORM PMF LEVELS

50 0 50 FEET

25 0 25 METERS

Figure 3-5. Topographic Cross Sections with Probable Maximum Flood Levels Under a General Storm Condition

these figures, the ES-1 and ES-2 surface locations are 5 and 11 m, respectively, above the PMF maximum levels for the thunderstorm event and 6 and 13 m, respectively, above the PMF maximum levels for the general storm event.

To illustrate the necessary peak flow required to reach the surface elevation of ES-1 and ES-2, curves illustrating the elevation versus flow rate at the ES-1 and ES-2 locations were prepared. These curves are shown in Figure 3-6. When the water reaches the ES-1 and ES-2 collars, the corresponding peak discharges are about 150,000 ft³/s and 820,000 ft³/s. These peak discharges are approximately 45 and 240 times the amount of discharge for the PMF for the thunderstorm event and suggest a large uncertainty in the computed flood volumes required to reach the collars of the shafts.

To further illustrate the low likelihood that flood waters will reach the elevation of the ES collar, Table 3-1 is presented here. This table lists peak discharges and associated drainage basin areas for other washes in the Yucca Mountain area. Fortymile Wash having a drainage basin of 312 mi² has a computed peak discharge of 540,000 ft³/s for a regional maximum flood. Yucca Wash having a drainage basin of 16.6 mi² has a computed peak discharge of 92,000 ft³/s. Because (1) these peak discharges are comparable to the discharges needed to reach the collars of the ESs and (2) the sizes of the drainage basins for Fortymile Wash and Yucca Wash are 1,560 and 83 times greater than the drainage basin associated with the ESs, we conclude that the likelihood that flood waters will enter the ESs directly is extremely small.

3.1.4 Sheet Flow over the Exploratory Shaft Pad

To determine the depth of sheet flow over the ES pad, the unit hydrograph methodology was used to develop the hydrographs. The unit hydrograph methodology used was identical to that used by Bullard (1986).

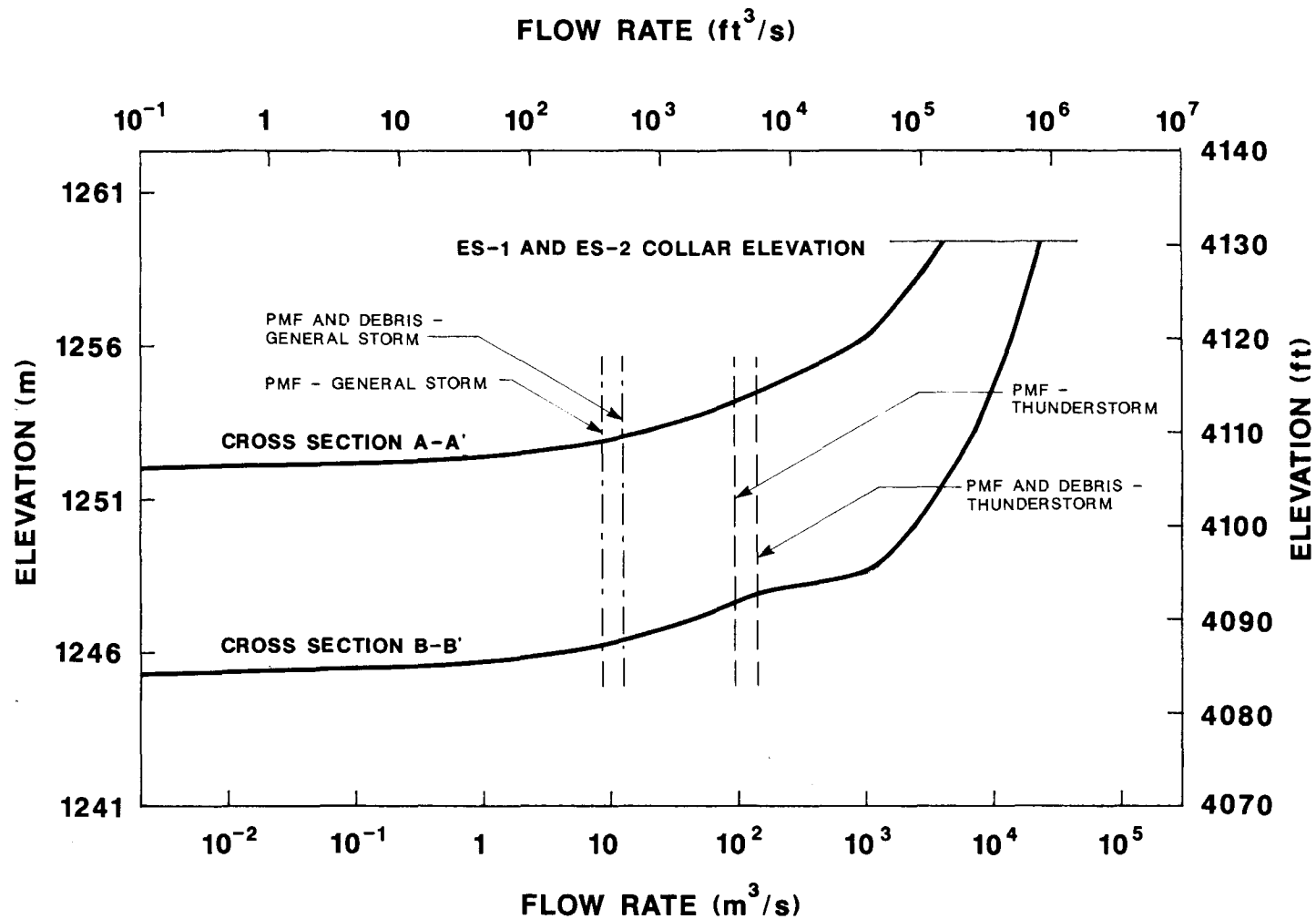


Figure 3-6. Flow Rate as a Function of Elevation for the Exploratory Shaft Locations (Locations of Cross Sections A-A' and B-B' are shown on Figure 3-2.)

Table 3-1. Comparative Peak Discharges from Floods in the Yucca Mountain Area

Wash	Drainage Area (mi ²)	Peak Flood Discharge (cfs)
Fortymile	312	540,000 ^(a)
Busted Butte	6.6	44,000 ^(a)
Drill Hole	15.4	86,000 ^(a)
Yucca	16.6	92,000 ^(a)
Coyote	0.2	3,350 ^(b)
Coyote, discharge to reach Exploratory Shaft-1 collar	0.2	~150,000 ^(c)
Coyote, discharge to reach Exploratory Shaft-2 collar	0.2	~820,000 ^(d)

(a) From Squires and Young (1984) for the regional maximum flood.

(b) From Bullard (1986) for thunderstorm probable maximum flood.

(c) Computed peak discharge to reach Exploratory Shaft 1 collar (~45 times PMF discharge).

(d) Computed peak discharge to reach Exploratory Shaft 2 collar (~240 times PMF discharge).

Following are the sequential steps used to compute the water depth over the ES pad.

- o Outline the drainage boundary tributary to the ES pad.
- o Determine the geometric characteristics of the watershed such as length of the longest water course, the length of the water course from the centroid, and the overall slope of the drainage area.*
- o Determine the lag time.

*This step assumes that limited restoration of the ES pad is performed.

- o Generate the unit hydrograph using the dimensionless graph presented in Plate 18 contained in Bullard (1986).
- o Develop the hydrograph for the drainage area tributary to the ES pad by using the unit hydrograph and the runoff curves for a thunderstorm and a general storm.
- o Calculate the water depth upstream from the ES pad using the hydrograph developed in the previous step and a modified version of the Manning equation.

Some of the details of the specific steps are discussed below.

The drainage area tributary to the ES pad is illustrated in Figure 3-7. The lag time used to compute the unit hydrograph is defined as

$$\text{lag time} = C \left[\frac{L \cdot L_{ca}}{\sqrt{S}} \right]^{0.33}, \quad (3-1)$$

where

- C = constant (0.5 for thunderstorms and 0.6 for general storms),
- L = length of the longest water course (miles),
- L_{ca} = longest channel length from the point of collection to a point opposite the area centroid (miles), and
- S = slope of the longest channel (ft/mile).

Knowing the lag time and using the dimensionless graph (Bullard, 1986, Plate 18), the unit hydrograph is developed. The unit hydrograph is then used with the runoff curve presented by Bullard (Tables 11 and 26) to compute the hydrograph for the watershed upgrade from the ES pad. Because the hydrograph is a graph of the flow rate versus time, it is possible to compute the depth of flow using this result and a modification of the Manning equation written in terms of the depth of water on the slope upgrade from the pad. This modification of the Manning equation is discussed below.

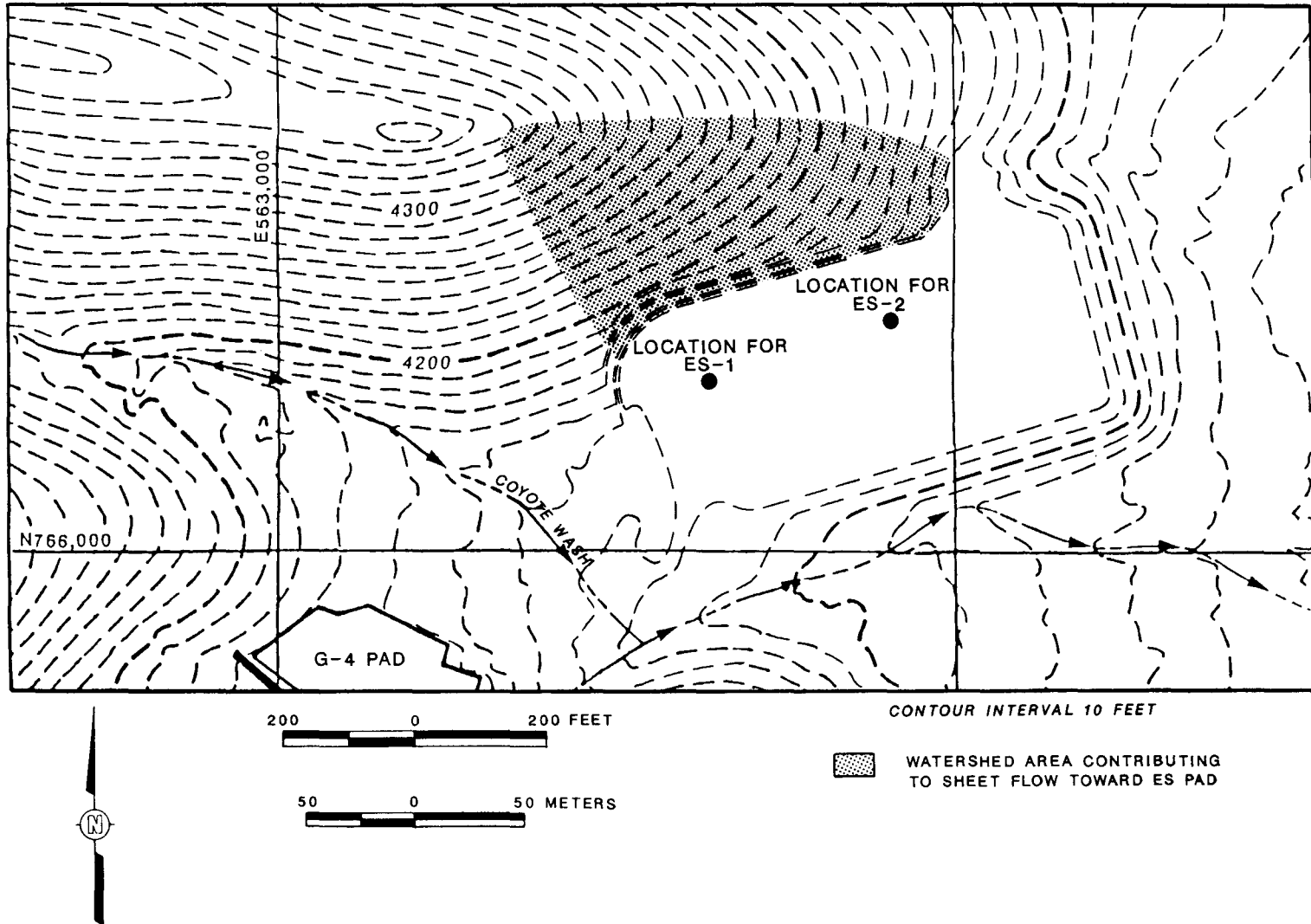


Figure 3-7. Watershed Above the Exploratory Shaft Pad

The Manning equation is given by Trefethen (1959, p. 422) as

$$V = \frac{1.49}{n} R^{2/3} S^{1/2}, \quad (3-2)$$

where

V = velocity of water flow on the slope,

n = roughness coefficient,

R = hydraulic radius defined as the area of flow (A) divided by the wetted perimeter (P),

P = wetted perimeter defined as the width of the channel flow plus twice the depth of flow, and

S = hydraulic slope.

Because $A = b \cdot d$ (b = width of channel flow and d = depth of channel flow) and $P = b$ (because the depth of flow is small in comparison to b), the value of $R = (b \cdot d)/b$ or d . Substituting these values in the following formula describing the flow rate, Q , from the hydrograph analysis

$$Q = A \cdot V \quad (3-3)$$

results in the following formula

$$d = \left(\frac{Q \cdot n}{1.49 S^{1/2} \cdot b} \right)^{3/5}. \quad (3-4)$$

The results obtained after applying the approach defined above are presented in Figure 3-8. For the thunderstorm conditions, the peak height over the ES pad is slightly >3 cm. Because the intensity and amount of rainfall is much less for the general storm, the height of water over the ES pad is much lower for the general storm conditions than for the thunderstorm conditions. The significance of these results on fracture flow into the ESs will be discussed in Section 3.2 of this report.

3.1.5 Erosion Potential at the Exploratory Shaft Locations

The ESs will be collared in the Tiva Canyon Member that caps most of Yucca Mountain. The Tiva Canyon Member is predominantly a densely welded,

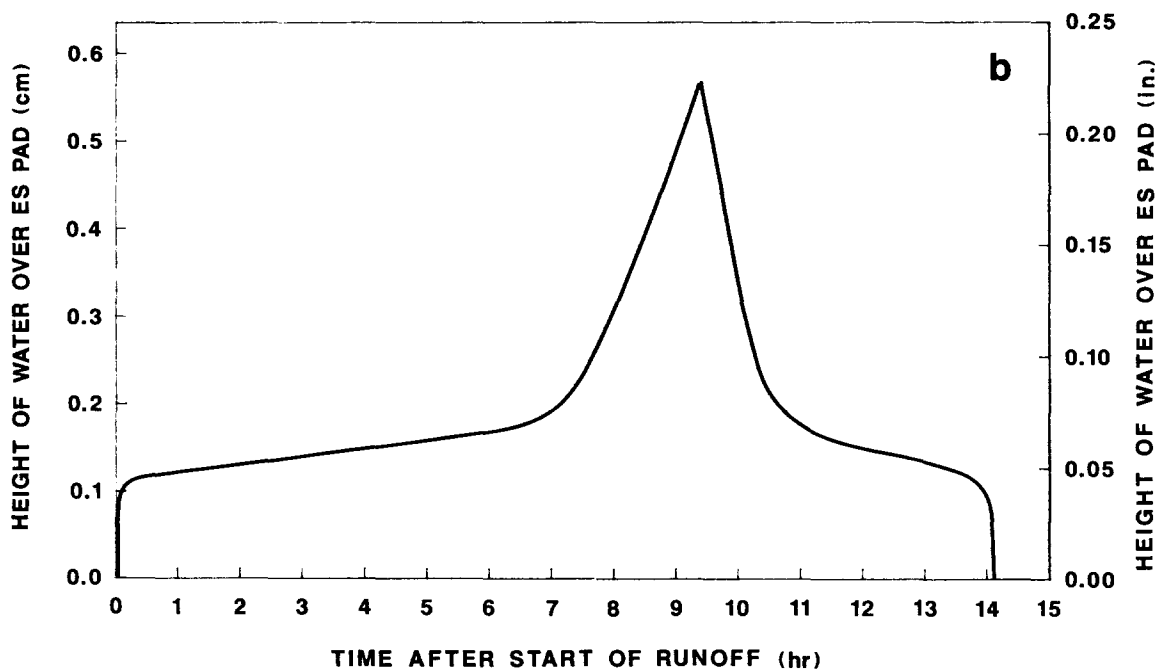
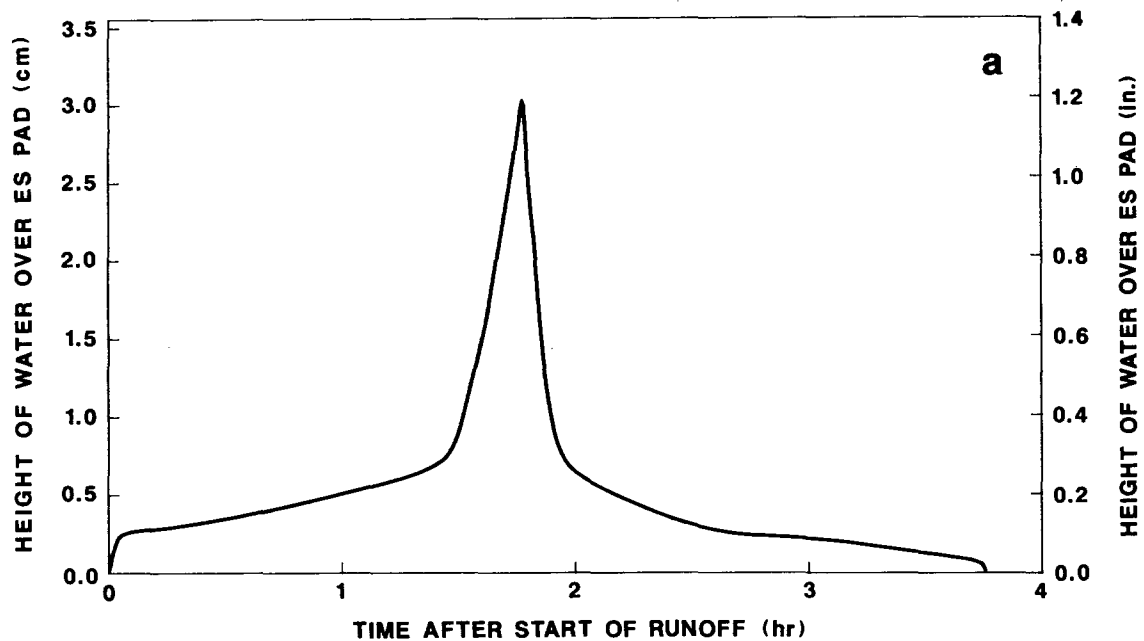


Figure 3-8. Height of Water over the Exploratory Shaft Pad During Sheet Flow Conditions Resulting from (a) a Thunderstorm and (b) a General Storm

highly fractured tuff. The exposed portion of the Tiva Canyon Member provides effective protection from rapid erosion. As indicated in the SCP (Section 1.1.3.3.2), the drainage feature characteristics, such as the broad, shallow, and widely spaced nature of the dip-slope drainage lines and the smooth and little-dissected nature of the upper slopes beneath the caprock-protected surfaces (DOE, 1988, p. 1-32), suggest the erosional stability of Yucca Mountain.

Average erosional rates for basalt-capped erosion surfaces are given in Table 1-2 of the SCP (DOE, 1988, p. 1-31). These erosion rates vary from 0.8 to 4.7 cm/1,000 years. If we applied these erosion rates to the upper portion of the Tiva Canyon Member, which outcrops in the area of the ES, a total erosion of <0.5 m would occur over 10,000 years. We feel that the application of these erosion rates is reasonable and appropriate because of the geomorphic form (discussed above) indicating the erosional stability of the Yucca Mountain area. Based on (1) the low erosion rate of <0.5 m/10,000 years, (2) the horizontal separation of the ES from the PMF channel (approximately 90 m; Figures 3-1 and 3-2), and (3) the minimum distance of 5 m from the surface elevation of the ES and the highest flood surface computed for a PMF, it is not likely that erosion will significantly impact the geologic repository.

3.2 Water Flow into the Exploratory Shafts Resulting from Fracture Flow

Flow through a near-surface, fractured media in the unsaturated zone is analyzed for water entry into the ES. Three scenarios are considered using a nonsteady-state numerical model of fracture flow: the rainfall rate, sheet flow, and channel flow scenarios. Model assumptions are discussed, and a range of input conditions are selected. Results for all scenarios are presented for both the general storm PMF and the thunderstorm PMF. These results are placed in context through a consideration of the drainage and storage capacities in the ESs followed by a discussion of results.

3.2.1 Description of Scenarios

The scenarios analyzed in this section consider water flow from a surface location, through the fractured Tiva Canyon Member, and into the

ES. Three different scenarios are considered. In the rainfall rate scenario, the flow of water into the fractures is controlled by the rate of the rainfall. Rain falling in excess of the fracture networks' ability to absorb water is assumed to drain off the ES pad. This scenario implies that no restoration of the ES pad occurs and that the engineered drainage features around the ES pad will function to maintain drainage. In the sheet flow scenario, sheet flow over the pad area is assumed to occur. This scenario implies that no restoration of the ES pad occurs and the amount of water entering the fracture network is limited only by the fracture networks' ability to absorb that water. In the channel flow scenario, channel flow is assumed to occur in Coyote Wash. This scenario is different from the second scenario because the flow channel will be significantly deeper than the sheet flow, and the water will not flow over the ES pad.

For each of the scenarios considered above, a variety of conditions are evaluated. First, for each scenario, two different PMFs are considered: the general storm PMF and the thunderstorm PMF. Further, for each storm type, three rock conditions are evaluated to account for the uncertainty in rock saturation and porosity. The first rock condition corresponds to the expected saturation and porosity of the Tiva Canyon Member. The second rock condition corresponds to an extreme of initial saturation and porosity, which leads to maximum matrix absorption and hence minimum fracture flow. The third rock condition corresponds to an extreme of initial saturation and porosity, which leads to minimum matrix absorption and maximum fracture flow.

An important characteristic of unsaturated flow is the dominant effect of capillary forces, which tends to confine flows to smaller pores while larger pores and fractures remain empty. Hence, water moving within the matrix, is expected to be constrained to remain in the matrix by naturally occurring capillary forces. Consequently, flow from the matrix to the shaft is not possible unless localized saturated conditions exist or the shaft backfill is constructed so that its pores are smaller than the pores of the surrounding rock. The existence of saturated rock above the water table (perched water) and below the surface is not considered in these scenarios, and will be evaluated later if site characterization gives any evidence of water perching. Further, shaft backfill will be designed

giving due consideration to the advantages offered by a capillary barrier. Based on the occurrence of capillary barriers in unsaturated rock, a scenario that considers water entry to the ESs by way of near-surface fractures is appropriate and reasonable.

3.2.2 Model Description

Flow of water through the near-surface, fracture network is modeled as shown in Figure 3-9. The fracture network is conservatively assumed to consist of many fractures that provide a direct connection between the surface and the ES. One of these fractures is shown in Figure 3-9. Because fractures in a real fracture network probably would not run directly from the surface to the ES, this assumption is conservative.

Water movement within a single fracture is depicted in Figure 3-10. Flow into the fracture will be governed by either

$$F_i(1) = \frac{b^3 \rho g}{12 \mu} \left(\sin \alpha + \frac{H}{z_{\max}} \right) \quad (3-5)$$

for those conditions where a fluid head of height, H, exists over the ground surface, or $F_i(1)$ is given by total precipitation reaching the ground as a function of time during a storm. In Equation 3-5,

- $F_i(1)$ = volumetric flow rate entering the first element per unit fracture width,
- b = fracture aperture,
- ρ = water density,
- g = acceleration of gravity,
- μ = water viscosity,
- α = dip angle,
- H = water height above ground level, and
- z_{\max} = total distance along a fracture having flowing water.

Equation 3-5 describes laminar flow between parallel plates under both gravitational and pressure heads. The pressure head is assumed to vary linearly over the flowing water column as discussed in Section 3.2.4.

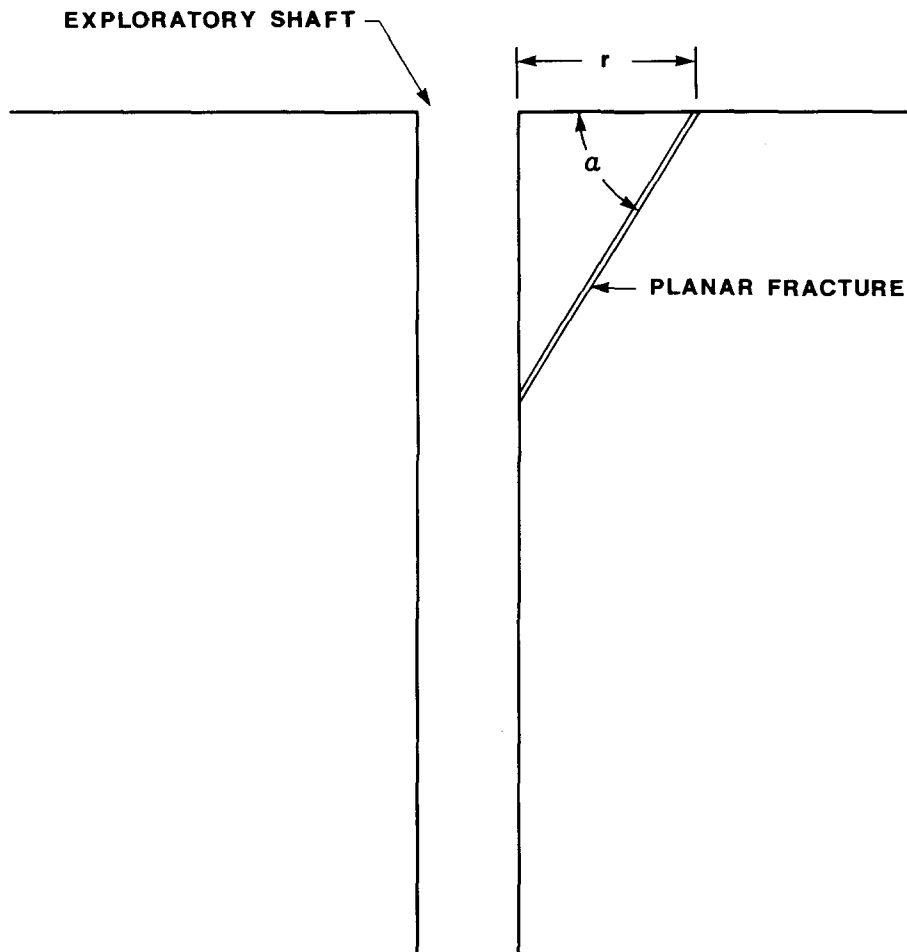


Figure 3-9. Schematic of Near-Surface Fracture Flow

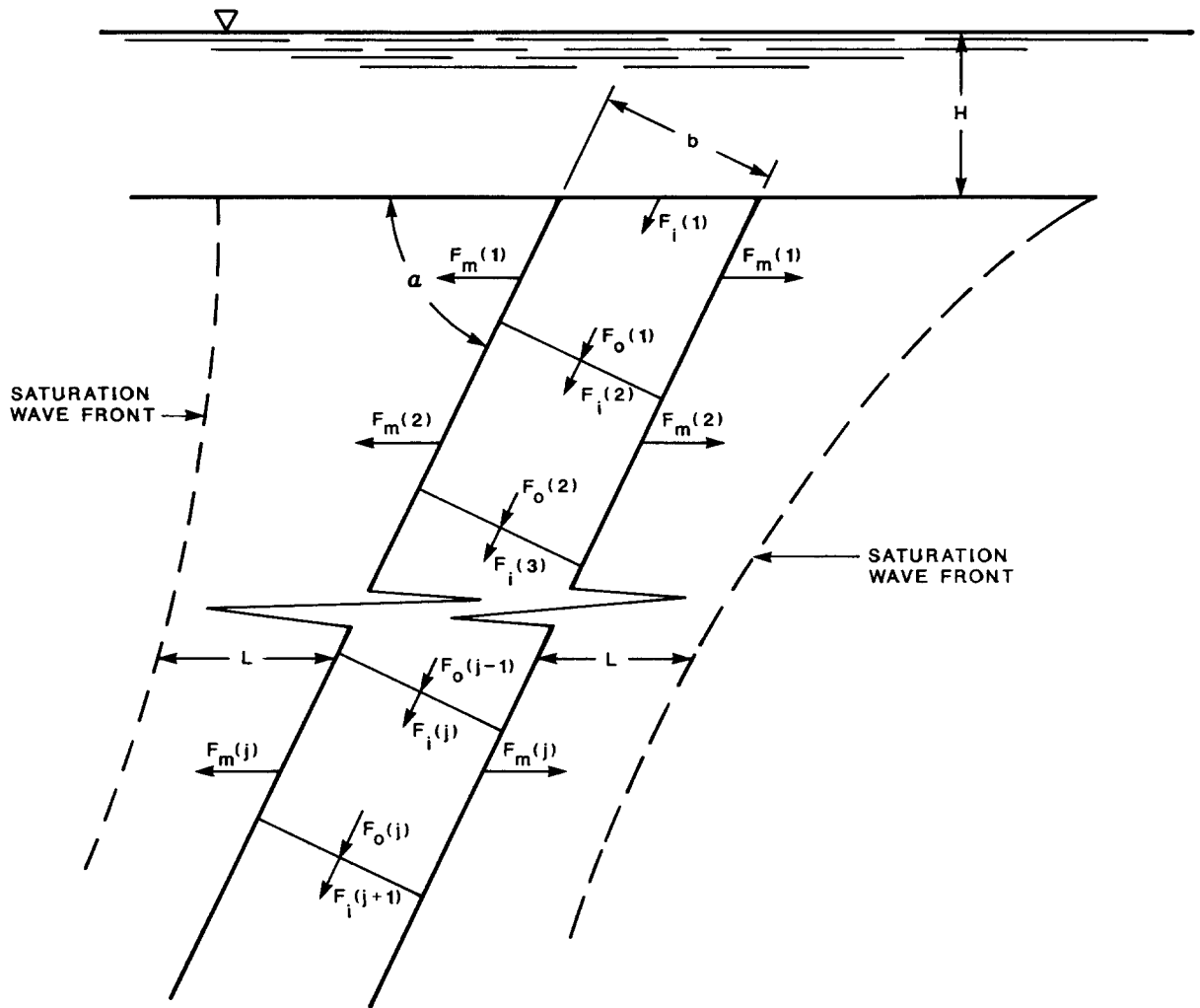


Figure 3-10. Schematic of Flow in a Single Fracture

Within the fracture, elements have been constructed of length, Δz , so that at any time, t , a mass balance for the j th element is

$$F_o(j) = F_i(j) - F_m(j) \quad , \quad (3-6)$$

where

$F_i(j)$ = volumetric flow rate per unit fracture width entering the j th element,

$F_o(j)$ = volumetric flow rate per unit fracture width leaving the j th element, and

$F_m(j)$ = volumetric flow rate per unit fracture width entering the matrix surrounding the j th element.

Further, it is recognized that

$$F_i(j + 1) = F_o(j) \quad (3-7)$$

so that a recursive calculation may be performed to determine the flow profile for the complete fracture.

Flow into the matrix is determined by an application of Darcy's law where flow is modeled as an advancing saturation wave. In front of this wave, the undisturbed matrix saturation is assumed to exist, while behind the wave, the porous media is assumed to be completely saturated. This model of matrix imbibition is similar to that of Green and Ampt (Hillel, 1971, p. 140). Hence, flow into the matrix is given by

$$F_m(j) = \frac{2 \Delta z k(p_f - p_m)}{\mu L} \quad , \quad (3-8)$$

where

k = saturated matrix permeability;

p_f = water pressure in the fracture at any element, j ;

p_m = water pressure in the matrix in front of the saturation wave front;

Δz = element length; and

L = distance from fracture face to saturation wave front within the matrix.

In Equation 3-8 the water pressure in the fracture, p_f , is given by

$$p_f = H\rho g \frac{z_{\max} - z}{z_{\max}}, \quad (3-9)$$

where

z = distance along a fracture to any element, j ,

and other parameters are as before. The matrix water pressure, p_m , is evaluated using the Van Genuchten parameters for the Tiva Canyon unit presented in Klavetter and Peters (1987, p. B-2), that is,

$$p_m = \frac{\left[\left(\frac{1 - S_r}{S - S_r} \right)^{1/\gamma} - 1 \right]^{1/\beta}}{\alpha} \rho g, \quad (3-10)$$

where

α = curve fit parameter, 0.0231 m^{-1} ;

β = curve fit parameter, 1.693;

$\gamma = 1 - 1/\beta$,

S_r = residual saturation, 0.0535; and

S = saturation.

Equations 3-5 through 3-10 may now be solved numerically to yield the total flow in a fracture, V , as a function of length along the fracture, z , the dip angle, α , and time, t .

The total amount of flow that enters either one of the shafts may then be determined by summing the flow through all fractures that intercept the shaft. This total is expressed as

$$V_{\text{Total}}(t) = \sum_{i=1}^{\infty} \sum_{j=1}^9 A V(\alpha_j, t, \frac{r_i}{\cos \alpha_j}) F(\alpha_j) \sin \alpha_j \Delta r, \quad (3-11)$$

where

$V_{\text{Total}}(t)$ = total volume of water entering a shaft as a function of time;

V = total volume of water in a fracture of dip angle, α_j , at time, t , passing a point that is a distance, $r_i/\cos \alpha_j$, from the surface;
 F = fracture frequency as a function of dip angle (SNL, 1987, Appendix O);
 A = width of the fracture, which corresponds to the ES diameter plus its associated MPZ;
 r_i = distance from the shaft to an arbitrary surface location;
 Δr = radial distance increment between r_i and r_{i+1} ; and
 α_j = dip angles where $\alpha_1 = 5^\circ$, $\alpha_2 = 15^\circ$, ..., $\alpha_9 = 85^\circ$.

3.2.3 Input Parameters

The evaluation of inflow into the ES was carried out for the three different scenarios. Precipitation data for the PMF events were obtained from Bullard (1986). The height of water in Coyote Wash (resulting from these PMF events) as a function of time is obtained from Section 3.1.3 of this report.

Because the total amount of matrix imbibition strongly depends on the initial saturation state as well as the porosity, three cases were run for each of the flooding events. These cases correspond to the average and extreme amounts of imbibition by the rock matrix. Based on data from the Reference Information Base, the saturation, S , of Tiva Canyon is expected to be $67 \pm 23\%$, while the porosity, ϵ , is expected to be $11 \pm 4\%$. Hence, the three cases selected were

for average imbibition, $S = 67\%$ and $\epsilon = 11\%$;

for maximum imbibition, $S = 44\%$ and $\epsilon = 15\%$; and

for minimum imbibition and maximum water entering the shafts, $S = 90\%$ and $\epsilon = 7\%$.

Further, the saturated matrix hydraulic conductivity of the Tiva Canyon Member was selected to be 0.1 mm/yr , and the fracture aperture in the densely welded Tiva Canyon was $89 \mu\text{m}$.

3.2.4 Assumptions Used in the Model

- o The real fracture network is approximated by a series of planar fractures that provide direct connection between the surface and the ES. This assumption is conservative because the tortuosity of a real fracture network will retard the extent of fracture flow.
- o All near-surface fractures are assumed to be open. Because fracture filling is routinely observed, the modeled fractures are likely to conservatively pass more water than real ones that are plugged or partially plugged.
- o No alluvial resistance is assumed to exist in the ES pad area or in Coyote Wash. Because alluvium provides a resistance to flow, a consideration of the absence of this resistance conservatively increases the fluid driving force in the fracture network.
- o Flow in the fracture network is computed assuming a linear pressure gradient across the column of fluid flowing in the fracture. This assumption has been verified in separate calculations performed by Martinez (1988, Figure 18).
- o The saturation wave front (Figure 3-2) is assumed to extend no more than half the distance between fractures. This assumption limits the amount of water that may be absorbed by the matrix. Therefore, if the matrix between fractures becomes fully saturated, water can no longer flow into the matrix, thus maximizing flow in the fracture.
- o The effect of gravity on the determination of flow into the matrix is assumed to be negligibly small. This is true because capillary forces in the densely welded tuff are much greater than gravitational forces.
- o Matrix imbibition is assumed to be modeled by the progression of a saturation wave front. This assumption is similar to that used by Green and Ampt (Hillel, 1971, p. 140). The Green and Ampt approach

was developed in 1911 and has been used for many years to successfully predict soil infiltration. The fundamental basis for the assumption lies in the fact that the movement of fluid through saturated porous media is more rapid than the movement of fluid through unsaturated media. An alternate computation of matrix imbibition was performed by Martinez (1988). His method uses a diffusion equation that gives results equivalent to the method selected here.

3.2.5 Model Results

Results for each of the three scenarios described in Section 3.2.1 are presented in this section. It is observed that once water enters the fracture network, the surrounding unsaturated matrix would remove water from the fractures and limit fracture flow. While the greatest extent of fracture flow tends to occur in the predominantly vertical fractures, these fractures are parallel to the ES and hence will not contribute to the total flow into the shafts. Further, the gravitational driving force is attenuated in the nonvertical fractures so that these fractures do not propagate water as far as the vertical fractures. Fractures located beyond a maximum distance, referred to as the zone of influence, will not contribute to the total flow into the shaft. For all of the scenarios, zones of influence are presented in tabular form. For those cases where water does flow into the shafts, the total amount of water entering both shafts from the fracture network in Tiva Canyon is also presented. The effect of the MPZ is accounted for in these calculations by assuming that all of the water in a fracture segment, whose width is equal to the total diameter of both the shaft and its MPZ, has the potential to drain into the shaft. Results are presented for three cases. Case 1 corresponds to the expected amount of imbibition and hence to expected zones of influence and water inflow. Case 2 corresponds to minimum zones of influence and water inflow, while Case 3 corresponds to maximum zones of influence and water inflow as defined in Section 3.2.3.

Flow into Fractures Controlled by Rainfall Rate

In the rainfall rate scenario, either the thunderstorm or the general storm PMF was assumed to occur in the vicinity of the ES pad. No alluvial

resistance was assumed to be present so that precipitation was modeled as passing directly to the fracture network. When the rainfall rate exceeded the ability of the fracture to accept water, the surplus water was assumed to run off.

For this scenario, the zones of influence for a general storm PMF and a thunderstorm PMF are given in Table 3-2, where while the zone of influence can be between 1.9 and 18.3 m, the more expected zone of influence (Case 1) will be approximately 4.5 m for either type of PMF storm.

Table 3-2. Zone of Influence Based on the Rate of Rainfall

	Case 1	Case 2	Case 3
Probable Maximum Flood Storm Type	S = 67% ε = 11% (m)	S = 44% ε = 15% (m)	S = 90% ε = 7% (m)
General Storm (14 hr)	4.6	1.9	18.3
Thunderstorm (6 hr)	4.5	1.9	17.5

The total amount of water entering both shafts from the fracture network in the Tiva Canyon is presented in Table 3-3. In this table it is seen that the expected amount of water entering the shaft from a PMF event (Case 1) will be 1.33 m³ for a general storm PMF (14 hours) and 1.02 m³ for a thunderstorm PMF (6 hours). Depending on the initial matrix saturation and porosity, the total water inflow from a general storm PMF may vary between 0.54 and 5.32 m³ while the water inflow from a thunderstorm PMF may vary between 0.43 and 4.01 m³.

Sheet Flow over the ES Pad

In this calculation, the ES pad was assumed to be covered by a sheet flow with a zero height for the entire PMF storm period. The impact of the zero height assumption is negligible and is discussed in Section 3.2.7.

Table 3-3. Total Volume of Water Entering Both Exploratory Shafts Based on the Rate of Rainfall

	Case 1	Case 2	Case 3
Probable Maximum Flood Storm Type	S = 67% ε = 11% (m ³)	S = 44% ε = 15% (m ³)	S = 90% ε = 7% (m ³)
General Storm (14 hr)	1.33	0.54	5.32
Thunderstorm (6 hr)	1.02	0.43	4.01

Hence, during a general storm PMF, the pad was under sheet flow conditions for 14 hours. Similarly during a thunderstorm PMF, the pad was under sheet flow conditions for 6 hours. Further, it was conservatively assumed that the alluvium and fill on the pad offered no resistance to flow. Future calculations will account for the resistance of the alluvium. Under these conditions the zones of influence are computed for each of the three cases and are presented in Table 3-4. The maximum zone of influence for a general storm PMF is expected to be 10.7 m and may vary between 4.5 and 41.8 m. The zone of influence for a thunderstorm PMF is expected to be 7.1 m and may vary between 3.0 and 27.5 m.

The total water entry into both shafts from the fracture network, including the effect of the MPZ, is given in Table 3-5. The total water entry into the shaft for a general storm PMF under the assumption of continuous sheet flow over a pad is 12.2 m³ and may vary between 5.27 and 47.4 m³ for low and high fracture penetration cases. For the thunderstorm PMF, the water entry is calculated to be 3.45 m³ and may vary between 1.49 and 13.3 m³.

Channel Flow Associated with a Probable Maximum Flood

Another source of potential water input to the ES is the PMF flood channel, which is expected to run in Coyote Wash during the storm. A description of this flood channel is found in Section 3.1.2 of this report.

Table 3-4. Zone of Influence for Sheet Flow over a Bare Fracture Network

	Case 1	Case 2	Case 3
Probable Maximum Flood Storm Type	S = 67% ε = 11% (m)	S = 44% ε = 15% (m)	S = 90% ε = 7% (m)
General Storm (14 hr)	10.7	4.5	41.8
Thunderstorm (6 hr)	7.1	3.0	27.5

Table 3-5. Total Volume of Water Entering Both Exploratory Shafts for Sheet Flow over a Bare Fracture Network

	Case 1	Case 2	Case 3
Probable Maximum Flood Storm Type	S = 67% ε = 11% (m ³)	S = 44% ε = 15% (m ³)	S = 90% ε = 7% (m ³)
General Storm (14 hr)	12.2	5.27	47.4
Thunderstorm (6 hr)	3.45	1.49	13.3

As determined from Figure 3-1, the closest this channel comes to the ES is 82 m. As shown in Figure 3-3, the flood channel will run for 4.3 hours in the thunderstorm case and for 14.7 hours in the general storm case. The zones of influence for water flow in Coyote Wash are presented in Table 3-6. The maximum zones of influence for water flow in fractures under Coyote Wash were determined to be 43.4 m for general storm PMF and 29.0 m for a thunderstorm PMF. Because the zone of influence for Coyote Wash does not extend to the ESs, water is not expected to enter the shaft from Coyote Wash as a consequence of the channel flow scenario.

Table 3-6. Zone of Influence for Channel Flow

	Case 1	Case 2	Case 3
Probable Maximum Flood Storm Type	S = 67% ε = 11% (m)	S = 44% ε = 15% (m)	S = 90% ε = 7% (m)
General Storm (14 hr)	11.5	5.0	43.4
Thunderstorm (6 hr)	7.8	3.5	29.0

3.2.6 Storage and Drainage Capacity of the Exploratory Shafts and Associated Facility

In designing the ESF, specific design features were included that contribute to containment and isolation of the radionuclides. These specific features included isolating the ESF as much as possible from the remainder of the underground facility by

- o limiting the number of interconnecting drifts between the ESF and the access drifts,
- o providing drift drainage within the ESF towards ES-1, and
- o controlling drainage around the ESF so that water outside the ESF is diverted to nonwaste emplacement drifts and thus is impeded from entering the ESF.

Incorporation of these design features provides a storage and drainage capacity in the ESF if waters enter the ESs. A discussion of the storage and drainage capacity of the ESF follows.

As discussed in the previous section, the maximum amount of water entering the ESs and associated MPZs is computed to be 0 to 50 m³ for a PMF. This volume was computed assuming direct entry of water into the fractures of the Tiva Canyon Member. This volume of water could easily be

stored and drained in the ES sumps as discussed below. If the ESF was backfilled with a crushed tuff having a porosity of 0.3, the storage capacity would be about 200 m³ in the shaft sumps. This volume is computed assuming a tail shaft 15 and 31 m long in ES-1 and ES-2, respectively. It is also important to note that the drifts in the ESF provide additional storage capacity and slope toward ES-1. The drainage pattern, illustrated in Figure 3-11, suggests that water entering ES-1 or ES-2 would first have to fill up the sumps of ES-1 and ES-2 as well as portions of the ESF drifts before water would exit the ESF into the connecting access drifts. The storage capacity of these ESF drifts is about 630 m³. If this total storage capacity were exceeded, the water entering the connecting access drifts would flow toward the low point of the repository near the emplacement exhaust shaft.

Using the Nasberg-Terletska analytical solution discussed in Appendix C and assuming a bulk rock hydraulic conductivity of 10⁻⁵ cm/s,* the potential drainage capacity from the sumps of both ESs, assuming the tail shaft is fully saturated, is 6,400 m³/year. Using the same bulk rock hydraulic conductivity, the potential drainage capacity through the ESF drift floor, corresponding to the storage capacity of the same portion of the ESF discussed above, is about 11,300 m³/year. If the mean value of the bulk rock hydraulic conductivity (1.2 x 10⁻³ cm/s) was used to compute the potential drainage capacity, the drainage capacity would be two orders of magnitude greater than the computed values above. Although these values are computed assuming Darcy flow under fully saturated flow, these calculations indicate that the ESF is sufficient to drain water entering from the shaft.

3.2.7 Discussion of Results

Because the shafts have been located a significant horizontal and vertical distance from Coyote Wash, the scenarios analyzed in this section predict no inflow from channel flow. Hence, the total volume of water to enter the shafts for any of the scenarios is relatively small, <50 m³.

*This value of 10⁻⁵ cm/s is at the lower range for the densely welded Topopah Spring Member as discussed in Fernandez et al. (1987).

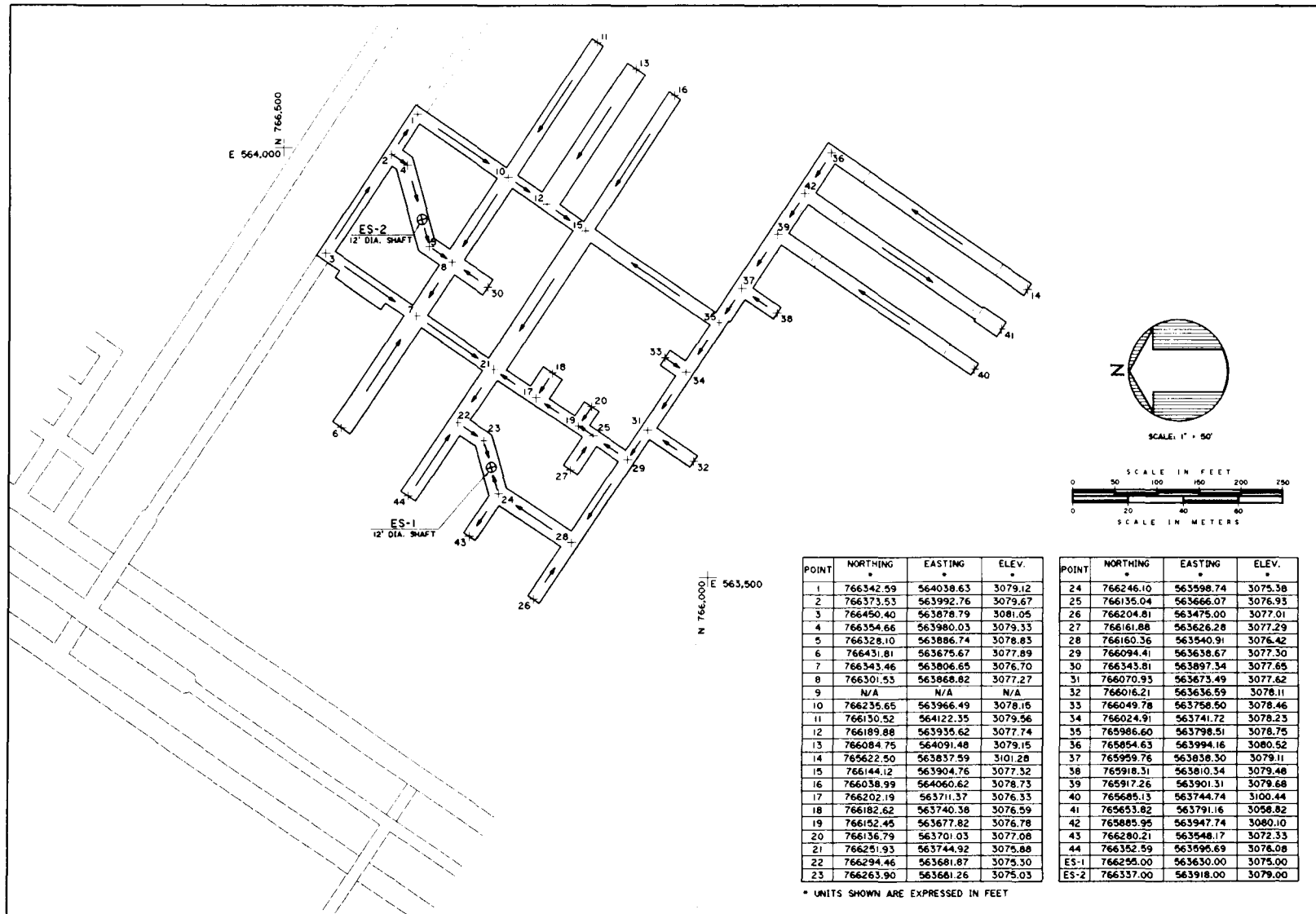


Figure 3-11. Drainage Direction for the Exploratory Shaft Facility

This water is then assumed to migrate to the bases of the shafts where it may be stored and drained. From the discussion in Section 3.2.6, the total storage capacity of the shaft sumps and ESF drifts is 830 m^3 , while the total drainage capacity of the shaft sumps and ESF drift flows is $17,700 \text{ m}^3/\text{year}$. Because both the storage and the drainage capacity of the ESF is so much larger than the predicted maximum inflow, this water entry is likely to have no significant effect on repository performance. Further, the assumption that the shaft will act as a perfect conduit to transport water from the surface to the base of the shaft ignores the physical mechanism presented in the fracture flow scenario, i.e., matrix imbibition. As in the fracture flow scenarios, water passing through the MPZ and the shaft fill will also tend to be imbibed by the matrix thus tending to eliminate locally saturated flow. This factor will further reduce the rate and volume of water entering the shaft sump and ESF.

A discussion of the hydraulic zones of influence around both ESs and Coyote Wash illustrates that the primary source of water entering the shafts is likely to be water on the surface of the ES pad. In Figure 3-12 the hydraulic zones of influence for Cases 1, 2, and 3 of the rainfall rate scenario are presented along with the Case 3, or the maximum zone of influence around Coyote Wash, for a general storm PMF. The same information for the thunderstorm PMF using the rainfall rate scenario is presented in Figure 3-13. In both of these cases, it is observed that the hydraulic zones of influence are completely contained within the ES pad. Further, Coyote Wash is seen to be hydraulically isolated from the ESs.

For the case where sheet flow over the pad area occurs as a result of pad drainage failure, hydraulic zones of influence are presented for both the general storm PMF and the thunderstorm PMF in Figures 3-14 and 3-15. Once again the thunderstorm event leads to zones of influence that are completely contained within the ES pad. The general storm PMF has zones of influence that are mostly contained within the ES pad.

A consideration of the results obtained for both the sheet flow and the channel flow scenarios can be used to justify the zero height assumption used in the sheet flow scenario. A comparison of the average of the zones of influence for sheet flow (Table 3-4), which assume zero height of

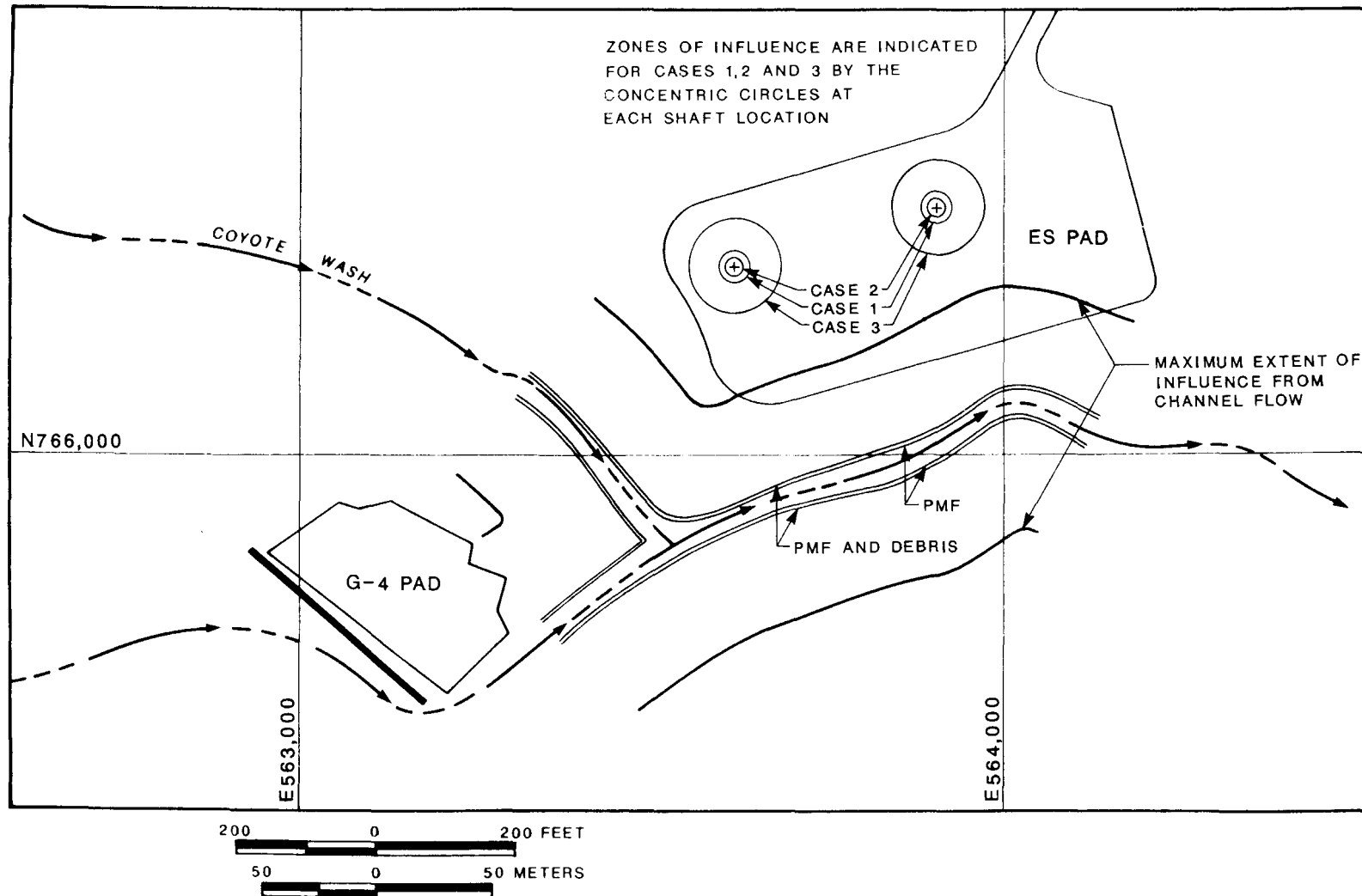


Figure 3-12. Zones of Influence for a General Storm Probable Maximum Flood Using the Rainfall Rate Scenario and the Maximum Zone of Influence, Case 3, for Channel Flow in Coyote Wash

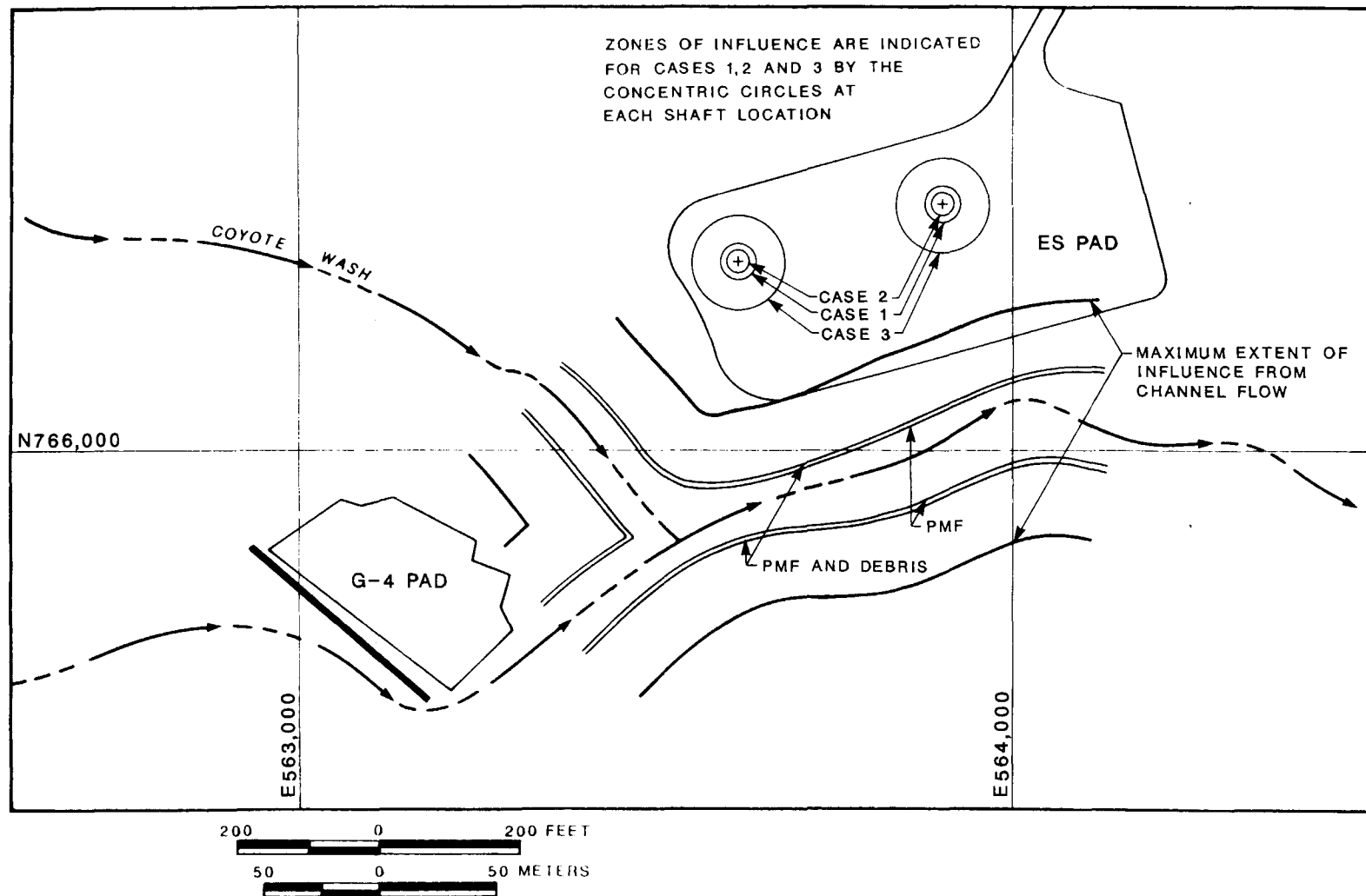


Figure 3-13. Zones of Influence for a Thunderstorm Probable Maximum Flood Using the Rainfall Rate Scenario and the Maximum Zone of Influence, Case 3, for Channel Flow in Coyote Wash

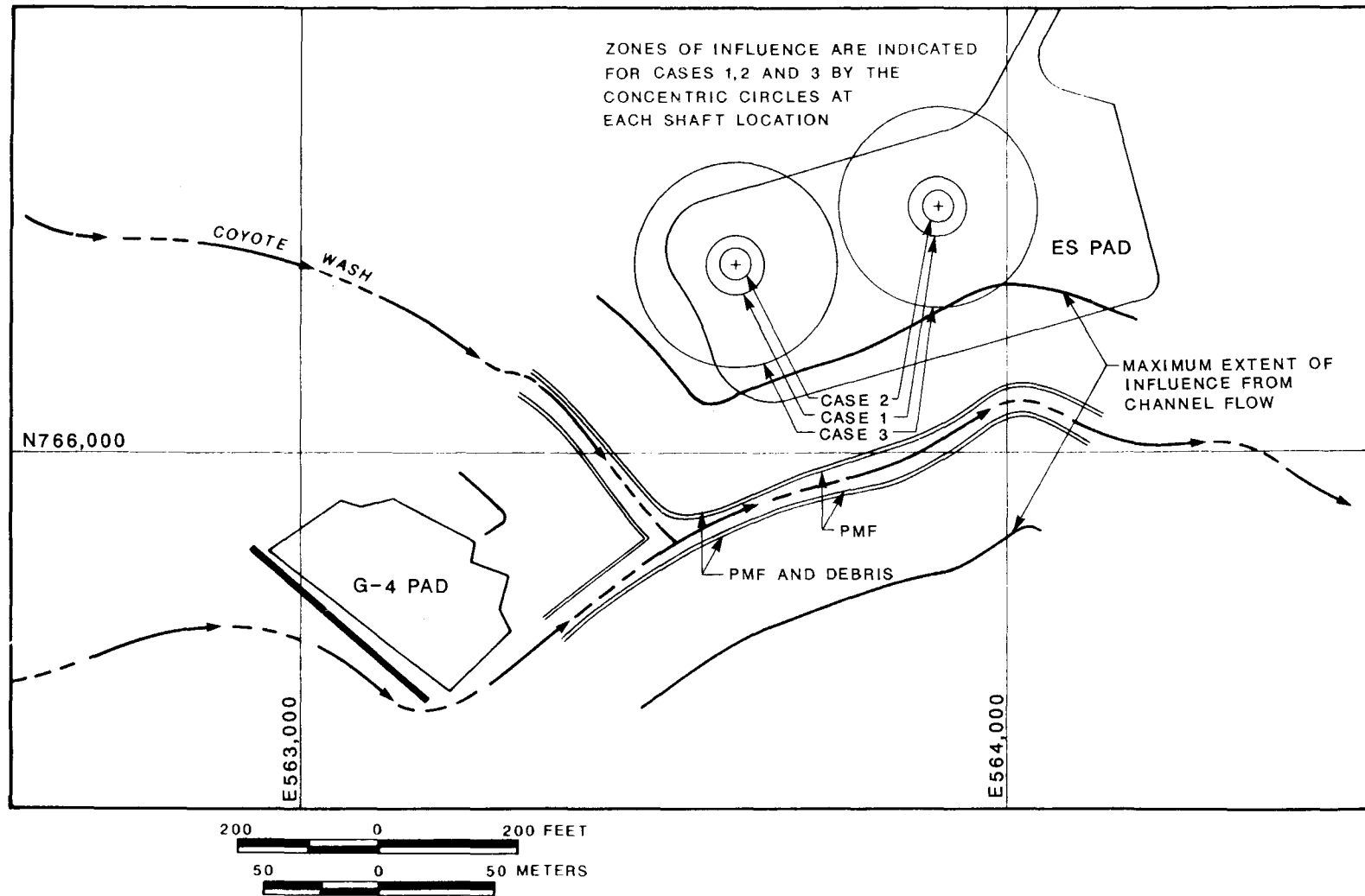


Figure 3-14. Zones of Influence for a General Storm Probable Maximum Flood Using the Sheet Flow Scenario and the Maximum Zone of Influence, Case 3, for Channel Flow in Coyote Wash

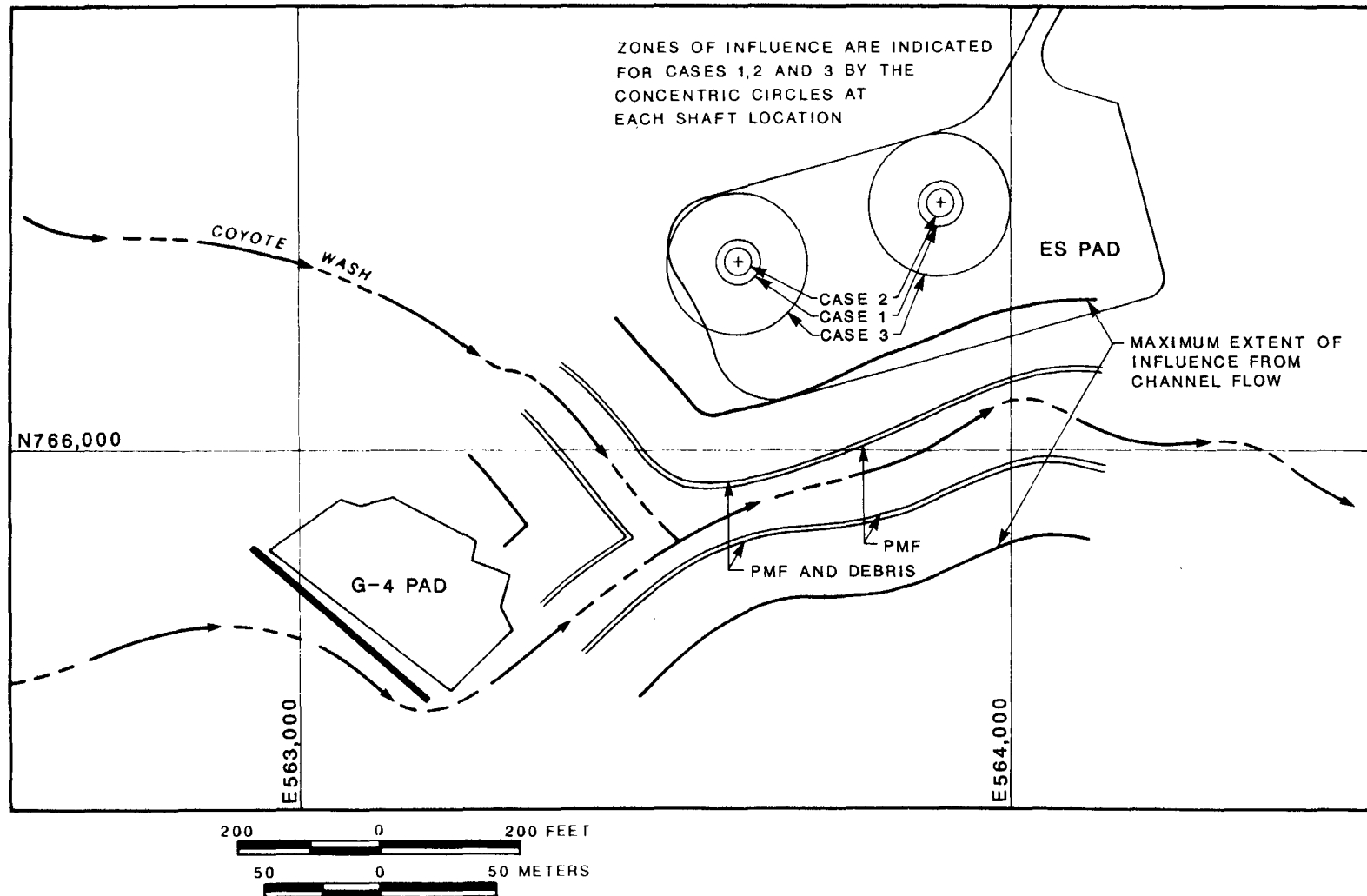


Figure 3-15. Zones of Influence for a Thunderstorm Probable Maximum Flood Using the Sheet Flow Scenario and the Maximum Zone of Influence, Case 3, for Channel Flow in Coyote Wash

water with the average of the zones of influence for channel flow (Table 3-6), shows that the channel flow average is approximately 10% larger. Further, the maximum depth of water in the channel is approximately two orders of magnitude greater than the maximum depth of water for sheet flow (2.5 m versus 3 cm). Because the difference between Table 3-4 and Table 3-6 is directly related to the depth of water in Coyote Wash, it is expected that the inaccuracy resulting from a zero depth would be much smaller than the differences noted between Tables 3-4 and 3-6. Hence, the zero depth assumption for the sheet flow scenario will lead to inaccuracies that are much smaller than 10%.

3.3 Scenario Describing Uniform Dispersion of Surface Water at Depth

An additional scenario of water flow into the ESs is discussed in this section. This scenario is selected to depict primarily fracture flow intercepting the shafts and associated MPZs anywhere below the surface. This scenario is believed to be less realistic than the scenario discussed in Section 3.2 because it is assumed (1) that the rock matrix is fully saturated so that rainfall is not imbibed into the rock matrix and fracture flow can occur over long distances and (2) that all of the rainfall infiltrates into the stratigraphic column with no surface runoff occurring. These assumptions are believed to lead to a conservative overprediction of the water that might enter a shaft.

This scenario involves intense rainfall over the drainage basin associated with the ESs. This rainfall is equivalent to the volume associated with a PMF (thunderstorm event). Following the rainfall, it is assumed that all of the water infiltrates into the ground surface either uniformly over the entire drainage area (Case 1) or over a more restricted area defined by the existing water courses (Case 2). These two cases are depicted on Figure 3-16. In Case 1 the area considered is upgrade from the ES locations. In Case 2 the area considered is upgrade and downgrade from the ES locations, acknowledging the fact that flow into the shafts can occur from surface locations downgrade from the surface location of the shaft. Superimposed on the drainage basin is a network of discrete areas or elements that define the zones where infiltration occurs. The amount of water entering each element is modeled as being proportional to its area

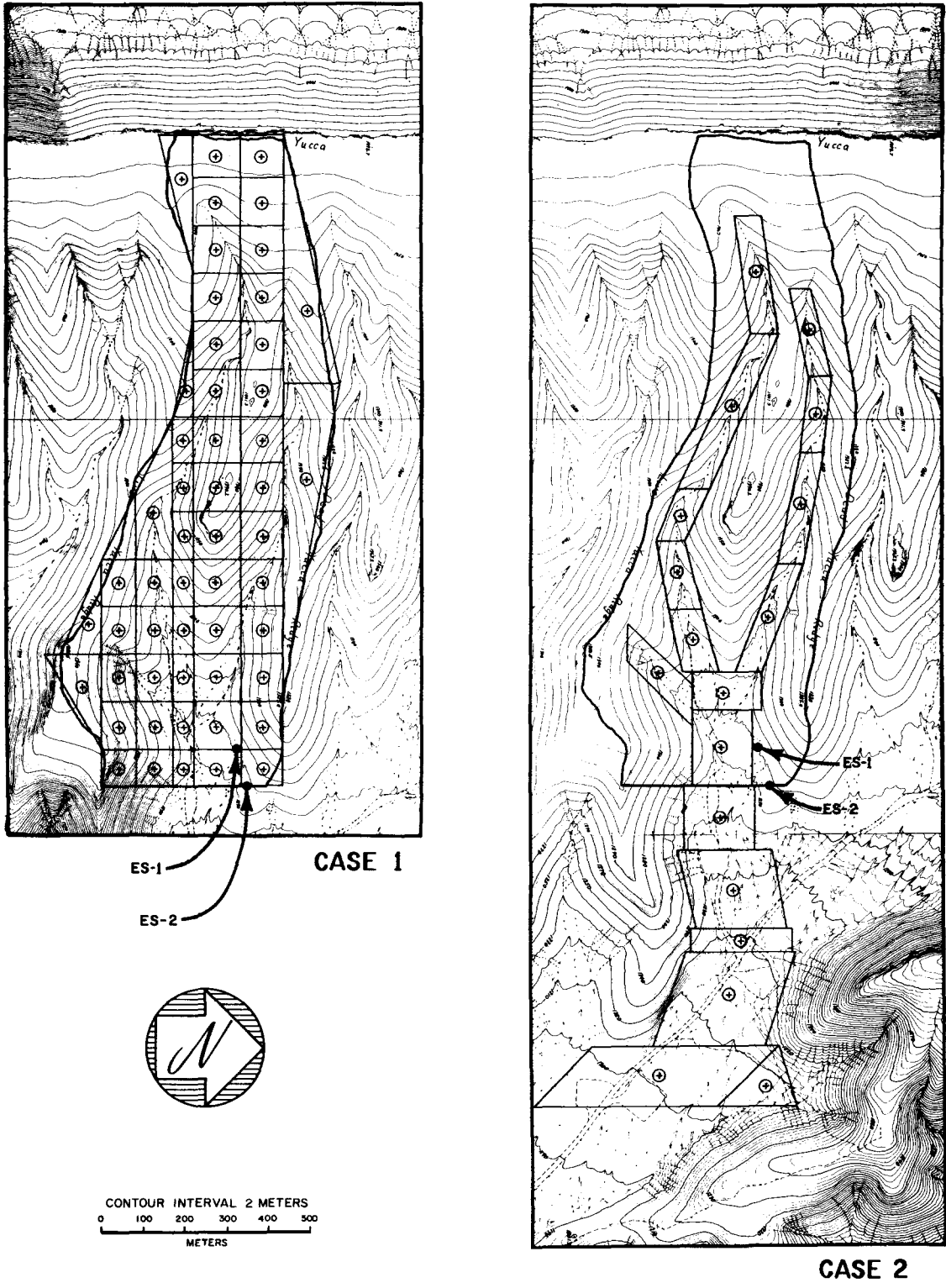


Figure 3-16. Topography, Drainage Basin Outline, and Grid Used in Developing the Uniform Dispersion Scenario

compared with the entire area into which infiltration is assumed to occur. In Case 1, infiltration occurs over the entire drainage basin. In Case 2, infiltration occurs only in the areas defined by the ephemeral stream locations.

In both cases it is assumed that all of the water from the rainfall is uniformly dispersed by the fractures in the stratigraphic column beneath each element. The portion of water that falls on each element and subsequently enters ES-1 and ES-2 is shown on Figure 3-17. The portion of water entering the shafts from each element is defined by

$$V_i = \frac{2\theta}{360^\circ} \frac{A_i}{A_{total}} V_{PMF} ,$$

where

V_i = volume of water entering the ESs from rainfall occurring over element "i,"

2θ = angle formed by the center point of each element and the assumed extent of the MPZ around each shaft (in degrees),

A_i = the area of an element "i,"

A_{total} = the total area of all the elements, and

V_{PMF} = volume associated with a PMF (13.9 in. of rainfall over the entire basin).

The total amount of water, V_{shafts} , entering both ES-1 and ES-2 from "n" elements would be

$$V_{shafts} = \sum_{i=1}^n V_i \text{ for ES-1} + \sum_{i=1}^n V_i \text{ for ES-2} .$$

The farther an element is away from an ES, the smaller will be the "2 θ " term and the lower will be the flow of water from an element to the shaft.

Using the formulas above, the total amount of water entering both ESs for the scenario is about 1,200 m³ for Case 1 and Case 2. This value is considered to be an upper bound for this scenario because it is assumed that all of the rainfall contributing to a PMF (thunderstorm condition), 13.9 in., falling over the entire basin, infiltrates down through the

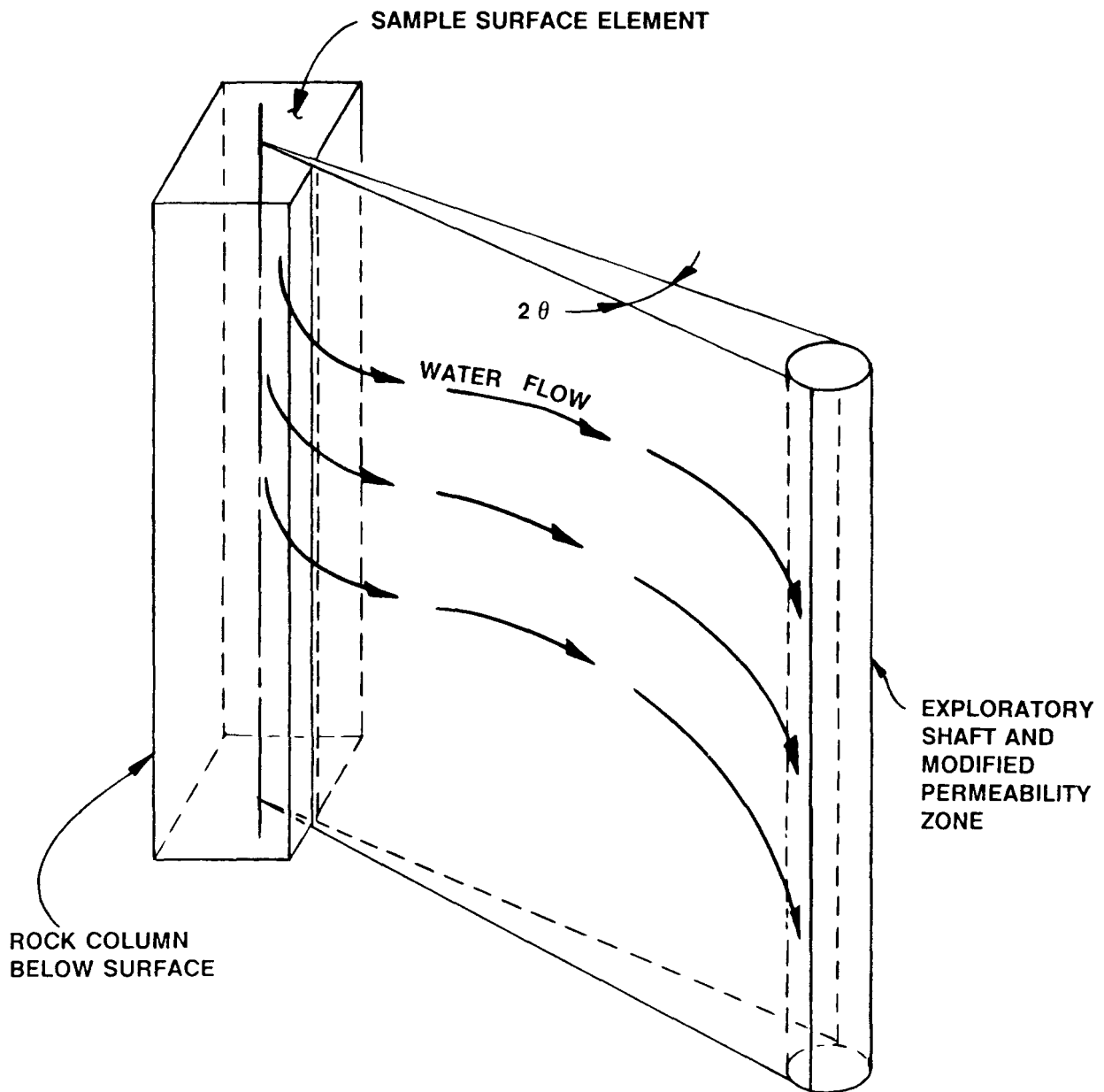


Figure 3-17. Illustration of the Water Flow That Enters the Exploratory Shaft and Modified Permeability Zone from a Single Surface Element

stratigraphic units and flows laterally to the ESs. In reality, all of the 13.9 in. is not likely to infiltrate downward into the stratigraphic column. The majority of rainfall would exit the drainage basin as a flood once the ground surface saturates to some threshold amount. If runoff occurs after 2 in. of rainfall, the upper bound of retention indicated by Bullard (1986), approximately 85% would exit the drainage basin as runoff. Only a portion of the rainfall that saturates the soils would percolate through the stratigraphic column. It is therefore reasonable to assume only a fraction of the 13.9 in. of rainfall would percolate through the stratigraphic column and migrate laterally to the ESs. A more realistic volume of water entering both shafts would be an amount one to two orders of magnitude lower than the amount computed earlier. Therefore, a more realistic estimate of water entering the shafts during a PMF is approximately 10 to 100 m³. In fact, in Section 3.2, realistic volumes were computed to range from 0 to about 50 m³ for an extreme rainfall event.

3.4 Scenario Describing Fully Saturated Alluvial Flow at the Old Exploratory Shaft Locations

At the initiation of the work that led to this report, the locations of the ESs were different from those currently proposed. The original locations for ES-1 and ES-2 were to the west of the currently proposed locations. ES-1 was within the alluvial filled valley, and ES-2 was located out of the alluvium southwest of ES-1. The old and current locations for ES-1 and ES-2 are shown on Figure C-1 of Appendix C.

Because the upper portion of the shaft was collared in alluvium, a scenario was proposed, which depicted flow from a fully saturated alluvium into the ES. This scenario presented an upper-bound estimate of water flow into ES-1 assuming a broad range of input parameters. When the locations for ES-1 and ES-2 were moved out of the alluvium upslope from the flow channel, it was apparent that the scenario of flow from fully saturated alluvium to ES-1 was not appropriate. It is also unlikely that a "dam" large enough to retain the flood waters from a PMF could be created at the ES location. Nonetheless, this description and the results from this scenario are presented in Appendix C. Both water flow into the shaft and drainage from the sump have been included to show that even if extremely large and unlikely water flows into the shaft occurred, it is likely that

they could be drained effectively (assuming extensions of the sump as currently proposed) through the sumps of the ESs and the floor of the ESF.

3.5 Conclusions

The intent of this chapter is to evaluate whether the presence of shafts could significantly enhance radionuclide release as a result of water flow into the shaft and the MPZ. Our overall conclusion is that the presence of the ESs at their currently proposed locations does not enhance radionuclide release as a result of water entering them. It is expected that the volume of water anticipated to enter the shafts can easily be contained and drained within the ESF. Some specific conclusions reached from the analyses in this chapter, which support the overall conclusion, are given below.

- o Direct entry of water into the shaft is considered unlikely because the ESs are collared in bedrock and are laterally removed from the wash. Further, the collars of the ESs are >5 m higher than the computed PMF levels, and the peak flood discharges would have to be 45 and 240 times the computed peak discharges for the thunderstorm event to reach the collars of ES-1 and ES-2, respectively.
- o The most probable way for water entering the ESs would be from precipitation or sheet flow over the ES pad, and the amount is expected to be low, 0 to <50 m³/PMF event.
- o The height of flow does not significantly change the zone of influence and the flow of water into the shafts. This conclusion is reached by comparing the computed zone of influence when the height of water at the surface is assumed to be zero, as in the case for sheet flow (Table 3-4), and when the height of water in the flow channel is up to 2.5 m (Table 3-6). The maximum difference in the zone of influence between the comparable cases presented in these Tables is 1.6 m for Case 3.
- o Erosion at the ESs should not impact the performance of the repository by directing waters into the shafts because of the

anticipated low erosion rate for the Tiva Canyon Member, the lateral incision into bedrock required to reach the ESs, and the horizontal and vertical separation of the ESs from the PMF channel.

- o Water flow into the ESs from fractures during a PMF event is expected to be low, 0 to 50 m³. It is also anticipated that the volume can easily be contained and drained within the ESF.

- o Even if extremely large and unlikely volumes of water flow into the ESs, it is anticipated that the water could be drained effectively (assuming extension of the sumps as currently proposed) through the sumps of the ESs and the floor of the ESF.

4.0 POTENTIAL FOR ENHANCING RADIONUCLIDE RELEASE BY AIR MOVEMENT RESULTING FROM CONVECTIVE FORCES

For a repository located above the water table, it is possible that airborne radionuclides can be released in the air flowing out of the repository through the shafts or the host rock. In Fernandez et al. (1987, p. 3-22) a performance goal was established for airflow through the shafts and their MPZs for the total gaseous releases of C-14 and I-129 that could potentially occur. The performance goal established was that air flowing through the shafts and their MPZs should not exceed 25% of the total flow of air from the repository. This section evaluates the potential magnitude of airflow rates from the repository and compares the relative influence of the shafts, ramps, and host rock on the airflow. More specifically, the calculations examine the influence of the MPZ around the shafts and ramps and the degree to which flow can be limited by backfilling or sealing the shafts.

After emplacing waste containers, heat is gradually transferred by conduction from the waste containers to the surrounding rock. Achieving a maximum temperature in the rock, as assumed here, could take 2,500 years (Richardson, in preparation). Vertical temperature gradients will develop from the repository horizon and potentially affect air and water density. If sufficient energy in the form of heat is imparted to the air or water vapor, convective transport is established.

4.1 Airflow Mechanisms

Two potential airflow mechanisms are illustrated in Figure 4-1. Mechanism A assumes that no upward flow occurs through the host rock relative to flow through the shafts, ramps, and drifts. ES-1 and ES-2 are within the repository area, and the temperature gradient is relatively high near the repository horizon because of the thermally hot waste packages. The men-and-materials shaft, the emplacement exhaust shaft, and the ramps are located outside or just inside the repository perimeter; and the temperature gradients are lower. In response to these temperature gradients, air will tend to rise in ES-1 and ES-2 and may be drawn in through the other entries. Mechanism A may occur if the shafts and drifts are open or

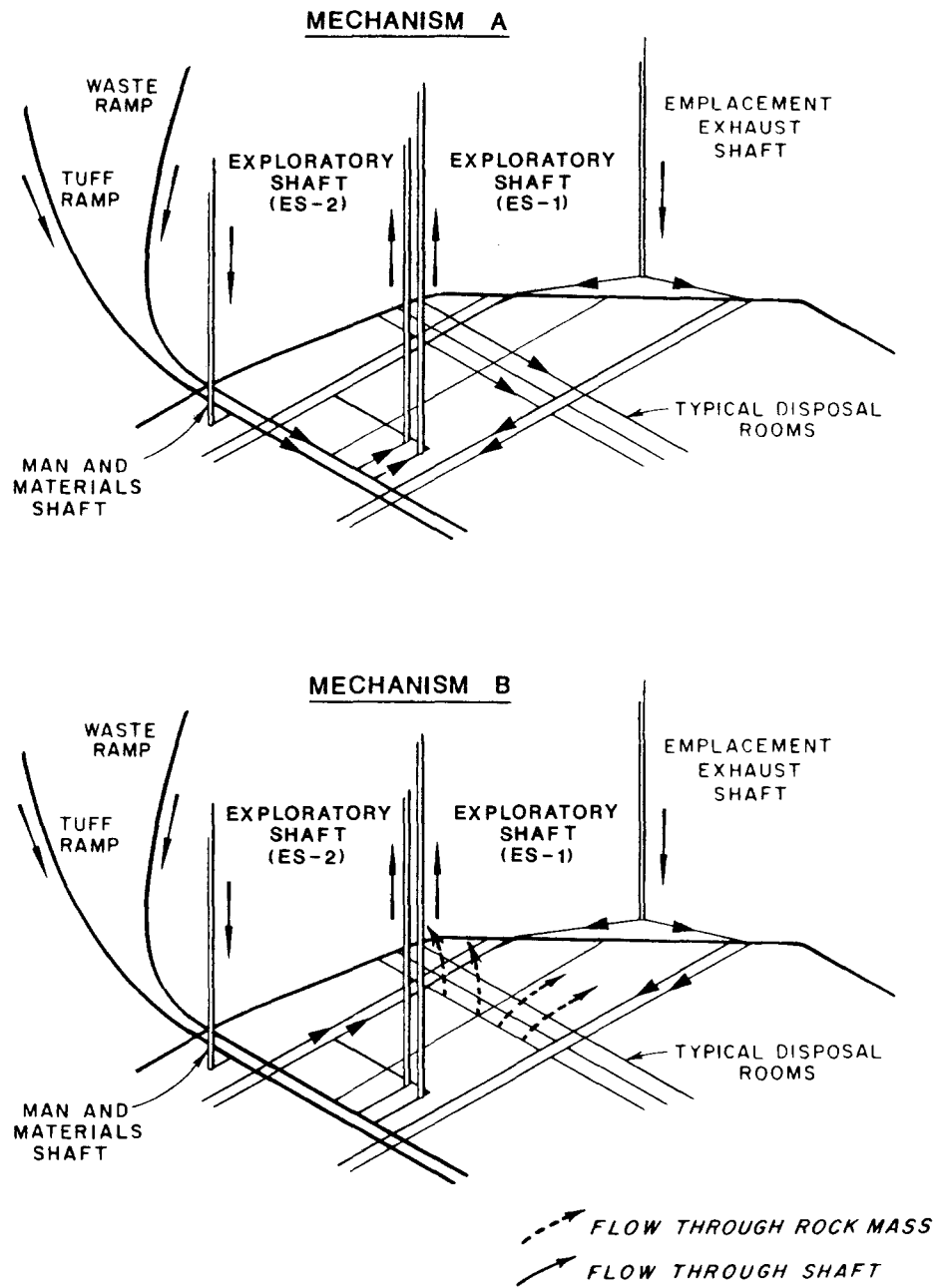


Figure 4-1. Mechanisms for Convective Airflow (a) Through Shafts Only and (b) Through Shafts and Rock

if the backfill is relatively permeable so that its resistance to airflow is less than the resistance to airflow through the rock. In Mechanism B, convective air transport is assumed to occur through the host rock. The waste disposal areas are relatively hot, and the heated air tends to rise vertically through the rock as well as through ES-1 and ES-2. Air is drawn in through the peripheral entries to maintain pressure in the rooms.

The analyses presented in this report consider Mechanism B in detail. A detailed discussion of Mechanism A and a comparison of the two mechanisms is presented in Appendix C of Fernandez et al. (1987).

4.2 Method of Analysis

The mechanism of convective airflow through a heated repository is considered analogous to the flow of air through an underground mine as a result of draft air pressure, which is calculated by using the density method and using the pressure-temperature-density relationship for natural ventilation presented in the SME Mining Engineering Handbook (Cummins and Given, 1973). The flow of air is assumed to be induced by the draft air pressure and is calculated using a network resistance model similar to that used in mine ventilation studies (Hartman, 1982, pp. 239-245). The flow is assumed to be governed by Darcy's law.

The principal input parameters are the resistance of the underground openings and the host rock to airflow and the pressure gradient calculated from the difference in pressure between the inlet and outlet points as derived from the air density profiles. A detailed discussion of the assumptions made in the analysis is presented in Appendix E. The assumptions may be summarized as follows: (1) Darcy's law is valid; (2) air temperatures in the shaft are the same as in the adjacent rock; (3) airflow is incompressible, and the air is dry; and (4) air circulation occurs along specified paths.

4.3 Model Description

Airflows were calculated by assembling a "network stiffness matrix" (Zienkiewicz, 1977, pp. 12-13) of various resistances representing the

network of underground openings and the rock mass, by applying pressure boundary conditions and by solving a system of linear simultaneous equations to calculate nodal pressures. Airflows were then calculated through the network. The following sections describe the temperature and pressure boundary conditions, air conductivities (material properties), and geometry of the model (networks) used in the analyses.

4.3.1 Temperature and Pressure Distributions

Draft pressures were calculated at the repository horizon (using the accepted mine ventilation practice of computing pressure gradients) based on the differences in air density at the inlet and outlet points. The first step requires the temperature profiles at the potential repository inlet and outlet points. The inlet and outlet temperatures at the ground surface were assumed to be 13°C. The temperature at the repository horizon for the inlet sources of air was computed to be 23°C, using the available information on the geothermal gradients. For purposes of calculating air densities, a peak temperature profile was estimated for ES-1 based on a peak temperature of 115°C at the repository horizon. (The source of this temperature is the heat from the radioactive waste contained in the waste packages.)

The draft pressure using the method described above was calculated as 0.35 kPa, which corresponds to a water gage of 1.4 in. By comparison according to Hartman (1982, p. 240), the natural ventilation pressure generated by natural geothermal energy in mines is usually <0.5 in. water gage and seldom exceeds 3 in. except in extreme cases. The calculated draft pressure falls within the range for this mechanism and is expected to be higher than 0.5 in. because the heat generated by the radioactive waste in an underground nuclear waste repository results in larger temperature contrasts than those experienced in a typical underground mine.

4.3.2 Flow Path Resistances

The resistance to airflow for incompressible fluid flow through shafts and drifts depends on the length and cross section of the flow paths and

the air conductivities of the backfill, surrounding the MPZ and host rock. In the present analyses, the MPZs were modeled around the shafts and ramps accessing the repository but not around the drifts (see below). The cross section and length of the flow paths for vertical and horizontal emplacement are summarized in Tables 4-1 and 4-2, respectively. The cross section of the MPZ developed around the shafts was assumed to extend one radius from the wall. For ramps with a noncircular cross section, the MPZ area was calculated from the equivalent radius of a circle with the same area.

For flow through undisturbed rock, it is necessary to know the cross-sectional area of the roof of the repository (waste rooms, mains, and drifts). This area is estimated to be 983,700 m² for vertical emplacement or 486,000 m² for horizontal emplacement. In these analyses, the roof areas above the mains and drifts were included in the calculation because thermal convection is expected to develop throughout the underground repository. The equivalent conductivity for flow through the rock to the ground surface was calculated assuming flow in series (Freeze and Cherry, 1979, p. 34). In the present analyses, the total thickness of the welded units (Tiva Canyon and Topopah Spring) is 260 m, and the total thickness of the nonwelded Paintbrush tuff is 40 m. The air conductivity* of the nonwelded Paintbrush, assumed to be either 3×10^{-7} or 3×10^{-5} m/min, corresponds to hydraulic conductivities of about 10^{-5} to 10^{-3} cm/s.** The welded tuff units (Tiva Canyon and Topopah Spring) were assumed to have either an air conductivity of 3×10^{-7} or 3×10^{-4} m/min, corresponding to hydraulic conductivities of 10^{-5} to 10^{-2} cm/s (Scott et al., 1983, p. 299).

Three combinations of bulk rock hydraulic conductivity were evaluated in the analysis. These combinations were selected to cover a range of conductivities for welded and nonwelded tuff and to examine the influence

*Air conductivity may be derived by calculating an intrinsic permeability from the hydraulic conductivity relationship presented by Freeze and Cherry (1979, p. 27) and then by calculating the air conductivity using the fluid properties of air. Slip flow has also been considered in computing the air conductivity

**The range considered here bounds the value for the bulk rock, saturated hydraulic conductivity of 2.4×10^{-4} cm/s given by Sinnock et al. (1984, p. 12) for the Paintbrush nonwelded unit.

Table 4-1. Summary of Areas and Lengths for Vertical Emplacement

Flow Path	Backfilled Area ^(a) (m ²)	Modified Permeability Zone ^(b) (m ²)	Length (m)
Waste Ramp	34.2	115.8	2,012
Tuff Ramp	42.8	136.8	1,410
Men-and-Materials Shaft	29.2	105.9	314
Emplacement Exhaust Shaft	29.2	105.9	314
ES-1	10.5	42.9	311
ES-2	10.5	42.9	311

(a) Backfilled area is based upon inside dimension of lined shaft or ramp.

(b) MPZ is based upon three times the excavated area of the shaft or ramp, which corresponds to an MPZ extending one radius from the edge of the excavated shaft wall.

Table 4-2. Summary of Areas and Lengths for Horizontal Emplacement

Flow Path	Backfilled Area ^(a) (m ²)	Modified Permeability Zone ^(b) (m ²)	Length (m)
Waste Ramp	28.3	96.5	2,012
Tuff Ramp	30.1	96.5	1,410
Men-and-Materials Shaft	29.2	105.9	314
Emplacement Exhaust Shaft	29.2	105.9	314
ES-1	10.5	42.9	311
ES-2	10.5	42.9	311

(a) Backfilled area is based upon inside dimension of lined shaft or ramp.

(b) MPZ is based upon three times the excavated area of the shaft or ramp, which corresponds to an MPZ extending one radius from the edge of the excavated shaft wall.

of a thinner less permeable layer of nonwelded tuff on overall airflow rates if the conductivities of the welded tuff were high (10^{-2} cm/s).

	Nonwelded Hydraulic Conductivity (cm/s)	Welded Hydraulic Conductivity (cm/s)
Combination 1 (Low)	10^{-5}	10^{-5}
Combination 2 (Intermediate)	10^{-5}	10^{-2}
Combination 3 (High)	10^{-3}	10^{-2}

The equivalent air conductivity of the MPZ was either 20 or 60 times higher than the conductivity of the undisturbed tuff averaged over an annulus one radius wide extending from the shaft wall. The equivalent conductivity factor of 20 corresponds to expected conditions at depth. The equivalent conductivity factor under worst-case assumptions ranged from 40 to 80 times the undisturbed tuff conductivity. The average value of 60 was selected for analysis. The equivalent conductivity factor of the overlying rock was determined, as explained previously, to take into account strata with varying conductivities, and the MPZ was assumed to be either 20 or 60 times more permeable than the undamaged rock in each stratigraphic unit.

Air conductivities in the backfill varied from 3.0×10^{-6} to 3.0 m/min, equivalent to hydraulic conductivities from 10^{-4} to 100 cm/s. The upper bound of air conductivity corresponds to a gravel, while the lower bound corresponds to a silty sand (Freeze and Cherry, 1979, p. 29). The lower bound might also correspond to a compacted backfill engineered for low permeability by adding silt or clay fines.

4.4 Model Results

The convective airflow analysis results are presented as a series of plots. The relationships of the total flow rate out of the repository to the shaft fill, the air conductivity for vertical and horizontal emplacement configurations, and the low and high MPZ models are presented in Figures 4-2 through 4-5. The flow rates through ES-1 and ES-2 expressed as a percentage of the total flow rate out of the repository are presented in Figures 4-6 through 4-9. The three curves on each plot represent the low, intermediate, and high rock conductivity combination presented previously.

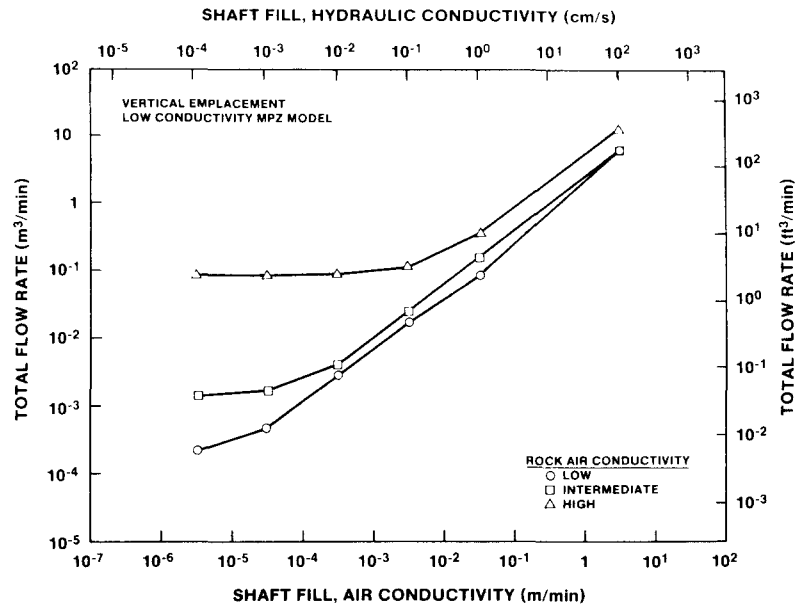


Figure 4-2. Total Flow Rate as a Function of Shaft Fill, Air Conductivity (Vertical Emplacement and Low Conductivity MPZ Model)

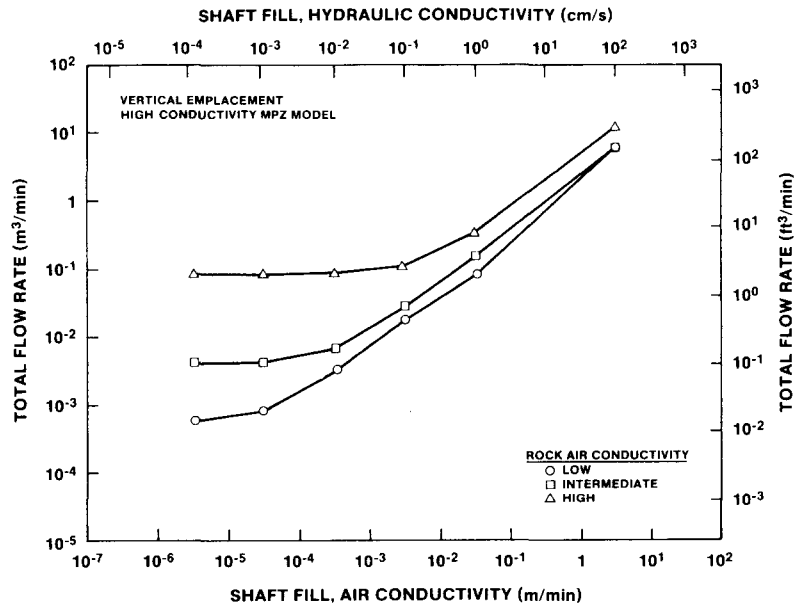


Figure 4-3. Total Flow Rate as a Function of Shaft Fill, Air Conductivity (Vertical Emplacement and High Conductivity MPZ Model)

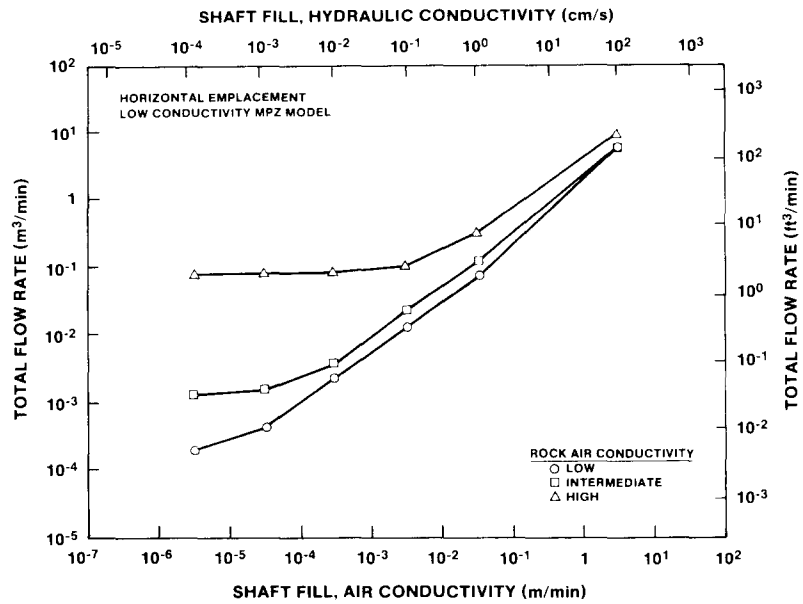


Figure 4-4. Total Flow Rate as a Function of Shaft Fill, Air Conductivity (Horizontal Emplacement and Low Conductivity MPZ Model)

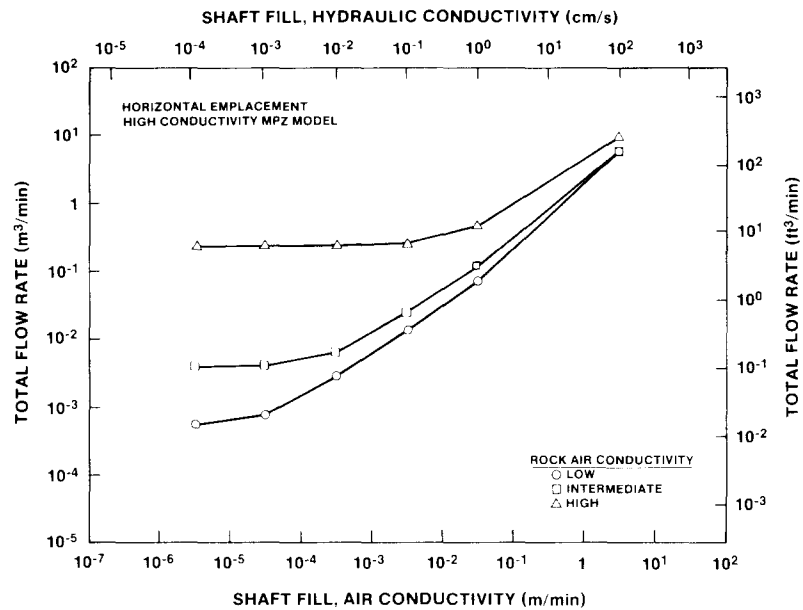


Figure 4-5. Total Flow Rate as a Function of Shaft Fill, Air Conductivity (Horizontal Emplacement and High Conductivity MPZ Model)

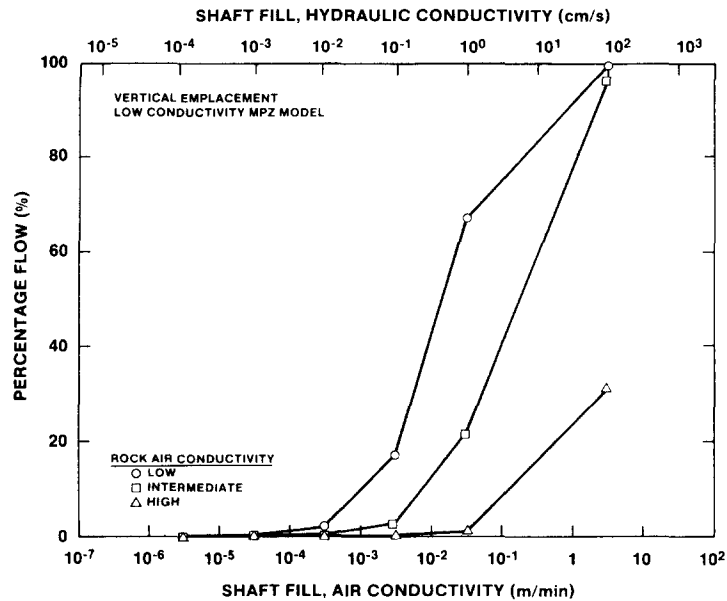


Figure 4-6. Airflow Through ES-1 and ES-2 (Shaft Fill and MPZ Flows Included) as a Percentage of Flow Through the Rock over the Repository Area (Vertical Emplacement and Low Conductivity MPZ Model)

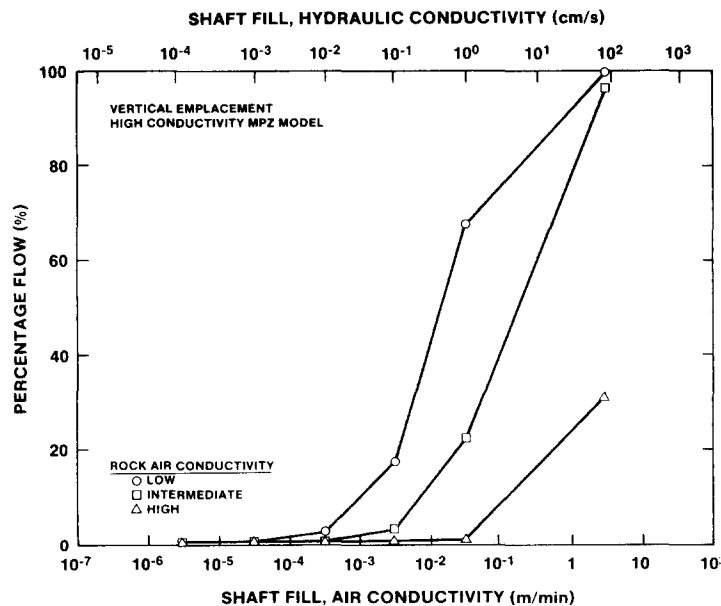


Figure 4-7. Airflow Through ES-1 and ES-2 (Shaft Fill and MPZ Flows Included) as a Percentage of Flow Through the Rock over the Repository Area (Vertical Emplacement and High Conductivity MPZ Model)

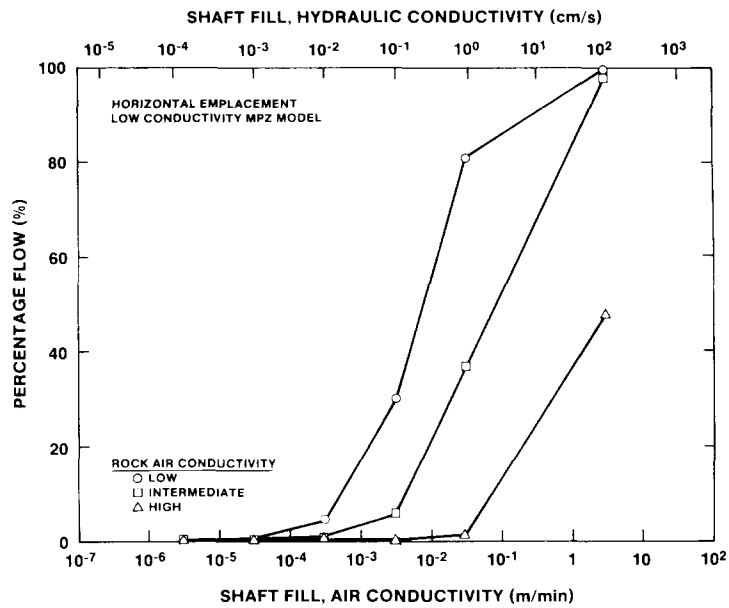


Figure 4-8. Airflow Through ES-1 and ES-2 (Shaft Fill and MPZ Flows Included) as a Percentage of Flow Through the Rock over the Repository Area (Horizontal Emplacement and Low Conductivity MPZ Model)

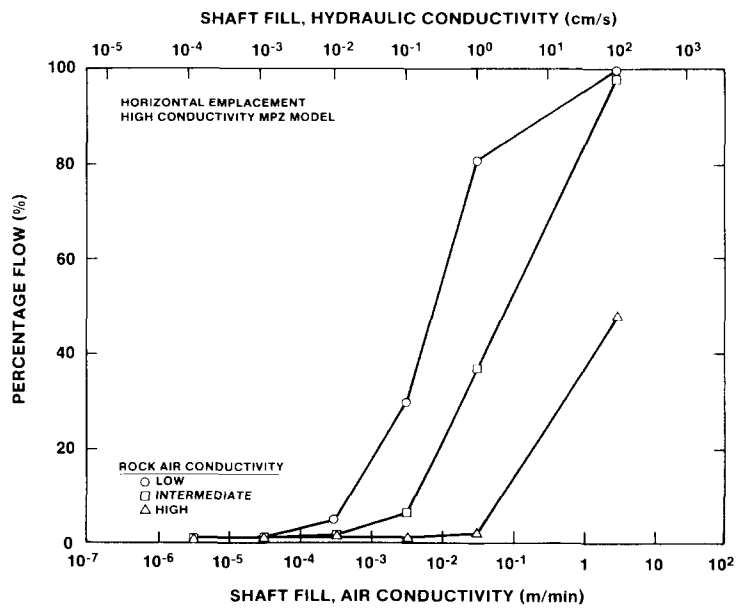


Figure 4-9. Airflow Through ES-1 and ES-2 (Shaft Fill and MPZ Flows Included) as a Percentage of Flow Through the Rock over the Repository Area (Horizontal Emplacement and High Conductivity MPZ Model)

The distribution of airflow through the shaft fill, the MPZ, and the tuff roof rock was found to depend on the air conductivity of the shaft fill. For shaft fill having a high air conductivity of 1 m/min, the flow into and out of the repository is mainly through the shaft fill with the total flow ranging from approximately 1 to 10 m³/min, depending on the conductivity of the roof rock. For shaft fill having low air conductivities of <10⁻⁵ m/min, the flow into the repository is primarily through the MPZ, while flow out of the repository is dominantly through the tuff roof, and total flow rates are <0.1 m/min. The high conductivity MPZ model results in a somewhat higher flow rate than the low conductivity MPZ model under these circumstances. The conductivity of the tuff units in series influences the total airflow through the repository. For the high conductivity combination, the total flow begins to level off toward a constant value at a shaft fill, air conductivity of about 10⁻³ m/min. For the intermediate and low conductivity combinations, this stabilization of total flow occurs at a shaft fill, air conductivity of approximately 10⁻⁵ m/min. At low, backfill air conductivity, the total flow rate varies more than two orders of magnitude depending on the air conductivity of the rock column above the repository.

In comparing total flow for the vertical and horizontal emplacement modes, it is apparent that the results are very similar. This is because the geometry of the shafts and ramps accessing the repository are similar. For shaft fill having a high air conductivity, airflow is mainly through the shafts and ramps. For shaft fill having a low air conductivity, airflow is mainly in the MPZ of the inlet shafts and ramps. In this analysis, no attempt has been made to distinguish between temperature fields of the two emplacement modes although this may have some influence on calculated upper-bound, convective airflow rates. It is reiterated that the assumption of the inlet shafts and ramps being at geothermal temperature is conservative for both emplacement modes.

The analysis indicates that the flow through ES-1 and ES-2 as a percentage of total flow depends on the air conductivity of the shaft fill. When the conductivity of the backfill is low, the percentage of flow through the shafts and ramps is also low, regardless of whether the conductivity of the MPZ is low or high. For example, for vertical

emplacement with a shaft fill having an air conductivity $<3 \times 10^{-4}$ m/min (equivalent to a hydraulic conductivity of 10^{-2} cm/s), the contribution of ES-1 and ES-2 to the total flow is $<2.5\%$. The percentage is somewhat higher for horizontal emplacement and can be attributed to a smaller roof area, which tends to increase the percentage of flow through ES-1 and ES-2. Nevertheless, for either emplacement mode, the percentage is smaller than 2.5% when the backfill air conductivity is $<10^{-4}$ m/min. As indicated at the beginning of this chapter, the performance goal established for airflow from the ESs was that no more than 25% of the total flow from the repository should go through these shafts. The value of 2.5% given above, therefore, represents an even more conservative release of air through the shafts; i.e., one order of magnitude less than the performance goal.

4.5 Conclusions

From the preceding discussion, it has been concluded that the ESs (including shaft fill and the MPZ) are not likely to be preferential pathways for gaseous radionuclide releases if the air conductivity of the shaft fill is less than about 3×10^{-4} m/min. Following are the reasons for reaching this conclusion.

- o When the air conductivity is $>3 \times 10^{-4}$ m/min, the airflow is predominantly through the shaft fill.
- o When the conductivity of the shaft fill is low, flow through the MPZ is proportionally greater than flow through the backfill. However, because the total airflow through the MPZ and the shaft fill as compared to flow through the roof rock over the repository is low ($<2.5\%$), the potential release of air through the MPZ will also be low.
- o The temperature gradients between the repository horizon and the ground surface are greater than those anticipated to occur at this location. Hence the driving force for this airflow scenario is larger than what would be expected under maximum thermal convection at the repository. Also, as the repository cools after the peak temperature is reached and before the repository heats up, thermally induced airflow is of lesser consequence.

Further, obtaining a shaft fill that has a hydraulic conductivity of 10^{-2} cm/s is achievable. For example, for cohesionless materials (i.e., with no clay), values may range from as high as 100 cm/s for a clean, coarse gravel or rock fill to 10^{-5} cm/s for a fine silt. Specific values within this range can be engineered by crushing and screening the tuff. Lower values of hydraulic conductivity can be obtained by adding clay or crushed tuff. For example, a value of about 10^{-10} cm/s can be obtained from a mixture of crushed tuff with 30% Na-bentonite (Fernandez et al., 1987, Appendix D).

5.0 POTENTIAL FOR ENHANCING RADIONUCLIDE RELEASE BY AIR MOVEMENT RESULTING FROM BAROMETRIC FORCES

This section evaluates the potential volumes of air displaced from ES-1 or ES-2 as a result of barometric forces. These barometric forces are created by pressure differences that are induced by postulated meteorological events occurring at the ES locations. The purpose of the analyses in this section is to predict what volume of air contained in the shaft fill and MPZ under unsaturated conditions can be displaced by several meteorological events. If only a portion of the shaft fill and MPZ air volume is displaced when the pressure drops at the surface, the surface air will be forced into the shaft fill and MPZ when the pressure at the surface reverses (pressure increase). As a result, contaminated air that reaches the shaft is not continuously displaced by barometric forces.

5.1 Model Description

The differences between the repository and surface air pressure will cause air to move through the accesses to the repository. Air may also move through the rock. The direction of air movement will be from areas of high pressure to those with low pressure. The magnitude of the flow rate will be proportional to the pressure difference, the air conductance, and the cross-sectional area through which air flows.

A one-dimensional, airflow model was developed to evaluate flow induced by barometric changes at the surface. The development of the model includes the following assumptions.

- o Darcy's law is valid for flow through the shafts and ramps; this assumption requires that airflow be laminar.
- o Atmospheric pressure follows a sinusoidal function. Individual pressure cycles occur within minutes to a year. The amplitude of the periodic functions is related to barometric pressure highs and lows found at Yucca Mountain for various events.
- o Air in the repository behaves according to the equation of state for an ideal gas. For this analysis, the temperature of the

repository is constant, while the mass of the air in the repository is allowed to change in response to barometric pressure variations.

- o Compressive storage of the air in the backfilled shafts and ramps and rock is negligible compared to the compressive storage in the repository.
- o The MPZ model is the same as that used in the previous analyses of convective flow.

This model is structured to describe porous media flow between the repository and the surface air in response to a sinusoidal variation in barometric pressure. The pressure within the repository will also vary sinusoidally as air leaves and subsequently reenters the repository by way of 13 parallel pathways. In this model, these pathways are the backfill and MPZs associated with all six shafts and ramps and the host rock itself.

5.1.1 Physical Model

For purposes of model development, the repository is conceived of as an enclosed volume with parallel conduits to the surface such as shown in Figure 5-1. Gas within the repository may enter or leave by way of the parallel conduits, and flow within each conduit is governed by Darcy's flow law. A pathway may consist of fill emplaced in a lined shaft or ramp, the surrounding MPZ, or the undisturbed rock. Because the fill and MPZ associated with each shaft and ramp have different conductivities, flow areas, and lengths, they are treated as independent flow paths.

5.1.2 Mathematical Model and Assumptions

Flow through each conduit is described by Darcy's law:

$$Q_i = \frac{K_i A_i}{L_i \rho g} (P_r - P_a) \quad , \quad (5-1)$$

where

K_i = air conductivity of the i^{th} flow path,

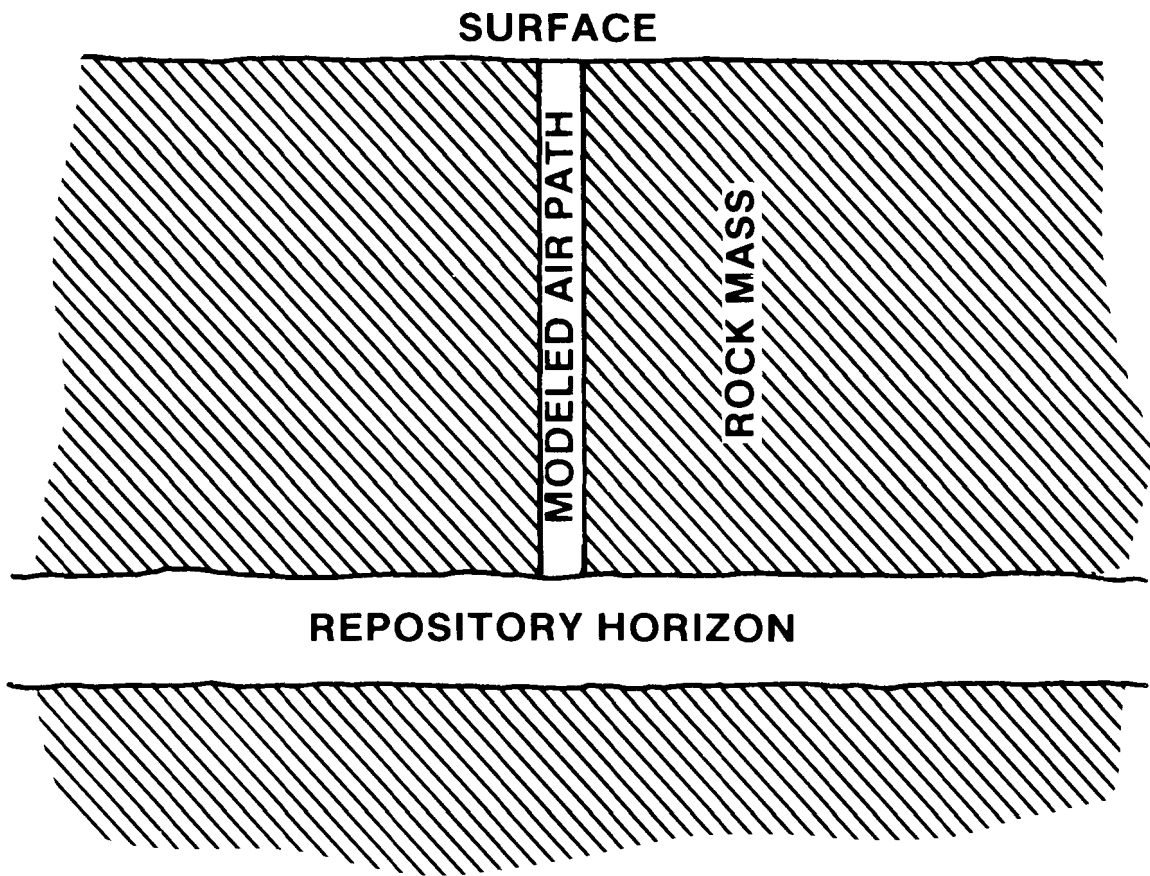


Figure 5-1. Repository Used in Barometric Pressure Model

A_i = cross sectional area of i^{th} flow path,
 L_i = length of i^{th} flow path,
 ρ = average density of air within the permeable conduit,
 g = acceleration resulting from gravity,
 Q_i = volumetric flow rate (positive for flow out of repository),
 $P_a = p_a - \rho g Z_a$,
 $P_r = p_r - \rho g Z_r$,
 p_r = repository pressure,
 p_a = atmospheric pressure,
 Z_r = repository elevation above a reference datum, and
 Z_a = surface elevation above a reference datum.

The use of P in Equation 5-1 inherently allows for variation in the static head resulting from repository and surface elevation differences. Hence, the difference $(P_r - P_a)$ is appropriate for all shafts and ramps.

The sum of the volumetric flow rates through all flow paths is also governed by a direct application of Darcy's law:

$$Q = \sum_i \frac{K_i A_i}{L_i \rho g} (P_r - P_a) \quad (5-2)$$

This volumetric flow rate may then be expressed as a molar flow rate,

$$\frac{dn_r}{dt} = -\frac{\rho Q}{M} \quad (5-3)$$

where

M = the molecular weight of air,
 n_r = moles of air contained within the repository, and
 t = time.

The molar flow rate is also assumed to be related to the repository pressure through the ideal gas law so that

$$\frac{dn_r}{dt} = \frac{dp_r}{dt} \frac{V_r}{RT_r} \quad (5-4)$$

where

$$\begin{aligned} V_r &= \text{repository volume,} \\ R &= \text{ideal gas constant, and} \\ T_r &= \text{repository temperature.} \end{aligned}$$

Noting that $\frac{n_r}{V_r} = \frac{\rho}{M}$ and combining Equations 5-2 through 5-4 yields an expression for the response of the repository pressure to atmospheric pressure variations:

$$\frac{dP_r}{dt} + c(P_r - P_a) = 0 \quad , \quad (5-5)$$

where

$$c = \frac{n_r RT_r}{\rho g V_r^2} \sum_i \frac{K_i A_i}{L_i} \quad . \quad (5-6)$$

The variation of atmospheric pressure with time is assumed to take the form of a sinusoid:

$$P_a = P_{ao} + m \sin(\omega t) \quad , \quad (5-7)$$

where

$$\begin{aligned} P_{ao} &= \text{the average barometric pressure;} \\ m &= \text{amplitude, which is defined as } m = (P_H - P_L)/2; \\ \omega &= \text{angular frequency} = 2\pi/T; \\ T &= \text{period;} \\ P_H &= \text{average high pressure for a specific event; and} \\ P_L &= \text{average low pressure for a specific event.} \end{aligned}$$

The solution to this problem will be presented for various values of amplitude and frequency.

The significance of the constant c is that it is proportional to the ratio of the volumetric flow rate to the volume of the repository. It also influences the amplitude and phase relationships of the repository pressure under periodic conditions as described subsequently. The constant c

depends on the air conductivity of all flow paths. The placement of shaft fill under certain circumstances affects the pressure response of the underground repository.

The solution to Equations 5-5 and 5-7 is

$$P_r = P_{ao} + \frac{m \sin(\omega t) - \frac{\omega m}{c} \cos(\omega t)}{1 + \frac{\omega^2}{c^2}} \quad (5-8)$$

The volumetric flow rate can be calculated by substituting the pressure relationships in Equations 5-7 and 5-8 into Darcy's law (Equation 5-2),

$$Q = \sum_i \frac{K_i A_i}{\rho g L_i} \left[m \sin(\omega t) \left(\frac{c^2}{c^2 + \omega^2} - 1 \right) - \frac{c \omega m}{c^2 + \omega^2} \cos(\omega t) \right] \quad (5-9)$$

or expressed as a sinusoid with a lagging phase angle,

$$Q = \sum_i \frac{K_i A_i}{\rho g L_i} \left[\frac{m \omega}{\sqrt{c^2 + \omega^2}} \sin \left((\omega t) - \pi + \sin^{-1} \frac{c}{\sqrt{c^2 + \omega^2}} \right) \right] \quad (5-10)$$

Equation 5-10 may then be integrated over half of any cycle to give the amount of air entering or leaving a shaft as a consequence of the assumed barometric pressure variation. Hence, the cyclic volume of displaced air, V , is given by

$$V = \sum_i \frac{2K_i A_i}{\rho g L_i} \frac{m}{\sqrt{c^2 + \omega^2}} \quad (5-11)$$

Further, the cyclic volume of displaced air may be computed for any flow path, i ,

$$V_i = \frac{2K_i A_i}{\rho g L_i} \frac{m}{\sqrt{c^2 + \omega^2}} \quad (5-12)$$

In Section 5.3, results are displayed in terms of the ratio of air displaced from a shaft, V_i , to the volume of air in the shaft fill and MPZ. The void volume in the shaft fill was calculated from the total volume of

the lined ES-1 with a porosity of 30% and the volume of the MPZ with an effective, unsaturated rock porosity of 4.2%. The calculated volume of the voids in the ESs is 1,540 m³. It is assumed that the porosity of the shaft fill has a constant value of 30%. This value is at the lower range of porosities (i.e., 25 to 50%) for natural granular materials and artificial materials, as indicated by standard texts (e.g., Winterkorn and Fang, 1979, p. 257; Davis and DeWeist, 1966, p. 375).

5.2 Input to the Mathematical Model

The cyclic volumetric displacement relationship developed in the previous section suggests that the displaced volume is proportional to the pressure amplitude and inversely proportional to the frequency of the weather event (proportional to the period). To cover a range of potential weather events, the following were considered:

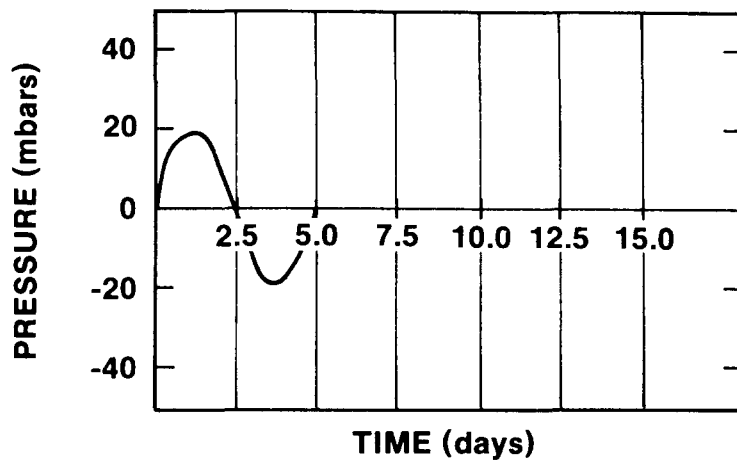
- o a severe thunderstorm event with a time period of five days;
- o a tornado event with a time period of one minute; and
- o a seasonal fluctuation of barometric pressure with a time period of one year.

These events are indicated schematically in Figure 5-2 and include a low frequency/low amplitude seasonal event, an intermediate frequency/intermediate amplitude event, and a high frequency/high amplitude tornado event.

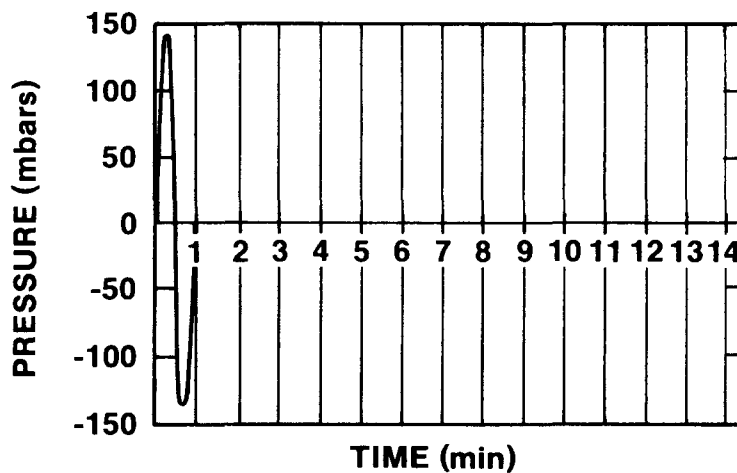
The severe thunderstorm event represents a bounding event to typify atmospheric pressure fluctuations (movement of weather fronts) that might occur at Yucca Mountain. The average high and low pressures for January through December have been compiled by the DOE (1986, p. 3-48) and indicate that the pressure amplitude ranges from 8.6 to 19.0 mbars (0.25 to 0.56 in. of Hg). Various strip charts at Yucca Mountain have been reviewed and indicate that a typical pressure variation for a thunderstorm event occurs over approximately five days.

There are no published values for barometric pressure fluctuations for tornadoes because it is difficult to measure pressure during such events.

EVENT 1 - THUNDERSTORM



EVENT 2 - TORNADO



EVENT 3 - SEASONAL FLUCTUATION

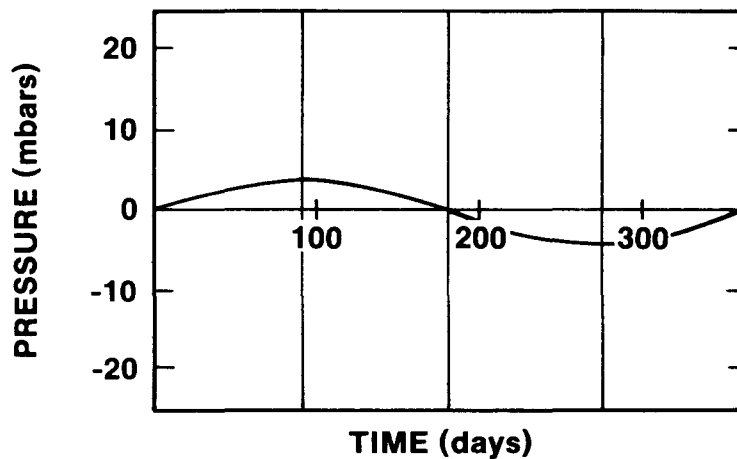


Figure 5-2. Barometric Pressure Events

An approximate value may be derived from the Bernoulli equation for conservation of energy for fluid flow and the equation of state for an adiabatic expansion of air. If it is assumed that the initial pressure is 850 mbars (25.1 in. of Hg) and that the tornado event results in an air velocity of 200 mph (89.4 m/s), then the calculated drop in pressure is 132 mbars (3.9 in. of Hg). This calculated value may be compared to the difference between high and low pressure extremes recorded in the United States (Valley, 1965, p. 3-30). The high and low extremes are 1,063.3 and 954.9 mbars, respectively, with a difference of 108 mbars or an equivalent pressure amplitude of 54 mbars. It is further assumed that the tornado would hover over the ES for approximately 1 minute.

The seasonal fluctuation in barometric pressure is derived from differences between average pressures in January and June (DOE, 1986, p. 3-48). The calculated difference is 3.0 mbars (0.09 in. of Hg).

Other parameters required for conducting these analyses include (1) the air conductivities of the shaft fill, the surrounding MPZ, and the undisturbed rock; (2) the lengths and areas of the parallel flow paths; (3) the volume of the repository; and (4) the repository temperature.

The same range of shaft fill, air conductivities; the same combination of rock conductivities; and the same MPZ models were used in these analyses as were used in the convective airflow analyses. The analyses were conducted for both vertical and horizontal emplacement options as in the convective airflow analyses. Tables 4-1 and 4-2 summarize cross-sectional areas and lengths for each of the flow paths.

The cross-sectional area of rock flow path was again taken to be equal to the combined roof area of all underground mains, access drifts, and emplacement drifts (983,700 m² for vertical emplacement or 486,000 m² for horizontal emplacement). The area of the MPZs surrounding the shafts or ramps in either configuration was taken as three times the excavated area. In addition, the temperature of the air underground was taken as 115°C for determining the mass of air in the repository.

5.3 Model Results

The results of the analysis are presented as a series of plots relating the ratio of total flow or displaced volume out of ES-1 to void volume in ES-1* and the surrounding MPZ versus shaft fill, air conductivity. A series of six plots for vertical emplacement is presented in Figures 5-3 through 5-8 for the three pressure events and the two MPZ models. The complementary set of six plots for horizontal emplacement are presented in Figures 5-9 through 5-14. Each plot presents three curves for the three cases of rock air conductivity presented previously.

For vertical or horizontal emplacement, results indicate that the displaced volume of air from ES-1 predominantly flows through the shaft fill when the air conductivity of the shaft fill is high and flows through the MPZ when the air conductivity of the shaft fill is low. For example, in Figure 5-3 for Event 1 and the low conductivity MPZ model, the analysis indicates that one to ten times the void volume might be displaced if the air conductivity of the shaft fill were >1 m/min. For shaft fill with an air conductivity of $<10^{-2}$ m/min, the MPZ is more dominant, and the displaced air volume becomes less dependent on the air conductivity of the shaft fill for the high, rock air conductivity combination. Similar trends are observed for all air conductivity combinations. The analysis indicates that 1/10,000 to 1/10 times the void volume would be displaced from the shaft for thunderstorms if a low conductivity backfill were emplaced in the shafts and ramps. Further for low conductivity backfill, flow through the shaft and MPZ is directly proportional to the conductivity of the MPZ because very little air escapes through the backfill. The analyses indicate that placement of a low conductivity backfill will be very effective in reducing the flow volume if the conductivity of the surrounding MPZ is low.

*While the discussion of these analyses focuses on ES-1, the results are equally applicable to ES-2 because ES-2 and its MPZ are the same size as ES-1.

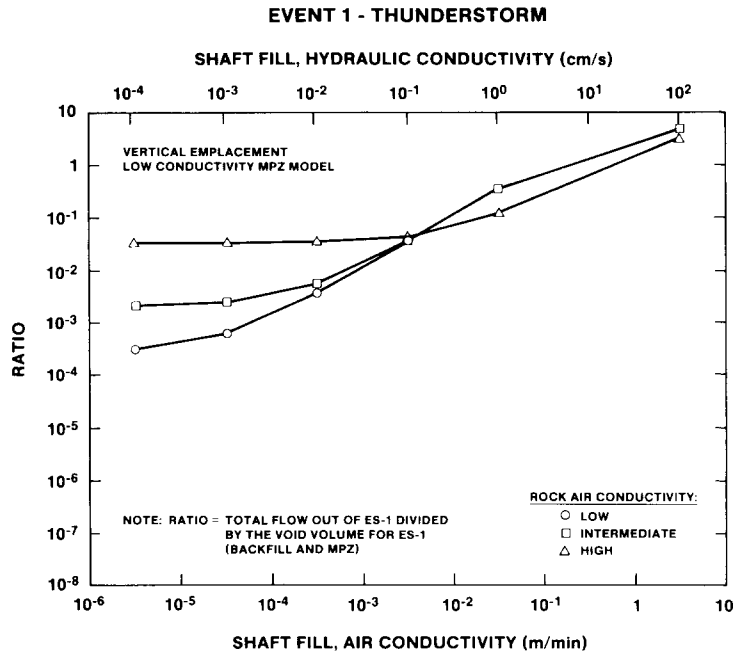


Figure 5-3. Ratio of Displaced Air Volume to Void Volume for ES-1 for a Severe Thunderstorm Event (Vertical Emplacement and Low Conductivity MPZ Model)

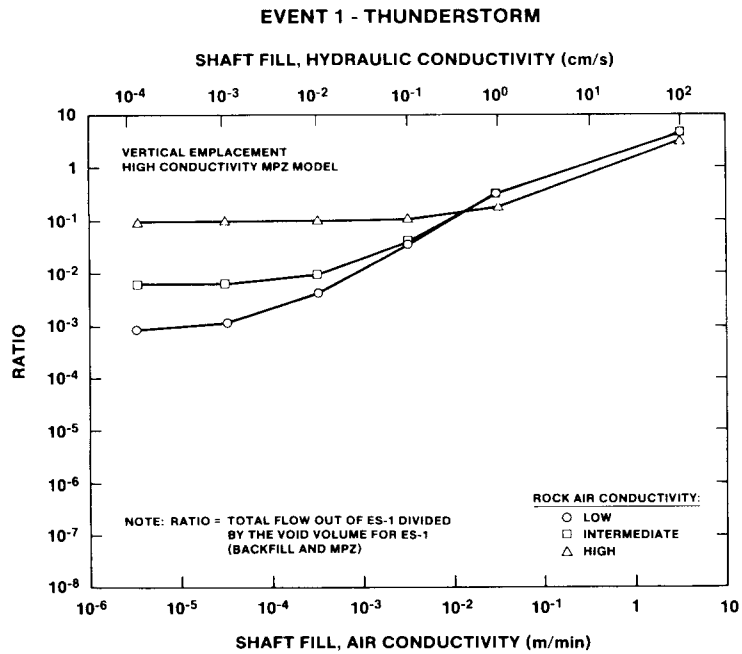


Figure 5-4. Ratio of Displaced Air Volume to Void Volume for ES-1 for a Severe Thunderstorm Event (Vertical Emplacement and High Conductivity MPZ Model)

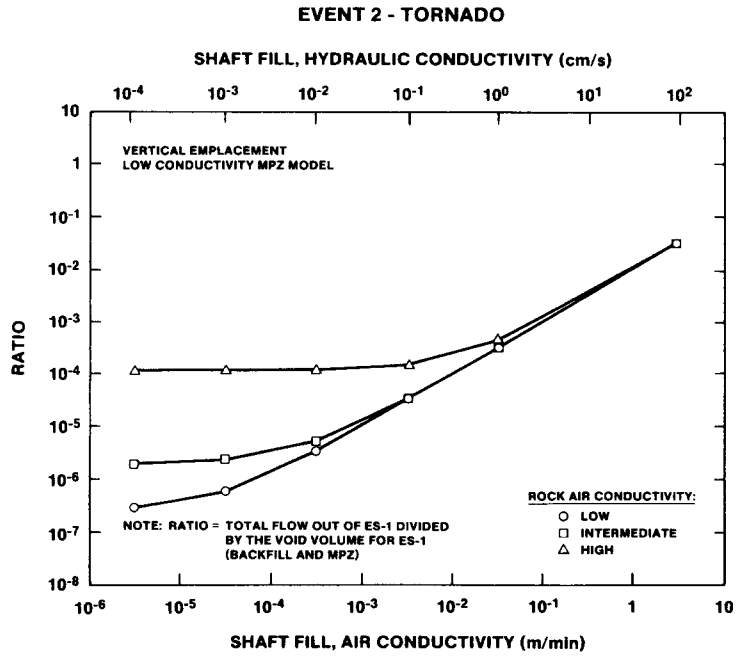


Figure 5-5. Ratio of Displaced Air Volume to Void Volume for ES-1 for a Tornado Event (Vertical Emplacement and Low Conductivity MPZ Model)

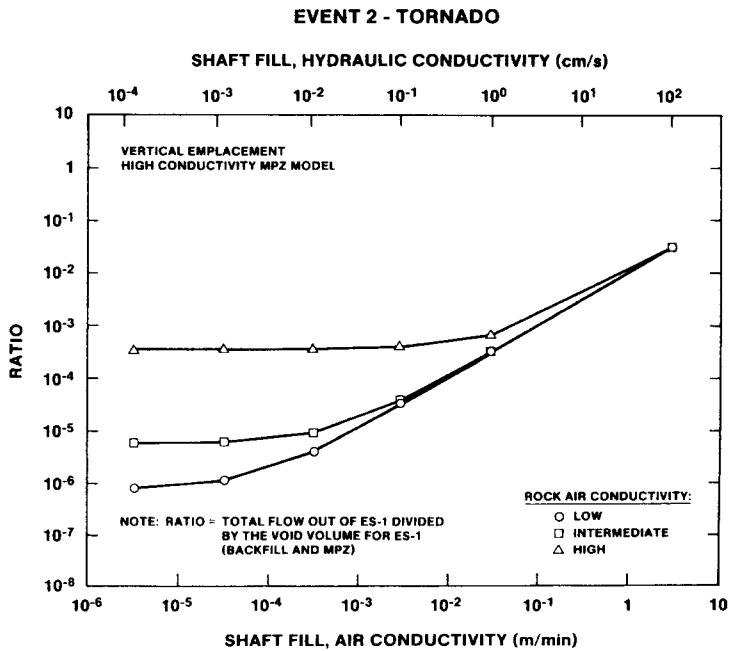


Figure 5-6. Ratio of Displaced Air Volume to Void Volume for ES-1 for a Tornado Event (Vertical Emplacement and High Conductivity MPZ Model)

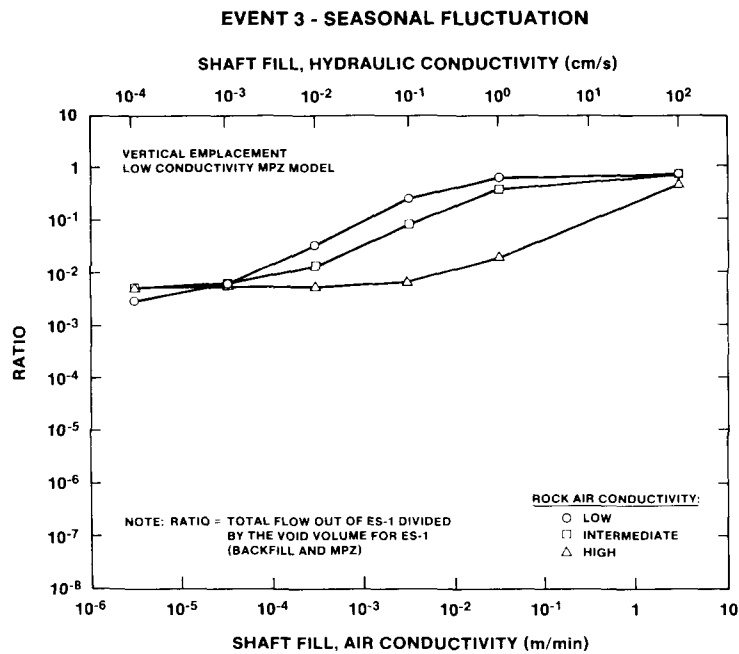


Figure 5-7. Ratio of Displaced Air Volume to Void Volume for ES-1 for a Seasonal Event (Vertical Emplacement and Low Conductivity MPZ Model)

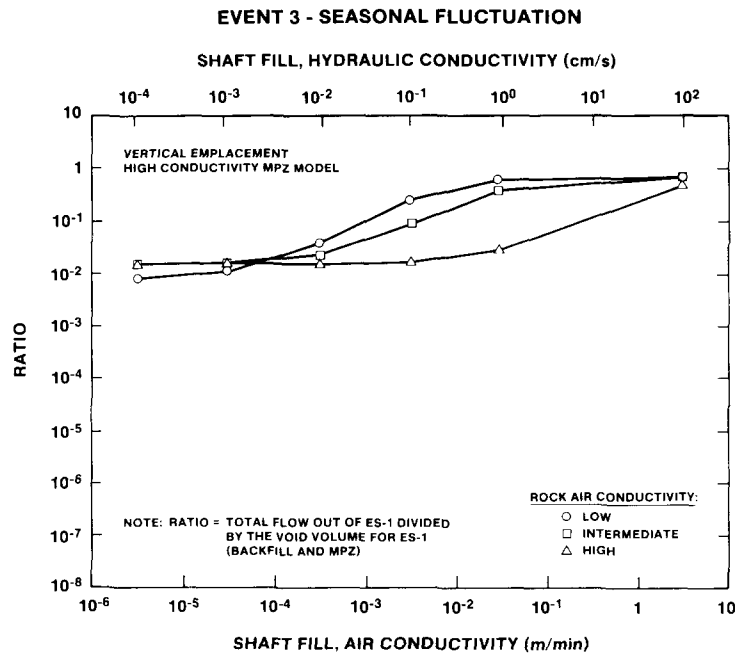


Figure 5-8. Ratio of Displaced Air Volume to Void Volume for ES-1 for a Seasonal Event (Vertical Emplacement and High Conductivity MPZ Model)

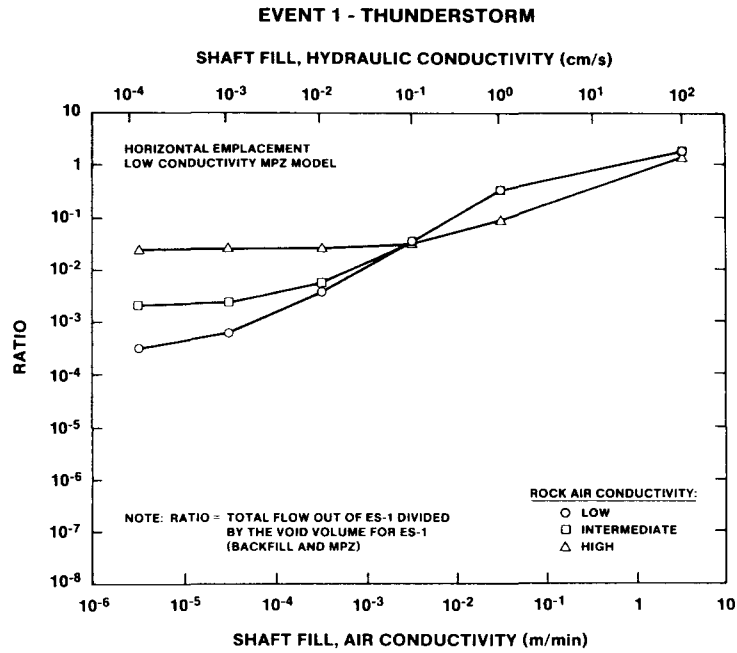


Figure 5-9. Ratio of Displaced Air Volume to Void Volume for ES-1 for a Severe Thunderstorm Event (Horizontal Emplacement and Low Conductivity MPZ Model)

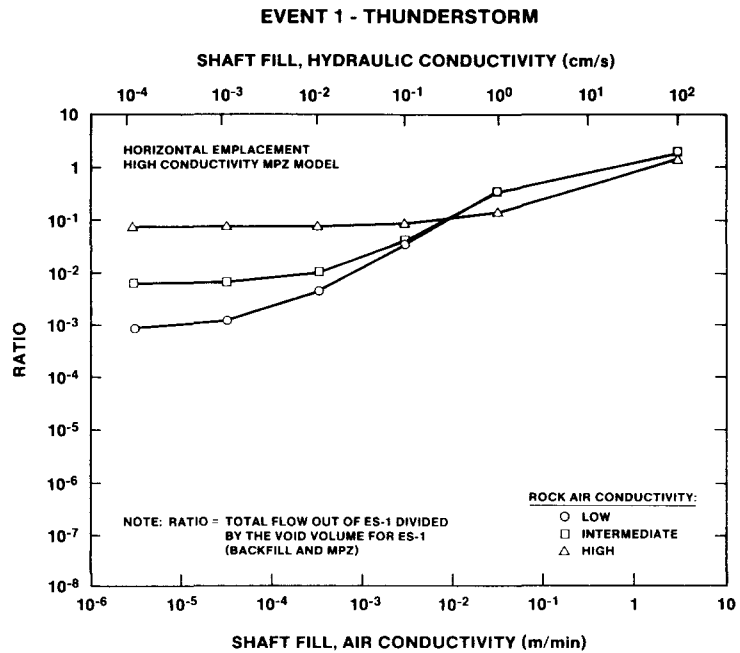


Figure 5-10. Ratio of Displaced Air Volume to Void Volume for ES-1 for a Severe Thunderstorm Event (Horizontal Emplacement and High Conductivity MPZ Model)

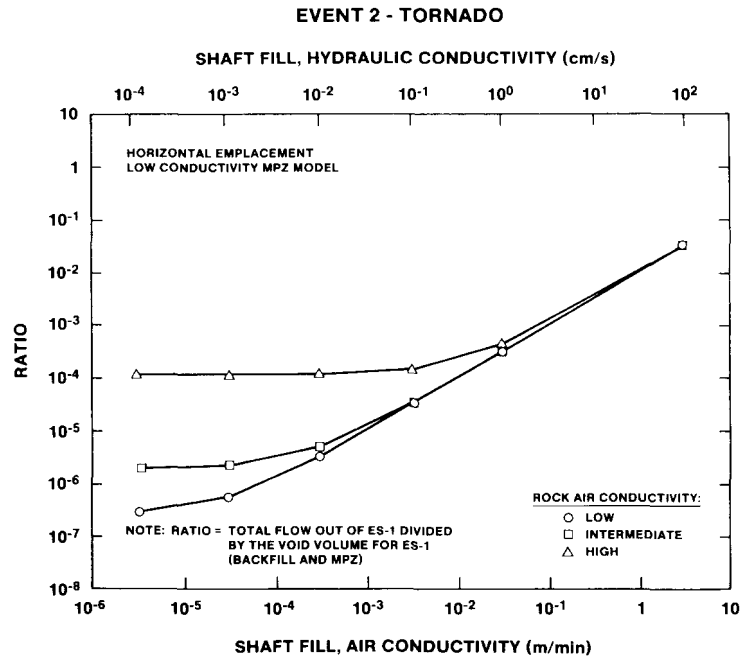


Figure 5-11. Ratio of Displaced Air Volume to Void Volume for ES-1 for a Tornado Event (Horizontal Emplacement and Low Conductivity MPZ Model)

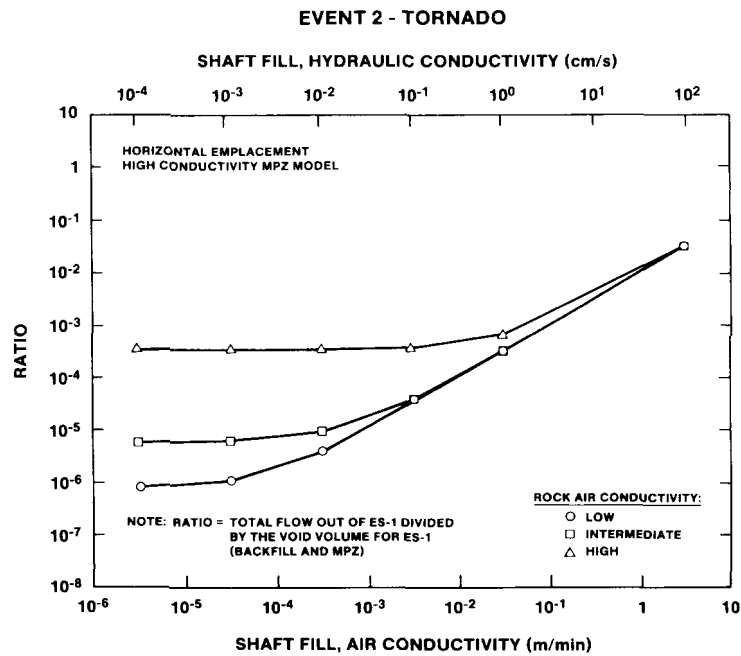


Figure 5-12. Ratio of Displaced Air Volume to Void Volume for ES-1 for a Tornado Event (Horizontal Emplacement and High Conductivity MPZ Model)

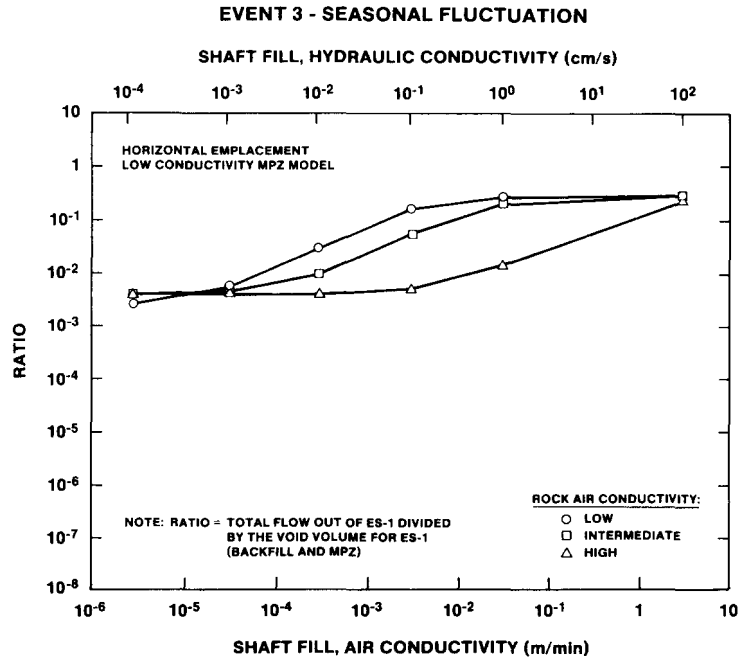


Figure 5-13. Ratio of Displaced Air Volume to Void Volume for ES-1 for a Seasonal Event (Horizontal Emplacement and Low Conductivity MPZ Model)

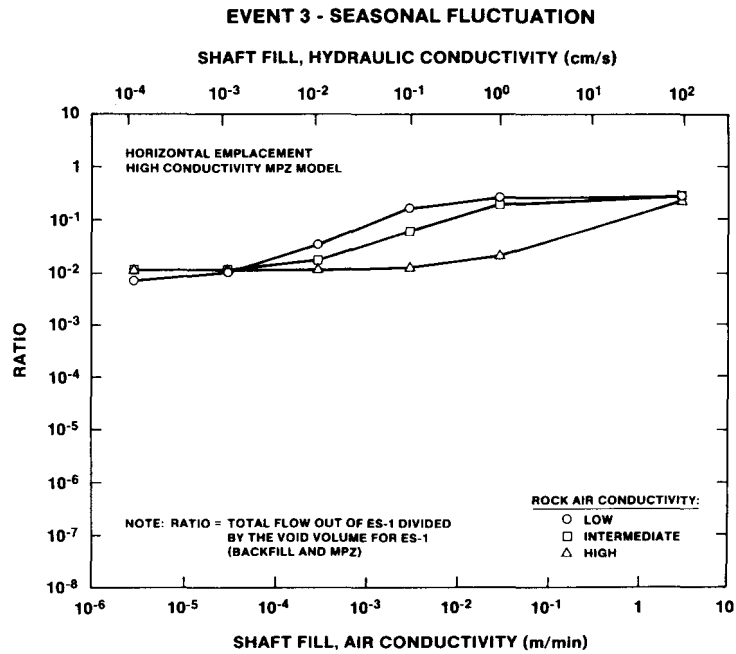


Figure 5-14. Ratio of Displaced Air Volume to Void Volume for ES-1 for a Seasonal Event (Horizontal Emplacement and High Conductivity MPZ Model)

It is interesting to note that a lower, rock air conductivity results in the displacement of somewhat greater amounts of air at higher shaft fill, air conductivities. This "cross over" phenomenon is related to the pressure phase relationship that develops between the surface and the underground repository. As seen from Equation 5-8, if the characteristic constant c is large, then the atmospheric and repository pressures are in phase and P_r is approximately equal to P_a . Consequently, the difference in the repository and the surface pressures is reduced resulting in a lower flow rate and displaced volume as indicated in Equation 5-2.

In comparing volumes of air displaced from the ES for various pressure events, it is apparent that the severe thunderstorm event is most significant, and the tornado event is least significant. As seen from Equation 5-12, when the frequency of the event is high (equivalent to a small period), the displaced volume is inversely proportional to the high frequency (proportional to the period) and is dominantly affected by it. The large pressure amplitude is of secondary importance for the tornado event. For a severe thunderstorm, the frequency is lower (by three orders of magnitude) and results in a higher displaced volume. The seasonal barometric pressure event is of intermediate significance. Because of the low frequency (equivalent to a large period) of this event, the ratio of the displaced air volume to the void volume in the ES at large, shaft fill, air conductivities approaches a constant of 0.7. This may be seen from Equations 5-6 and 5-12 in which the frequency of the pressure event is much smaller than the c constant. The substitution of the relationship for the c constant (Equation 5-6) into the displaced volume relationship (Equation 5-12) results in the displaced air volume approaching a constant where the air conductivity of the shaft fill is high and air flows dominantly through the fill of shafts and ramps.*

The results of the analysis for the horizontal emplacement option are similar to the results for the vertical emplacement option at low backfill conductivities for the three events. This is because at low, shaft fill, air conductivities, flow is dominantly through the MPZ of ES-1, which is

*The displaced volume of air approaches an asymptote, which depends on the initial air in the repository, the pressure amplitude, and the ratio of the conductance of the ES-1 flow path to the sum of the conductances of the other flow paths.

identical for the two emplacement options. At high, shaft fill conductivities, the ratio of displaced air volume to void volume of the ES is somewhat lower because of the smaller mass of air in the underground repository for the horizontal emplacement option.

5.4 Conclusions

From the barometric airflow analyses presented above, it is concluded that the ESs (including shaft fill and the MPZ) are not likely to be preferential pathways for gaseous radionuclide releases when the air conductivity of the shaft fill is less than about 10^{-1} m/min. This conclusion is reached because the volume of air in the ESs is not fully displaced during a broad range of meteorological conditions when the air conductivity of the shaft fill is less than about 10^{-1} m/min.

Further, if the air conductivity of the shaft fill is restricted to 3×10^{-4} m/min, as concluded from the convective airflow analysis, the proportion of air displaced from the ESs is computed to be very low for the three meteorological conditions considered.

- o For a thunderstorm event, the volume of displaced air from the ES is always computed to be $<1/10$ of the total volume of air in the shaft fill and the MPZ when the air conductivity of the shaft fill is $<3 \times 10^{-4}$ m/min. Even when the air conductivity of the shaft fill is high, less than approximately 0.1 m/min, the total volume of air in the shaft fill and the MPZ is not displaced.
- o For a tornado event, in all cases evaluated, the displaced volume of air is always less than the total volume of air for the shaft fill and MPZ. When the air conductivity of the shaft fill is 3×10^{-4} m/min, the amount of air displaced is always $<1/1,000$ of the total volume in the shaft fill and MPZ.
- o For a seasonal fluctuation event, in all cases evaluated, the displaced volume is always less than the total volume of air in the shaft fill and the MPZ. When the air conductivity of the shaft

fill is 3×10^{-4} m/min, the amount of air displaced is about 1/10 or less of the total volume of air in the shaft fill and the MPZ.

6.0 POTENTIAL FOR CHANGING THE CONDUCTIVITY OF THE SHAFT LINER, MODIFIED PERMEABILITY ZONE, SHAFT FILL, AND SHAFT SUMP

In this chapter, the potential for changing the conductivity of the shaft liner, the MPZ, the shaft fill, and the shaft sump is evaluated. Conductivity may be affected in two ways: chemically and hydraulically. When a concrete liner is placed in the ESs, it will alter the ground-water chemistry and in turn be altered by the ground water as shown in the analyses presented in this chapter. The expected changes are the result of alkaline species that leach from the cement, causing the concrete to become more permeable as the minerals dissolve. Similarly, the ground water that comes in contact with the concrete liner will become unstable when its pH is increased, and precipitates will form in the ground water. These precipitates will then lodge in pores within the shaft fill and in the MPZ. The potential for changing the hydraulic conductivity of the liner is evaluated in Section 6.1, and the effect of precipitate formation in the shaft fill and the MPZ is evaluated in Section 6.2. The effect of water percolating through the shaft fill and transporting fines to the shaft sump is discussed briefly in Section 6.3.

6.1 Effect of Elevated Ground-Water Temperature on the Conductivity of the Liner

It is anticipated that the concrete liner will be formed with conventional materials including aggregate, sand, and cement. For these formulations, the aggregate and sand portions of the concrete are essentially inert, and all chemical interactions occur with the cement phase. Also, the hydraulic conductivity of concrete depends almost completely on the hydraulic conductivity of the cement phase.

When ground water comes into contact with a cement, naturally occurring aqueous carbonate reacts with alkali and excess portlandite to modify the structure of the cement. Carbonate minerals are deposited within the pores of the cement, so that the natural tendency of the cement to shrink and crack will be partially offset by the deposition of new minerals.

In assessing how the hydraulic conductivity of the concrete liner may change as a result of chemical alterations, it is first important to know the initial hydraulic conductivity. The range of typical hydraulic conductivities for concrete is 10^{-8} to 10^{-6} cm/s, although hydraulic conductivities $<10^{-10}$ cm/s are achievable (Mather, 1967). Values for saturated conductivities obtained through laboratory testing of a grout, mortar, and a concrete (determined as part of the YMP Repository Sealing Program) varied from 1.6×10^{-10} to 9.5×10^{-10} cm/s (Fernandez et al., 1987, Appendix G).

Because the waste emplaced in the repository can elevate the temperature of the rock around the waste disposal area, it is important to know how the elevated temperatures could affect sealing components. Hydro-thermal experiments were performed at Pennsylvania State University (PSU) (Licastro et al., in preparation) to determine the effect of temperature and moisture on selected seal materials. Two of the materials (grouts and mortars) had the same composition as the grout and mortar reported in Fernandez et al. (1987, Appendix G). The hydraulic conductivity of these materials was evaluated at 38°, 60°, and 90°C after the materials were exposed to water with the same composition as J-13* water. Initial conductivities in all PSU cases were between 10^{-10} and 10^{-11} cm/s. These initial conductivities are at the low end of the range for grouts. For all of the materials evaluated, no increase in hydraulic conductivity was observed at 38°C over a 1-year period. At 60°C, one cement sample showed a small increase in conductivity after 30 days, with no other changes noted after that. Finally, at 90°C, one sample showed a small increase in conductivity after 90 days. It is recognized that the application of short-term, high-temperature experiments to long-term performance may require further evaluation.

Using the results of Blanford reported in Morales (1986), the temperature field for different portions of the liner can be approximated. We estimate that the temperature at the top 220 m of the shaft will always be

*Water from Well J-13 has been selected as the reference water for experimental studies in the YMP (DOE, 1988, pp. 4-39 and 7-10).

<38°C, and all but the 40 m above and below the repository horizon will always be <60°C. Because alteration of the shaft liner at 38° and possibly 60°C will probably be limited, as indicated by the laboratory experiments cited above, surface-water infiltration through the shaft liner will be impeded significantly.

From the preceding discussion, the potential for a four-order-of-magnitude increase in the hydraulic conductivity of the concrete liner is expected to be low. Therefore, the shaft liner will impede surface-water infiltration. Certainly, the assumption that the hydraulic conductivity of the shaft liner is 10^{-2} cm/s* is extremely conservative. This assumption implies that the hydraulic conductivity over the entire length of the concrete liner would have to change from a range of 10^{-6} to 10^{-10} cm/s to 10^{-2} cm/s.

If the liner at the base of the shaft behaves in a similar way, water within the shaft fill would be impeded from draining into the surrounding rock. This discussion suggests that if it is desirable to restrict surface-water flow, it would be prudent to leave the concrete liner in place above the repository horizon, particularly in the upper portion of the shaft where the temperature field is lower. If water drainage from the base of the shaft is desired, the liner should probably be removed below the repository horizon.

6.2 Effect of Ground-Water Chemistry on the Hydraulic Conductivity of the Exploratory Shaft Fill and Modified Permeability Zone

In addition to modification in the hydraulic conductivity of the shaft liner, the liner itself may cause minor modifications to the ground water, which may impact the conductivity of the shaft fill and the MPZ. In this section we provide a first approximation to these changes. In Section 6.2.1 we consider the consequences to the ground-water chemistry after contact with the concrete liner. Both analyses and experiments are presented to show that the primary change to the ground water is an increase in pH.

*This value represents a silty sand.

In Section 6.2.2 we show that when the pH of J-13 ground water is increased, calcium, magnesium and iron minerals are expected to precipitate. Both hand calculations and the computer code, WATEQ, are used to estimate the total volume of precipitate per volume of solution. It is assumed that all calcium, magnesium, and iron precipitate as their least soluble minerals. Section 6.2.2.1 considers the likely migration of these precipitates considering both diffusional rate processes and chemical kinetics. In Section 6.2.2.2 Berner's (1980) model of precipitate buildup in porous media is adopted, and precipitate deposition is described as a frontal advance. The frontal advance rates of the precipitates are presented in Section 6.2.3.

Water entering the ES could have a range of possible concentrations and a variety of compositions, depending upon the source of the water. These sources of water could be rainwater, water equilibrated with alluvium, water equilibrated with tuff, or any of a variety of ground waters. In this paper, we have assumed that the starting composition of the water is the same as Well J-13 water (Ogard and Kerrisk, 1984, pp. 9-12). In future work, we will consider the other possible choices as well as the use of the Computer Code EQ3/6 (Wolery, 1979).

We have also assumed that local equilibrium will apply throughout the ES. In actuality, several rate phenomena are operative. For example, leaching of minerals from cement is governed by the diffusion of ionic species in the pores of the cement and by the diffusion and dispersion of those same chemical species in the rock backfill and MPZ. There are also chemical kinetic rate processes to be considered. The rate processes already mentioned will tend to limit an increase in the pH of the ground water and limit the release of precipitates. Hence, the assumption of local equilibrium is a conservative one that leads to the maximum calculable change in the ground-water chemistry.

6.2.1 Leaching of Alkaline Species from the Concrete Liner

A typical Portland cement is composed of calcium silicate hydrate, tricalcium aluminate hydrate, and tetracalcium aluminoferrite hydrate. In the presence of sulphate, we also have an ettringite phase. In addition to these major phases, minor amounts of unreacted portlandite, Ca(OH)_2 , and

sodium and potassium alkalis are present. A typical Portland cement will contain between 0.05 and 0.15% of dissolvable alkali (Glasser et al., 1984). It is these alkalis that are primarily responsible for increasing the pH of any water that comes in contact with cement. As will be seen in Section 6.2.2, these alkalis are the primary cause of ground-water instability. Further, the cement pore fluid will contain increased concentrations of H_4SiO_4 , Na^+ , K^+ , OH^- , and perhaps $\text{SO}_4^{=}$. The actual concentration of these species in the ground water that comes in contact with the cement liner will depend on the flow rate of the water, where higher concentrations are expected at lower flow rates. Barnes (1983, p. 298) gives the pore fluid concentration of alkali as 0.75 M after 7 days of hydration. This corresponds to a pH of 13.88 for the pore fluid. After this initial small percentage of alkali has been leached from the cement, the pH of the fluid in the pores is dominated by the $\text{Ca}(\text{OH})_2$ equilibrium (Glasser et al., 1984) and is expected to drop to 12.5 (Lea, 1971, p. 185).

Leaching of cement is represented by the diffusion of Na^+ , K^+ , OH^- , and possibly $\text{SO}_4^{=}$ through the pores of the cement. All other ionic species are not expected to be present in significantly increased concentrations. In related experiments at PSU, B. E. Sheetz and D. M. Roy (in preparation) have considered the leaching of a particular ettringite-bearing concrete, Formulation 82-022,* by J-13 ground water. The test was an immersion test performed at 90°C for 4 months; the water-to-solid mass ratio was 10:1. Results of this experiment are shown in Table 6-1.

As may be seen in the Table 6-1, only the concentrations of the Na^+ , K^+ , $\text{SO}_4^{=}$, Si, and OH^- ions are significantly greater than in the J-13 composition. All other species are no more than 1 mg/l greater than their starting composition. Of these species, OH^- is potentially the most important in affecting the performance of the ES, as will be discussed in Section 6.2.2.

A diffusion model of the cement liner is postulated to estimate the concentration of ions that reach the ground water. The cement liner is a

* Formulation 82-022 is one of several cementitious mixtures evaluated in the YMP Repository Sealing Program.

Table 6-1. Chemical Analyses of Water Before and After Contact with PSU 82-022 Concrete

Species	J-13 Concentration, (a) mM (mg/l)	J-13 Concentration (b) mM (mg/l)	Concentration After 4-mo Contact with PSU 82-022 Concrete (b) mM (mg/l)
Al	.0010 (0.03)	<0.007 (<0.2)	0.008 (0.22)
Ca	0.29 (11.5)	.30-.41 (12.0-16.3)	0.181 (7.25)
Fe	0.0008 (0.04)	<0.0004 (<0.02)	0.006 ^(c) (0.34)
K	0.136 (5.3)	0.13-0.24 (5.1-9.5)	1.48 (57.9)
Mg	0.072 (1.76)	0.079-0.086 (1.93-2.1)	0.013 (0.32)
Na	1.96 (45)	1.56-1.78 (36-41)	5.70 (131)
Si	1.07 (30.0)	0.93-1.18 (26-33)	2.14 (60.1)
NO ₃	0.16 (10.1)	- -	0.15 (9.3)
SO ₄	0.19 (18.1)	0.20-0.24 (19-23)	0.54 (52.0)
HCO ₃	2.34 (142)	- -	1.85 ^(d) (113)

pH	6.9	7.7-8.13	9.9

(a) Data from Ogard and Kerrisk, 1984, pp. 9-12.

(b) Data from Sheetz and Roy, in preparation.

(c) Data taken after 3 months.

(d) Data taken after 2 months.

slab 30.5 cm thick, where the cement pore fluid is at equilibrium with the cement. Under this assumption the maximum flux of any ionic species may be determined through an adaptation of Example 11.1-2 in Bird et al. (1960, p. 354). Using the analog between heat and mass transport and differentiating the analogous expression for concentration versus distance, the flux may be calculated. As a result of the model, the maximum ionic flow occurs initially and is expressed as

$$\text{Flux} = \frac{2D_e(C_o - C_{\text{initial}})}{L} , \quad (6-1)$$

where $C_o - C_{\text{initial}}$ is the concentration in excess of the ground-water concentration of any ionic species within the cement pore fluid; L is the half thickness of the cement slab; and D_e is related to the cement void fraction, ϵ , and the molecular diffusivity, D_{AB} (Smith, 1970, p. 416) by

$$D_e = D_{AB}\epsilon^2 . \quad (6-2)$$

The concentration of species in the ground water passing below the shaft liner is then estimated by

$$C = C_{\text{initial}} + \frac{(C_o - C_{\text{initial}}) 2D_e A_{\text{shaft}}}{L Q} , \quad (6-3)$$

where A_{shaft} is the shaft liner surface area, and Q is the volumetric flow rate through the shaft and the MPZ. In Equation 6-3 the following values are used to determine the concentration:

$$\begin{aligned} A_{\text{shaft}} &= 4.17 \times 10^7 \text{ cm}^2, \\ \epsilon &= 0.28, \\ D_e &= 10^{-5} \text{ cm}^2/\text{s}(0.28)^2 = 7.84 \times 10^{-7} \text{ cm}^2/\text{s}, \text{ and} \\ L &= 15.24 \text{ cm}. \end{aligned}$$

Focusing our attention on the concentration of hydroxide with an initial pH of 6.9, the initial molar concentration is 7.94×10^{-8} M. The concentration of hydroxide in the cement pores, C_o , is 0.75 M (Barnes, 1983, p. 298). To evaluate the concentration of hydroxide in the ground water after contact with cement, the flow rate through both the shaft and the MPZ must be estimated. Flow in the shaft fill and the MPZ will be unsaturated

most if not all of the time. We have, however, allowed for the possibility of saturated flow in these zones; and during saturated flow periods, the flow rate is governed by the hydraulic conductivity of the shaft fill and of the MPZ. The concentration of hydroxide, expressed as pH, as a function of flow rate is shown in Figure 6-1. The concentration of other ionic species will be similar in shape to the pH curve shown in Figure 6-1 and inferred from Equation 6-3.

6.2.2 Chemical Equilibrium Model of Ground-Water Reactions

When ionic species, primarily hydroxide, are leached from the cement, these ions will interact with the ground water. As a consequence, it is shown below that some precipitation is expected as determined through the use of the computer code WATEQ developed by Truesdell and Jones (1974). This code was used to expedite the assessment of mineral precipitation for a large number of minerals. These precipitates may then lodge in existing pores and reduce the hydraulic conductivity of both the MPZ and the shaft fill. The purpose of the present analysis is to estimate the nature and quantity of the precipitates formed from the interaction of ground water with a concrete liner. This was accomplished by conservatively assuming that 100% of any ionic specie that tends to precipitate will do so in its least soluble compound. We leave, as a necessary adjunct to the present work, a detailed analysis of the interaction between ground water, tuff, and cement as a function of temperature. The estimates provided here, however, indicate the likely consequences of ground water making contact with a cement liner.

We have examined the equilibrium of J-13 water after several changes have been superimposed on the water chemistry. The base case was J-13 water using the water analysis presented in Ogard and Kerrisk (1984). Variations on this base case are increasing the pH to 9.5, the temperature to 100°C, and the Na^+ , K^+ , SO_4^- , and SiO_2 concentrations, each by an order of magnitude. These studies were performed using a water chemistry equilibrium code, WATEQ. WATEQ includes more than 100 equilibria and displays both ion activity products and equilibrium constants. When the ion activity product was greater than the equilibrium constant, a mineral would have a tendency to precipitate.

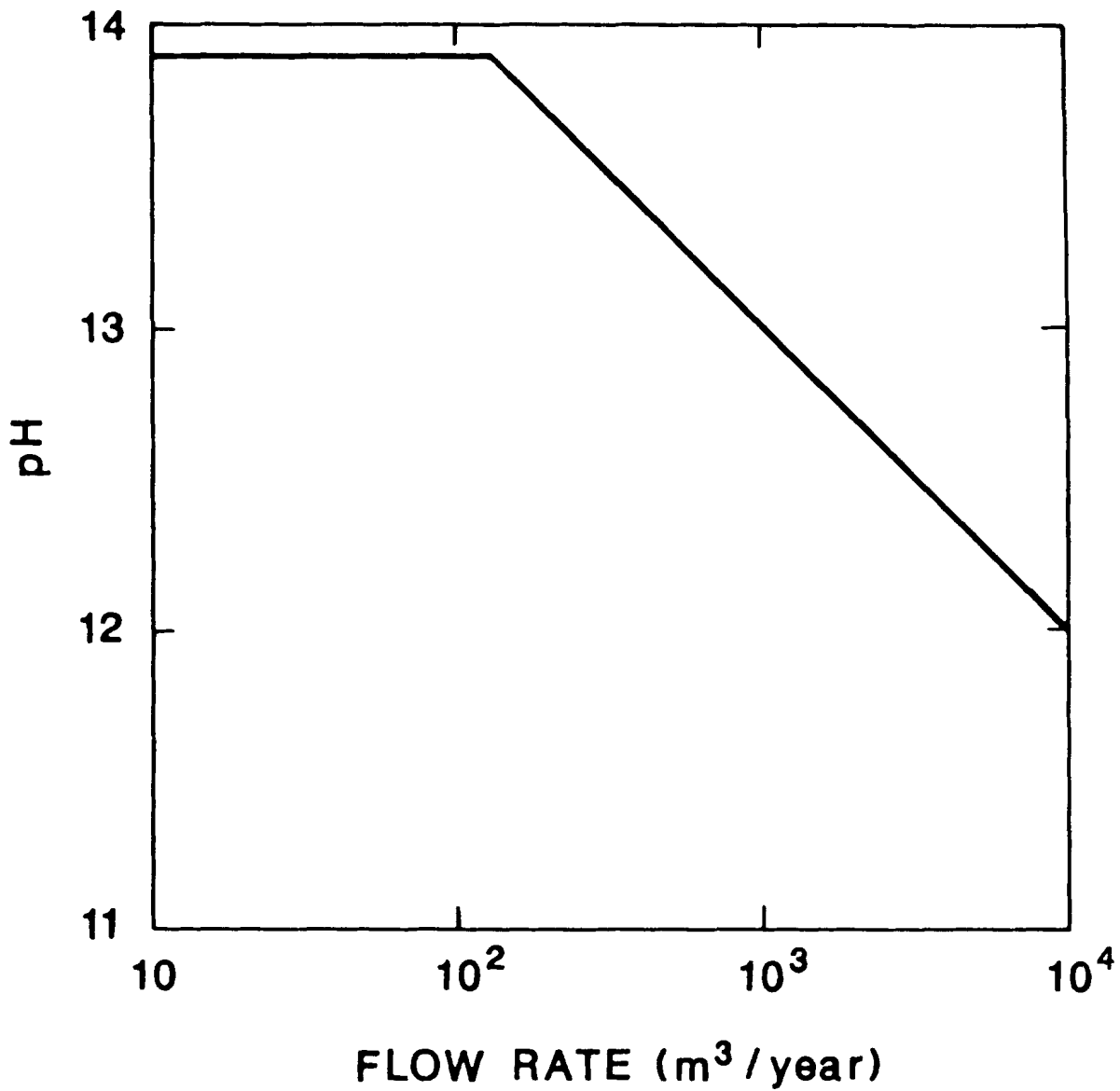


Figure 6-1. The pH of Water from Below the Shaft Liner as a Function of the Volumetric Flow Rate Through the Shaft or MPZ

For the base case, the J-13 water pH was taken to be 6.9, the water temperature 25°C, and the partial pressure of CO₂ was 0.033 atmospheres. While the Eh of J-13 water is not given in Ogard and Kerrisk (1984), the authors do state that the best estimates of water Eh at depth is given by the samples whose Ehs were -18 and -143 mv. Calculations using WATEQ indicated that the iron minerals, hematite, magnetite, and goethite are insoluble at these Ehs. Because these minerals would be expected to precipitate readily, the Eh was lowered to -256 mv to keep those minerals in solution. As will be seen below, the iron minerals exceed their solubility when the pH is increased, and it is a conservative assumption to set the solution Eh to -256 mv.

In the base case, 22 minerals had already exceeded their equilibrium solubility products. In every case, however, these minerals were aluminum bearing, with the least soluble of these being clay minerals. Further, the concentration of aluminum in J-13 water was reported to be 0.03 mg/l. By varying the aluminum concentration in J-13 water, it was determined that the maximum concentration of soluble aluminum was 1% of 0.03 mg/l; or by implication, practically all of the aluminum in J-13 water is present in microscopic clay particles carried along with the water. It is assumed that these clay particles are so small they would probably not clog the pores within the MPZ or the shaft fill.

Next we consider the effects of increasing the pH of the water to 9.5. In this case, WATEQ shows 14 new minerals as exceeding their solubility products. These minerals were aragonite (CaCO₃), calcite (CaCO₃), dolomite (CaMg(CO₃)₂), diopside (CaMgSi₂O₆), hematite (Fe₂O₃), maghenite (Fe₂O₃), magnetite (Fe₃O₄), goethite (FeO(OH)), Fe(OH)₃, siderite (FeCO₃), clinoenstatite (MgSiO₃), talc (Mg₃Si₄O₁₀(OH)₂), sepiolite (Mg₂Si₃O_{7.5}OH 3H₂O), and chrysotile (Mg₃Si₂O₅(OH)₄). The least soluble of these minerals, as determined by increasing the pH in small steps, is the iron mineral magnetite, followed by the magnesium and calcium minerals, talc, and calcite. If we assume that iron, magnesium, and calcium are all deposited as their least soluble mineral, then 37.9 mg/l of precipitate will form as a consequence of raising the pH of the J-13 ground water. Equivalently, the total volume of this precipitate formed per volume of solution is 1.40×10^{-5} , to be referred to as ν in the following text.

Other possible changes to the ground water were also considered in addition to raising the pH. We raised the temperature to 100°C and increased the concentration of the Na⁺, K⁺, SO₄⁼, and SiO₂ ions by one order of magnitude in each case. These additional changes caused some variation in the solubilities of the various minerals, but these variations are considered to be small. For example, when the temperature increases, calcite is actually less soluble than at a lower temperature. Thus, the mineral that accounts for the most precipitate will tend not to redissolve as the temperature is raised. Increasing the concentrations of Na⁺, K⁺, SO₄⁼, and SiO₂ similarly appears to have small additional effects, and detailed analysis of their effects has been postponed until a later date.

6.2.2.1 Migration of Precipitates

The precipitation of minerals from a supersaturated solution is a rate-controlled process. When considering the formation of calcite, solid calcite is found to precipitate at nucleation sites on existing solid surfaces rather than precipitating homogeneously (Berner, 1980). The rate at which further precipitate forms on existing nucleation sites is governed by diffusional rate processes because chemical kinetic rates are much faster than diffusional rates. In a quiescent fluid where the bulk of the fluid is supersaturated, excess ions will migrate to the solid surfaces and then precipitate causing the concretion to grow. As the fluid moves through the pores or fractures, the process of solid deposition is controlled by the rate of diffusion of ions from the bulk of the fluid to the walls of the pores or fractures. Where pores or fractures are narrowed by ongoing precipitation, further precipitation is favored because the length of the path of diffusion has been reduced (Figure 6-2).

The precipitates formed in the pathway of the fluid will result in the precipitate spreading out over a thin shell thus reducing fluid flow and hydraulic conductivity. Moreover, the precipitate will tend to seal off the MPZ and the shaft fill so that high conductivity will be reduced locally provided sufficient quantities of water enter the shaft fill and MPZ and react with the liner.

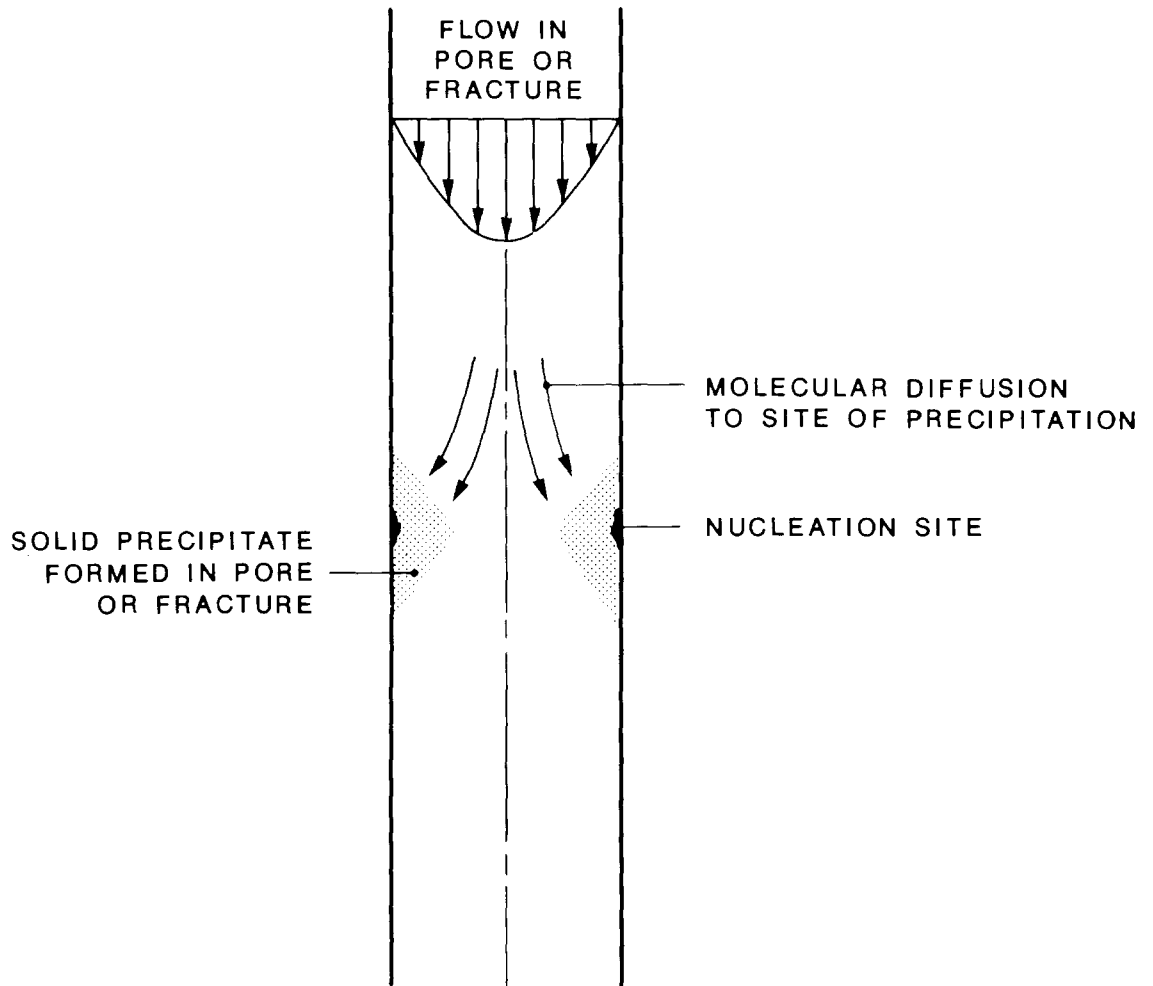


Figure 6-2. Deposition of Precipitate

To estimate how rapidly this shell will form, the time it takes for ions in the center of a pore to migrate to a pore wall must be considered. If we use the conservative Einstein relationship to describe diffusion, then

$$t = \frac{x^2}{D} \quad , \quad (6-4)$$

where t = the time for a molecule to migrate in a random way through a distance, x , and

D = the fluid diffusion coefficient.

The aperture of a pore or fracture is assumed to be 50 μm . Therefore, the value of x used in Equation 6-4 is 25 μm . Using a representative liquid diffusivity of $10^{-5} \text{ cm}^2/\text{s}$, the time for ions to migrate from the stream centerline to the wall is 0.6 s (Equation 6-4). In the more likely case, where flow occurs primarily within the matrix, the pore diameters are inferred to be 0.05 μm based on matrix hydraulic conductivities. In this instance, the migration time is 0.5 μs . Hence, we conclude that super-saturated solutions will not persist, and precipitate deposition will be almost instantaneous.

6.2.2.2 Model for Precipitate Deposition

A model describing the rate at which the buildup of precipitates occurs in the flow through porous media has been proposed by Berner (1980). In this model, a front of solid precipitate progresses through the porous media, and the void spaces behind the front are assumed to be completely filled. A small residual permeability is allowed so that the deposition process may continue. Beyond the front, the water is saturated so that no further deposition is assumed. As derived from Berner, the frontal velocity, U_F , is

$$U_F = \frac{\nu Q}{A(\Phi_U - \Phi_d)} \quad , \quad (6-5)$$

where

ν = the volume of precipitate per unit volume of water,

Q = the volumetric water flow rate,

A = the cross-sectional area of the flow,

Φ_U = the undisturbed porosity, and

Φ_d = the porosity behind the deposition front.

Based on Berner we assume that Φ_d is zero. Equation 6-5 may be applied to two regions: the shaft fill and the MPZ. Equation 6-5 is also applied for the modeled, anticipated flow rate of $44.2 \text{ m}^3/\text{year}^*$ and for flooding events where the fractures are saturated. This latter type of flow will be very transient in nature (flow for less than one-half year per event) and is expected to occur only infrequently over the lifetime of the repository.

6.2.3 Results

The normal flow of water passing through the MPZ and the shaft fill annually will be unsaturated. Within the matrix, the undisturbed porosity is 0.11. Within the shaft fill the porosity is assumed to be 0.3. The total flow of $44.2 \text{ m}^3/\text{year}$ is partitioned between the MPZ and shaft fill in proportion to the relative conductivities and areas. The frontal velocities in each case are then calculated from Equation 6-5 to be

$$U_{F \text{ MPZ}} = 0.1 \text{ } \mu\text{m}/1,000 \text{ year}$$

and

$$U_{F \text{ shaft fill}} = 0.2 \text{ m}/1,000 \text{ year} \text{ .}$$

In the anticipated water passage case, we conclude that no significant migration of precipitate occurs because the frontal velocities in both cases are small.

*This value, taken from Fernandez et al. (1987), is the amount of water calculated to enter the upper portion of each ES. In computing this number it was assumed that rain falls directly on the shaft fill. Any protective cover over the ES pad or seal within the shaft would substantially reduce this computed in flow.

At the other extreme of the water flow spectrum is the highly improbable PMF scenario presented in Appendix C, which assumes that the ES is located in alluvium. In this case, we assume that water flow fills the fractures and saturated flow results. Up to 20,000 m³ may enter the shaft in a single event. The hydraulic conductivity of the backfill is assumed to be 10⁻² cm/s, while that of the MPZ may vary between 60 x 10⁻² and 20 x 10⁻⁵ cm/s. The porosity of the MPZ for flow in fractures is assumed to vary between estimates (0.001 and 0.0001) for natural fractures (Erickson and Waddell, 1985, p. 1). The frontal advance in the MPZ behind the shaft liner is shown in Figure 6-3. While the advance of the precipitation front (Figure 6-3) may become as large as 60 m for the improbable flooding event described in Appendix C, this advance rate is appropriate only for flow behind the shaft liner. Once the flow advances beyond the base of the liner, the appropriate porosity is no longer the very small value assigned to fracture flow in the MPZ. Here, because of the intimate communication between the shaft fill and the MPZ, the porosity of the backfill allows the interstitial flow rate to decrease. As a result, the maximum frontal advance below the shaft liner is predicted to be 0.016 m/event. Within the shaft fill inside of the liner, the frontal advance is never >0.08 m for any of the above cases. Flow between the MPZ and the shaft fill can also occur periodically along the length of the shaft as a result of the horizontal joints in the liner. We have not taken credit for this communication in the above analysis, which would further reduce precipitate advance.

6.2.4 Conclusions

The deposition of solids from the interaction of the shaft liner with ground water will therefore most likely be a localized phenomenon, even considering highly improbable amounts of water, because

- o precipitation occurs rapidly after ground water contacts the shaft liner;

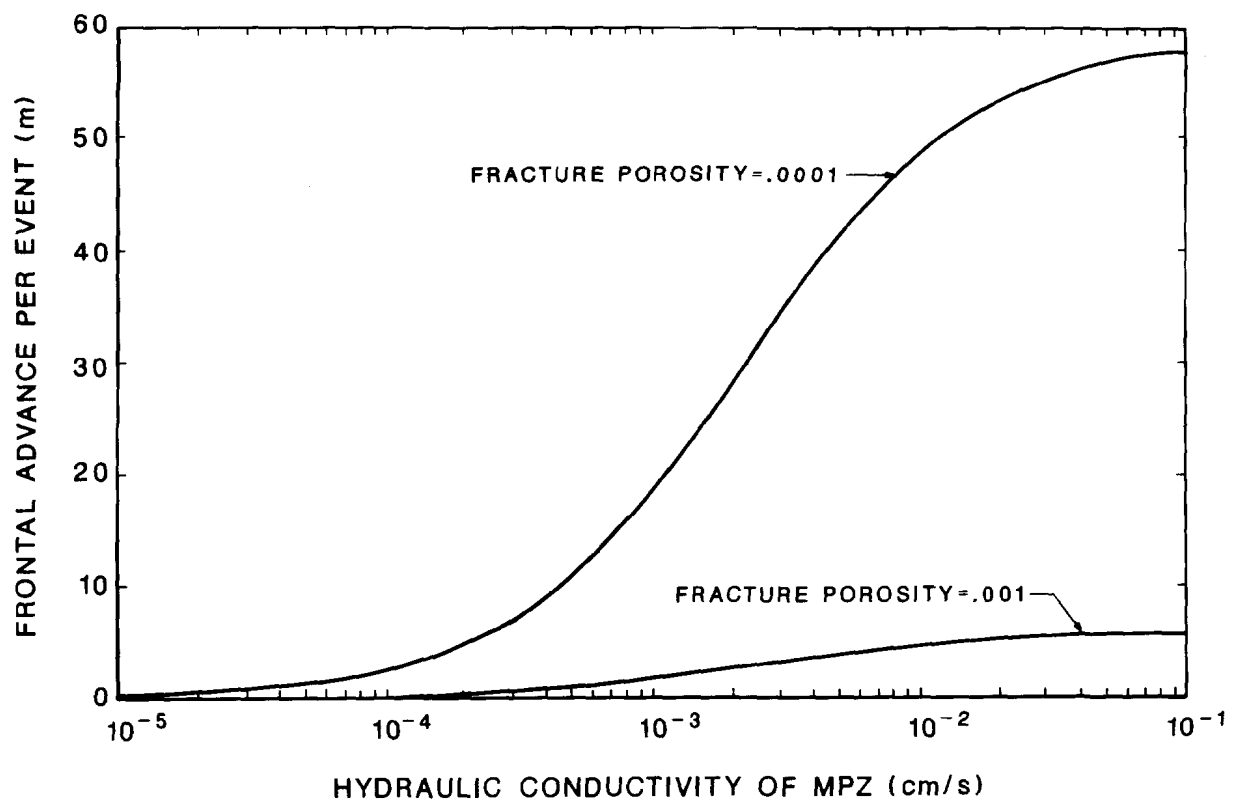


Figure 6-3. Advance of the Precipitation Front in the Modified Permeability Zone

- o precipitation occurs as a result of a progressively advancing front; and

- o the frontal advance is limited to regions near the shaft liner.

6.3 Effect of Fines Migration on the Hydraulic Conductivity of the Shaft Sump

As indicated in Chapter 2, the concept is to fill the majority of the shaft with a crushed tuff material. Depending on the preparation, placement, and consolidation of the shaft fill, fines may be introduced into the shaft fill. If the amount of water entering the shaft is sufficient to mobilize the fines, migration is possible. The potential consequence of fines migration, as discussed in this section, is a reduction of the hydraulic conductivity of the shaft sumps. As discussed in Chapter 3 and Appendix C, the shaft sump could perform effectively as a water drainage zone. It is necessary, therefore, to consider the effect of fines on the hydraulic conductivity of the shaft fill.

The sumps of the ESs are located in the densely welded, highly fractured Topopah Spring Member. Drainage through the Topopah Spring will occur predominantly through the fractures, under fully saturated conditions, because of their high conductivity compared to the conductivity of the matrix. Therefore, if sufficient water percolates down through the shaft fill and transports the fines, these fines could plug the highly transmissive fractures. It is our judgment, however, that fines migration, as discussed above, is not expected to significantly reduce the drainage capacity of the shaft sump for the following reasons.

First, the ES is located in a region where direct inflow of water is not anticipated. Hence, it is anticipated that the interstices of the rock backfill will be dry, and it is unlikely that a mechanism for significant fines migration will exist.

Second, the response of the unsaturated zone to periodic flooding is to rapidly remove water from fractures and backfill interstices to the rock matrix. The zone in which saturated flow exists is expected to be limited and even for the extreme case considered in Peters (1988), it does not

propagate below the Paintbrush Tuff nonwelded unit.* Hence, no significant mechanism for the movement of fines at the base of the sump is likely to exist.

Third, near-surface water diversion from the ES pad and an anchor-to-bedrock plug/seal will further limit interstitial water movement within the ES fill.

And finally, it is within accepted engineering practice to design specifically a layered system that is capable of stopping fines migration (Khilar et al., 1985). This type of barrier to fines migration works on the principle of physical exclusion of fines whose median particle size exceeds one-third of the median pore or fracture size (Abrams, 1977; Kelsall et al., 1982). In the case of the shaft sump, the average fracture aperture is not expected to be smaller than about 6 μm (DOE, 1988, Section 8.4.3.2.1.2), so that particles smaller than 2 μm will pass through these fractures without plugging the shaft sump. Theoretically, if the pore size between three spheres were 2 μm , the diameter of the spheres would be approximately 13 μm as determined from the relationship discussed by Herzig et al. (1970). Therefore, inclusion of this size of particle (13 μm) in a properly graded shaft fill could affect a reduction in the migration of fines that would plug fractures. A further indication of the ability to retard fines migration is suggested based on the work of Khilar et al. (1985), who concluded that a material whose hydraulic conductivity is 10^{-4} cm/s will have very large particle buildups.

*The case evaluated by Peters assumed a 10-m surface pond lasting for 2.2 days.

7.0 POTENTIAL FOR IMPACTING REPOSITORY PERFORMANCE RESULTING FROM PENETRATION OF THE CALICO HILLS UNIT BY THE EXPLORATORY SHAFT

7.1 Changes in the Sorption of the Calico Hills Unit as a Result of Elevated Ground-Water Temperature

Ground water entering the ES will be heated as it descends the shaft and MPZ to the repository horizon. From there it will continue downward to eventually cooler regions in the Calico Hills unit. As will be shown in Section 7.1.1, the temperature of this water will approximate the temperature of the rock surrounding the ES. Hence, the first consideration will be to determine the rock temperature in the vicinity of the ES. Using this temperature profile and the assumed phase condition within the shaft and MPZ, the temperature of the fluid entering the top of the Calico Hills unit is estimated next. The temperature of the fluid is then compared with the temperature required to maintain the mineralogical stability of Calico Hills zeolites.

7.1.1 Temperature Elevation of Water Entering the Shaft

The temperature of the ground water passing through the ES will increase globally because of the presence of the repository. Far-field calculations have been made by M. L. Blanford (Morales, 1985, pp. 36-39), assuming a thermal load of 57 kW/acre for the repository (SNL, 1987, p. 7-33). At a location approximating the ES at the edge of the repository, these calculations indicate that the temperature at the top of the Calico Hills unit 500 years after emplacement is expected to be 47°C and that the maximum temperature is expected to be 52°C. These temperatures are calculated assuming that conduction of heat is the only heat transfer mechanism and that there is no barrier pillar around the shafts. The temperature of the rock mass around the shaft in an area where waste is not emplaced will tend to be lower. Indeed, more recent results (Richardson, in preparation, Appendix B), which account for the presence of the barrier pillar, show that the maximum temperature at the top of the Calico Hills

unit will be $<40^{\circ}\text{C}$ assuming a thermal load of 57 kW/acre at the repository horizon.*

To address the thermal impact of the ES on water that might enter the Calico Hills unit, a separate analysis (Appendix G) has been conducted, which assumes various water flow rates downward through the shaft fill and the MPZ around the ES. These calculations were directed at determining the maximum water temperature at the base of the ES, entering the Calico Hills unit. Conservative assumptions in all cases reveal that the fluid temperature never deviated greatly from the formation temperature. Under the PMF water flow conditions where the temperature at the top of the Calico Hills unit was 52°C , the water temperature increase was 0.01°C above the rock temperature. Increasing the flow rate to correspond to the highly improbable PMF scenario presented in Appendix C, which assumes that the ES is located in alluvium, increases the water temperature by 0.8°C above the rock temperature. Hence, the formation temperature, computed assuming conduction alone, accurately approximates fluid temperatures within the ES and shows that the ES has little additional impact on the ground-water temperature.

7.1.2 Impact of Increased Ground-Water Temperature on the Sorption of the Calico Hills Unit

Within the Calico Hills unit, the principal zeolite phases are clinoptilolite, mordenite, and analcime. Of these, clinoptilolite is the most important sorbent phase (Daniels et al., 1982, p. 92 and Smyth, 1982, p. 195). Moreover, the ability of the Calico Hills to sorb radioactive materials at elevated temperature depends on two factors: the dependence

*The thermal profiles discussed here and presented in Appendix G (Figure G-1) show the repository at a greater depth than currently proposed. This assumption will result in a higher computed temperature at the repository horizon because the ambient temperature will be greater for the greater depth. Also, because Figure G-1 was developed assuming a greater depth and no barrier pillar, the computed rock temperature at the repository horizon and the top of the Calico Hills unit will be overestimated.

of the distribution coefficient (e.g., K_d^*) on temperature and the hydrothermal stability of the mineral phase, clinoptilolite. Also, as has been shown above, the upper limit of temperature computed in this discussion is approximately 52.8°C. The concern about the upper margin of the Calico Hills does not involve extreme temperatures but rather represents the potential impact of more moderate temperatures on the sorption potential.

The dependence of the distribution coefficient (e.g., K_d) on temperature has been addressed in several studies (Wolfsberg et al., 1979; Daniels et al., 1982; and Ogard et al., 1983). In these studies, increases in K_d are reported in every case for temperature increases of up to 85°C. Hence, it may be stated that the distribution coefficients of the Calico Hills minerals improve as temperature increases.

The second phenomenon to be addressed is the hydrothermal stability of the zeolite phases within the Calico Hills unit. Smyth (1982) and Smyth et al. (1981) report on two types of stability: dehydration stability and mineralogical stability. Dehydration reactions occurring up to 200°C are found to be reversible and will not be considered further. However, an irreversible deleterious mineralogical reaction is also observed. Clinoptilolite is a thermally sensitive mineral that undergoes transformations to mordenite and analcime. While the consequence of these transformations has not been investigated, it is assumed that the sorption potential will decrease. The exact transition temperature depends on the sodium concentration and pH. For conditions at Yucca Mountain, Smyth predicts a transition temperature of 105°C; at extreme sodium concentration levels, this transition temperature may drop to 95°C. Data gathered to date indicate that the actual temperature of any part of the Calico Hills unit will be less than that required to cause any significant reaction of clinoptilolite.

*The distribution coefficient is a parameter commonly used to describe the sorption behavior of radionuclides in geologic systems. The distribution coefficient, K_d , is defined as "the concentration per gram of a species on a solid phase divided by its concentration per milliliter in the liquid phase at equilibrium" (Wolfsberg et al., 1979, p. 4). The higher the K_d value, the higher the sorption potential of the material being evaluated.^d

7.2 Changes in the Thickness of the Calico Hills Unit Above the Ground-Water Table

An additional consideration associated with ES-1 is its penetration into the Calico Hills unit. Such a penetration can reduce the effective thickness of the Calico unit used in performance assessment calculations. The current YMP position is that any penetration associated with the ESF including ES-1 should not reduce the effective thickness (total thickness^{*}) of the Calico Hills unit to less than its minimum thickness anywhere within the perimeter of the repository. Figures 7-1a and 7-1b illustrate this point.

The Calico Hills unit can be divided into a nonzeolitic portion and a zeolitic portion. At the new ES-1 location, none of the nonzeolitic portion of the Calico Hills unit is present above the prevalent zeolites. The zeolitic portion of the unit (Figure 7-1b) is approximately 100 m thick at ES-1. Thus, the effective thickness of the Calico Hills unit will be about 100 m. This thickness is greater than the minimum thickness of the unit (70 m).

7.3 Conclusions

The impact of water percolating through the shaft fill and MPZ on the sorption potential of the Calico Hills unit has been found to be negligible. This conclusion has been reached for the following reasons.

- o First, water passing through the ES will be completely separated from waste stored in the repository and will not constitute a preferred pathway.
- o Second, if ES-1 penetrates 15 m into the Calico Hills unit as originally proposed, the minimum thickness of the Calico Hills unit will be preserved, while much valuable information is gained from sinking the ES into the upper margin of the Calico Hills unit.

*The total thickness of the Calico Hills unit at the ES locations can be obtained by adding the thicknesses of the vitric and zeolitic portions of the Calico Hills unit shown in Figures 7-1a and 7-1b, respectively.

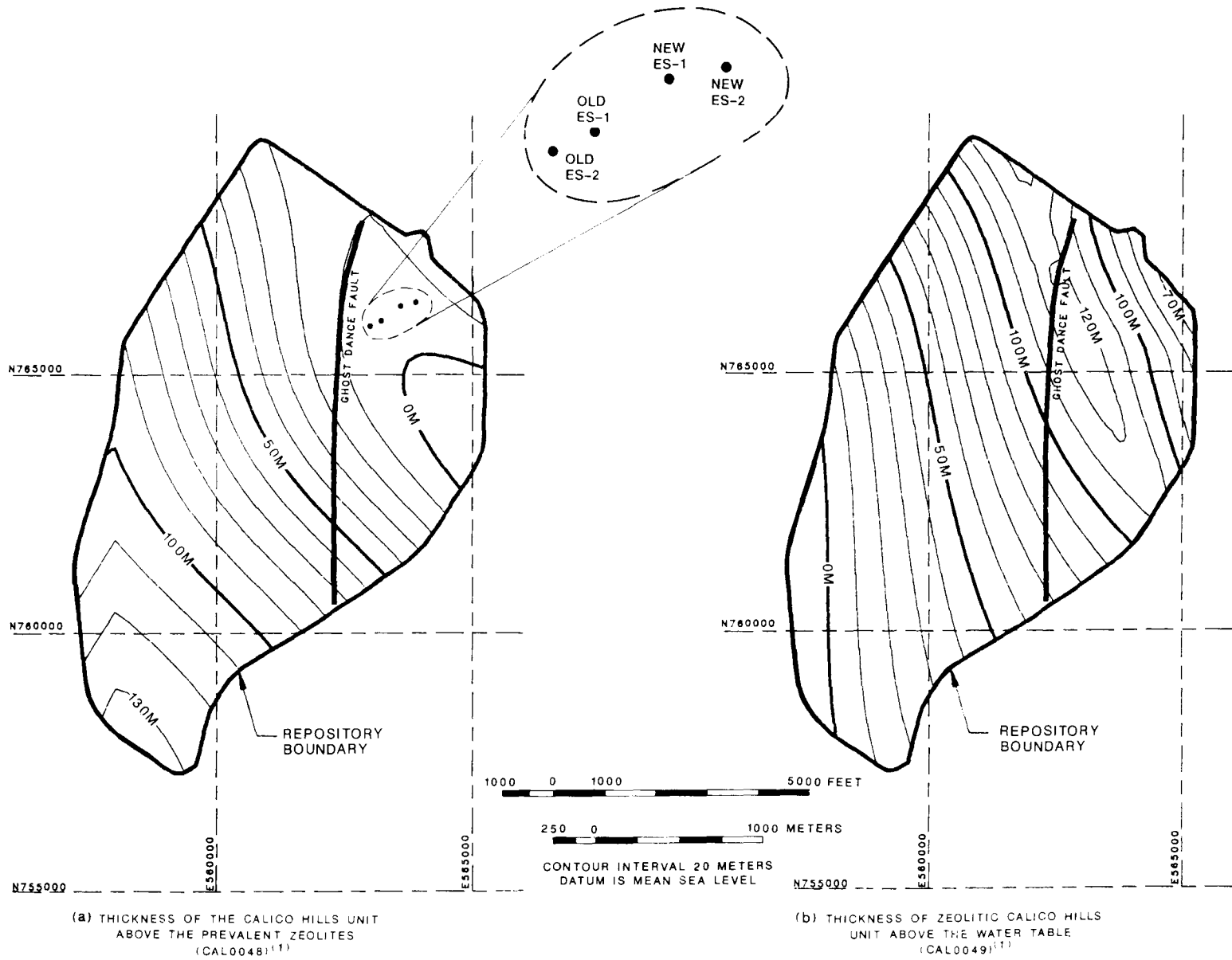


Figure 7-1. Contours of the Thickness of the Unsaturated Portion of the Calico Hills Unit Beneath the Repository

- o Third, if ES-1 is extended into the Calico Hills unit, the maximum temperature of the ground water percolating through the shaft fill is computed to be 52.8°C at the top of the Calico Hills unit, which is less than the minimum value of 95°C (Smyth, 1982, p. 195) observed to cause mineralogical transition of zeolites.

8.0 POSSIBLE REMEDIAL MEASURES TO MODIFY PHYSICAL FEATURES ASSOCIATED WITH THE EXPLORATORY SHAFT FACILITY

In this chapter, remedial measures are identified to remove the liner in the shafts (Section 8.1), to restore the MPZs surrounding the shafts (Section 8.2), and to restore the ES pad area (Section 8.3). Should future analyses indicate that these measures could significantly influence the performance of the repository, these measures can be implemented.

8.1 Remedial Measures to Remove the Liners from the Exploratory Shafts

Removal of the shaft liner will require breaking the concrete over some portion of the shaft and removing the chunks of concrete to the surface. Liner removal techniques are discussed in Section 8.1.1, and muck removal is discussed in Section 8.1.2.

8.1.1 Liner Removal

Six methods of breaking concrete (liner removal) are identified below:

- o handheld pneumatic breakers,
- o drill and blast,
- o drill and the use of a hydraulic splitter,
- o drill and the use of a nonexplosive demolition agent,
- o impact breaker, and
- o roadheader boom.

In the first four methods, it is assumed that several operations (drilling, breaking, and removing the liner; and backfilling the shaft) would be performed from a single stage that retreats from the repository as each cycle of operations is performed (Figure 8-1). In the production cycle, the concrete lining is removed upward, and the backfill is placed below the working stage. During this method of liner removal, approximately 10 m of the shaft wall is unsupported. It may be necessary to install occasional temporary support to facilitate muck removal and reduce the unsupported length of shaft wall in weaker zones. In the last two methods, the impact breaker or the roadheader boom (Figure 8-2) is mounted

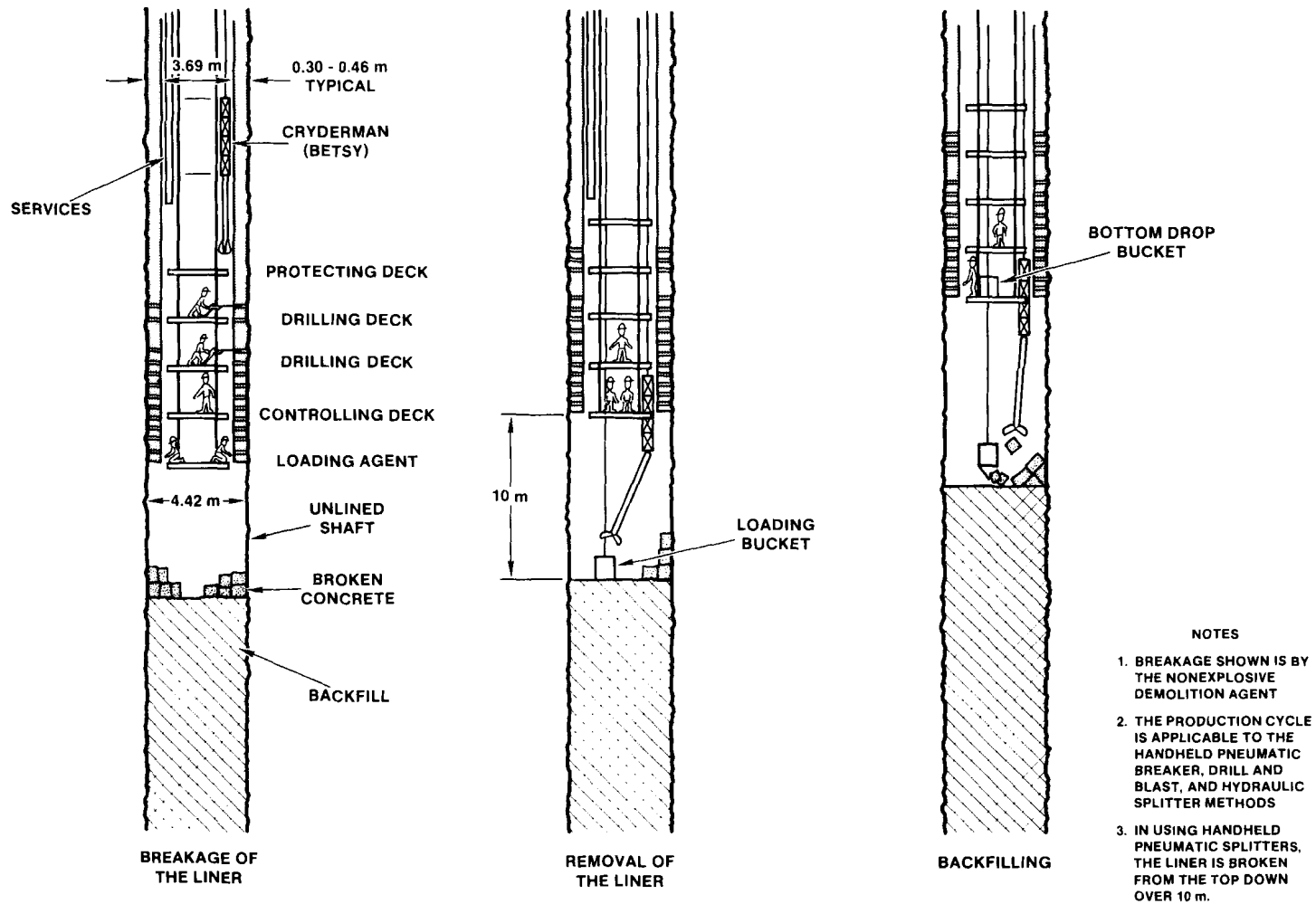


Figure 8-1. Production Cycle for Breaking and Removing the Liner and Placing the Backfill

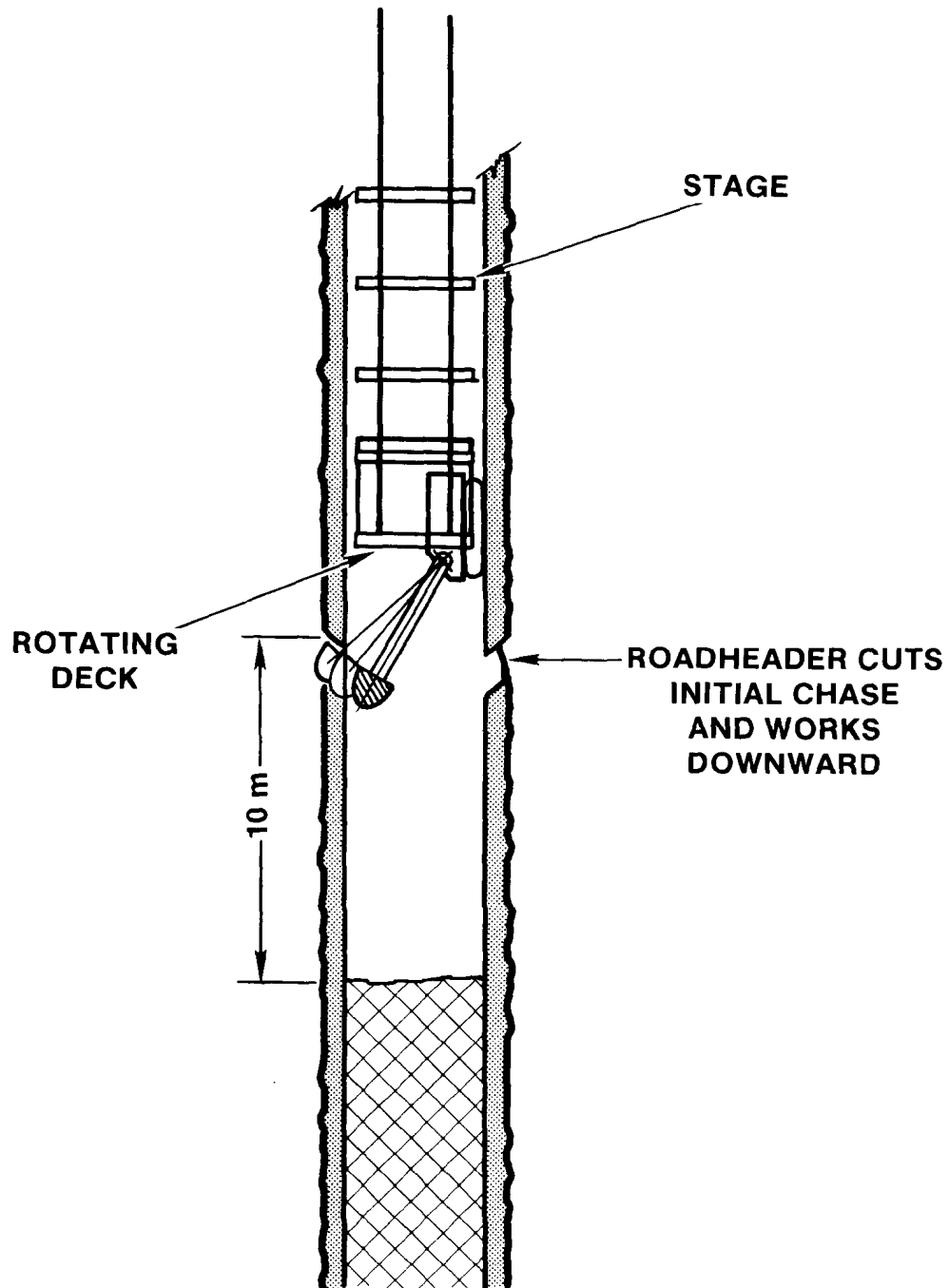


Figure 8-2. Breaking the Liner with the Roadheader Unit

on the base of one stage, and mucking and backfilling occur from a second stage.

Handheld pneumatic breakers have been used previously on high-strength concrete. In one unpublished experience at Blue Mesa Dam between Montrose and Gunnison, Colorado, pneumatic breakers were used to remove a 0.5-m lining of a spillway that was constructed of 25-year-old concrete with an unconfined compressive strength of 28 to 55 MPa. With handheld breakers, it is essential to maintain support at the breaker point; otherwise, when the liner fractures, support is lost and the breaker drops. To avoid this problem, a 10-m length of liner can be removed downward, or the breakers can be suspended by chains or other adjustable supports that would allow the liner to be removed upward. It has been estimated that horizontal drillholes would have to be spaced approximately on 0.3-m centers to break out the concrete.

The drill-and-blast method requires that horizontal drillholes with a horizontal spacing of 0.5 m and a vertical spacing of 0.3 m be loaded with explosives and the explosives be detonated. Drilling and loading operations are performed in series. During blasting, the stage is raised, and personnel are kept clear of the blasting area for about 30 minutes following each blast. Hole lengths penetrate the surrounding rock. This method is suitable where the liner is removed to enhance drainage, as discussed previously.

The drill and hydraulic splitter operate on the "plug-and-feather" principle. Pairs of wedges inserted into the series of drillholes penetrating the liner are forced apart, resulting in tension and splitting. It is estimated that this method would require twice as many holes as in the drill-and-blast method. Also, it is necessary to suspend the splitters on chains to retrieve them from the broken concrete. Hydraulic splitting is performed from the lower platform of the stage with drilling operations performed from the higher platforms.

Use of a drill and nonexplosive demolition agent consists of drilling holes and loading them with an expansive agent. The technique has been described by Dowding and Labuz (1982, pp. 1289-1299), in a series of tests to fracture rock and concrete. These authors and subsequent investigators

(Ingraffea and Beech, 1983, pp. 1205-1208) have interpreted tests on the basis of linear elastic fracture mechanics. It is estimated that a number of holes similar to the hydraulic splitter method would be required. The liner would be fractured 24 to 48 hours after placing the agent.

The impact breaker is mounted on a hydraulically operated boom and is suspended on ropes below the stage. Impact breakers mounted on rubber-tired base units have been used successfully to break concrete in surface operations. This unit breaks concrete at a high rate of speed and would have to be supported in a fashion similar to the handheld breaker. With this method, it is necessary to make a cut about every 10 m to break out the liner in the downward direction. Because of the limited space, it is not possible to muck out the broken liner and backfill unless the stage is removed after every 10-m lift.

The roadheader boom is used extensively in underground mining operations. Single head or double cutting heads are capable of excavating medium-hard rock (D'Appolonia, 1976, pp. 2-62 through 2-66) and are suitable for removing concrete liner. In this method, the roadheader boom is mounted below the base platform of the stage and can reach the liner from a single support point. It is best suited for cutting downward and has an advantage over the impact breaker because it can cut as it is being swung into the concrete lining. In this manner, it can readily make the first cut to allow removal downward. The use of hanging rods in the concrete liner, however, could complicate its removal using this technique.

The advantages, disadvantages, and equipment and material costs for several methods of removing the liner are summarized in Table 8-1. This study emphasizes conventional methods and gives preference to the use of equipment that has already been developed. The impact breaker and roadheader methods are not as practical as other methods for removing concrete from the muck pile because either one would have to be pulled out of the shaft to remove concrete and place backfill.

Further comparisons of production cycle times and costs for the four remaining methods are presented in Tables 8-2 and 8-3, respectively. These costs apply to complete removal of the liner from the base of the shaft to the surface. This cost comparison would suggest that the drill and

Table 8-1. Summary of Advantages, Disadvantages, and Cost of Liner Removal Methods(a)

Removal Method	Advantages	Disadvantages	Equipment and Material Costs
Handheld Pneumatic Breakers	There is experience in removing concrete liners.	The method is labor intensive and requires more production time. The method poses a potential safety problem if the breaker drops suddenly.	The cost of eight breakers and four drills is approximately \$15,000. Drilling equipment spares cost \$120,000.(b)
Drill and Blast	The method is well-known.	An overbreak zone may form. Drilling and loading operations cannot be performed simultaneously. Blasting would require raising the stage and clearing the area after each detonation.	The cost of six drills and four breakers is \$15,000; the cost of drilling equipment spares is \$57,000. The cost of explosives and caps is \$51,000.
Drill and Use of a Hydraulic Splitter	Drilling and splitting may occur simultaneously. The method is clean and does not leave chemical residue.	It is not as efficient as drilling and blasting. The method may need to be supplemented with hand methods such as the handheld pneumatic breakers. The splitters must be suspended to avoid being dropped into the broken concrete.	The cost of six drills and four breakers is \$15,000. Drilling equipment spares cost \$102,000. Rental costs for the splitters are estimated at \$54,000.

Table 8-1. Summary of Advantages, Disadvantages, and Cost of Liner Removal Methods (Concluded)

Removal Method	Advantages	Disadvantages	Equipment and Material Costs
Drill and Use of a Nonexplosive Demolition Agent	Drilling and splitting may occur simultaneously.	Operations must be carefully planned because a period of 24 to 48 hours is required for liner fracturing.	The cost for six drills and four breakers is \$15,000. Drilling equipment spares cost \$102,000. The cost of the expansive agent is \$306,000.
	The method has been used to fracture plain concrete (Dowding and Labuz, 1982, p. 1297).	The chemical agent could not be recovered from the muck pile.	
Impact Breaker		Mucking and backfilling operations must be performed from a second stage.	The initial costs of power and stage modifications are \$16,000 and \$8,000, respectively. A suitable unit with equipment spares may be rented at a rate of \$100.00/hour or an estimated cost of \$300,000.
		The breaker point must be supported.	
Roadheader Boom	No drilling is necessary, and the production rate is high.	Mucking and backfilling operations must be performed from a second stage.	The initial costs of power and stage modifications are \$18,000 and \$8,000, respectively. A suitable unit with equipment spares may be purchased for \$125,000.
	It can cut as it is being swung into the concrete lining so that it can readily cut the starting chase to allow downward excavation.	The roadheader boom has been used very little in shaft operations.	

(a) Note that the costs apply to complete removal of the liner.

(b) Drills are required to expedite liner removal and increase productivity.

Table 8-2. Comparison of Production Cycle Times for Various Methods Used to Remove Concrete Liners^(a)

<u>ACTIVITY</u>	<u>Number of Shifts</u>
<u>Handheld Pneumatic Breakers</u>	
Remove liner with pneumatic breaker	15.0
Muck out broken liner, 63 m ³	1.5
Backfill, 160 m ³	1.5
Remove 9 m of service lines	0.5
Allow for other hoist runs, movement of stage	<u>0.5</u>
Total	19.0
<u>Drill and Blast</u>	
Drill approximately 800 holes 0.6 m deep	2.0
Load 60% of the holes and blast	3.0
Muck out broken liner, 63 m ³	1.5
Backfill, 160 m ³	1.5
Remove 9 m of service lines	0.5
Allow for other hoist runs, movement of stage	<u>0.5</u>
Total	9.0
<u>Drill and Hydraulic Splitter</u>	
Drill 1,700 holes 0.6 m deep and simultaneously use splitter in 25% of the holes	4.0
Muck out broken liner, 63 m ³	1.5
Backfill, 160 m ³	1.5
Remove 9 m of service lines	0.5
Allow for other hoist runs, movement of stage	<u>0.5</u>
Total	8.0
<u>Drill and Nonexplosive Expansive Demolition Agent (NEDA)</u>	
Drill 1,700 holes 0.6 m deep and simultaneously load 25% of the holes with NEDA	4.0
Muck out broken liner, 63 m ³	1.5
Backfill, 160 m ³	1.5
Remove 9 m of service lines	0.5
Allow for other runs, movement of stage	<u>0.5</u>
Total	8.0

(a) Cycle times are calculated for a 9-m length.

Table 8-3. Comparison of Costs for Breaking Out the Concrete Lining and Rock^(a,b)

Cost Item	Handheld Pneumatic Breakers	Drill and Blast	Drill and Hydraulically Split	Drill and NEDA
Time	3,447	1,149	912	912
Equipment				
Drilling	15	15	15	15
Blasting Winch Rental		2		
Blasting Cable		17		
Firing Switch, etc.		2		
Consumables				
Drilling	120	57	102	102
Explosives and Caps		51		
Rental of Splitters		6	54	
Bristar				306
Total	3,582	1,299	1,083	1,335
Weeks	42.6	14.2	11.3	11.3

- (a) Includes only costs directly related to breaking out the entire concrete liner from the shaft, i.e., 420 m assumed in the old ES-1 design.
 (b) Thousands of dollars.

hydraulic splitter method is the most economical, although when offsite preparation, onsite preparation, and other costs are factored in (Appendix F), the differences in adopting any single method are not significant.

8.1.2 Muck Removal

Two methods of muck removal suitable for removing the broken liner are the

- o Cryderman mucker (The Betsy) and
- o remote controlled, orange-peel-grab unit.

The smallest Cryderman mucker would suit the small 3.66-m finished diameter of the ESs. This unit is normally suspended from the surface on a winch and held against the side of the excavation or concrete lining by a

frame-and-bolt arrangement. The unit is pneumatically operated and may be hoisted out of the area of the shaft stage while drilling and breaking operations are in progress. During mucking operations, the unit can remove broken concrete and place it in a conventional bucket hoisted through a trap door to the surface. During backfilling operations, the conventional bucket is replaced by a bottom drop bucket.

The other mucking method is the orange-peel-grab unit that operates below the stage (Figure 8-3). This unit is raised and lowered by a winch that operates from the bottom of the shaft stage. The broken concrete liner is loaded into a bucket that may be hoisted to the surface.

An alternative method of removing the broken liner when using hydraulic splitters or pneumatic breakers is to transfer the broken liner directly into a hoist bucket. This bucket could be positioned on a platform below the working level. In this arrangement broken pieces of material would be pushed to retractable chutes that empty directly into a central hoist bucket. The size of the concrete pieces could be controlled by making breakline cuts with circular saws equipped with diamond or high-strength carbon-steel blades.

8.1.3 Conclusions

After evaluating the advantages and disadvantages of methods to remove the liner, we selected the hydraulic splitter although the other approaches are technically feasible. Conventional equipment modified by suspending the splitters from chains may be used in this method. It is also possible that drilling and splitting patterns could be optimized by analyzing the effects of an array of splitters. Also, this method does not leave undesirable chemical residue. While supplemental hand methods may be required, this is not considered a significant disadvantage. Either of the two muck removal techniques are acceptable. It is recognized that additional efforts may be required during liner removal and backfilling operations to ensure safety. For example, in areas where additional stability is required (where the liner has been removed and no lateral support from the backfill is provided) additional shoring of the existing liner may be required. If necessary, other means of providing rock

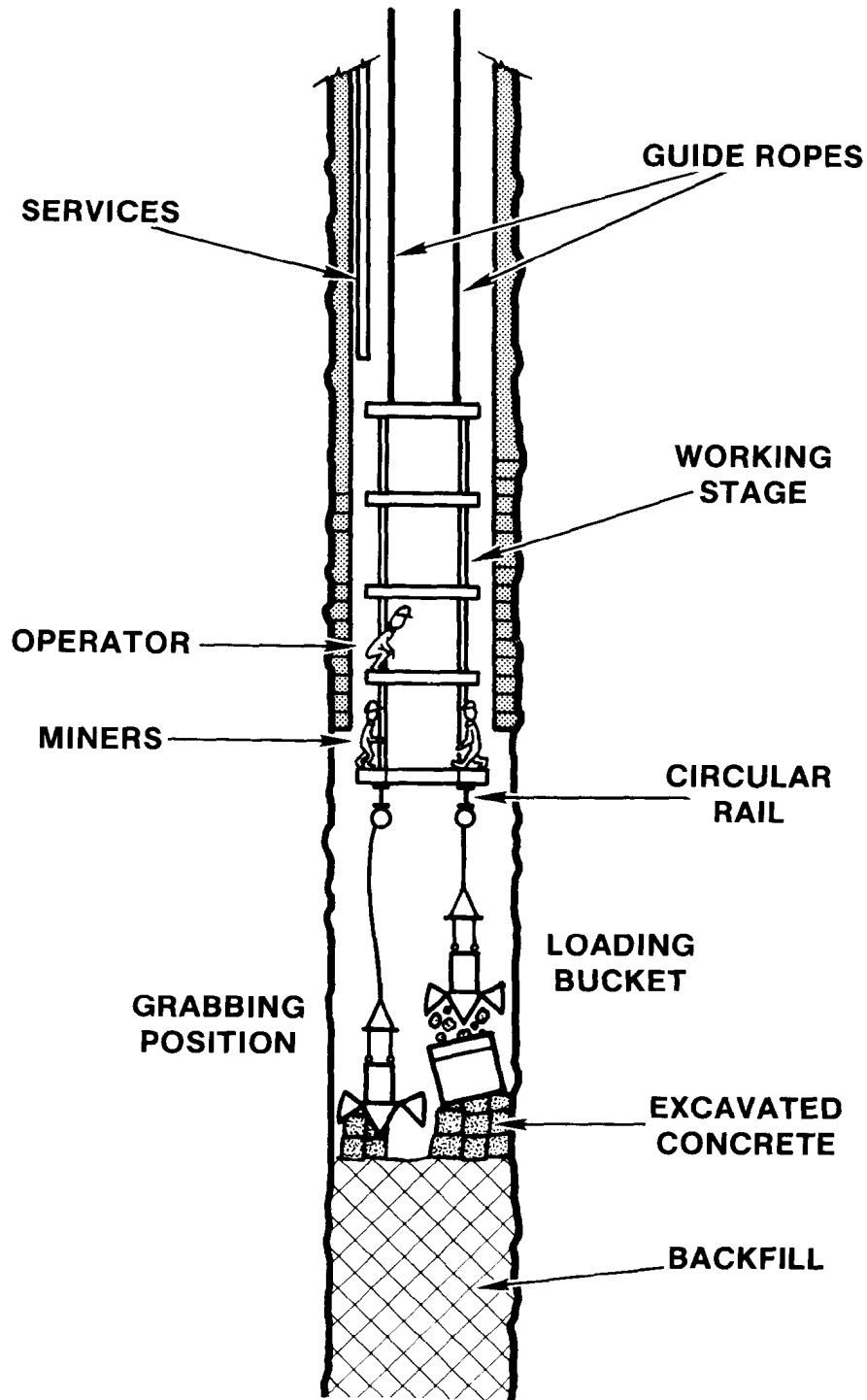


Figure 8-3. Removing the Pieces of Concrete Using the Orange-Peel-Grab Unit

support, such as rock bolts and wire mesh, can be used to achieve rock mass stability.

8.2 Remedial Measures To Restore the Modified Permeability Zone

When considering methods of restoring the MPZ, it is assumed that a plug would be constructed to reduce the flow of water down the shaft or the shaft and rock interface zone. It is further assumed that the plug is keyed into the rock (Figure 8-4). This provides the most direct treatment or localized restoration of the MPZ because when a keyway is excavated the more intensely fractured portion of the MPZ is removed. The structural performance of a plug keyed into the surrounding rock is also advantageous because overlying backfill loads are transferred in bearing compression to the surrounding rock. A plug keyed into the rock should exhibit a higher rigidity when subjected to thermal or seismic loads than a simple, nonkeyed plug.

The construction sequence entails making saw cuts at the top and bottom of the plug, removing the liner, excavating the keyway, backfilling to the underside of the plug, placing the concrete, and contact grouting. Initial saw cuts ~23 cm deep around the top and bottom of the plug are made. A series of holes is drilled horizontally at the top of the seal to the full depth of the keyway and perhaps loaded with an expansive agent. Because of the high strength of welded tuff, mechanical excavation of a keyway may not be feasible, and other methods similar to those used in liner removal supplemented by hand methods could be used for rock excavation. The keyway is fragmented and excavated over a length of several meters to provide a larger working area. Excavation of the keyway then proceeds from the top to the bottom of the plug. To accomplish this excavation, vertical holes are drilled in a precise pattern and loaded with an expansive agent from this working area to remove the rest of the keyway. The rock is removed to the surface. Fill is then emplaced to the base of the plug. The concrete is poured and allowed to mature for a period of time to achieve adequate strength and stiffness.

Methods for the treatment and restoration of the MPZ surrounding the keyway include

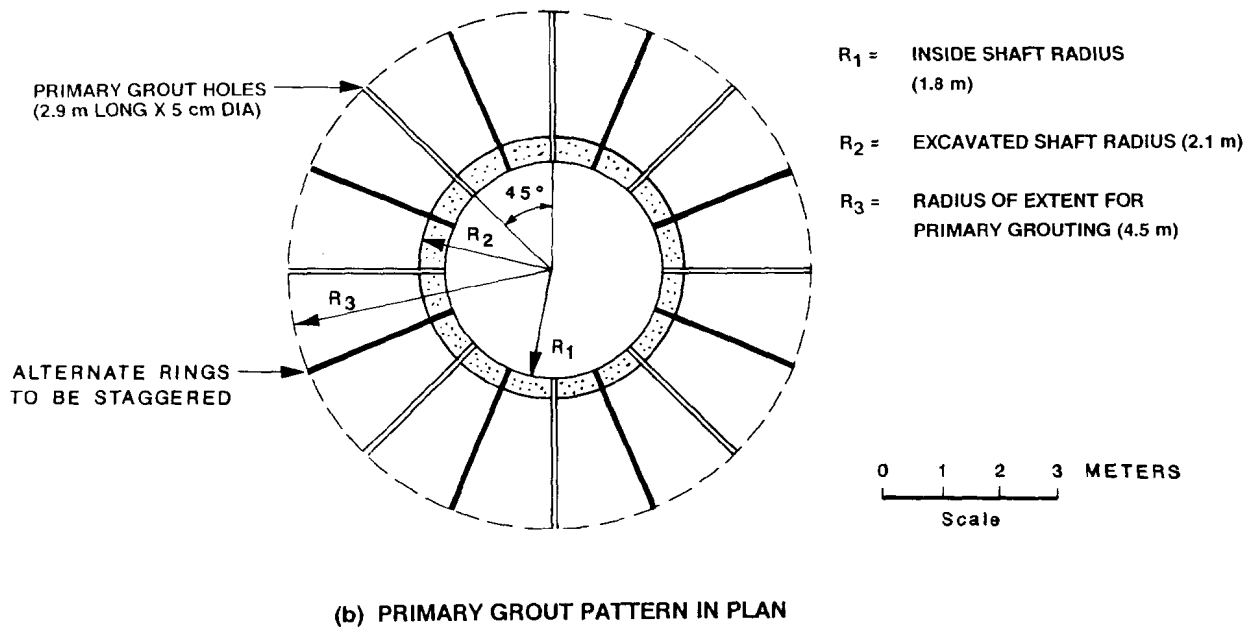
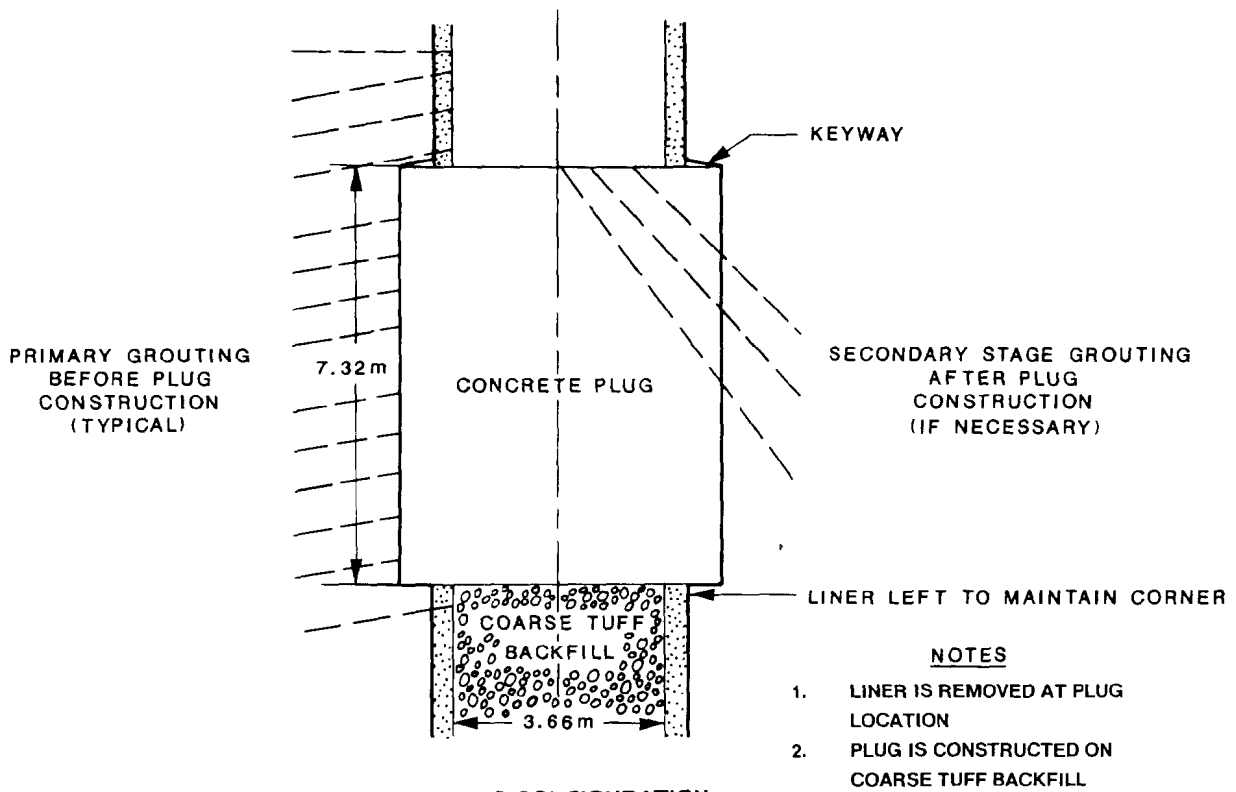


Figure 8-4. Restoration of the Modified Permeability Zone and Emplacement of the Shaft Seal

- o the use of an expansive concrete and temperature control to develop interface stress and close fractures in the MPZ and
- o primary and secondary grouting of the MPZ.

8.2.1 Restoration of the Modified Permeability Zone by Grouting

Emplacing grout in fractures is expected to reduce permeability in the MPZ. Grouting will reduce permeability in both the blast-induced and stress-induced fractures, irrespective of whether the rock deformed elastically or inelastically. However, grouting is not likely to increase rock mass strength significantly or increase structural stability. If grouting is needed, selection of the grout type and the method of grout application will be made based on the characteristic of the fractures defined during ES testing.

Grouting might be performed either before liner removal and plug emplacement (primary) or after liner removal and plug emplacement (secondary). There are advantages to pregrouting the plug location before removing the liner. After removing the liner, there would be a gap of approximately 0.6 m or more between the work stage and the shaft walls. It is easier to locate grout pipes on the smooth surface of the concrete liner. The grouting pattern might consist of a series of eight holes with alternate rings staggered. This pattern would result in a hole spacing of approximately 1.5 m near the shaft and 3.5 m at a distance of 4.5 m from the centerline of the shaft excavation (Figure 8-4). Note that the distance would depend on the size of the MPZ at the plug location. At the ends of the holes, only the open fracture zones would have continuity of grout between holes. By redrilling holes several times and grouting, a nearly impermeable barrier would be formed by a "laced" grout structure similar to the pattern proposed by Kelsall et al. (1982, p. 122) for drilled cutoffs.

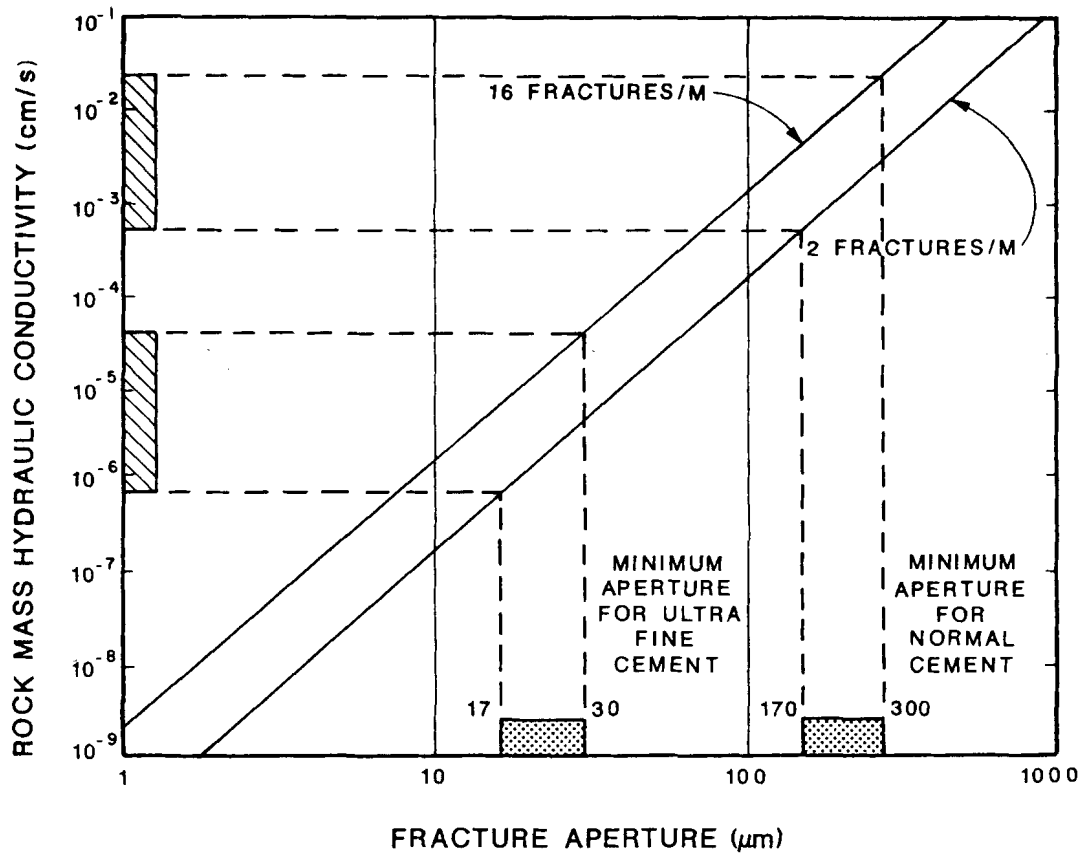
Primary and secondary grouting might be effective in reducing the permeability of the MPZ. A series of holes is drilled to intercept conductive fractures either before (primary) or after (secondary) plug emplacement. Grout with a small particle size and low viscosity is selected to penetrate

the thin fracture zones under pressure. Tests by the Waterways Experiment Station, (Kelsall et al., 1982, p. 113) showed that the ratio of crack thickness to grout particle size should be at least 1.7 and preferably 3.0 or more for adequate penetration. For ordinary cements, the maximum particle size is about 100 μm , but this can be reduced to 10 μm using ultrafine cement. Therefore, the minimum aperture that could be grouted is 17 to 30 μm . The relationship of rock mass hydraulic conductivity to fracture aperture over a range of fracture spacing (Langkopf and Gnirk, 1986) is shown in Figure 8-5. Over the expected range of bulk rock, saturated hydraulic conductivities for welded tuff of 10^{-5} to 10^{-2} cm/s (Fernandez et al., 1987), grouting is feasible using either a normal cement for a welded tuff conductivity of 10^{-3} to 10^{-2} cm/s or an ultrafine cement for a welded tuff conductivity of 10^{-5} to 10^{-6} cm/s.

While there is precedence for pressure grouting of shafts and tunnels under a variety of conditions (Dietz, 1982, pp. 602-608), there are a number of operational factors to be considered in constructing a grout curtain. These include the distance and time for transporting the grout, the injection pressure required, frictional losses through pipes, and grout setting time. At shallow depths, the use of packers may suffice to seal off sections of the injection hole; at greater depths, steel grout pipes may be required because greater injection pressures would be used. These factors increase the complexity of the design before field operations and require sampling the grout for physical properties during grouting.

8.2.2 Restoration of the Modified Permeability Zone Using Expansive Concrete

The use of an expansive concrete has been proposed elsewhere (Case et al., 1984). In this method, a concrete is selected that forms the expansive agent ettringite during cement hydration, resulting in volumetric expansion. The volumetric expansion in turn results in the development of interface stress, which will close fractures in the adjacent MPZ and thereby reduce the permeability in the MPZ. The degree to which volumetric expansion is effective depends on a number of factors: the temperature and moisture environment, evolution of the thermomechanical properties, and the



LEGEND

-  MINIMUM CONDUCTIVITY THAT MAY BE GROUTED USING ULTRA FINE OR NORMAL CEMENT
-  MINIMUM APERTURE THAT MAY BE GROUTED USING ULTRA FINE OR NORMAL CEMENT

Figure 8-5. Minimum Conductivity for Grouting

degree of external restraint. Placement temperatures affect volumetric expansion of the concrete. A lower placement temperature results in elimination or reduction of the heating and cooling cycle and the development of higher interface stress. In using an expansive concrete, it is desirable to pour the plug (250 m³) in one operation to avoid potential leakage paths through construction joints. Auld (1983, pp. 209-211) describes methods of cooling aggregates and mixing water to eliminate undesirable thermal effects. An alternative is to provide pipes, filled with circulating water during cement hydration, that are subsequently grouted.

The use of an expansive concrete to apply stress to the surrounding MPZ is most efficient where the stress-induced disturbance is caused by elastic deformation. If deformations are elastic, then the reapplication of stress would result in closure of fractures. If deformations are inelastic, then the reapplication of stress might not result in the closure of fractures and restoration of permeability. The use of an expansive concrete would result in increased rigidity and confining stress in the plug and surrounding rock. The structural stability of the plug, when subjected to backfill, thermal, and seismic loads, would be enhanced. There would be less tendency for shear failure at the interface between the plug and rock when the plug is subjected to combined loading.

The constructibility of the plug may be a key issue in the use of expansive concrete because use of an expansive concrete to restore an MPZ has not been demonstrated. As mentioned previously, the success of the method depends on control of moisture and temperature in the environment. Sampling concrete and monitoring temperature and other performance parameters may be required during and following construction of the plug. For these reasons use of an expansive concrete alone to restore the MPZ is not recommended.

8.2.3 Conclusions

From the preceding discussion, it is concluded that grouting in welded tuff is feasible and is currently the preferred method for restoring the MPZ. This method is preferred because drilling smooth-walled grout holes

allows an examination of fractures in the MPZ. Also, at present, it is not certain how large an interface stress can be developed through the use of only an expansive concrete or how effective such stress development would be in closing fractures.

Grouting the MPZ, however, does incur a greater cost. In Appendix F, the costs for liner removal in the vicinity of the plug and the construction of the plug are given. The estimated costs for pregrouting and constructing the plug are \$134,000 and \$380,000, respectively. At this stage of the design process, these costs are intended to be used only in a comparative way.

8.3 Remedial Measures to Restore the Exploratory Shaft Pad Area

The NWPA of 1982 requires that site characterization activities be conducted "...in a manner that minimizes any significant adverse environmental impacts..." Also, it is the intention of 43 CFR 3809, which discusses surface management of federal lands, "...to establish procedures to prevent unnecessary or undue degradation of federal lands which may result from operations authorized by the mining laws." Based on this guidance and because construction of the ESs will require modification of the land surface, some type of restoration of the ES pad will be considered.

Two strategies for remedial measures are discussed below. In Section 8.3.2 a strategy to further limit surface water infiltration is discussed, and in Section 8.3.3 a strategy to provide additional control of erosion is discussed. Section 8.3.1 briefly discusses the removal of rock and soil to construct the ES pad.

8.3.1 Excavation and Fill Required to Construct the Exploratory Shaft Pad

A pad will be constructed around each of the ESs that will result in removal of up to 17 m of soil and rock in the northwestern portion of the pad and up to 11 m of fill in the southeastern portion of the pad. Figure 8-6 displays contours of the cut and fill depths associated with the ES pad as configured during the Title I design of the ESF. Because the shafts are

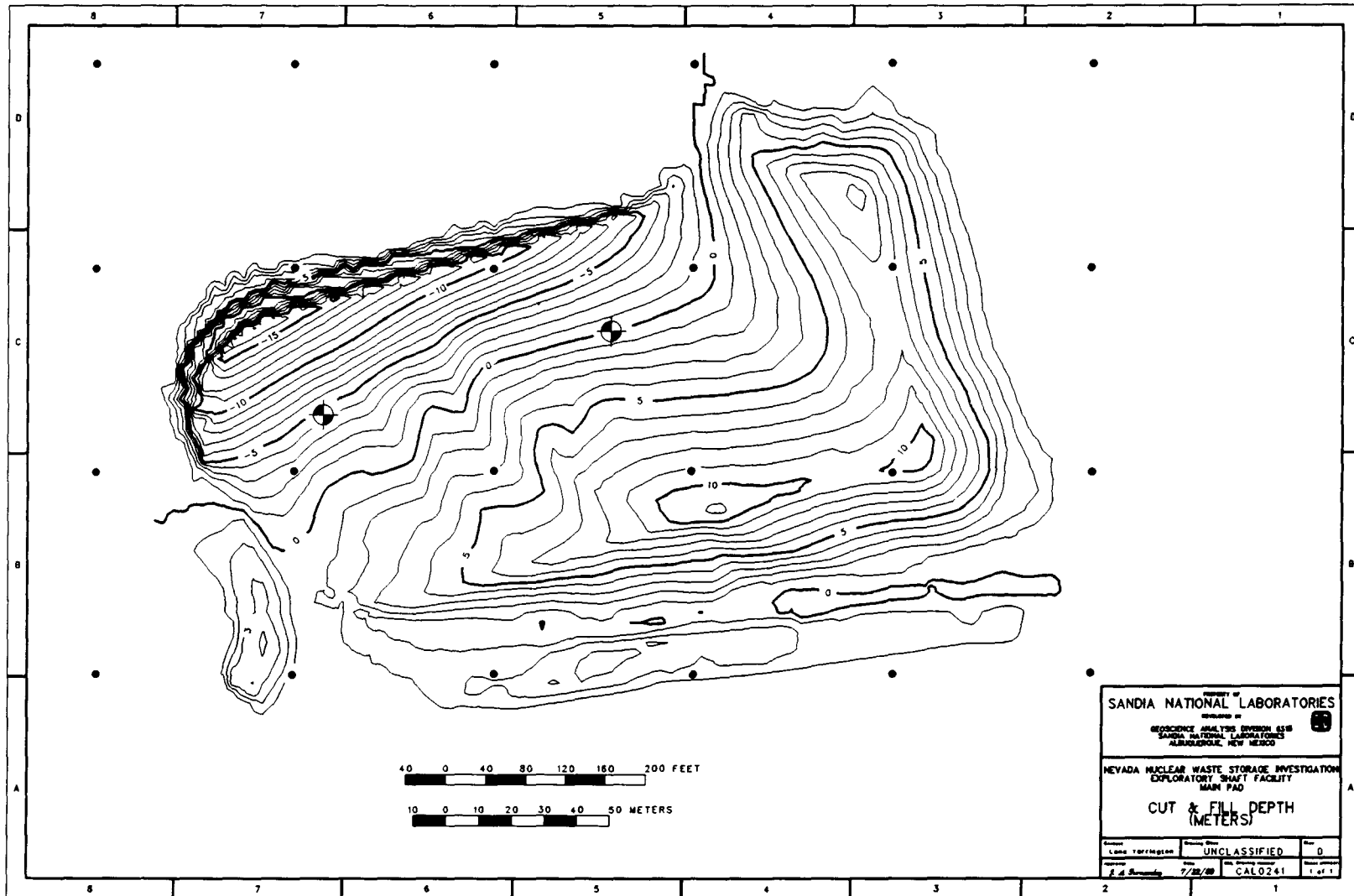


Figure 8-6. Contours of the Cut and Fill Depths Associated with the Exploratory Shaft Pad

located out of the alluvial-filled valley, the majority of the excavated material for the pad will be rock. A thin and discontinuous layer of rock fragments and soil is present at the ES location.

8.3.2 Design Strategies to Control Infiltration of Precipitation

As indicated in Section 3.2, the estimated, maximum amount of water entering both shafts was computed as 47.4 m³ during a PMF general storm event. The majority of the water would be expected to enter from precipitation falling directly on the pad or from sheet flow over the pad. Figures 3-12 to 3-15 illustrate the maximum zone of influence surrounding the shafts. These zones of influence indicate that some of the precipitation or sheet flow occurring within the zones reaches the shafts. Because the estimated maximum amount of water entering the shafts is small and, as concluded in Section 3.6, is not likely to influence the performance of the repository, a surface cover probably would not enhance the performance of the repository. Nevertheless, the following simple measures could be implemented to further reduce the small amounts of water that might enter the shaft, thereby, providing greater assurance that the presence of the shafts would not compromise the performance of the repository.

Because (1) the predicted maximum zone of influence in Figures 3-12 to 3-15 is generally no larger than the extent of the pad and (2) a layer of unsaturated soil at the surface would be expected to be very effective in controlling the downward infiltration of precipitation, a simple design reestablishing the original slope with a soil and soil-rock mixture could be effective in retarding vertical infiltration of water. This simple concept is depicted in Figure 8-7a. The entire soil sequence could be designed to retard vertical water flow while the upper layer could be designed to promote vegetative growth. This vegetative growth would not only increase the evapotranspiration rate over the pad area when compared to the evaporation rate over a bare soil but also be expected to increase erosional stability.

Another design concept incorporates alternating layers of coarse- and fine-grained materials that could also result in an effective barrier under unsaturated and saturated flow conditions (Finley et al., 1985). This

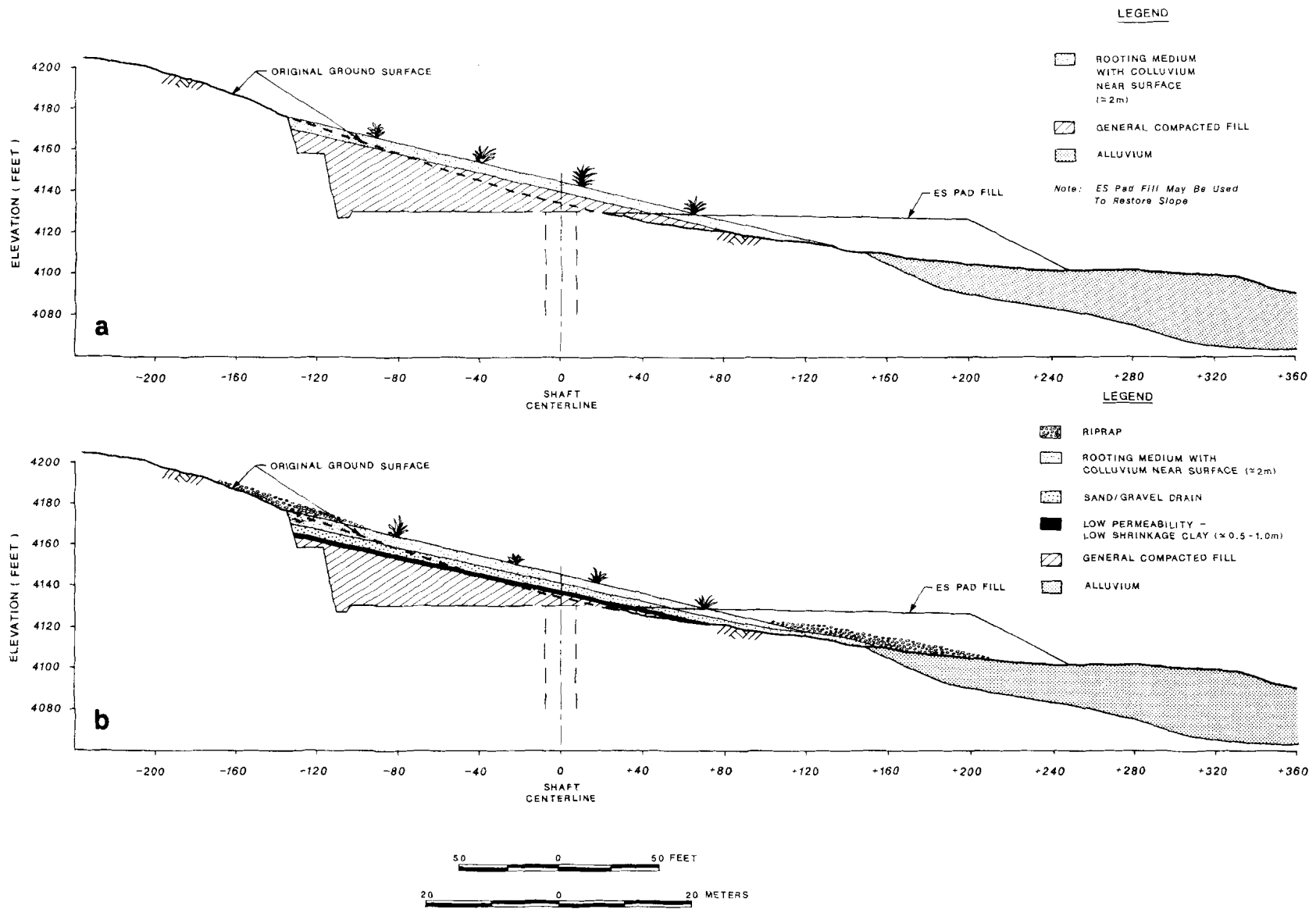


Figure 8-7. Reestablishing the Original Slope in the Area of the Exploratory Shaft

design is illustrated in Figure 8-7b. In this figure the uppermost layer could in itself retard flow. Its effectiveness would depend on its saturated and unsaturated properties and its initial saturation state. Under unsaturated conditions, this fine-grained, upper layer combined with an underlying layer of coarse sand can provide a capillary barrier to infiltration (Herzog et al., 1982). Under saturated conditions that may occur during intense precipitation events, the volume of moisture in the upper layer would increase, and the effectiveness of the capillary barrier would decrease. The upper layer, when fully saturated, would still tend to reduce vertical infiltration because it has a lower hydraulic conductivity than the underlying sand layer. As water enters the coarse-grained material from the saturated upper layer, it can be transported laterally as a result of its high hydraulic conductivity. A very low hydraulic conductivity material is placed beneath this coarse-grained material to enhance lateral drainage (Maestas et al., 1985). Lateral drainage could be facilitated by sloping the layers as illustrated in Figure 8-7.

To increase the effectiveness of the alternating layers concept above, reducing the possibility of fines migration from the uppermost layer into the coarse layer should be considered. A filter criterion such as that recommended by Keshian et al. (1985) may be appropriate. This recommended criterion is

$$\frac{D_{15_{\text{filter}}}}{D_{85_{\text{soil}}}} < 5 \quad ,$$

where

$D_{15_{\text{filter}}}$ = the particle diameter at which 15% of the soil by weight is finer for the coarse-grained material; and

$D_{85_{\text{soil}}}$ = the particle diameter at which 85% of the soil by weight is finer for the upper soil layer.

The coarse-grained material will be expected to prevent the excessive movement of fines and passively act as the filter provided not more than 5%

of the coarse-grained material passes the No. 200 mesh and the gradation curves of the two materials are approximately parallel in the fines-sized range.

An additional concern is the need to prevent cracking of the clay layer beneath the coarse-grained material. As reported in Herzog et al. (1982), a minimum of 2 ft of soil above the clay layer is recommended.

The concepts above indicate that these technically feasible approaches can be adapted to provide additional assurance that shaft inflow can be reduced. Future evaluations of these restoration activities on the flow into the shafts can be performed to show their effectiveness in reducing flow.

8.3.3 Design Strategies to Control Erosion

Remedial measures to control erosion of soil from the pad area include emplacement of riprap, especially at the base of the restored slope. If it was determined that a multilayer cover would be needed to maintain the slope, then a cover composed of a coarse layer and a fine layer of riprap could be placed over the slope. The cover design would consider the grain size of available materials; the velocities of floods for overland flow that may contact the cover considering the PMP and PMF events for drainage tributary to the pad; erosional factors (areas of potential concentration of flow or areas where changes in bedslope occur); and construction requirements.

Keshian et al. (1985) provide a method for the selection of the riprap to protect underlying layers. The layers could be designed against the erosive forces associated with the PMP resulting in overland flow for the area of interest. The riprap sizing will depend on the precipitation intensities and runoff velocities.

An alternative remedial measure that could contribute to controlling slope erosion is to restore the vegetation. Habitat restoration needs at Yucca Mountain are summarized by Mitchell (1984). Some generalized "rule-of-thumb" activities cited by Mitchell are the following.

- o Stabilize soils before planting. Because reestablishing the original land contours would require adding up to 17 m of fill, the majority of the fill above the pad would probably be a crushed rock and soil mixture.
- o Prepare a good seedbed that will hold seeds and "harvest" later.
- o Use native plant species the are adapted to the local environment.

Revegetation of the ES area once the slope is built up to the original land surface can be expected to contribute not only to erosion control but also to a potential increase in the evapotranspiration rate, which will tend to maintain a "drier" soil profile. A thickness of about 2 m for the upper layer is expected to be sufficient to contain the root systems of shrubs that could be used to provide erosion control over the recontoured slope. An evaluation of root systems of some shrubs by Wallace and Romney (1972) indicates that the vertical depth of the root systems is <2 m.

Restricting root penetration may be desirable to maintain good drainage through the coarse-grained layer beneath the surface layer and to avoid penetration of the low permeability soil layer beneath the coarse-grained layer.

8.3.4 Conclusions

As stated in Section 3.6, the presence of the ESs is not expected to compromise the performance of the repository with respect to water infiltration into the shafts. This conclusion was reached assuming no restoration of the ES pad occurs. Nevertheless, restoration of the ES pad area, could potentially reduce even further the amounts of surface water predicted to possibly enter the shaft. While additional work is necessary to develop a specific design, some simple, technically feasible concepts are proposed to provide additional assurance that precipitation entering the shafts and erosion will be limited.

9.0 CONCLUSIONS

The analyses in this report support the overall conclusion that the design and construction of the ESs, as currently planned, are not expected to significantly influence the performance of the potential nuclear waste repository at Yucca Mountain. Not all analyses related to the ES performance are presented in this report. Specifically, additional analyses and scenarios are considered in Section 8.4 of the Site Characterization Plan (DOE, 1988). In this report, a reasonably conservative approach was used. This approach incorporated evaluating various radionuclide release mechanisms, evaluating variations in site-specific properties when performing the numerical analyses, and considering the potential modifications on the rock mass resulting from construction of the ESs. Some specific conclusions reached in this report that support the overall conclusion are given below.

- o Flooding and erosion at the current shaft locations are not expected to adversely affect long-term repository performance. In reaching this conclusion, surface-water infiltration, sheet flow, and erosion potential were considered. The estimated amount of water entering the shafts and their associated MPZs from a PMF event is small, 0 to $<50 \text{ m}^3$ (Section 3.2), compared to the estimated storage (830 m^3) and drainage ($17,700 \text{ m}^3/\text{year}$) capacity of the ESF and ES sumps (Section 3.2.6). Because both the storage and the drainage capacity of the ESF are much larger than the maximum inflow of 50 m^3 , this water entry is likely to have no significant effect on repository performance. Erosion at the ESs should not impact the performance of the repository by directing waters directly into the shafts because of the anticipated low erosion rates for the Tiva Canyon Member, the lateral incision into bedrock required to reach the ESs, and the horizontal and vertical separation of the ESs from the PMF channel.

- o The ESs (including shaft fill and MPZ) are not likely to be preferential pathways for gaseous radionuclides if the air conductivity of the shaft fill is less than about $3 \times 10^{-4} \text{ m/min}$. In reaching this conclusion, both convectively driven airflow and

barometrically driven airflow were considered. For convective airflow, when the air conductivity is less than about 3×10^{-4} m/min (Chapter 4), airflow out of the ESs is less than about 2.5% of the total airflow out of the repository. This value of 2.5% is one order of magnitude less than the airborne performance goal established for the shafts in Fernandez et al. (1987). From the barometric airflow analyses presented in Chapter 5, it is concluded that the ESs (including shaft fill and the MPZ) are not likely to be preferential pathways for gaseous radionuclide releases if the air conductivity of the shaft fill is less than about 10^{-1} m/min. This conclusion is reached because the volume of air in the ESs is not fully displaced during the occurrence of a broad range of meteorological conditions and because shaft fill with an air conductivity of 10^{-1} m/min can be emplaced (Fernandez et al., 1987, Appendix D).

- o Precipitation and siltation in the shaft are not likely to have a significant or adverse effect on the drainage capacity of the ESF and sump. In reaching this conclusion, geochemical interaction of the shaft liner with ground water and the migration of fines through the shaft backfill were considered. The deposition of solids from the interaction of the shaft liner with ground water will most likely be a near-surface phenomenon, even considering highly improbable amounts of water. Therefore, the effectiveness of the ES sumps to drain is not expected to be reduced significantly (Chapter 6).

The migration of fines is expected to be limited because water movement in the shafts is limited. In particular, the shafts are located out of a region of direct water inflow; the matrix imbibition potential of the rock in the unsaturated zone will further limit free water movement; and seals and surface drainage features can be expected to further limit water movement. Additionally, an engineered fines migration barrier may be constructed (Chapter 6).

- o Simple and technically feasible remedial measures are available, which can provide additional assurance that the postclosure

objectives for the repository can be achieved. These remedial measures include removal of the liner, emplacement of a shaft seal, and restoration of the ES pad (Chapter 8).

- o The impact of episodic water percolating through the shaft fill and the MPZ on the sorption of the Calico Hills unit is believed to be negligible (Chapter 7). It is assumed that the temperature of this percolating water becomes slightly elevated as it passes through the repository horizon. Although ESSs are currently not planned to penetrate into the Calico Hills unit, this evaluation is presented in the event that a decision is made to penetrate this unit.

APPENDIX A

POTENTIAL FOR RADIONUCLIDE TRANSPORT

CONTENTS

	<u>Page</u>
A.1 Downward Water Movement Through the Shafts	166
A.2 Downward Water Movement in Fractures from the Repository Horizon to the Base of the Exploratory Shafts	167
A.3 Upward Movement of Water in the Sumps of Shafts	170
A.4 Transport as a Result of Solid-Solid Diffusion	171
A.5 Gaseous Transport as a Result of Diffusion	172
A.6 Gaseous Transport as a Result of Convective Forces	175
A.7 Gaseous Transport as a Result of Barometric Forces	176

FIGURES

A-1 Results from the Green and Ampt Solution for Transient Flow Through Shaft Backfill	168
A-2 Detailed Repository Layout in Vicinity of the Exploratory Shaft Facility	169
A-3 Concentration of Two Gaseous Systems as a Result of Binary Gaseous Diffusion	174

APPENDIX A

POTENTIAL FOR RADIONUCLIDE TRANSPORT

The purpose of this appendix is to provide a perspective into the potential for radionuclide transport as a result of the presence of the exploratory shafts (ES). To provide this perspective, descriptions of several mechanisms that can potentially enhance radionuclide releases from the underground facility are given. These descriptions are supplemented by simple calculations that compute the travel distance and/or travel time of the transporting medium. The authors recognize that these mechanisms do not represent a comprehensive evaluation of all conceivable mechanisms and processes, e.g., effects of the presence of organics and microbial organisms are not considered. However, the mechanisms do represent some of the more common mechanisms that could affect radionuclide transport as a result of the presence of shafts. The mechanisms considered include

- o downward movement of water through the shafts,
- o downward movement of water in fractures from the repository horizon to the base of ES-1,
- o upward movement of water in the sumps of the shafts,
- o transport of radioactive solids through the shafts,
- o gaseous transport through drifts and shafts because of gaseous diffusion,
- o gaseous transport through drifts and shafts because of convective forces, and
- o gaseous transport through shafts because of barometric forces.

A.1 Downward Water Movement Through the Shafts

Shafts are pathways to the underground facility that could potentially increase the amount of water entering the waste disposal areas. The

analyses presented in the following sections illustrate the time required to saturate shaft fill to a 300-m depth assuming a constant supply of water at the upper portion of the shaft. It is presumed in the analysis that if water does not reach the repository horizon over a substantial period of time, there is no potential for water to reach the waste disposal areas, and this mechanism should not be considered further.

The Green and Ampt solution (Hillel, 1971, pp. 140-143) was used to calculate the saturated vertical infiltration into the initially dry shaft fill. A discussion of the Green and Ampt solution is provided in Fernandez et al. (1987). The results illustrating the time to saturate 300 m of backfill are given in Figure A-1. This figure suggests there is a time delay for a fully saturated front to reach the repository horizon. Depending on the hydraulic conductivity of the shaft fill, this time delay can vary by many orders of magnitude. Figure A-1 also illustrates that if a coarse material is placed in the shaft, water from the surface is transmitted to the repository level over a short time. Because there is some potential for water to be transmitted down to the repository horizon (depending on the condition encountered at the surface), water flow down the shafts is considered further in Appendix C of this report.

A.2 Downward Water Movement in Fractures from the Repository Horizon to the Base of the Exploratory Shafts

In this section, the potential for the ESs to act as preferred pathways in releasing radionuclides is discussed. The ESs are considered here because they extend below the repository horizon. The mechanism for the release of radionuclides is transport by water from the waste disposal area to the sump of the ES through the fracture system. The geometric relationship between the waste disposal area and the ESs is shown in Figure A-2. Because waste is stored a minimum of about 140 m away, an effective barrier of rock results. The effectiveness of this barrier is further enhanced because (1) fracture flow from the repository to the ESs is not anticipated based on current knowledge of flow conditions* and (2) even if

*As discussed in Section 8.4 of the SCP (DOE, 1988, p. 8.4.1-18), the rock matrix must attain a high degree of saturation before significant water movement occurs along fractures. Further, the predominant flow in the unsaturated zone probably is through the matrix.

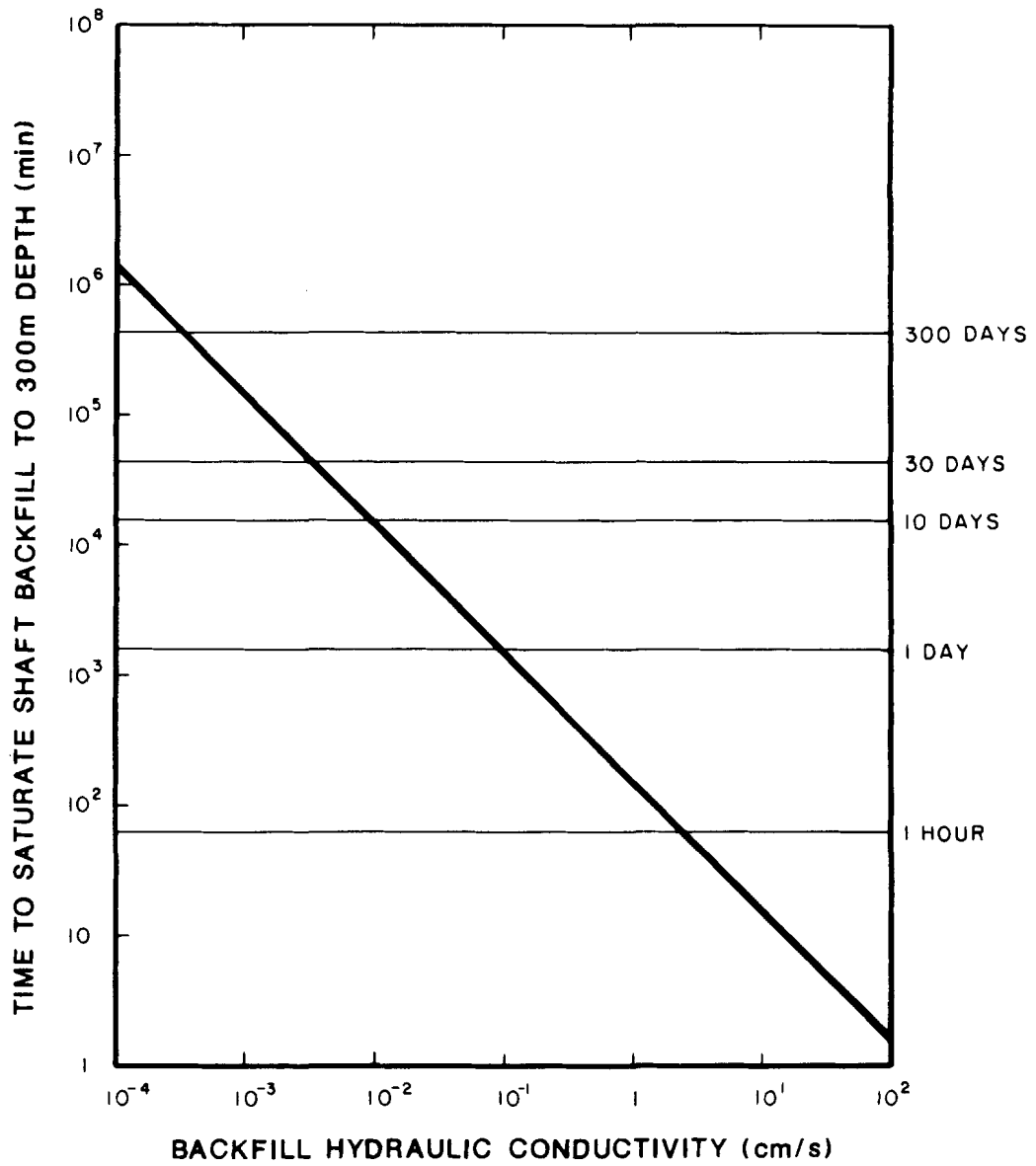


Figure A-1. Results from the Green and Ampt Solution for Transient Flow Through Shaft Backfill (from Fernandez et al., 1987)

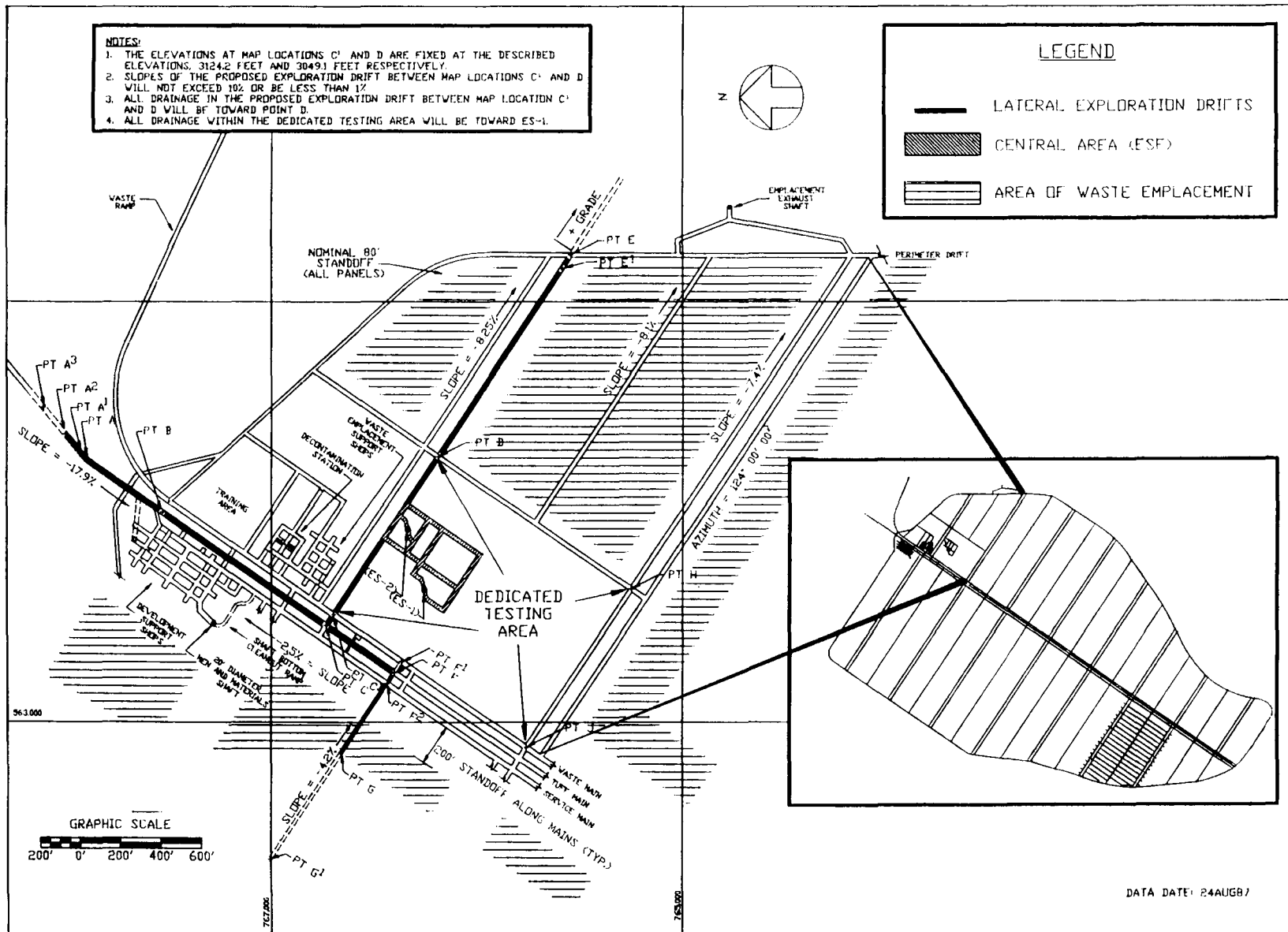


Figure A-2. Detailed Repository Layout in Vicinity of the Exploratory Shaft Facility (modified from DOE, 1988, p. 8.4.2-92)

fracture flow occurs, the dip for the majority of fractures (~98%) is >13° (SNL, 1987, Appendix O, Table O-7 for fracture frequency in the Topopah Spring Member). Because the angle from the base of ES-2 to the edge of the waste disposal area is approximately 13°, the majority of flow will not intercept ES-2 assuming that it is controlled by fractures whose dip is >13°.*

A.3 Upward Movement of Water in the Sumps of Shafts

The mechanism discussed in this section involves the transport upward of standing water at the base of a shaft as a result of fracture and matrix capillary forces. This mechanism assumes that radionuclides are dissolved in water at the base of the shaft, implying transport of contaminated water to the shaft. Assuming that contaminated water is transported to the shaft, in itself, may totally negate the feasibility of this mechanism because a drainage pattern has been designed so that no drainage occurs from the access and emplacement drifts into ES-1. This constraint, therefore, significantly reduces the possibility that radionuclides may reach ES-1. The following discussion, nevertheless, evaluates and calculates the effect of this mechanism.

Because the sump at the base of ES-1 is located predominantly in welded tuff, which is highly fractured, capillary forces within fractures in the MPZ are considered. The upward transport of water in fractures as a result of capillarity was computed using the formula

$$h = 2\sigma \cos \theta / (\rho g b) \quad , \quad (A-1)$$

(Lohman, 1972, p. 2)

where

h = height of water in a fracture, m;

σ = surface tension of water against air, newton/m;

*ES-2 is discussed here because the current tailshaft (or sump) is 31 m which is greater than the sump for ES-1. Additionally, ES-2 is closer to the waste than ES-1.

θ = contact angle between the water in the fracture and the tuff
(assumed to be 0°);
 ρ = density of water, kg/m^3 ;
 b = fracture aperture, m; and
 g = acceleration resulting from gravity, m/s^2 .

This situation could be applied to fractures penetrating saturated zones such as the water table or a shaft containing water at the base. For fractures having aperture widths of $71 \mu\text{m}$ (Sinnock et al., 1984, p. 12) and $25 \mu\text{m}$, the rise of water in the fracture was computed to be approximately 0.21 and 0.58 m, respectively. The temperature of the water was assumed to be 30°C . At 52°C (Section 7.1.1), the rise of water in fractures having apertures of 71 and $25 \mu\text{m}$ would be 0.20 and 0.56 m, respectively. Because of the limited extent to which capillary forces within a fracture can transport water upward, radionuclide transport upward in a fracture is considered insignificant.

If water stands in the shaft fill in the sump, it is possible for the water to move up through the shaft fill by capillary forces. The rise of water above the fully saturated level or the phreatic surface is termed the capillary rise. The extent of capillary rise depends on the pore sizes of the shaft fill. For example, capillary rise in a material that has large pores, such as a coarse sand, would be low (2 to 5 cm). For a shaft fill having small pores, such as a clay, the capillary rise could range from 200 to 400 cm (Bear, 1976, p. 481). Therefore, because (1) capillary forces within the shaft fill can transport water over a limited extent; (2) transport of radionuclides to the shaft sump is unlikely; and (3) the duration of ponding of water, if it occurs at all, is anticipated to be short; it is postulated that water can be effectively drained through the base of the shaft, and radionuclide transport upward because of capillary forces in the shaft fill is insignificant.

A.4 Transport as a Result of Solid-Solid Diffusion

The scenario considered here involves bare waste adjacent to rock. The process being considered is transport of waste through the rock. Using

a one-dimensional solution to Fick's second law, we can compute the time for solid diffusion of radionuclides. The formula used to compute the time for radionuclide migration for the specified conditions is

$$\frac{C_A}{C_{A_0}} = \operatorname{erfc} \frac{X}{\sqrt{4\vartheta_{AB}t}} \quad , \quad (\text{A-2})$$

(Freeze and Cherry, 1979, p. 393)

where

- C_A = concentration of A at point X, moles/l;
- C_{A_0} = concentration of A at point of origin, moles/l;
- X = distance from original point of diffusion, m;
- ϑ_{AB} = binary diffusivity for system A-B, m^2/s ; and
- t = time over which diffusion occurs.

The most significant unknown in this formula is the diffusion coefficient for uranium through welded tuff. The diffusion coefficient used below is $10^{-15} \text{ cm}^2/\text{s}$, which is believed to be extremely conservative because it is at the higher end of the solid-solid diffusion coefficients given in Bird et al. (1960, p. 505). Using this diffusion coefficient and evaluating the condition where the solid portion of the radioactive waste migrates 0.1 m and its concentration is 99% of its original concentration, we computed a transport time of about 10^{13} years. However, the diffusion coefficient of uranium or uranium oxide because of its molecular size would probably be less than the value of $10^{-15} \text{ cm}^2/\text{s}$ used above. A diffusion coefficient of $10^{-30} \text{ cm}^2/\text{s}$ yields a transport time of 10^{28} years. Because of these long transport times, the potential for radionuclide release by solid-solid diffusion is considered insignificant.

A.5 Gaseous Transport as a Result of Diffusion

Some radionuclides can be released in a gaseous form and therefore the potential significance of binary-gaseous diffusion is considered here. Some potential gaseous species (Xe isotopes, Rn, Kr-85, and H-3) can be eliminated from concern because of their short half-lives, assuming the containment period is 300 to 1,000 years. The radionuclides that

potentially could enter the repository in a gaseous state are C-14 and I-129 (Van Koynenburg et al., 1984, p. 1). Equation A-2 is used to compute the relative concentration-versus-time curves for I-129 and C-14. However, in order to apply Equation A-2, the diffusivity values for the gaseous forms of I-129 and C-14 are needed. It is assumed that I-129 occurs as I_2 and C-14 occurs as CO_2 . Using an approach described in Reid et al. (1977, pp. 548-550) for binary-gas diffusion coefficients and in Smith (1970, p. 406) for Knudsen diffusion coefficients, diffusivities are computed for air-iodine and air-carbon dioxide systems. The computed binary diffusion coefficients for these two systems are $0.081 \text{ cm}^2/\text{s}$ for the air-iodine system and $0.156 \text{ cm}^2/\text{s}$ for the air-carbon dioxide system. The computed Knudsen diffusion coefficients are $10.6 \text{ cm}^2/\text{s}$ for I_2 and $25.3 \text{ cm}^2/\text{s}$ for CO_2 . These diffusivities are combined by the method described in Mason and Evans (1969, p. 362) to give overall gaseous diffusion coefficients of $0.080 \text{ cm}^2/\text{s}$ for the air-iodine system and $0.155 \text{ cm}^2/\text{s}$ for the air-carbon dioxide system. These values assume open drifts and shafts. If backfill is emplaced, migration of the gas is partially restricted. The magnitude of this restriction can be computed using the effective diffusivity, which is a function of the porosity of the material through which the gas is diffusing and of the tortuosity of the material. The following equation is used to compute the effective diffusivity.

$$D_e = \frac{\epsilon}{\tau} D \quad (\text{Froment and Bischoff, 1979, p. 167}) \quad , \quad (\text{A-3})$$

where

D_e = effective diffusivity, cm^2/s ;

ϵ = porosity of material through which diffusion occurs;

τ = tortuosity; and

D = diffusion coefficient, assuming no restriction to diffusion, cm^2/s .

The porosity assumed for the drift and shaft fill is 0.3. The value for tortuosity is assumed to be 3, which corresponds to a loose random pore structure (Froment and Bischoff, 1979, p. 167).

Figure A-3 illustrates the relationship between the relative concentration of the gas under consideration versus time for a distance of

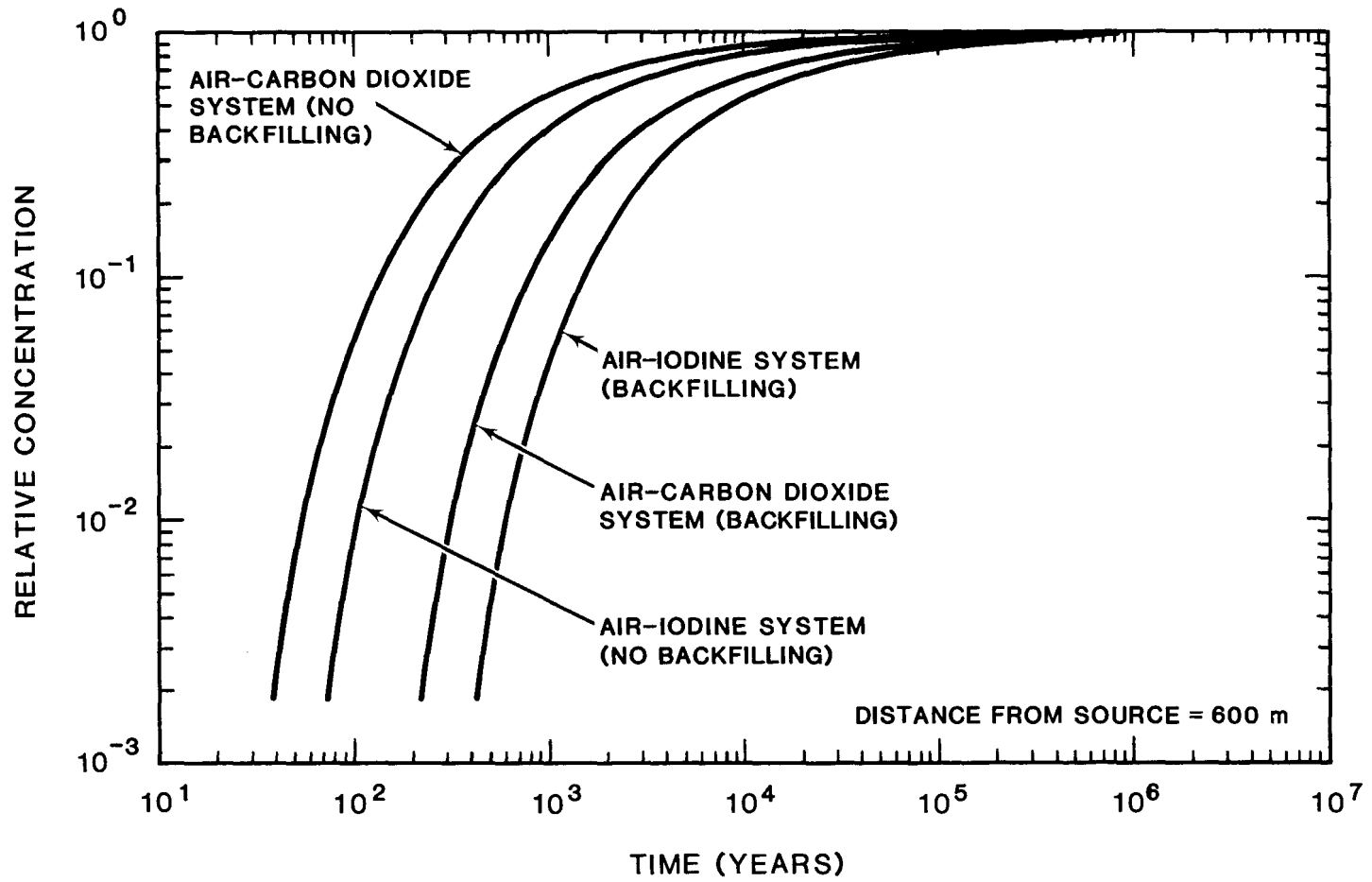


Figure A-3. Concentration of Two Gaseous Systems as a Result of Binary Gaseous Diffusion (600 m from Point of Release and at Various Times Following Release)

600 m from the waste disposal area. This distance is an approximation of the distance from the waste disposal area to the surface entry point of ES-1 or ES-2.

Two sets of curves are presented. The first set assumes no backfilling of the shafts and drifts. The second set assumes the shafts and drifts are backfilled with a material that is emplaced loosely. Figure A-3 illustrates that if only binary diffusion occurs, considerable time, 10^5 to 10^6 years, is required to release I_2 or CO_2 at ~99% of the original concentration in the waste disposal areas. Lesser concentrations are released at much shorter times following release of the gas at the disposal area. Also, a substantial reduction in the concentration exiting the shaft can be achieved by emplacing loose shaft and drift fill. Emplacement of consolidated shaft fill or a single shaft or drift seal can further reduce the release through the shaft. Because (1) binary gaseous diffusion is a slow process as indicated by Figure A-3, (2) travel times can be reduced substantially by simple backfill, and (3) the original concentrations of I-129 and C-14 at the waste package remain constant, binary gaseous diffusion is not considered to be a significant release mechanism.

A.6 Gaseous Transport as a Result of Convective Forces

For a repository located above the water table, there is the possibility of release of radionuclides by airflow out of the repository through the shafts or through the host rock. Airflow may develop as a convective circulation in response to the thermal gradient.

After the waste containers have been emplaced, heat is initially transferred by conduction from the waste containers to the surrounding rock. Vertical temperature gradients will develop from the repository horizon and potentially affect air and water density. If sufficient energy in the form of heat is imparted to the air or water vapor, convective transport is established.

Two potential convective airflow mechanisms are illustrated in Figure 4-1. Mechanism A assumes that no upward flow occurs through the

host rock relative to flow through the shafts, ramps, and drifts. ES-1 and adjacent ES-2 are within the repository boundary, and the temperature is relatively high near the repository horizon. The men-and-materials shaft, the emplacement exhaust shaft, and the ramps are located outside or just inside the perimeter of the repository, and the temperature gradients for these locations are lower. In response to these gradients, air will be drawn in through the other entries and will tend to rise in ES-1 and ES-2. This mechanism may occur if the shafts and drifts are open or if the backfill is relatively permeable compared to the host rock. In Mechanism B, convective air circulation is also assumed to occur through the host rock. The waste disposal areas are relatively hot, and the heated air tends to rise vertically through the rock as well as through ES-1 and ES-2. Because temperature rises in the rock are expected and it is uncertain what the effects of this temperature rise will be, this mechanism is considered further in the text.

A.7 Gaseous Transport as a Result of Barometric Forces

Another potential flow mechanism for the transport of radionuclides is the development of a differential air pressure between the repository and the ground surface. A weather front suddenly moving across the repository site might result in a drop in barometric pressure, producing a pressure gradient between the repository and the surface. Pressure gradients may also develop more gradually in response to changing seasons. These changes in barometric pressure are cyclical or periodic in nature, so that air would eventually move back into the repository. The ease with which air moves in and out of the repository will depend upon the properties of the backfill placed in the shafts and ramps and the surrounding rock. Conceptually, large volumes of air may move through shafts and ramps containing coarse backfill with a high conductivity. Smaller volumes of air might move through shafts and ramps containing a fine backfill with a low conductivity, although a proportionally greater amount of flow might occur through the modified permeability zone around the shafts and ramps. In addition, a low conductivity backfill will isolate the repository from pressure variations at the surface, while a high conductivity backfill will result in a more significant pressure response within the repository. Because barometric fluctuations will occur at the surface and because it is

uncertain what the effects of these fluctuations are, this mechanism is considered further in Chapter 5.

APPENDIX B

A MODEL OF THE MODIFIED PERMEABILITY ZONE

CONTENTS

	<u>Page</u>
B.1 Approach Used to Develop the Model of the Modified Permeability Zone	180
B.2 Modeling Results	182
B.3 Model Appropriateness	184
B.3.1 Orientation of Fractures Relative to the Stress Field	184
B.3.2 Assumption of Blast-Damaged Zone	185
B.3.3 Effect of Shaft Liner Removal	186

TABLES

B-1 Relative Permeability Factors Associated with the Modified Permeability Zone	184
--	-----

APPENDIX B

A MODEL OF THE MODIFIED PERMEABILITY ZONE

Excavation of the exploratory shafts (ES) at the site will modify the rock mass permeability as a result of stress redistribution and blast damage in zones immediately surrounding the shafts. To perform selected calculations in this report, it is necessary to predict how the rock mass permeability has been modified in these zones. This appendix presents a brief synopsis of the modified permeability zone (MPZ) model. A more complete description of the model and site-specific parameters at Yucca Mountain that were used in the development of the model is presented by Case and Kelsall (1987). The technical approach adopted for modeling stress redistribution and blast-damage effects is also presented by Kelsall et al., 1982 and Kelsall et al., 1984.

B.1 Approach Used to Develop the Model of the Modified Permeability Zone

As excavation occurs, stresses are relieved and blast-induced fracturing may occur in the rock surrounding the shaft. Considering a representative volume of rock adjacent to the shaft, it is expected that the geomechanical response to excavation will be most influenced by rock mass properties (which take into account the effect of fractures) rather than by the properties of the intact rock because the range of fracture spacing is small relative to the shaft diameter. Similarly, the permeability of the rock mass will be influenced by fractures as well as by the rock matrix in welded tuff.

It is postulated that the significant mechanisms for modifying permeability in fractured, welded tuff are (1) opening or closing of fractures in response to stress changes and (2) creating new fractures or causing the opening of preexisting fractures by blasting. The approach for developing the MPZ model includes the following five steps.

- o Calculate stress changes around a shaft by using an appropriate closed-form solution for elastic or elastoplastic analysis of a

circular shaft located in a uniform stress field (Jaeger and Cook, 1976, p. 251; Hoek and Brown, 1980, p. 250).

- o Obtain relationships from published laboratory and field testing results that describe the effects of stress on the permeability of single fractures and fractured rock (Peters et al., 1984; Zimmerman et al., 1985).
- o Calculate rock mass permeability as a function of radius away from the shaft, based on the calculated stresses and the stress-permeability relationships obtained from testing.
- o Calculate rock mass permeability changes resulting from blasting based on an evaluation of case histories (Montazer and Hustrulid, 1983; Kelsall et al., 1982, 1984; Wilson et al., 1983; Miller et al., 1974; Cording et al., 1971; Worsey, 1985; Siskind et al., 1973), which indicate the depth of damage and estimate the probable increase in fracture frequency in the damaged zone.
- o Combine the results derived from performing Steps 3 and 4 to obtain the combined effects of stress redistribution and blasting.

Analyses are conducted for depths of 100 and 310 m. The 100-m depth represents the upper part of the Topopah Spring unit, whereas 310 m is the approximate depth at which the ES intersects the repository horizon. Analyses are conducted to represent a range of expected rock conditions at each of these depths as follows.

- o A lower-bound estimate of the increase in rock mass permeability is obtained by considering an upper bound for the expected rock mass strength properties, a lower bound for the expected in situ stress, and a lower bound for the sensitivity of permeability to stress as indicated by laboratory and field testing.
- o An expected estimate of the probable increase in rock mass permeability is obtained using the expected mean values for

strength and in situ stresses and values for the mean sensitivity of permeability to stress.

- o An upper-bound estimate of the increase in rock mass permeability is obtained by using values for lower-bound strength properties, upper-bound in situ stresses, and the upper-bound sensitivity of permeability resulting from stress.

In the analyses of stress redistribution presented by Case and Kelsall (1987), the intact rock compressive strength varies from 110 to 230 MPa, with an expected value of 171 MPa. Values for the rock mass quality, as indicated by the Rock Mass Rating (Langkopf and Gnirk, 1986), vary from 48 to 84 with an expected value of 65. Values for the in situ stress vary from 0.25 to 1.0 times the weight of overburden with an expected value of 0.6 times the weight of overburden. These properties cover a wide range of rock mass properties in the prediction of the MPZ.

Estimates of the effects of blasting on rock mass permeability are based initially on a review of case histories that indicate the extent of blast damage around underground openings. Because these case histories indicate only the width of the damaged zone and not the permeability, it is necessary to base the estimates of increased permeability on assumptions regarding the increased fracture frequency within the blast-damaged zone. Case histories suggest that the width of blast damage may vary from approximately 0.3 m, for cases in which controlled blasting methods such as smooth blasting are used, to approximately 2.0 m, for cases in which uncontrolled blasting methods are used. For purposes of estimating increases in rock mass permeability resulting from blasting, it is assumed that blasting will be controlled and will result in a threefold increase in fracture frequency within a zone extending 0.5 m from the shaft wall. In a second upper-bound, blast-damage model, it is assumed that the annulus extends 1.0 m from the shaft wall.

B.2 Modeling Results

Elastic and elastoplastic stress analyses were performed for the ES at depths of 100 and 310 m. The results indicate that a wide variation in

rock mass behavior might be observed depending on depth, in situ stress, and rock properties. Because rock mass strength* may vary with depth (as a result of variations in porosity and fracture spacing), rock mass behavior may vary even within a lithologic unit. For the welded units, the expected response is elastic in nonlithophysal zones, but plastic response may occur in lithophysal zones or in intensely fractured zones where strength is lower.

The results of the stress redistribution and blast-damage analyses are combined to form a series of models for the MPZ representing a range of rock mass properties and in situ stress conditions.

The increase in permeability resulting from stress relief and blast damage effects for the ES for several cases (Case and Kelsall, 1987) are presented in Table B-1 and expressed as relative permeability factors** for two depths. The expected case is based on an elastic stress analysis and the 0.5-m-wide blast-damaged zone, while the upper-bound case is based on an elastoplastic analysis with a 1-m-wide blast-damaged zone. For the expected conditions at a 310-m depth (i.e., considering mean values for rock mass strength, in situ stress, and stress-permeability sensitivity, and a 0.5-m-wide blast-damaged zone), the relative permeability factor is 20. For the upper-bound condition at the 310-m depth (considering low values for rock mass strength, a high value for in situ stress, high stress-permeability sensitivity, and a 1-m-wide blast-damaged zone), the equivalent rock mass permeability is 80 times the undisturbed permeability.

*Rock mass strength is defined as the maximum stress that can be carried by the rock mass (Hoek and Brown, 1980, p. 150). The maximum stress level is found to depend on the strength properties of intact rock and discontinuities and is dependent on confining stress.

**The relative, rock mass permeability factor for the expected case is calculated by first performing the radial integration of relative rock mass permeability from the shaft radius (2.2 m) to approximately a radius of 10 m and then by calculating a factor by dividing by the area of the annulus extending from 2.2 to 10 m from the shaft.

Table B-1. Relative Permeability Factors Associated with the Modified Permeability Zone^(a,b)

Depth	Stress Redistribution Without Blast Damage		Expected ^(c) Case	Upper-Bound ^(d) Case
	Elastic	Elastoplastic		
100	15	20	20	40
310	15	40	20	80

- (a) Relative permeability factors are averaged over an annulus one radius wide around the 4.4-m diameter ES.
- (b) Source: After Case and Kelsall (1987).
- (c) This case is based upon an elastic analysis with expected strength, in situ stress, sensitivity of permeability to stress, and a 0.5-m-wide, blast-damaged zone.
- (d) This case is based upon an elastoplastic analysis with lower-bound strength; upper-bound, in situ stress; greatest sensitivity of permeability to stress; and a 1.0-m-wide, blast-damaged zone.

B.3 Model Appropriateness

Several specific issues exist in the evaluation of MPZ models. These issues include the orientation of the fractures with respect to the stress field near the shaft and their mode of deformation, blast damage during shaft excavation, and liner removal before seal construction. These issues as they relate to the MPZ zone model are discussed below.

B.3.1 Orientation of Fractures Relative to the Stress Field

The excavation of the ES will result in alteration of both normal and shear stress across fractures with the amount of alteration dependent on the in situ stress state before excavation, the distance of the fracture from the shaft excavation, and the orientation of the fracture with respect to the stress state. The alteration of stress across the fracture will result in normal and shear deformation.

The MPZ model assumes that "onionskin" fractures will open in the direction normal to the radial direction or the direction of maximum stress relief and are predominant in the altered rock mass permeability. Under

elastic conditions, the radial stress will decrease to zero assuming no support at the shaft wall while the tangential or boundary stress will increase and close a system of "radial" fractures. Because permeability depends on changes in aperture for "onionskin" and "radial" fractures, which will close and open respectively, the model overestimates the effects of normal stress relief in this case. It can also be shown that the model overestimates the effects of normal stress relief for the elastoplastic case. However, the model neglects the effects of shearing along fractures that might result in shear dilatancy and subsequently in an increase in the apertures of the affected fractures.

In a recent study, a detailed numerical analysis of the response of jointed rock to shaft excavation was conducted by Dial et al. (1988) using the explicit finite difference computer code STEALTH with the CAVS jointed rock constitutive model. The response of an orthogonal system of discontinuities was modeled by partitioning the total strain within a computational zone into intact rock strain and void(aperture) strain. The changes in void strain include changes in normal stress across discontinuities, slip induced dilatancy, and the initiation and propagation of fractures. The analysis was performed using lumped siltstone-dolomite properties for the Queen/Grayburg formation at a depth of 545 m in Deaf Smith County, Texas. The conclusion was reached that qualitatively, the excavation response predicted by STEALTH was similar to the joint response predicted by the analytic model in Kelsall et al. (1982) for basalt, which is identical to the technical approach adopted here for the MPZ model in welded tuff (Case and Kelsall, 1987). Further, it was concluded that the simple analytic model proposed by Kelsall et al. (1982) is appropriate for estimating excavation-induced joint response.

B.3.2 Assumption of Blast-Damaged Zone

The blast-damage model is assumed to increase the fracture frequency by a factor of three in a zone adjacent to the shaft where blast-induced fracturing might occur. Further, the newly created fractures are assumed to have the same deformability characteristics as existing fractures. Because the changes in fracture frequency associated with blasting have not been well documented (in particular in welded tuff), the blast-damage model

is considered preliminary (Kelsall et al., 1984). Further, the assumption that fractures created by blasting have similar characteristics to natural fractures is at present unsubstantiated.

In view of the potential unknown effects of blast-induced damage, the current design of the ESs uses measures to control blasting. The number, depth, location, spatial orientation, explosive charge, and firing sequence for the blast holes will be designed to meet the requirements of controlled drilling and blasting to limit change in rock mass permeability and to minimize overbreak. Several methods have been surveyed in Section 8.4 of the Site Characterization Plan (DOE, 1988), and the method that appears most appropriate is smooth blasting.

B.3.3 Effect of Shaft Liner Removal

The current position in the Yucca Mountain Project repository sealing program is to remove that portion of the shaft liner that extends below the repository horizon. In the event that removal of the liner is required to emplace a seal above the repository horizon, the location selected will most probably be in an area where the rock mass is least affected by the construction of the shaft. This suggests that the most logical location for a shaft seal will be in a competent zone of welded tuff. Because the in situ stress state at a potential seal location is not expected to be high and because welded tuff has an adequate rock mass strength, we expect the seal location to behave in a linearly elastic fashion. We would also expect that shaft convergence following excavation of the shaft is low, certainly lower than that expected in the less competent nonwelded tuff zones penetrated by the shaft (Costin and Bauer, 1988).

Damage resulting from liner removal at key seal locations placed above the repository horizon might adversely affect hydrologic performance at these locations. In the event that removal of the liner is required to emplace a seal in a location above the repository horizon, the location selected will most probably be in an area where the rock mass is least affected by the construction of the shaft. This location would be in a competent zone of welded tuff. Further, following shaft excavation, the shaft convergence is expected to be lower than in less competent zones penetrated by the shaft.

The MPZ model assumes that no support is provided to the shaft wall from the shaft liner and that the radial stress is zero at the shaft excavation. This assumption is believed to be conservative because the effects of support from interaction of the liner and the rock mass would likely reduce the degree of stress relaxation and the degree to which "onionskin" fractures normal to the direction of radial stress relief would open. Therefore, because (1) no credit is taken for liner support pressures and (2) because the portion of liner removed would most likely be in competent rock that would display little convergence (most of which would occur after initial excavation and before shaft liner emplacement), the MPZ model is believed to bound the effects of removing the liner.

APPENDIX C

**SCENARIO DESCRIBING FULLY SATURATED ALLUVIAL FLOW AT THE
OLD EXPLORATORY SHAFT LOCATIONS**

CONTENTS

	<u>Page</u>
C.1 Scenario Description	193
C.2 Model Used for Water Flow into the Shaft	194
C.2.1 Model Description	195
C.2.2 Input Values Used	202
C.2.3 Inflow Volumes	203
C.2.4 Duration and Rate of Flow Into Shaft	205
C.3 Model Used for Water Flow out of the Shaft	211
C.3.1 Model Description	211
C.3.2 Input Values Used	217
C.4 Water Balance in the Exploratory Shaft	218

FIGURES

C-1 Old and Current Locations for the Exploratory Shafts	192
C-2 Geometry of Model Used to Estimate Flow into a Shaft from Saturated Alluvium	196
C-3 Phases of Flow into a Shaft from Saturated Alluvium	197
C-4 Types of Flow Considered in Estimating Flow into a Shaft	199
C-5 Capture Zone Near a Shaft	200
C-6 Estimated Volumes of Water Entering ES-1 (PMF, Shaft Fill Conductivity = 10^{-2} cm/s, Excavated Shaft Diameter = 4.42 m)	204
C-7 Estimated Duration of Flows into ES-1 (PMF, Hydraulic Conductivity of Alluvium--100 and 10 cm/s)	206
C-8 Estimated Duration of Flows into ES-1 (PMF, Hydraulic Conductivity of Alluvium--1 and 0.1 cm/s)	207

FIGURES (concluded)

	<u>Page</u>
C-9 Estimated Duration of Flows into ES-1 (PMF, Hydraulic Conductivity of Alluvium-- 10^{-2} and 10^{-3} cm/s)	208
C-10 Estimated Duration of Flows into ES-1 (PMF, Hydraulic Conductivity of Alluvium-- 10^{-4} and 10^{-5} cm/s)	209
C-11 Model Used to Compute the Water Balance in the Exploratory Shaft	213
C-12 Comparison of Methods Used to Compute Drainage from a Shaft	216
C-13 Estimated Buildup of Water in the Sump of ES-1 (Hydraulic Conductivity of Alluvium--100 and 10 cm/s)	219
C-14 Estimated Buildup of Water in the Sump of ES-1 (Hydraulic Conductivity of Alluvium--1 and 0.1 cm/s)	220
C-15 Estimated Buildup of Water in the Sump of ES-1 (Hydraulic Conductivity of Alluvium-- 10^{-2} and 10^{-3} cm/s)	221

APPENDIX C

SCENARIO DESCRIBING FULLY SATURATED ALLUVIAL FLOW AT THE OLD EXPLORATORY SHAFT LOCATIONS

The purpose of this appendix is to determine whether the presence of the exploratory shafts (ES) at their old locations (Figure C-1) and the resulting rock damage surrounding the shafts caused by excavation can significantly enhance the release of radionuclides. The release mechanism considered here is water entering the waste disposal areas through the ESs and contacting the waste. Therefore, it is necessary to establish the hydrologic properties of the zone through which water can be transmitted to the base of the shaft. This zone includes the shaft interior and the modified permeability zone (MPZ). Therefore, it is important to define the MPZ and establish a scenario of water entry into the shaft and potentially into the waste disposal area. Relative permeability factors for the MPZ are given for the expected and the upper-bound cases (Appendix B). Both MPZ models include a blast-damaged zone and are evaluated to provide a range of water flows through the MPZ. The scenario of water entry postulated in this section includes two major events occurring at the ground surface, which establish hydrologic conditions that could lead to water flow into the upper portion of the shaft (Section C.1). The water from one of the events then migrates to the base of the shaft where it builds up if the volume entering is greater than water draining from the shaft. This portion of the overall model is described in Section C.3. If the water level in the shaft is higher than the floor of the repository station, water can enter the underground facility through the connecting repository drift. This scenario and the hydrologic model used are described below in Sections C.1, C.2, and C.3. While the results of this analysis are no longer directly applicable to the current locations of the ESs, the scenario and results have been presented to illustrate the effectiveness of the shaft sumps in draining extremely large water flows and to fully document the evaluations completed in support of the YMP.

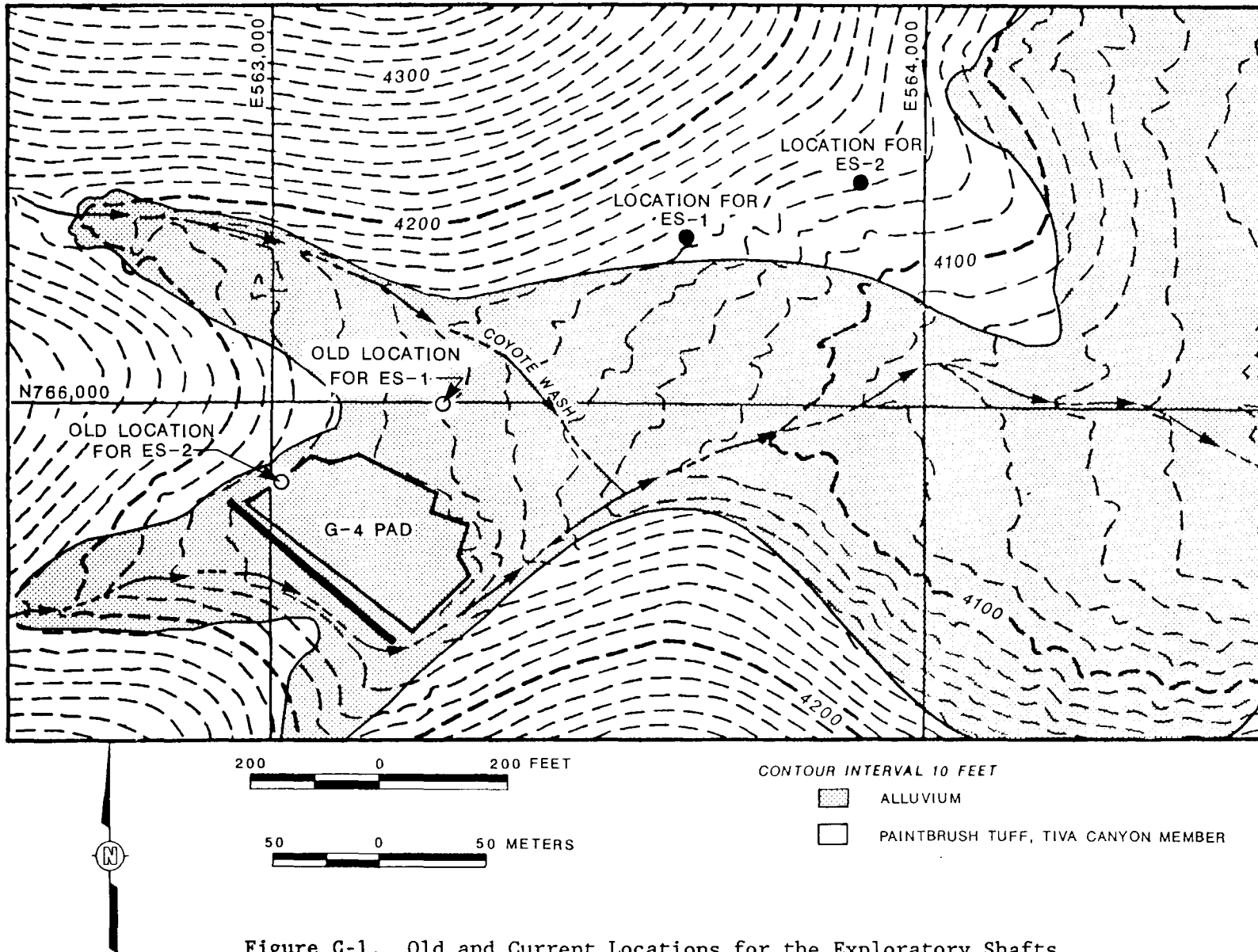


Figure C-1. Old and Current Locations for the Exploratory Shafts

C.1 Scenario Description

To arrive at a reasonable, upper-bound estimate of water flow into ES-1, the scenario developed here assumes the occurrence of two events. The first event is surface, earth movement downgrade from the ES which substantially retards drainage. Following this event, a probable maximum flood (PMF) thunderstorm is assumed to occur, and the waters of this PMF thunderstorm are assumed to be fully retained in the portion of the drainage basin upgrade from the shafts. These waters are then assumed to flow into the underlying bedrock, horizontally in the alluvium, and into the shaft and MPZ. No evapotranspiration is assumed to occur.

While it is reasonable to assume that a PMF can occur at the ES location, it is highly unlikely that earth movement sufficient to retain all the waters from a PMF would occur because

- o Earth movement, enough to retain all the waters from a PMF, is not credible given the thin cover of alluvium and weathered rock on the adjacent slopes. To impound a volume of water approximately half of the volume of 159,000 m³ computed for a PMF (Bullard, 1986, Table 10) would require a dam 12 m high across the entire drainage course. Further, at Yucca Mountain there is at present no evidence of surface impoundments formed by landslides (DOE, 1986, p. 6-232) and of the size needed to contain this flood volume. As indicated in Fernandez et al. (1987, p. 4-2 to 4-4), the occurrence of small obstructions blocking portions of the wash and slowing down the flow is a more probable and realistic scenario.

- o Four areas where slide blocks occur have been identified in the Yucca Mountain area. These slide blocks can be described as rock-slumps that are gravitationally driven. Three rock slumps, which are very small (0.01 to 0.03 km²), are located on the steep west-facing scarp of Yucca Mountain. A larger rock slump, about 0.13 km² in area, is located midslope on the ridge south of Yucca Wash (DOE, 1988, p. 1-32, 33). The common characteristic between these rock slumps is that they occur on steep slopes estimated to be about 25°. The slope near the ESs is about 15° to 20°.

Because (a) the slope in the vicinity of the ESs is less than that occurring in the areas where slumps do occur and (b) massive lateral movement sufficient to block Coyote Wash is not characteristic of these rock slumps, blockage of the drainage basin associated with the ESs by massive rock slumps is not considered credible.

Nevertheless, while this scenario is considered to be even more highly improbable at the new locations for the ESs, which are out of the flood area, we have decided to model the scenario to obtain a larger than expected inflow into the underground facility.

C.2 Model Used for Water Flow into the Shaft

In Figure C-1 the upper portion of ES-1* is located in the alluvial-filled portion of the drainage basin; whereas, the upper portion of ES-2 is located in bedrock upgrade from ES-1. Because the upper portion of ES-1 is located in alluvium at the confluence of two washes, Coyote Wash and the wash to the south, a greater potential exists for surface-water entry into ES-1 than into ES-2. The mechanism modeled in this section is water flow from saturated alluvium to the shaft. Because the upper portion of ES-2 is near the boundary of the bedrock and alluvium, this mechanism is less likely to occur. It is, therefore, assumed that water from a major flooding event that saturates the alluvium can enter ES-1 only. Using this logic, a hydrologic flow model was developed (Fernandez et al., 1987) to estimate the amount of water that could enter the upper portion of the ES. This model, discussed below, assumes that the alluvium surrounding the ES becomes saturated and that water can enter the shaft. In reality, alluvium in an initially unsaturated state can provide an effective barrier to downward water infiltration, thereby limiting flow into the shaft.

*The ES-1 and ES-2 locations used in the analysis are the old locations presented in the final EA (DOE, 1986, p. 4-11). The current locations are out of the alluvium as discussed in Chapters 2 and 3.

C.2.1 Model Description

The model used to compute the flow into the upper portion of the shaft is illustrated by Figure C-2. Alluvium overlies the welded, highly fractured Tiva Canyon Member. For the present analysis, the upper portion of the shaft through the alluvium is assumed to be filled with a coarse fill to minimize restriction of flow into the shaft. The lower portion of the shaft is modeled as containing a fill having a saturated hydraulic conductivity of 10^{-2} cm/s, extending to the outside diameter of the shaft. (In reality, a shaft liner, having a lower hydraulic conductivity than the shaft fill, remains in place. By ignoring the presence of the shaft liner in the analysis, a higher flow through the shaft is computed.) The MPZ is modeled as extending one radius from the shaft wall. Two cases for the MPZ are considered in which the MPZ is either 20 or 60 times the undisturbed, rock mass hydraulic conductivity. The value of 60 is the average of two values (40 and 80, Table B-1), associated with MPZ models at 100- and 310-m depths. This is believed to be a conservative assumption because it implies the permeability of the MPZ is 60 times the undisturbed, rock mass permeability over the entire length of the shaft, including the MPZ down to a depth of 100 m. For more details of the MPZ model used, see Case and Kelsall (1987) or Appendix B.

Flow is assumed to progress in three phases: an initial desaturation phase, a steady-state phase, and a final desaturation phase (Figure C-3). Before initiation of Phase I, it is assumed that the alluvium becomes fully saturated, and the water in the shaft above the alluvium-Tiva Canyon contact enters the upper portion of the shaft. Desaturation of the alluvium occurs first at curve "l" and progressively to curve "n" (Figure C-3a). As the radius of influence changes in response to desaturation, the radius of influence associated with curve "n" represents quasi-steady-state conditions that are held constant until the supply of water replenishing the alluvium no longer exists (Figure C-3b). As Phase III begins, the only water remaining is that contained under curve "n." Desaturation then proceeds from curve "n" to curve "m."

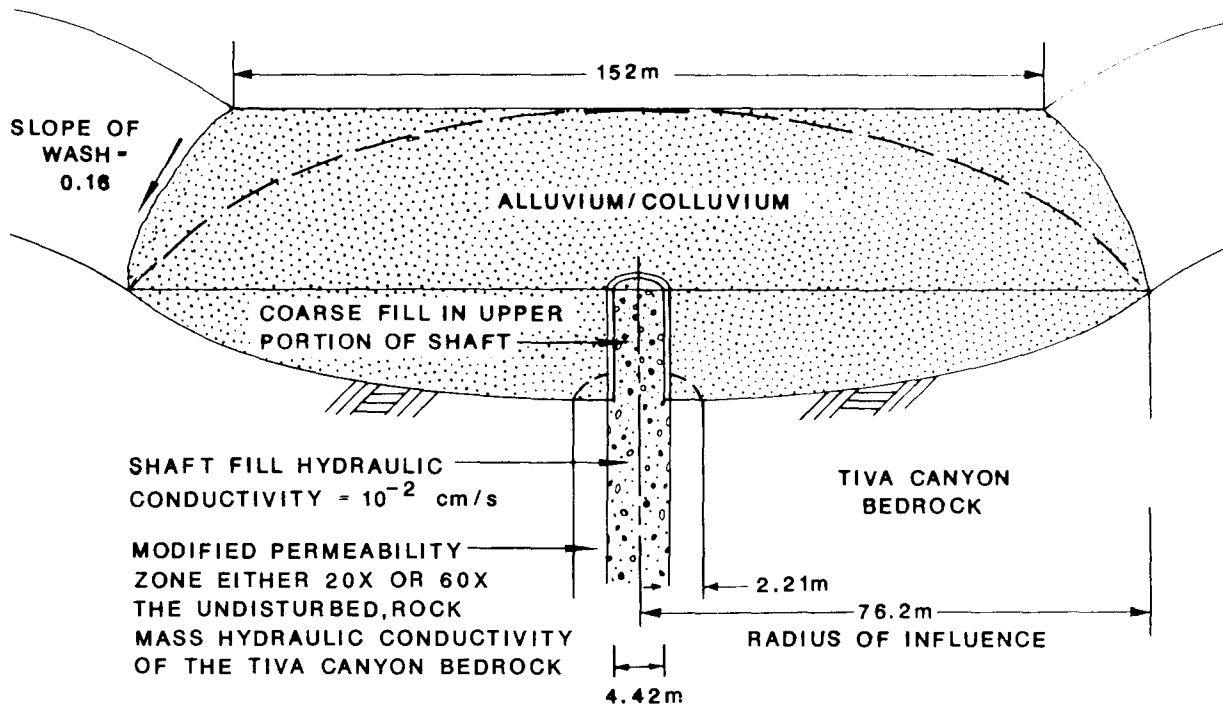


Figure C-2. Geometry of Model Used to Estimate Flow into a Shaft from Saturated Alluvium

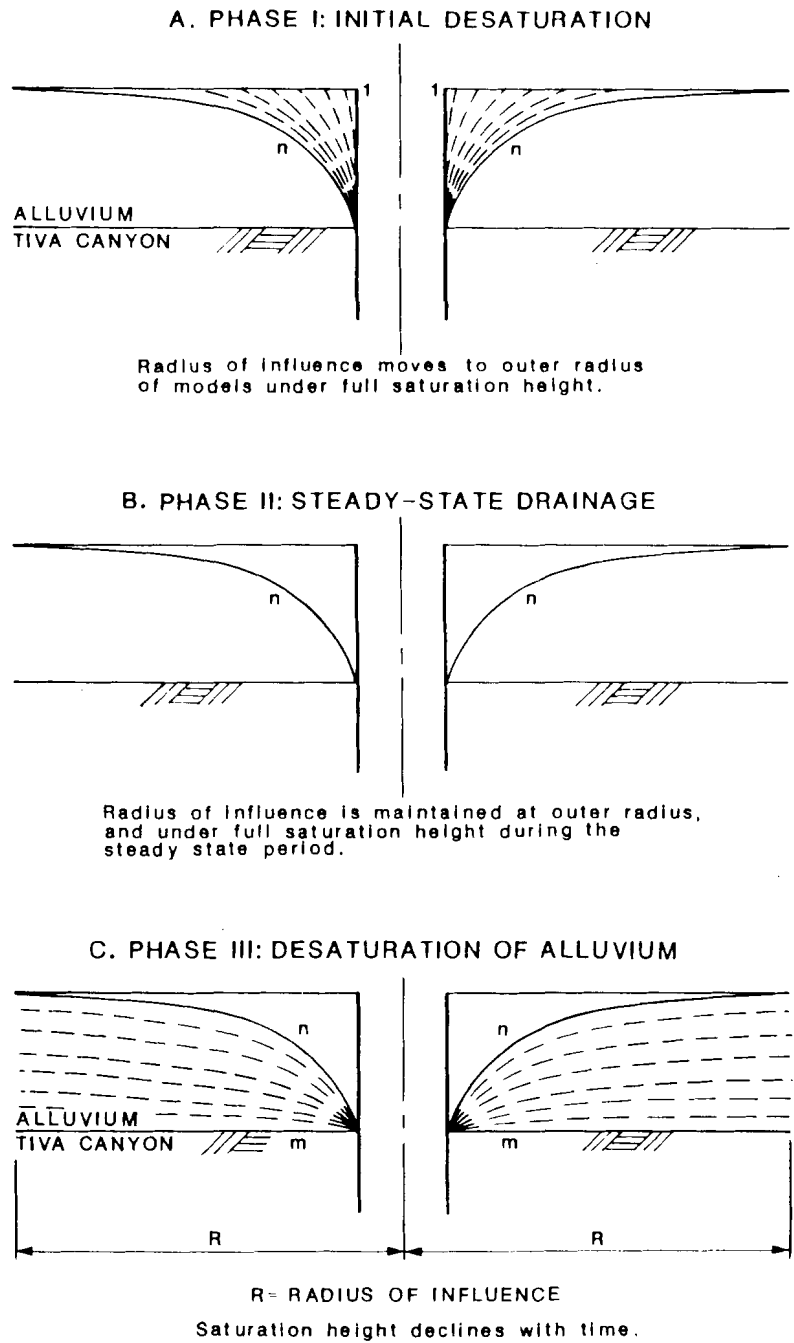


Figure C-3. Phases of Flow into a Shaft from Saturated Alluvium

During each phase of drainage, four types of flow are considered: unconfined radial flow under the Dupuit flow assumption, alluvial flow, Tiva Canyon flow, and flow through the MPZ and the shaft fill. Each of the flows are discussed below.

Radial flow is computed using the following equation:

$$Q_s = \frac{\pi K(H^2 - H_o^2)}{\ln\left(\frac{R}{r_o}\right)}, \quad (C-1)$$

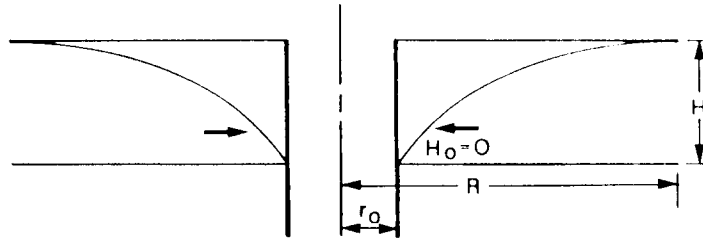
where

- R = radius of influence,
- Q_s = flow rate into the shaft,
- K = hydraulic conductivity,
- H = piezometric level at radius R,
- H_o = piezometric level at radius r_o , and
- r_o = shaft radius.

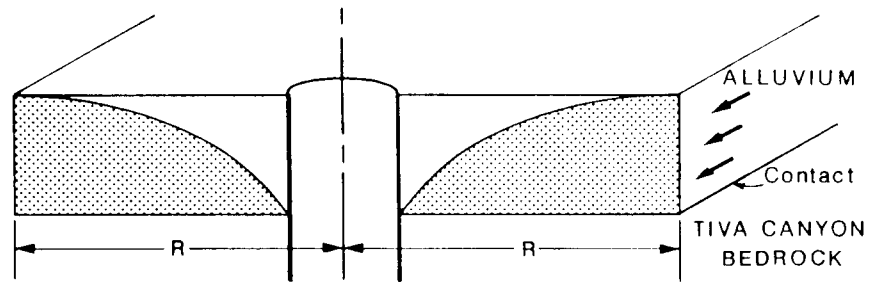
This equation, taken from Terzaghi and Peck (1967, p. 167), assumes steady-state flow in the horizontal direction under unconfined conditions. Radial flow is illustrated in Figure C-4a.

Alluvial flow is assumed to occur through the shaded area as shown in Figure C-4b, under a hydraulic gradient that coincides with the average alluvial grade. This approach was adopted to simplify the calculations and was compared to an alternate calculation that involved uniform flow above the shaft and a "zone of capture" near the shaft (Fernandez et al., 1987, Appendix A-4). In the "zone of capture" calculation (Figure C-5), all water flowing down the wash lying within the capture zone is predicted to eventually flow down the shaft. In this zone, the radial flow velocity induced by the drawdown of water on the surface near the shaft is sufficiently strong to overcome the tendency for flow to occur laterally down the alluvium in the wash. A more detailed calculation indicates that the simplified approach of computing the alluvial flow rate as the product of the saturated hydraulic conductivity (the shaded area) and the alluvial grade is reasonable.

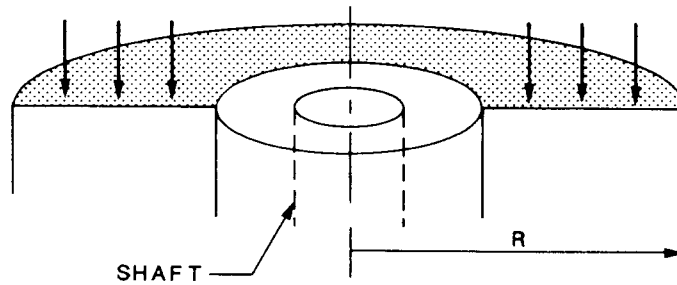
A. DUPUIT (RADIAL) FLOW



B. ALLUVIAL FLOW



C. TIVA CANYON FLOW



D. MPZ AND SHAFT FLOW

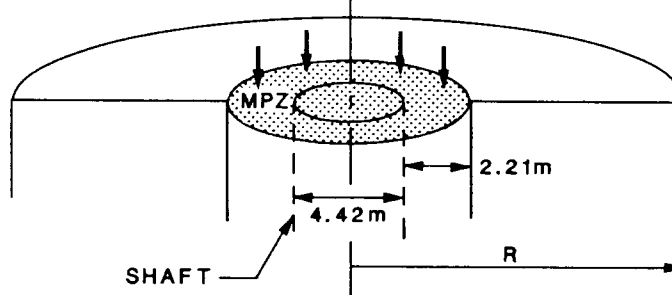
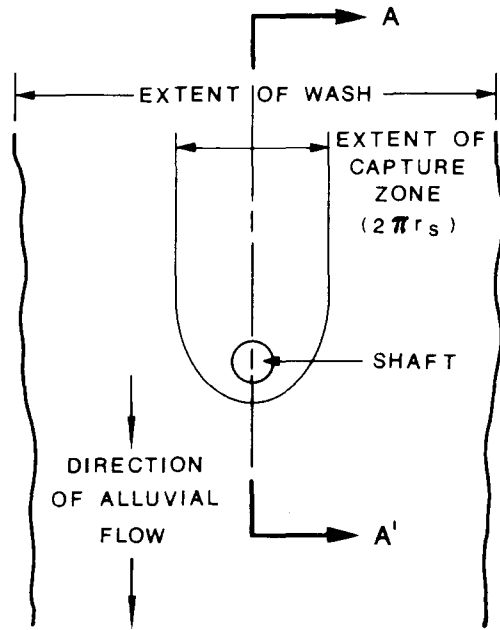
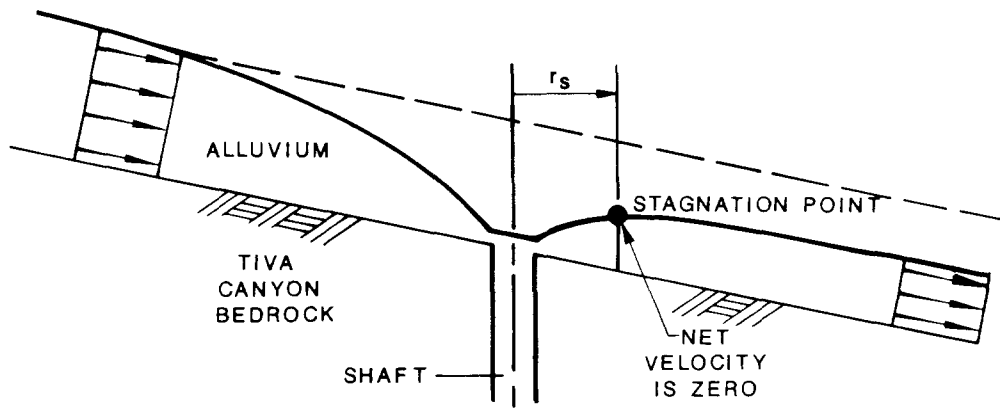


Figure C-4. Types of Flow Considered in Estimating Flow into a Shaft (Flows Occur Concurrently During Phases I, II, and III)



(a) PLAN VIEW
(Not to Scale)



(b) ELEVATION VIEW A-A'

Figure C-5. Capture Zone Near a Shaft

Tiva Canyon flow is the assumed vertical infiltration of water through the Tiva Canyon unit. It is assumed to occur through the shaded area under a unit gradient as might occur for fractured rock that is saturated. It is recognized that the bedrock is unsaturated and that infiltration rates are likely to be higher; nevertheless, the flow calculation is conservative in underestimating this component of flow (greater proportion of flow is directed to the shaft).

MPZ and shaft flow is the vertical infiltration through the MPZ and the shaft fill and the shaft liner. In this analysis, it is assumed that the hydraulic conductivity of the shaft liner is equivalent to the hydraulic conductivity of the shaft fill. It is also assumed that the shaft fill is near saturation and is exposed to atmospheric conditions. Accordingly, flow occurs under unit gradient. It is noted that the degree to which infiltration would occur at unit gradient depends on the level of saturation and that initially the hydraulic gradient could exceed unity. These high infiltration rates would be associated with the saturation of voids because of capillarity and not transmission of water to the base of the shaft. As the infiltration front reaches the base of the shaft, at which point water could potentially enter the repository, the hydraulic gradient would be approximately one.*

These flows are superimposed such that flow can occur as Tiva Canyon flow, alluvial flow, or shaft flow. Therefore, as a volume of water is computed for each portion of each phase, flow occurs proportionately through the Tiva Canyon Member, alluvium, and the shaft, as determined by

*This can be shown by the Green and Ampt solution for vertical infiltration (Hillel, 1971, p. 142). At the base of the shaft, the hydraulic gradient is given by $1 + \frac{H_o - H_f}{L_f}$ where H_o equals the pressure head at the surface, H_f equals suction head at wetting front, and L_f equals the length over which the wetting front has moved. If we assume the pressure head at the surface is 9.1 m (height of saturated alluvium above bedrock), the suction head for the backfill is -1.0 m (a typical value for coarse material), and the length over which the wetting front has moved is 311 m, then the calculated hydraulic gradient is nearly one.

the flow rate computed for each. Flow through the shaft is either the amount computed using the radial formula or the amount computed by the MPZ and shaft fill model, whichever is lower. The entire process of desaturation continues until the water supply is depleted. The potential water supply is assumed to be the waters associated with specific flooding events. The input values and assumptions used for this model are discussed below in Section C.2.2.

To arrive at the maximum inflow to the shaft, it is assumed that all the water associated with a flooding event is retained above the shaft location. This implies that the alluvium has sufficient capacity to retain all the water from the flood event, an overly conservative assumption that involves no losses by evapotranspiration or sheet flow downgrade from the shaft locations. In reality, a high percentage of the precipitation is expected to exit the drainage basin, with only a small part percolating into the alluvium or exposed bedrock. Further, it is assumed that water flow is directed vertically downward inside the shaft liner or in the shaft fill as the water percolates to the base of the shaft. It is further assumed that flow occurs through fractures within the MPZ and is not absorbed within the tuff matrix.

To verify the numerical results obtained from the model presented in this section, an alternate calculation was performed to check major assumptions, analyses methods, and input (materials properties and geometry). This alternate calculation incorporates the concept of the "capture zone" illustrated in Figure C-5. A comparison of the results from the model presented above and the model of the "capture zone" are in good agreement as discussed in Fernandez et al. (1987).

C.2.2 Input Values Used

In applying this model, the following assumptions were developed and specific conditions were evaluated for water flow.

- o PMF occurs at the ES location. The volume of water used for the PMF is $159,000 \text{ m}^3$ (Bullard, 1986) computed from a rainfall of 13.9 in. occurring over a 6-hour period.

- o No sheet flow or evapotranspiration occurs, and all of the flood waters are retained in the alluvium upgrade from ES-1.
- o ES-1 has an inside diameter of 3.7 m.
- o Both ES-1 and ES-2 in the Tiva Canyon Member have an outside diameter of 4.3 m. In this analysis an overbreak of 0.08 m on each side of the shaft is assumed giving an excavated diameter of 4.4 m.
- o MPZ in Tiva Canyon Member extends from shaft wall to a radius of 4.4 m from the centerline of the shaft.
- o Hydraulic conductivity of the alluvium varies from 10^{-5} to 100 cm/s (Freeze and Cherry, 1979, pp. 29, 147).
- o Hydraulic conductivity of the Tiva Canyon Member varies from 10^{-5} to 10^{-2} cm/s (Fernandez et al., 1987).
- o Alluvial grade of the water course is 0.16 (based on average water course grade in Coyote Wash).
- o Radius of influence is 76.2 m (based on the approximate width of alluvium at the ES-1 location).
- o Depth of alluvium is 9.1 m (based on the depth of the alluvium at borehole USW G-4).
- o Porosity of the alluvium is 0.30 (Fernandez et al., 1987, Appendix D).

C.2.3 Inflow Volumes

Applying the model described above, the maximum, yearly flow into ES-1 is computed following a PMF event. Because no evapotranspiration and sheet flow out of the drainage basin are assumed, flow into the shaft will continue until the total volume of water associated with the PMF has been depleted. For the majority of cases evaluated, the initial flood volume is depleted within the first year following the flooding event. Figure C-6 illustrates the flow into the shaft for a broad range of conditions that have been predicted by the model described in Section C.2.1 and that use the input volumes given in Section C.2.2. The flow volumes can range from approximately 30 to 20,640 m³/year. In some instances, differences between the two models assumed for the MPZ have been observed. Differences occur for two reasons. First, flow occurs through the MPZ and the shaft fill. If the majority of the total flow occurs through the shaft fill, the

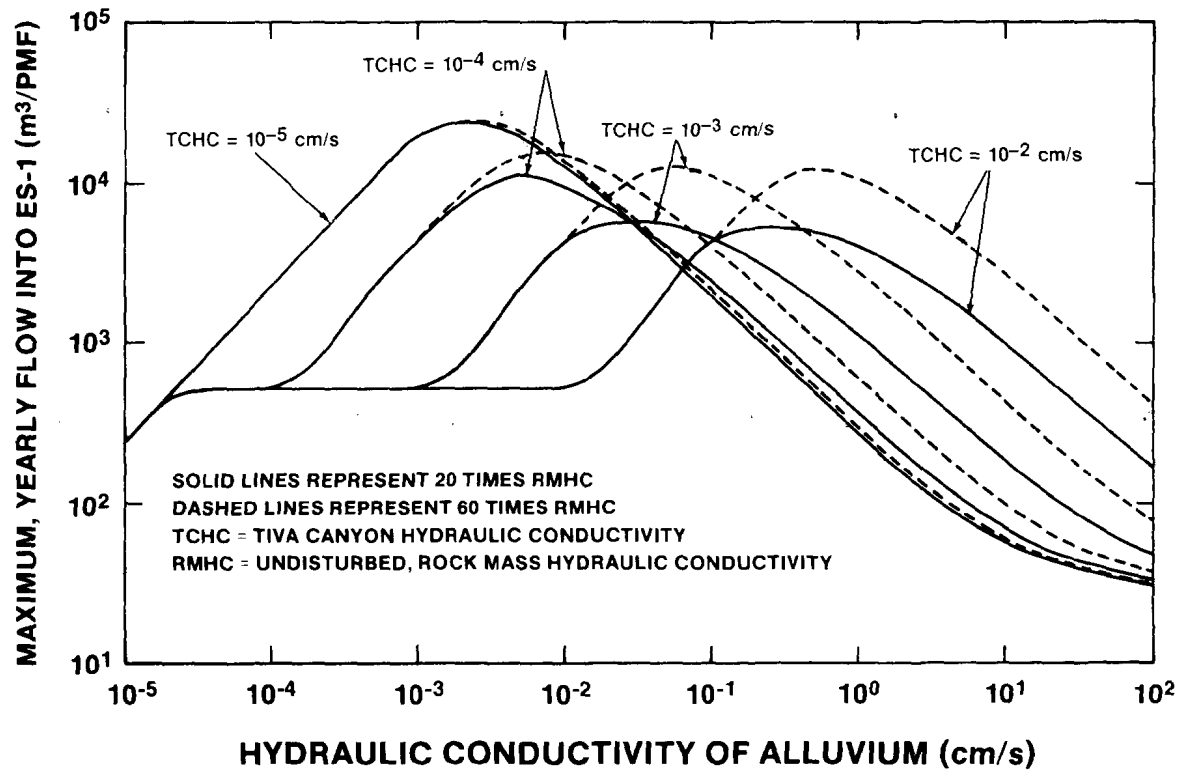


Figure C-6. Estimated Volumes of Water Entering ES-1 (PMF, Shaft Fill Conductivity = 10⁻² cm/s, Excavated Shaft Diameter = 4.42 m)

difference between the flows associated with each MPZ model is negligible. Second, flow into the MPZ and shaft fill can be no greater than the rate at which the water is released from the alluvium using the Dupuit assumption of radial flow to the shaft. Thus, when the saturated, hydraulic conductivity of the alluvium is low, the volume of water entering the MPZ and shaft fill is less than the full capacity of the MPZ and shaft fill. Therefore, no discrimination between the models is observed. A more complete explanation of the shape of the curves, presented in Figure C-6, is given in Appendix D.

C.2.4 Duration and Rate of Flow Into Shaft

In addition to knowing the total flow down the shaft, it is also important to understand the rate and duration of flow into the shaft. Figures C-7 to C-10 illustrate the duration of flow into the upper portion of the shaft. The duration is the time at the right end point of each curve. The data presented by these figures are used as the input functions of water flow into shaft to evaluate the potential for water buildup in the sump of the ES.

Each graph in Figures C-7 to C-10 illustrates water flows into the ES assuming a constant value of hydraulic conductivity of the alluvium. The range of hydraulic conductivity values for alluvium is 10^{-5} to 100 cm/s (Freeze and Cherry, 1979, p. 29). Each graph further illustrates the effect of altering the hydraulic conductivity of the Tiva Canyon Member, located immediately below the alluvium. Because the MPZ models are related to the undisturbed, rock mass hydraulic conductivity of the Tiva Canyon, a distinction between the different MPZ models is also displayed.

As indicated earlier, duration and rate of flow (Figures C-7 to C-10) are important considerations about how water can potentially build up at the base of the shaft. Both considerations are discussed below. Duration of flow depends on the flow that occurs as described in Section C.2.1, i.e., Tiva Canyon, alluvial, and radial or shaft flows. These flows depend on the selected hydraulic properties of the alluvium and the Tiva Canyon Member. If the selected hydraulic properties of the alluvium are low, the time to drain the waters retained in the alluvium can be long. Conversely,

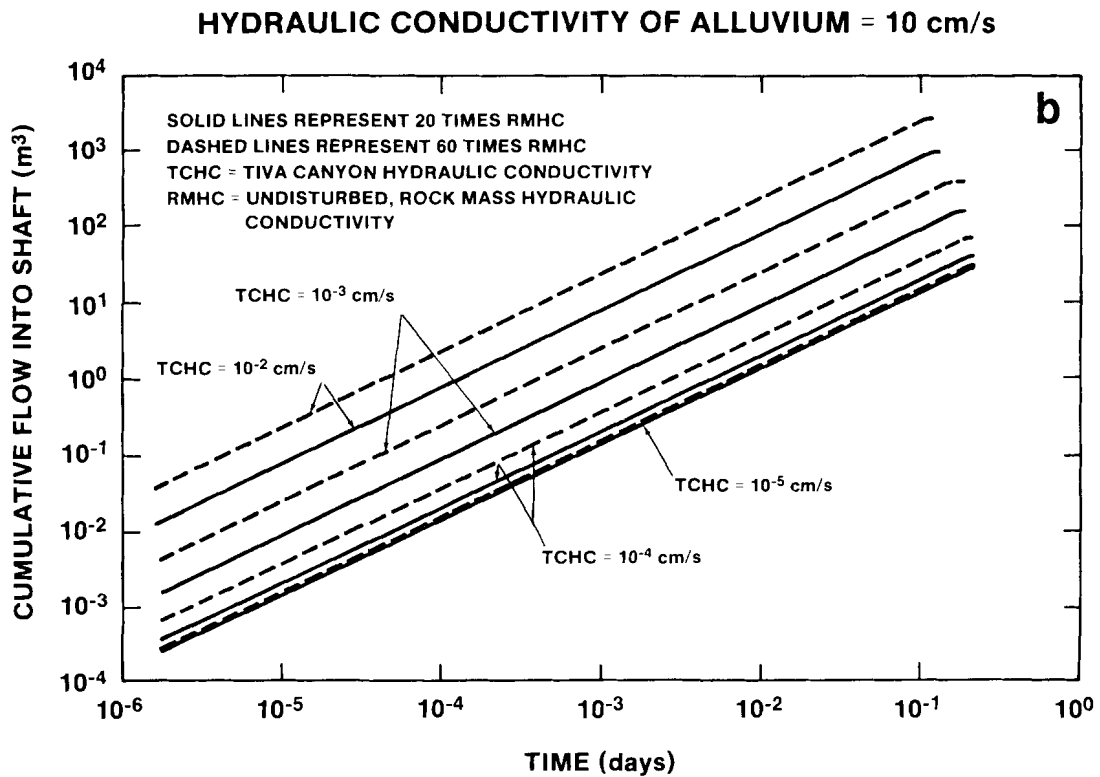
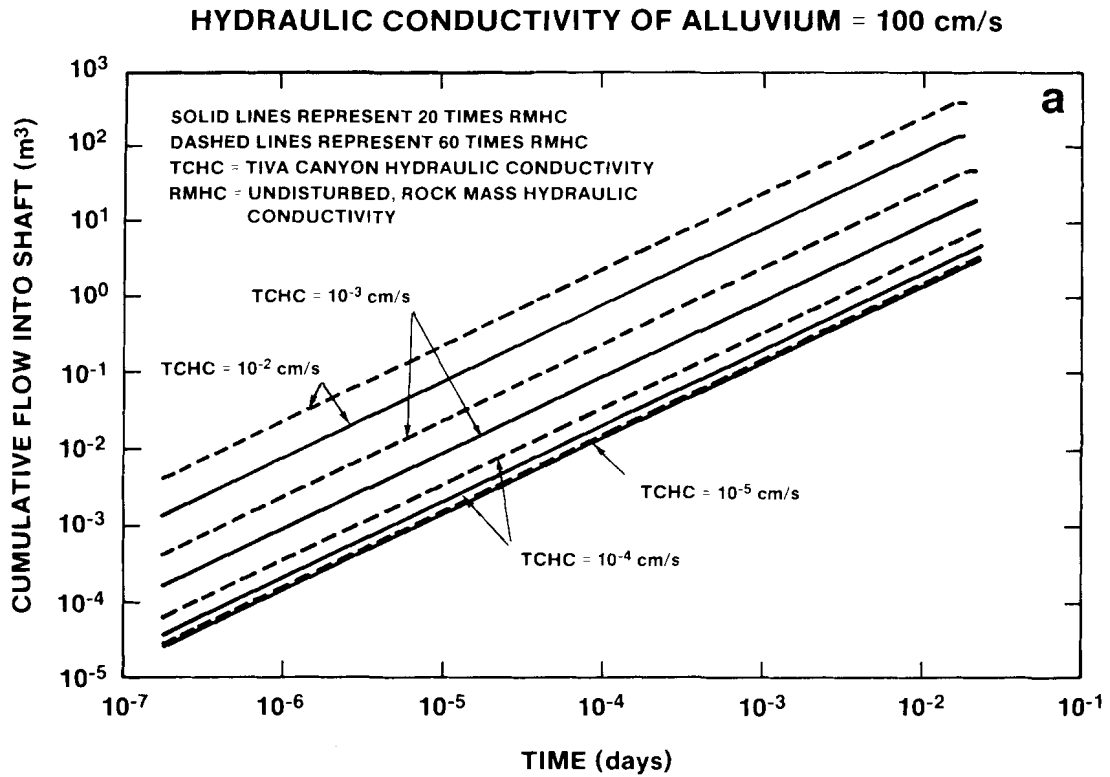


Figure C-7. Estimated Duration of Flows into ES-1 (PMF, Hydraulic Conductivity of Alluvium--100 and 10 cm/s)

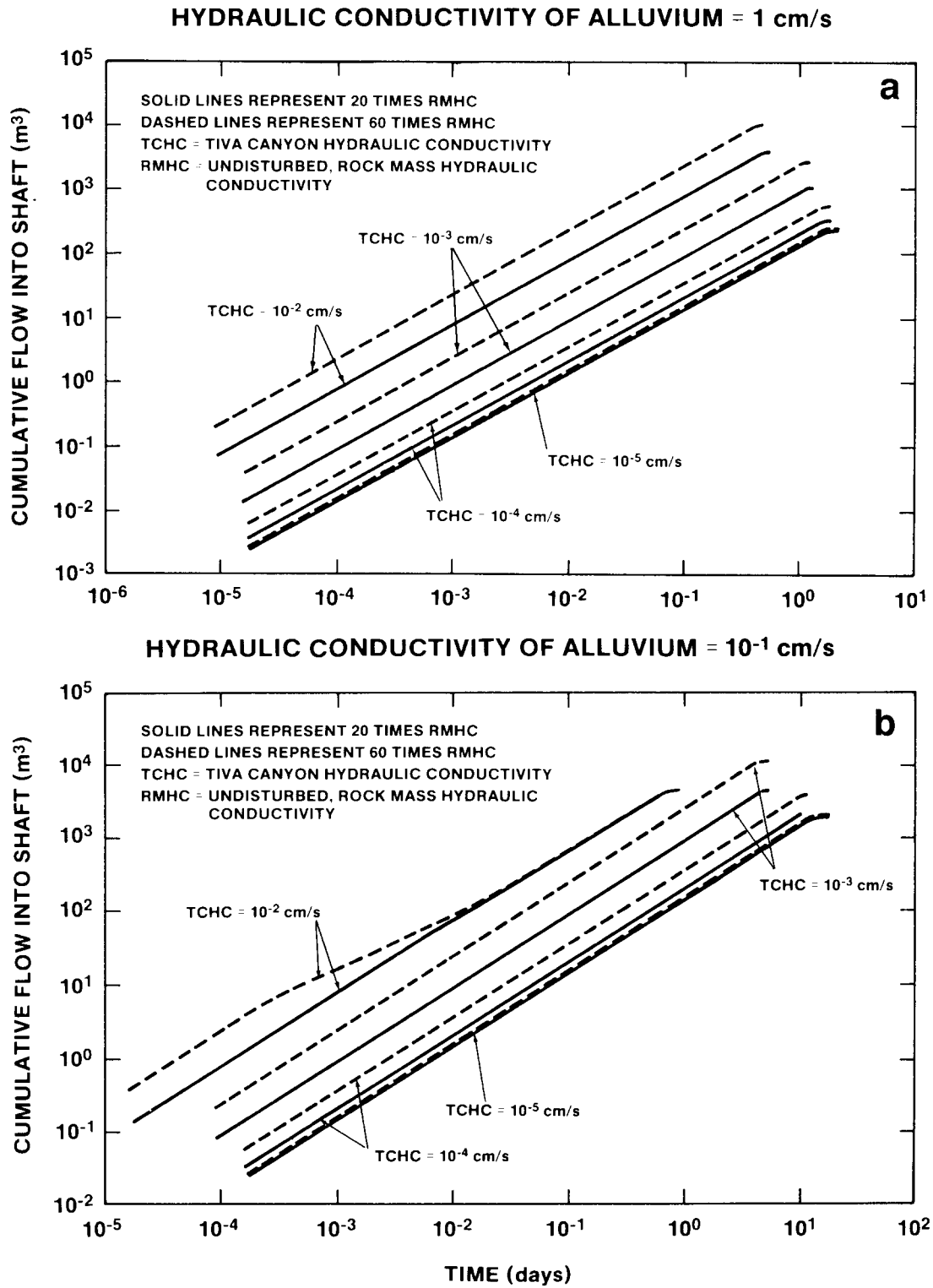


Figure C-8. Estimated Duration of Flows into ES-1 (PMF, Hydraulic Conductivity of Alluvium--1 and 0.1 cm/s)

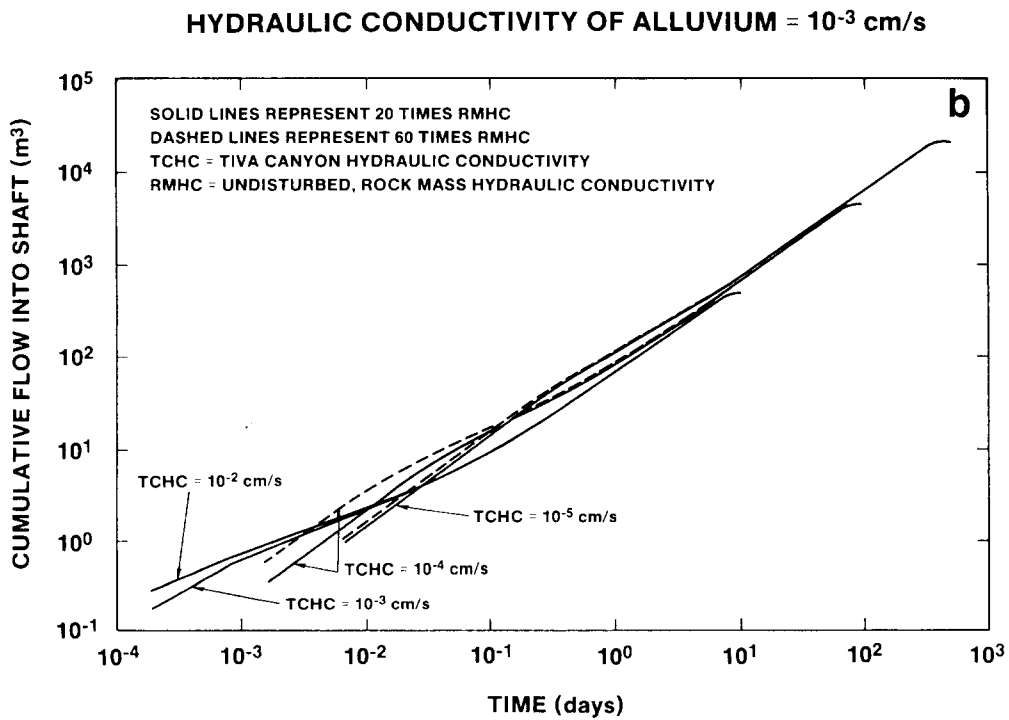
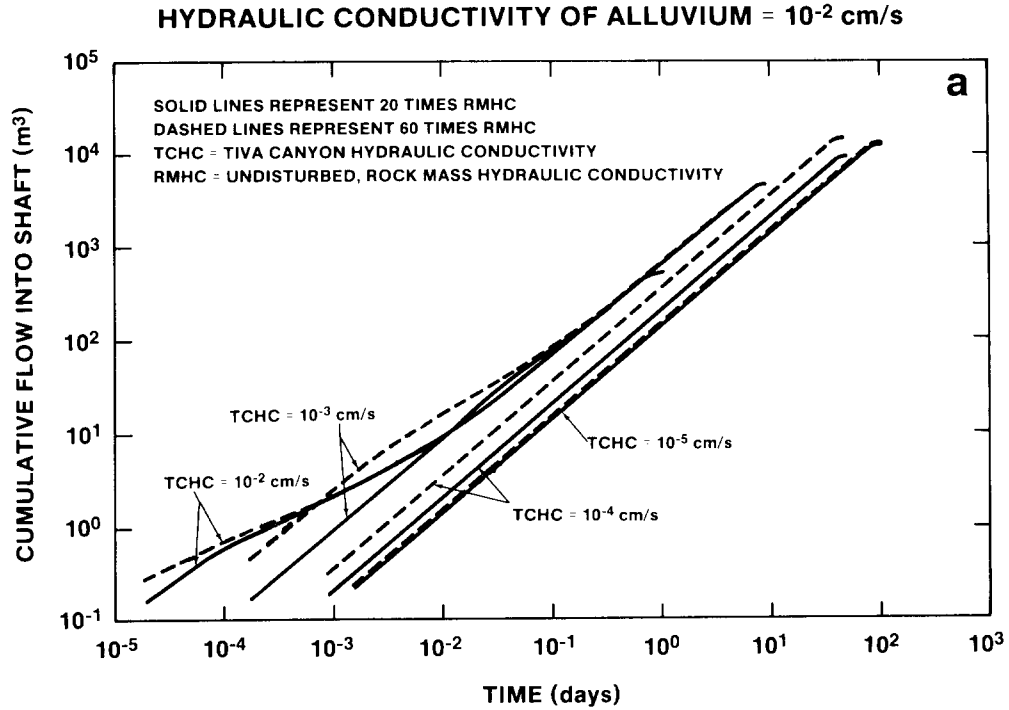


Figure C-9. Estimated Duration of Flows into ES-1 (PMF, Hydraulic Conductivity of Alluvium-- 10^{-2} and 10^{-3} cm/s)

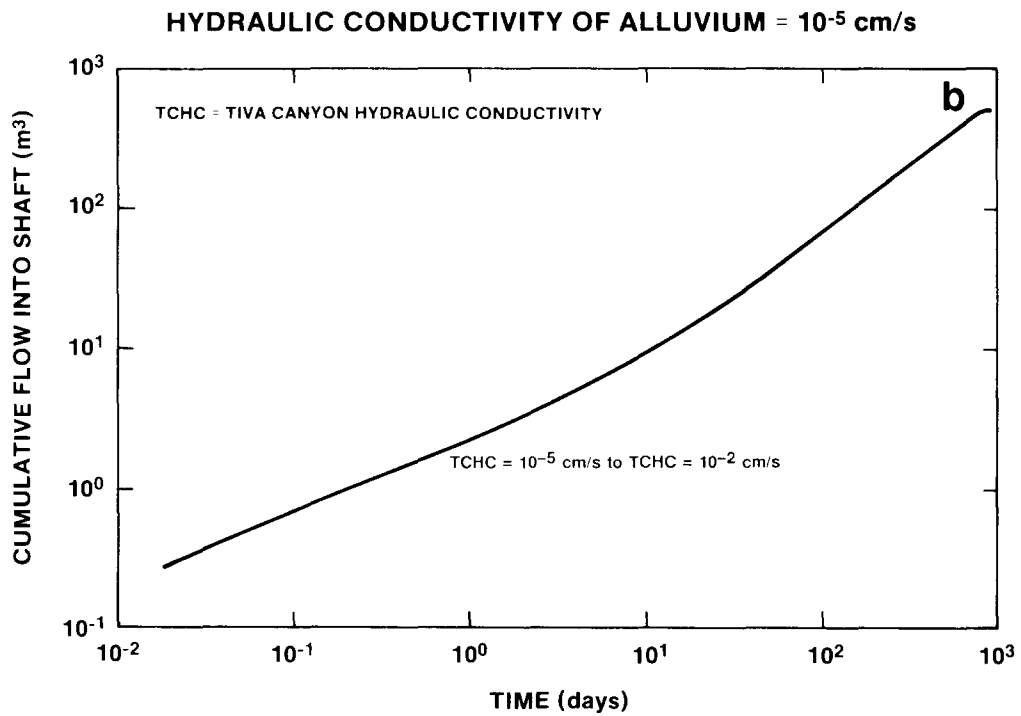
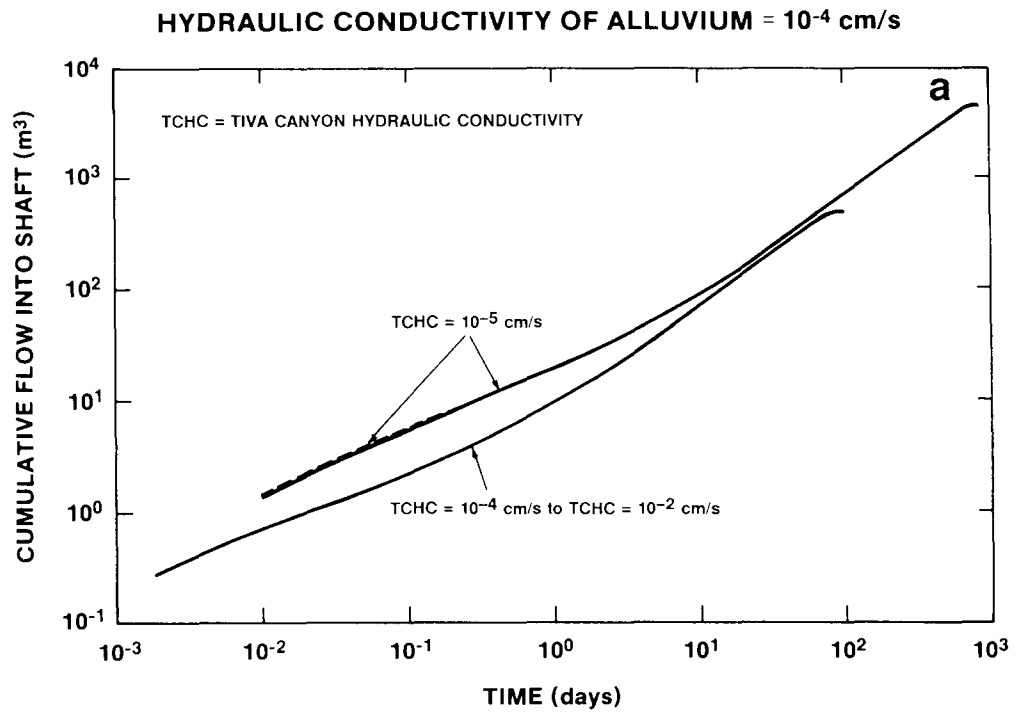


Figure C-10. Estimated Duration of Flows into ES-1 (PMF, Hydraulic Conductivity of Alluvium-- 10^{-4} and 10^{-5} cm/s)

if the hydraulic conductivities are high, the duration of flow into the shaft is limited. This effect is clearly displayed in Figures C-7 to C-10. When the hydraulic conductivity of the alluvium is high, 100 cm/s, the duration of flow into the shaft is computed as approximately 10^{-2} days or <15 minutes (Figure C-7a). When the alluvial hydraulic conductivity is low, 10^{-5} cm/s, drainage of flow into the shaft is computed to occur up to 1,000 days (Figure C-10b) following the PMF. The effects of changing duration are also noticed when the hydraulic conductivity of the Tiva Canyon Member changes. As the hydraulic conductivity of the Tiva Canyon Member decreases from 10^{-2} to 10^{-5} cm/s, the duration of flow into the shaft increases. This effect is noticed on the graphs in Figures C-7 to C-10a. However, the effect is more pronounced in total durations when the alluvial hydraulic conductivity decreases.

Another important consideration, aside from the duration of flow, is the rate of flow into the shaft, which is discussed in greater detail in Appendix D. Flow into the upper portion of the shaft is controlled by the radial flow from the alluvium to the shaft or the flow through the MPZ and the shaft fill. If the radial flow is greater than the potential for flow through the MPZ and shaft fill, the flow entering the MPZ and shaft fill will be controlled by the hydrologic properties of the MPZ and shaft fill. This condition suggests that the more water flow is restricted from entering the shaft and the MPZ because of the properties of the shaft fill and the MPZ, the greater will be the flow down the wash in the alluvium further reducing flow into the shaft. If the radial flow is less than the potential for flow through the shaft fill and MPZ, then the flow entering the shaft fill and MPZ is limited by the radial flow toward the upper portion of the shaft (Figures C-7 to C-10). For example, when the alluvial hydraulic conductivity is 100 to 0.1 cm/s, radial flow to the shaft is greater than the capacity for flow through both the shaft fill and MPZ. Therefore, a distinction between the cumulative flows for both MPZ models is noticed. As the hydraulic conductivity of the alluvium decreases further, the radial flow into the shaft decreases until the radial flow into the upper portion of the shaft is less than full flow capacity of the MPZ and shaft fill. This effect is first noticed (Figure C-8b) when the flow model is 60 times the Tiva Canyon hydraulic conductivity of 10^{-2} cm/s.

The flow rate into the upper portion of the shaft is further reduced as the alluvial hydraulic conductivity is reduced. When the alluvial hydraulic conductivity is extremely low, 10^{-5} cm/s, the flow through all MPZ and shaft models is controlled by the radial flow toward the shaft. In this case (Figure C-10b), no distinction between any of the MPZ models is possible. It is also true that when flow through these MPZ models is less than their full flow capacity, the model is only partially saturated. As mentioned earlier, the data presented in Figures C-7 to C-10 are used as input to estimate the potential for water buildup at the base of the ES.

C.3 Model Used for Water Flow out of the Shaft

If water enters the shaft faster than it can be effectively drained, buildup of water is possible. Further, if water buildup is greater than the capacity of the sump, then lateral migration through the repository station seal, into the underground facility, and ultimately, toward the waste disposal areas is possible. The model and input used to determine the potential for water buildup in the sump of ES-1 are discussed below. As indicated in Section C.2, because the upper portion of the old ES-2 location is near the boundary of the alluvium and bedrock, the mechanism of water flow from the alluvium into the shaft as described in Section C.2 is not likely.

C.3.1 Model Description

The purpose of this section is to describe the model used in assessing the potential for water buildup at the base of the ES. It is assumed that the concrete liner at the base of the shaft has been removed. This corresponds to an unlined portion of the shaft approximately 145.5 m from the base of the shaft to the crown of the repository station drift. The modeled sump depth is about 140 m, i.e., the distance from the invert* of

*The invert is the lowest point in elevation of the drift. This sump depth of 140 m corresponds to that presented in the "Site Characterization Plan Conceptual Design Report" (SNL, 1987, p. 4-69).

the repository station drift to the base of the shaft. The excavated diameter of the sump is 4.4 m. The entire shaft is assumed to be back-filled with a shaft fill having a porosity of 0.3. Figure C-11 illustrates the physical model described above.

To compute the maximum buildup of water at the base of the shaft, the following conservative assumptions have been made: (1) the amount of water entering the upper portion of the shaft (Section C.2.4) is transported immediately to the base of the shaft and (2) no leakage outside the MPZ occurs above the buildup of water in the base the shaft. In reality, water can leak into the rock mass outside the MPZ as it migrates down the MPZ. The reason for restricting the downward flow of water to the MPZ and shaft fill is primarily to maximize the potential for water buildup at the base of the shaft. If water flowing into the shaft is dispersed into the undisturbed rock mass, the significance of the MPZ and shaft fill is diminished.

Once water reaches the base of the shaft, it builds up, increasing the saturation levels in the bulk rock. As water builds up, it can also drain through the bulk rock at the base of the shaft, predominantly through fractures. Only when the water in the shaft reaches the invert of the repository station drift does it have the potential to pass through the repository station seals. (Two repository station drifts extend from the ES.)

Flow from the base of the shaft is predicted by analytical solutions used for calculating the saturated hydraulic conductivity above the water table using borehole infiltration tests. Flow through the repository station seals is described by Darcy's law.

Several analytical solutions described in Stephens and Neuman (1982, p. 642) were considered in computing the flow through the sump of the shaft. It should be noted that Stephens and Neuman evaluated the suitability of several analytical solutions to predict the saturated hydraulic conductivity of soils. The pressure head in the soils evaluated ranged from 0 to -1.6 m of water (Stephens and Neuman, 1982, p. 644). The

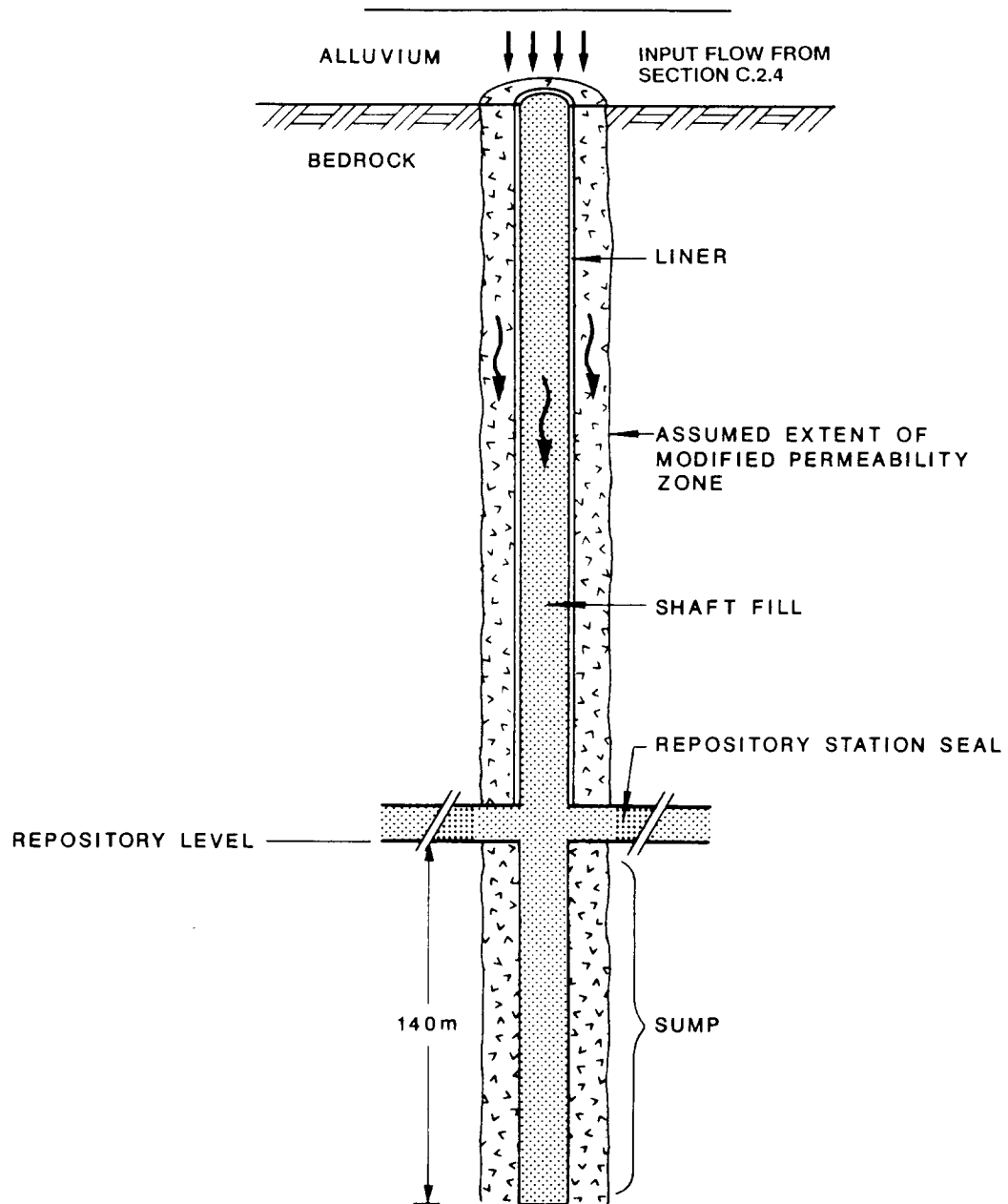


Figure C-11. Model Used to Compute the Water Balance in the Exploratory Shaft

pressure head in the matrix of tuff can range from 0 to -1,000 m of water (Peters et al., 1984, p. 2). However, because we are computing the drainage of water from a shaft sump that is predominantly in highly fractured welded tuff, drainage will occur primarily through the fractures. Because these fractures are closely spaced and because the range of pressure heads (0 to -1 m) for fractures (Wang and Narasimhan, 1984, p. 24; Klavetter and Peters, 1986, p. 20) is similar to that of coarse sand, we feel that selected analytical solutions presented by Stephens and Neuman can reasonably approximate the drainage from a shaft. Furthermore, a better understanding of the hydrologic characteristics and the drainage properties of fractured tuff will be obtained by field tests associated with the ES testing.

The analytical solutions considered in this report include those developed by Glover, Nasberg-Terletskaia, and Zanger (Stephens and Newman, 1982, pp. 640-659). To evaluate the differences between these analytical solutions, Stephens and Neuman defined two dimensionless quantities, C_u and H_D , defined as

$$C_u = \frac{Q_s}{K_s r H}$$

and

$$H_D = \frac{H}{r} ,$$

where

Q_s = infiltration or drainage rate at steady state, m^3/s ;

K_s = saturated, hydraulic conductivity, m/s ;

r = shaft radius, m ; and

H = height of water column in shaft, m .

The dimensionless value, C_u , was defined as follows:

$$C_u = \frac{2\pi H_D}{\sinh^{-1}(H_D) - 1} \quad (\text{Glover})$$

$$C = \frac{2.364 H_D}{\log_{10} (2 H_D)} \quad (\text{Nasberg-Terletska})$$

$$C_u = \frac{2\pi \left(\frac{A}{H}\right) H_D \left(2 - \frac{A}{H}\right)}{\sinh^{-1} \left[\left(\frac{A}{H}\right) H_D \right] - \left(\frac{A}{H}\right)} \quad (\text{Zanger})$$

The value of A in the Zanger equation represents the length of the shaft in hydraulic contact with the rock. Because the drainage rate is directly proportional to C_u , a relative comparison of C_u factors can illustrate a difference in the drainage rate out of the shaft. A comparison of the C_u factor for the analytical solutions considered is presented in Figure C-12a. In Figure C-12b the flow rates from the shaft, as computed for each analytical solution, are displayed. To be conservative, the lowest drainage rate is selected to compute the drainage from the shaft sump. This suggests that the Nasberg-Terletska formula is used for most of the shaft, i.e., the lower 325 m. In the upper part of the shaft, the Zanger formula provides a lower drainage rate. Stephens and Neuman (1982) compare the results obtained from various analytic solutions with the results from a finite element program FREESURF. They concluded that the C_u factor computed by the Nasberg-Terletska method is less than the C_u factor computed by FREESURF by 5 to 10% when $H_D > 50$ and by 25% or more when $H_D < 30$. Therefore, we feel that the selection of the Nasberg-Terletska method is reasonably conservative and appropriate.

When the height of water in the shaft is greater than the depth of the sump, drainage can also occur through the station seals. Flow through the station seals is defined by the following equation:

$$Q_p = K_s \frac{dh}{dl} A_p \quad ,$$

where

Q_p = drainage rate through the repository station plug;

$\frac{dh}{dl}$ = gradient of flow between the two faces of the repository station seal;

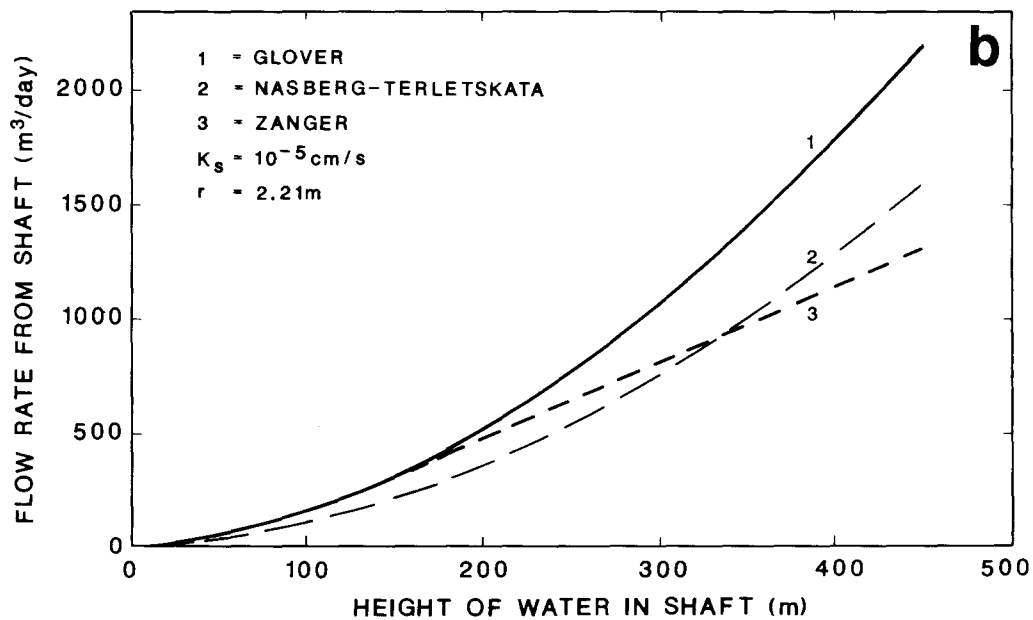
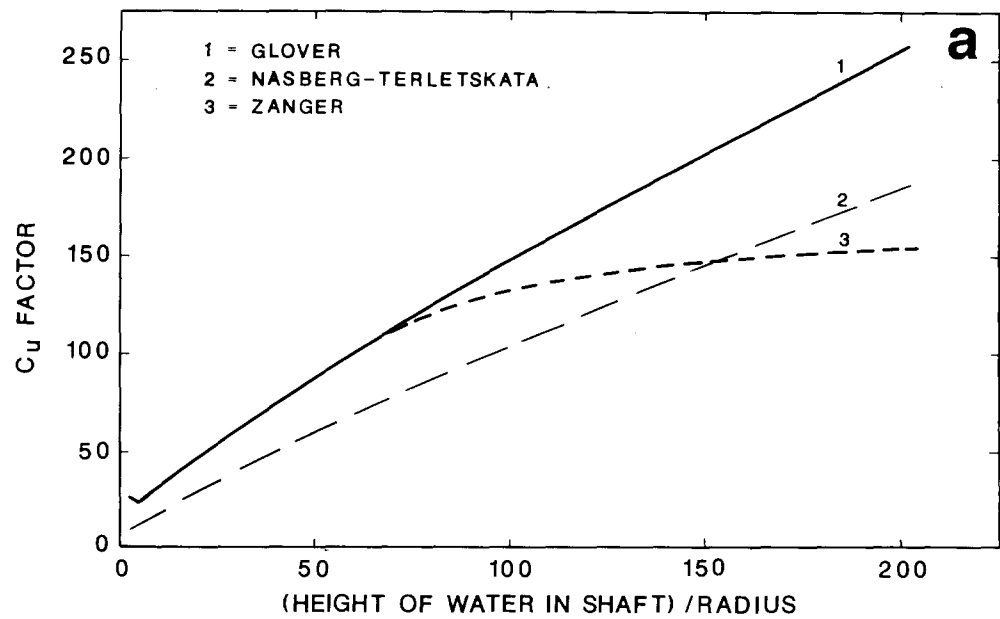


Figure C-12. Comparison of Methods Used to Compute Drainage from a Shaft

dh = change in hydraulic potential over the length of the seal;
dl = assumed length of the seal, i.e., twice the width of the drift
cross section; and
 A_p = cross section of the plug.

The pressure head acting on the face of the repository station plug is assumed to be equal to the height of water above the repository station flow. As the height of water builds up in the shaft, the gradient across the plug increases. It is further assumed that the repository station plug is fully saturated. This assumption maximizes the amount of water that passes the plug. The following sections describe the input values of K_s used in the formulas given above.

C.3.2 Input Values Used

The sump of ES-1 (old design) was designed to be predominantly in the densely welded portion of the Topopah Spring Member with approximately 15 m penetrating the nonwelded zeolitic portion of the tuffaceous beds of Calico Hills.* The Topopah Spring Member is considered to be freely draining and has a high permeability because of its pervasive and abundant fractures. The nonwelded portion of the tuffaceous beds of Calico Hills is not expected to be as intensely fractured. However, the saturated, bulk-rock hydraulic conductivity of either the densely welded portion of the Topopah Spring Member or the nonwelded Calico Hills vitric or zeolitic units is higher than their matrix hydraulic conductivities. Estimates for the bulk, saturated hydraulic conductivity are approximately 10^{-2} to 10^{-5} cm/s (Scott et al., 1983, p. 299) for the Topopah Spring Member and 2.4×10^{-4} or 10^{-3} cm/s for the tuffaceous beds of Calico Hills (Sinnock et al., 1984, pp. 11-12; Scott et al., 1983, pp. 299). In calculating the drainage rate from the sump, the saturated, rock mass hydraulic conductivity is assumed to range from 10^{-5} to 10^{-2} cm/s. The selection of a specific value depends on and is consistent with the undisturbed, rock mass hydraulic conductivity assumed for the MPZ model. For example, if the undisturbed, rock mass

*This represents the old design depth. The current design for ES-1 does not penetrate into the tuffaceous beds of Calico Hills.

hydraulic conductivity is 10^{-4} cm/s, then the saturated hydraulic conductivity at the base of the shaft is also assumed to be 10^{-4} cm/s. Because ES-1 was planned to penetrate slightly into the vitric and zeolitic portion of the Calico Hills nonwelded unit (approximately 23 m; DOE, 1988, p. 8.4-31), the bulk saturated hydraulic conductivity of the rock surrounding the sump has been restricted to a maximum value of 10^{-3} cm/s for the tuffaceous beds of Calico Hills when the undisturbed rock mass hydraulic conductivity is assumed to be 10^{-2} cm/s for the MPZ model. This restriction only slightly reduces the overall, rock mass, hydraulic conductivity of the sump because most of the sump (assumed to be 140 m in SNL, 1987, p. 4-69) will be surrounded by welded and highly fractured tuff.

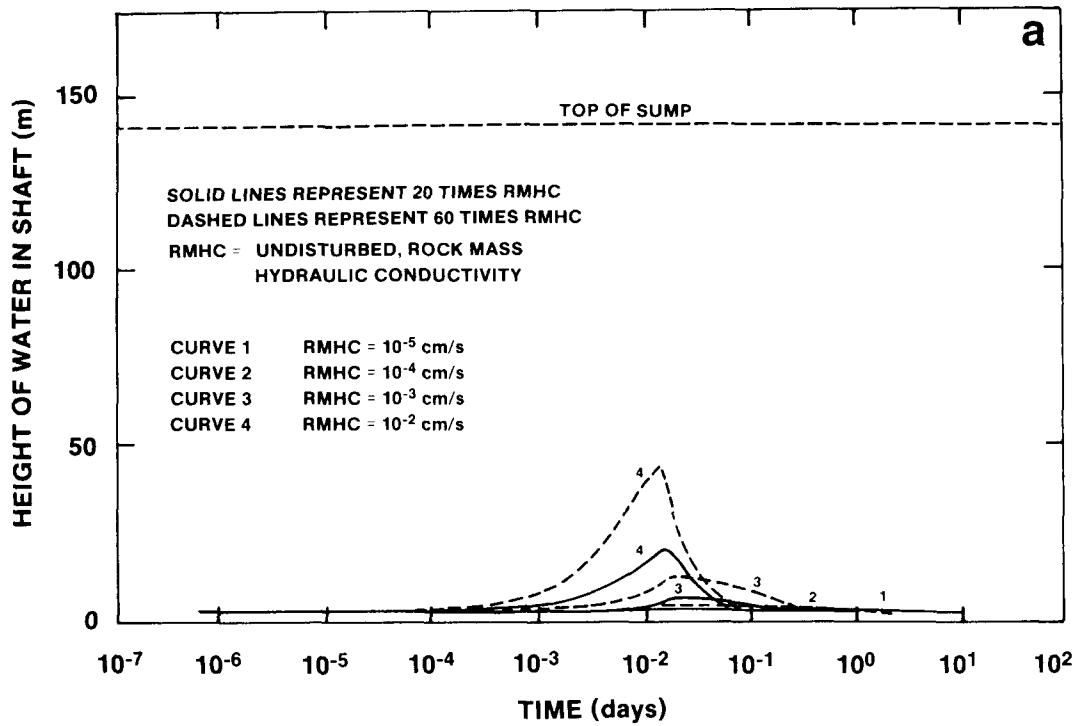
A similar logic is used in selecting the saturated, hydraulic conductivity of the repository station seal. In general, the repository station drift seal restores the surrounding rock mass to its original, undisturbed, hydraulic conductivity. The repository station seal if needed will be located in the densely welded portion of the Topopah Spring Member.

C.4 Water Balance in the Exploratory Shaft

Using the inflow rates described in Figures C-7 and C-10 in Section C.2 and the appropriate drainage rate from Section C.3, we computed the water balance in the ES. In all cases, water builds up. However, in two cases (when the saturated hydraulic conductivity of the alluvium is 10^{-5} and 10^{-4} cm/s), the buildup is limited because the flow into the shaft and MPZ is very low. Therefore, graphs of the height of water in the shaft versus time are displayed for only six cases (when the hydraulic conductivity of the alluvium is between 100 to 10^{-3} cm/s).

The results displayed in Figures C-13 to C-15 show that the height of water in the shaft varies from essentially no water to 126 m. In all cases when the MPZ model is 20 or 60 times the undisturbed rock mass hydraulic conductivity, the maximum height of the water in the shaft is below the repository station invert. In all cases evaluated, no flow through the repository station seal is computed. Again, it should be stated that shaft inflows predicted here are unanticipated and highly improbable. The

HYDRAULIC CONDUCTIVITY OF ALLUVIUM = 100 cm/s



HYDRAULIC CONDUCTIVITY OF ALLUVIUM = 10 cm/s

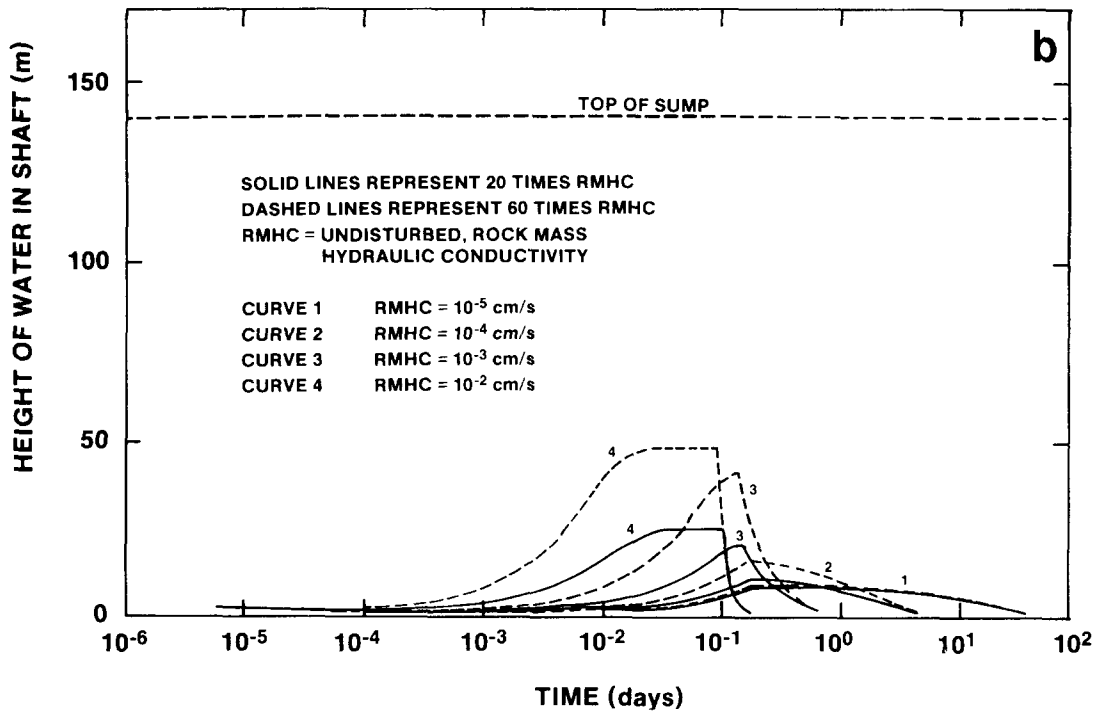
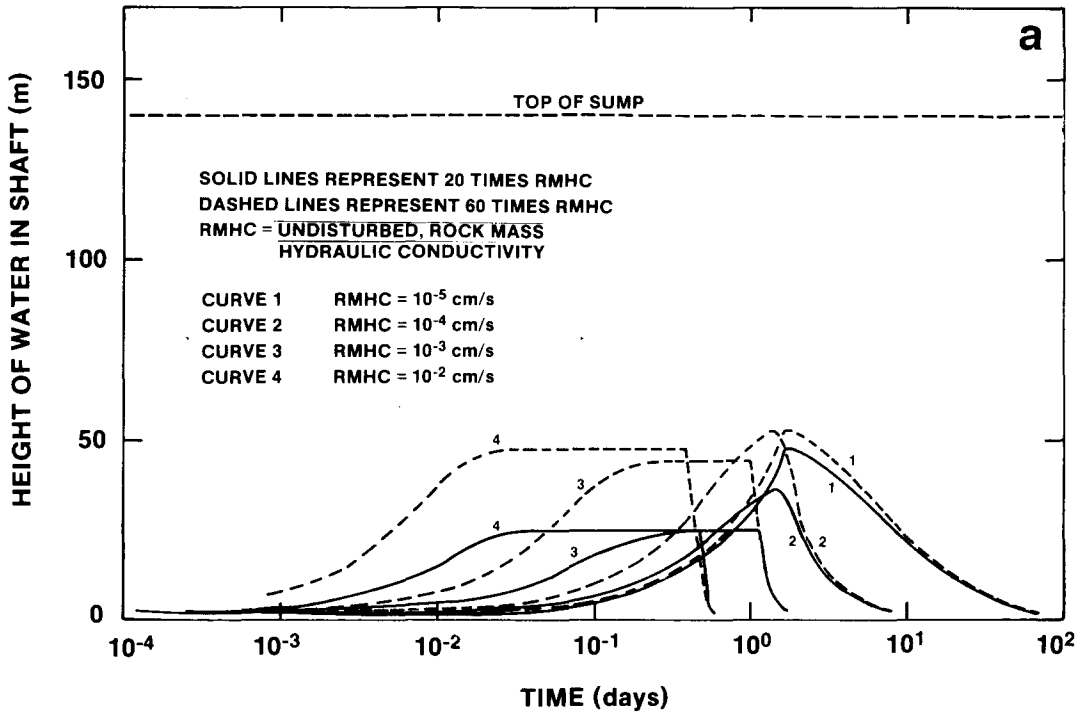


Figure C-13. Estimated Buildup of Water in the Sump of ES-1 (Hydraulic Conductivity of Alluvium--100 and 10 cm/s)

HYDRAULIC CONDUCTIVITY OF ALLUVIUM = 1 cm/s



HYDRAULIC CONDUCTIVITY OF ALLUVIUM = 10⁻¹ cm/s

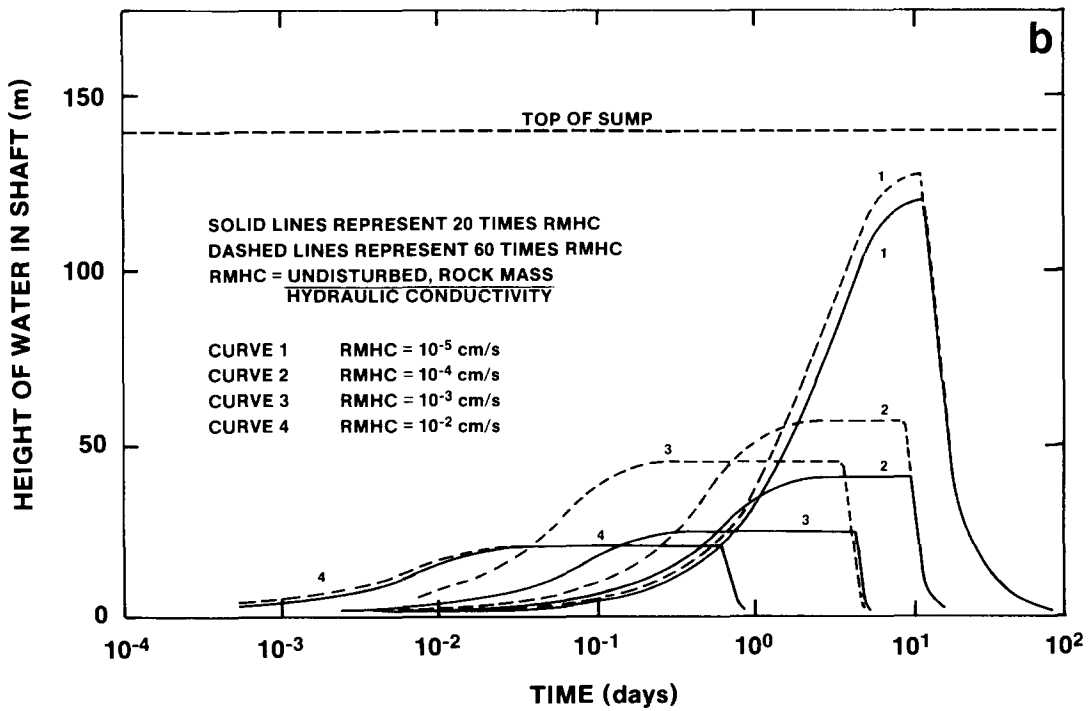
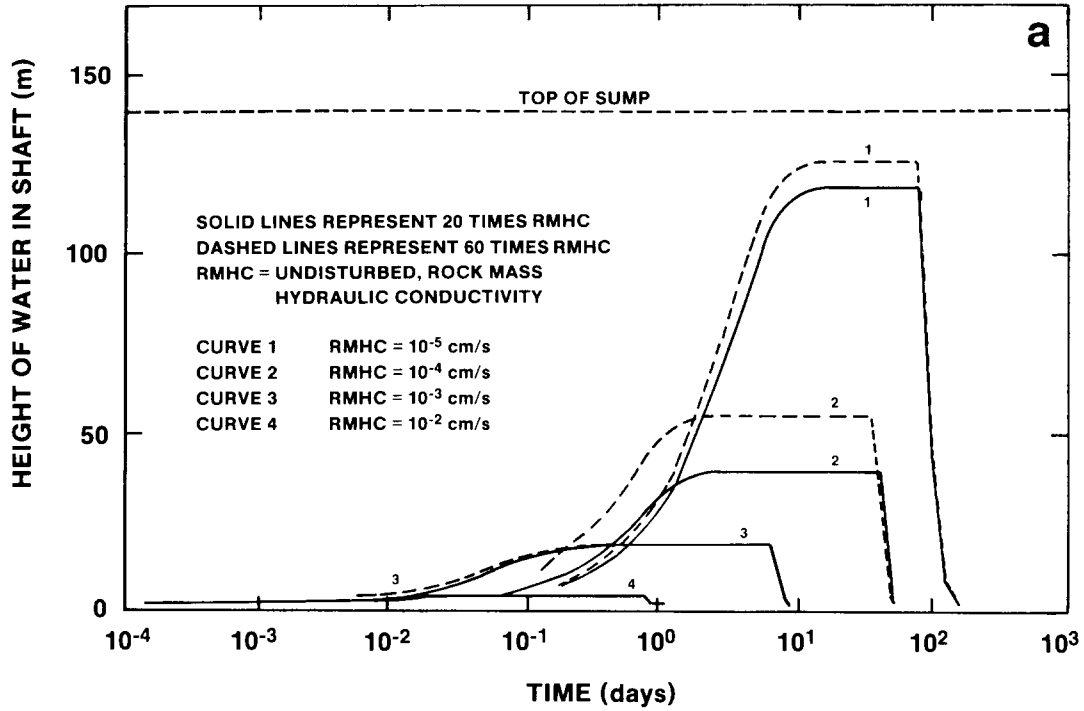


Figure C-14. Estimated Buildup of Water in the Sump of ES-1 (Hydraulic Conductivity of Alluvium--1 and 0.1 cm/s)

HYDRAULIC CONDUCTIVITY OF ALLUVIUM = 10^{-2} cm/s



HYDRAULIC CONDUCTIVITY OF ALLUVIUM = 10^{-3} cm/s

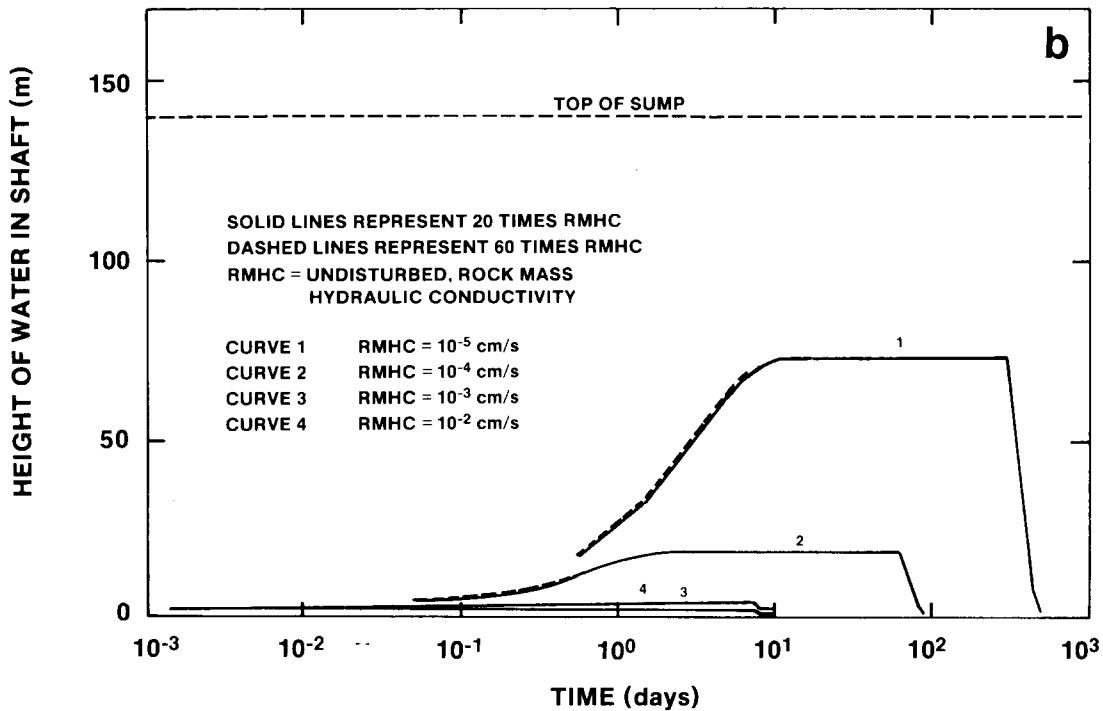


Figure C-15. Estimated Buildup of Water in the Sump of ES-1 (Hydraulic Conductivity of Alluvium-- 10^{-2} and 10^{-3} cm/s)

approach used in this report was to develop a scenario that would have an improbable, upper-bound water flow into the shafts.

Several general features have been observed in the curves in Figures C-13, C-14, and C-15. The duration of inflow in all curves is greatest when the hydraulic conductivity of Tiva Canyon is the lowest of the assumed range, 10^{-5} cm/s. This is to be expected as indicated by the duration of flows in Figures C-7 to C-10. The portion of the curves to the left of the peaks represents the period during which drainage from the sump is less than the flow into the upper portion of the shaft. The slopes of the curves beyond the peaks depend on the hydraulic conductivity of the rock mass through which the water is draining and the height of water in the shaft. The greater the rock mass hydraulic conductivity, the greater is the slope. The lower the height of water in the shaft, the slower is the drainage and the longer it takes for the water to fully drain from the shaft. In some cases plateaus are observed. These plateaus represent the condition when the rate of flow into the shaft is equal to the rate of flow out of the base of the shaft. Also, when the inflows are greater for the condition where the MPZ is 60 times the undisturbed rock mass hydraulic conductivity, the height of water reached in the shaft is greater.

An additional observation is the point at which the peaks occur for a specific, undisturbed rock mass hydraulic conductivity. Two factors important in noting where these peaks occur are the magnitude and the duration of inflow. For example, when the alluvial hydraulic conductivity is 100 cm/s, the duration of inflow into the shaft is short. As the hydraulic conductivity of the alluvium decreases, the time for inflow and drainage from the base of the shaft is extended. This extension results in an increase in the height of water in the shaft. When the hydraulic conductivity of the alluvium is approximately 10^{-2} cm/s, the trend is reversed. The high water level is reached when the hydraulic conductivity of the alluvium is about 10^{-2} cm/s and the hydraulic conductivity of the rock mass is 10^{-5} cm/s. As the hydraulic conductivity of the alluvium decreases from 1 cm/s, the maximum height reached in the sump becomes comparatively lower for the case where the rock mass, hydraulic conductivity is 10^{-2} cm/s (Figures C-14 and C-15). Conversely, more water builds up in the shaft for

the case when the rock mass hydraulic conductivity is 10^{-5} cm/s. This greater buildup occurs when the rock mass hydraulic conductivity is 10^{-5} cm/s because inflow occurs over a long period of time (Figures C-14 and C-15), and the drainage from the sump is lower than when the rock mass hydraulic conductivity is 10^{-2} cm/s.

APPENDIX D

EXPLANATION OF WATER INFLOW TO EXPLORATORY SHAFT 1
FROM SCENARIO IN APPENDIX C

FIGURES

	<u>Page</u>
D-1 Estimated Volumes of Water Entering ES-1 (Probable Maximum Flood, Shaft Fill Conductivity = 10^{-2} cm/s, Excavated Shaft Diameter = 4.42 m, Tiva Canyon Hydraulic Conductivity = 10^{-2} cm/s)	227
D-2 Approximation of the Flow Rates Used in the Model Presented in Appendix C, Section C.2.1 (Saturated Hydraulic Conductivity of the Tiva Canyon Member and the Shaft Fill = 10^{-2} cm/s)	228

APPENDIX D

EXPLANATION OF WATER INFLOW TO EXPLORATORY SHAFT 1 FROM THE SCENARIO IN APPENDIX C

The purpose of this appendix is to describe the shapes of the curves in Figure C-6. A single curve from Figure C-6 has been duplicated in Figure D-1. For the curves presented in Figure D-1, the saturated hydraulic conductivity of the Tiva Canyon Member is assumed to be 10^{-2} cm/s. For ease in explaining the shape of the curve in Figure D-1, portions of the curve are labeled A through E.

To explain each segment of the curve in Figure D-1, it is necessary to understand the different types of flow that the model comprises (Appendix C, Section C.3.1). The types of flow are alluvial, Tiva Canyon, Dupuit (or radial), and MPZ model. Figure D-2 illustrates the flow rate for each type of flow as a function of hydraulic conductivity of the alluvium. When the hydraulic conductivity of the saturated alluvium is less than the saturated hydraulic conductivity of the underlying Tiva Canyon Member, it is assumed that the rate of vertical infiltration into the Tiva Canyon Member is equal to the vertical infiltration rate of water leaving the alluvium. When the hydraulic conductivity of the Tiva Canyon Member is less than the hydraulic conductivity of the alluvium, vertical infiltration into the Tiva Canyon Member is controlled by its saturated hydraulic conductivity. (In both instances the gradient of flow vertically downward in the alluvium and the Tiva Canyon Member is conservatively assumed to equal one.) This explains why the Tiva Canyon flow rate increases from a saturated hydraulic conductivity for the alluvium of 10^{-5} to 10^{-2} cm/s. Above 10^{-2} cm/s, the flow through Tiva Canyon is controlled by the ability of the Tiva Canyon Member to transmit water.

Another type of flow is through the modified permeability zone (MPZ) and the shaft fill. This flow is assumed to depend on the saturated hydraulic conductivity of the Tiva Canyon Member. Therefore, the flow rate of the MPZ model for the Tiva Canyon Member has a constant value of 10^{-2} cm/s as assumed in this appendix.

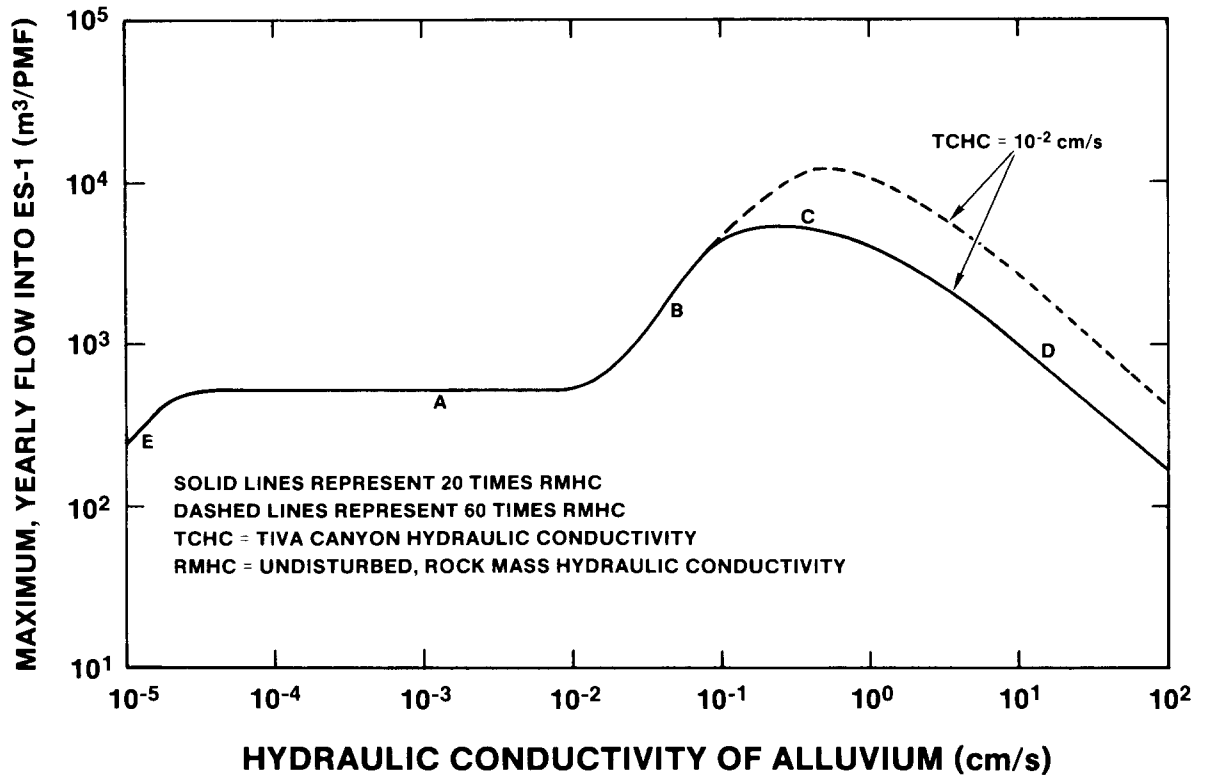


Figure D-1. Estimated Volumes of Water Entering ES-1 (Probable Maximum Flood, Shaft Fill Conductivity = 10^{-2} cm/s, Excavated Shaft Diameter = 4.42 m, Tiva Canyon Hydraulic Conductivity = 10^{-2} cm/s)

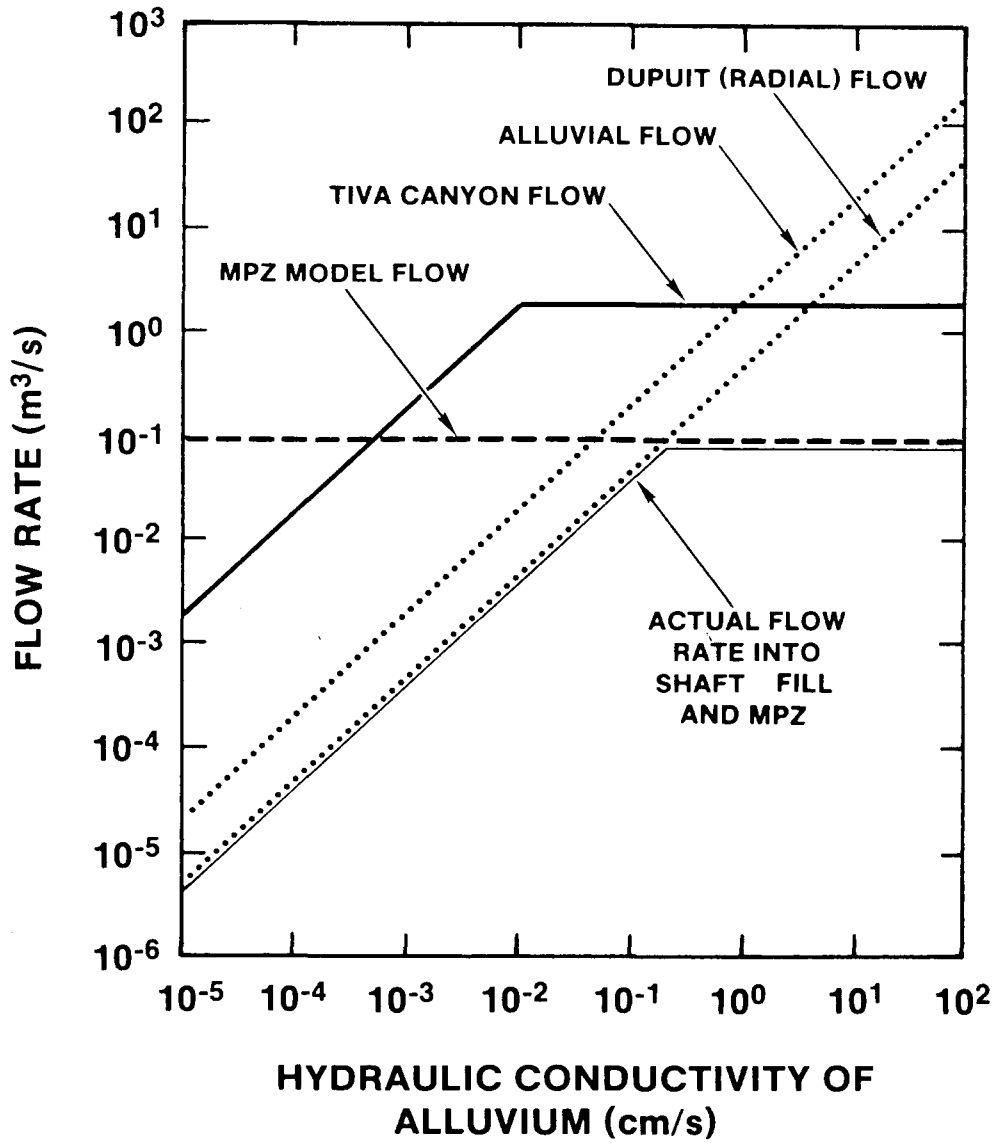


Figure D-2. Approximation of the Flow Rates Used in the Model Presented in Appendix C, Section C.2.1 (Saturated Hydraulic Conductivity of the Tiva Canyon Member and the Shaft Fill = 10⁻² cm/s)

Alluvial flow was described in Appendix C as being parallel or nearly parallel to the bedrock-alluvium interface. The alluvial flow rate as computed in this report depends on the hydraulic conductivity of the alluvium as well as the area of the alluvium that is fully saturated. The radial (Dupuit) flow rate towards the shaft depends on the hydraulic conductivity and the height of the alluvium, above the bedrock-alluvium contact. Because the area of alluvial flow and the height of saturated alluvium above the bedrock-alluvium contact vary with time, a representative area and height of saturated alluvium have been selected to illustrate how the alluvial flow rate and the radial (Dupuit) flow rate vary with the saturated hydraulic conductivity of the alluvium.

The relationship between these various flows and the total flood volume can be described by the following water balance equation:

$$V_{PMF} = V_s + V_{tc} + V_{all} \quad , \quad (D-1)$$

where

- V_{PMF} = cumulative flow for the probable maximum flood (PMF);
- V_s = cumulative flow down the shaft;
- V_{tc} = cumulative infiltration in the Tiva Canyon formation; and
- V_{all} = cumulative alluvial flow.

If the shaft flow is assumed to be governed by the radial Dupuit flow, then

$$V_{PMF} = \frac{\pi K_{all} (H^2 - H_o^2)}{\ln \frac{R}{r}} \cdot t + K_{tc} A_{tc} \cdot t + K_{all} i A_{all} \cdot t \quad , \quad (D-2)$$

where

- K_{tc} = Tiva Canyon hydraulic conductivity;
- K_{all} = alluvial hydraulic conductivity;
- t = time;
- i = alluvial gradient;
- R = outer radius;
- r = inner radius;
- A_{all} = alluvial area; and
- A_{tc} = Tiva Canyon area.

If it is assumed that the Tiva Canyon has a saturated hydraulic conductivity of 10^{-2} cm/s, and the range of alluvial hydraulic conductivity is from 10^{-5} to 10^{-2} cm/s for Segment A of Figure D-1, then the Tiva Canyon flow will be controlled by the rate of vertical flow through the alluvium. Equation D-2 can then be written as ($10^{-5} \leq K_{all} \leq 10^{-2}$)

$$V_{PMF} = \frac{\pi K_{all} (H^2 - H_o^2)}{\ln \frac{R}{r}} \cdot t + K_{all} A_{tc} t + K_{all} i A_{all} t \quad (D-3)$$

Assuming constant geometry, Equation D-3 can be simplified further to several constant values:

$$C_1 = C_2 t K_{all} + C_3 K_{all} t + C_4 K_{all} t \quad (D-4)$$

where

$$\begin{aligned} C_1 &= V_{PMF}, \\ C_2 &= \frac{\pi(H^2 - H_o^2)}{\ln(\frac{R}{r})}, \\ C_3 &= A_{tc}, \text{ and} \\ C_4 &= iA_{all}. \end{aligned}$$

Because all flows occur over the same period of time, this equation can be further simplified as

$$C_1 = C_2 t K_{all} + K_{all} t C_5 \quad (D-5)$$

and

$$C_1 = K_{all} t(C_2 + C_5) \quad (D-6)$$

where

$$C_5 = C_3 + C_4 \text{ and } 10^{-5} \leq K_{all} \leq 10^{-2}.$$

The term, $C_2 t K_{all}$, represents shaft plus MPZ flow, and the term $K_{all} t C_5$ represents nonshaft flow.* In Equation D-6, there are only two

*Nonshaft flow is the combination of alluvial flow plus Tiva Canyon flow.

variables, K_{all} and t . For this relation to be correct, K_{all} and t are inversely proportional to each other. Further, for any K_{all} and t combination, the flow into the shaft and MPZ and the nonshaft flow will also be constant. Therefore, the maximum, yearly flows into ES-1 that have hydraulic conductivities of between 10^{-5} to 10^{-2} cm/s for the alluvium (Figure D-1) are constant. The reason for the lower flow in the range of 10^{-5} to 2×10^{-5} cm/s (Figure D-1) is that when the alluvium has a low saturated hydraulic conductivity the time to drain the water from the modeled area is greater than one year. The values plotted in Figure D-1 are yearly inflows.

As the saturated hydraulic conductivity becomes $>10^{-2}$ cm/s, the flow rate into the Tiva Canyon Member can be no greater than the product of the hydraulic conductivity of the Tiva Canyon Member, K_{tc} or K_{all} , whichever is lower, and the cross-sectional area, A_{tc} . The term in Equation D-4, $C_3 K_{all} t$, that describes the Tiva Canyon flow rate no longer applies. The Tiva Canyon flow rate is constant and equal to $C_3 K_{tc} t$. As the hydraulic conductivity of the alluvium increases between 10^{-2} to about 2×10^{-1} cm/s on Figure D-1 (Segment B), the Dupuit and alluvial flows will increase, but the Tiva Canyon flow remains constant. Therefore, the combined nonshaft flow and MPZ flow is proportionally less than the actual flow entering the shaft. This results in a greater amount of flow directed to the shaft.

Once the peak "C" is reached on Figure D-1, there is a new factor to consider. The Dupuit flow will no longer dominate the flow into the shaft and MPZ. Rather, the flow rate described by the MPZ model controls flow. This flow rate is constant from 2×10^{-1} to 100 cm/s as indicated in Figure D-2. However, because the nonshaft flow is increasing (as a result of the increasing alluvial flow) and the total PMF flow is constant, the proportion of total flow entering the shaft and MPZ is decreasing. This phenomenon describes the decreasing flow into the shaft and MPZ (Segment D of Figure D-1). An additional consideration that contributes to the decreasing flow in Segment D is that as the time to drain the PMF volume decreases with an increase in the hydraulic conductivity of the alluvium, the alluvial flow becomes greater. This effect is very noticeable when the alluvial flow becomes greater than the Tiva Canyon flow, i.e. when the alluvial conductivity is about 7×10^{-1} cm/s.

APPENDIX E

THE DENSITY METHOD AS APPLIED TO FLOW THROUGH A POROUS MEDIA

This appendix provides the detailed assumptions used in the convective air transport analysis. These assumptions are used to develop a formula for the convective flux rate, which may be compared with flux rate relationships for convective transport through a porous media. A discussion of the development of thermal instability and convective air transport is also presented.

The model has been developed based on the following assumptions.

1. Darcy's law is valid.

The resistance to airflow through open or backfilled drifts may be characterized as either laminar or turbulent. In turbulent flow, resistance is nonlinearly related to potential. In laminar flow, resistance is linearly related to potential, and flow may be calculated using Darcy's law.

The results of the analyses were used to check the validity of Darcy's law by calculating the Reynolds number from the air velocity or specific discharge, the air kinematic viscosity, and the characteristic dimension. For laminar flow through backfill, the characteristic dimension is the mean grain diameter, and Darcy's law is valid as long as the Reynolds number does not exceed a value between 1 and 10 (Freeze and Cherry, 1979, p. 73). The calculated Reynolds number was within the specified limits, and the assumption of head loss varying linearly with flow rate was found to be justified.

2. Air temperatures in the shaft are the same as in the adjacent rock.

Convective airflow through a heated repository will involve a complex coupling of heat transfer from the rock to the air, which will tend to drive airflow and cool the rock by passage of the air thus reducing the driving mechanism. In the modeling which follows, the effects of cooling the rock are ignored. The air

is assumed to be at the same temperature as the adjacent rock at all points in the repository including the shafts.

Intuitively, this simplified approach is most valid for the case of a backfilled repository in which air flows relatively slowly, and temperatures are able to equilibrate. The faster the air flows, the greater will be the volume of air moving through the repository, and the more likely that the rock will be cooled to the extent that convection slows down. A converse effect to rapid airflow could occur if the flow of air is not sufficient to significantly cool the rock in the repository. Flow through the repository would be greater than that calculated using our simplified approach if air in the shafts (or rock) is not cooled by heat transfer to the rock. In this case, there is a potential for the repository to act as a heat engine. The driving pressure could then be about three times higher than that calculated assuming that temperatures equilibrate. This higher driving pressure occurs, however, because air is expelled at the ground surface at the same temperature as the repository rooms, a condition which is intuitively overly conservative.

3. Airflow is incompressible, and the air is dry.

Because convective transport evolves from air-buoyancy effects that depend on temperature, thermal properties such as air density and air viscosity will change through the circuit. In reality, flow is compressible with the actual resistance to the mass flow rate dependent on density and viscosity. In the analyses presented in this report, air compressibility effects on fluid flow are ignored for reasons of simplification. This assumption is considered to be reasonable because the pressures involved are small (<0.1 psi). According to Hartman (1982, p. 160), compressibility effects may be ignored for mine static head pressure drops of <5 kPa (0.72 psi) or where differences in elevation are <430 m.

Convective transport can, in general, involve both the transport of air and water vapor. However, the model assumes that the air

is dry. The authors recognize that water vapor may be present in the mine air at varying relative humidities. However, because of the general nature of this calculation, we made this assumption to simplify this analysis and to be consistent with the data available on the repository.

4. Air circulation occurs along specified paths.

The model assumes that a particular path for air circulation (Mechanism A or B, Figure 4-1) is established and that flow is one-dimensional either through shaft or ramp backfill, open drifts, or damaged or undamaged tuff. The model ignores the development of secondary circulation currents that might develop in the host rock above or below the repository away from the waste containers.

The following derivation is presented to illustrate that the use of the density approach is the same as the relationship presented by Bear (1972) for convective flow through a porous media. The derivation presented below is not identical to and as detailed as that used in Chapter 4. The derivation differs primarily in two ways. First, the pressure in Chapter 4 is calculated by summing the pressure differential over several increments of shaft length. Second, resistances to flow in Chapter 4 are calculated for drifts, shafts, the rock mass, and the MPZ. However, the derivation illustrates that the technical approach of calculating draft pressures by a density method and then substituting the draft pressures into Darcy's law is appropriate.

The draft pressure may be calculated by the density method for the circuit (Hartman, 1982):

$$\Delta p = (\gamma_i - \gamma_o)L \quad , \quad (E-1)$$

where

γ_i = mean air density of an inlet shaft, pcf;

γ_o = mean air density of an outlet shaft, pcf; and

L = flow path length, ft.

If it is assumed that the mean temperatures T_i and T_o correspond to the densities γ_i and γ_o , respectively, then the following relationship may be used to express volumetric thermal expansion effects (Bear, 1976, p. 655):

$$\gamma_i = \gamma_o [1 - \beta(T_o - T_i)] \quad , \quad (E-2)$$

where

β = coefficient of volumetric thermal expansion, $^{\circ}\text{C}^{-1}$;

T_i = mean temperature at density γ_i , $^{\circ}\text{C}$; and

T_o = mean temperature at density γ_o , $^{\circ}\text{C}$.

Substituting Equation E-2 into Equation E-1, the draft pressure differential is

$$\Delta p = -\beta(T_o - T_i)L\gamma_o \quad . \quad (E-3)$$

Expressing the above reaction as a potential difference, the following expression is obtained:

$$\Delta h = \frac{\Delta p}{\gamma_o} = -\beta(T_o - T_i)L \quad . \quad (E-4)$$

Substitution of the change in potential (head loss) into Darcy's law is used to calculate the flux rate. If it is assumed that the resistance to flow occurs in backfilled shafts with the underground repository drifts open, then

$$V = -K'_e \cdot \frac{\Delta h}{L} = -K'_e(T_o - T_i)\beta \quad , \quad (E-5)$$

where K'_e equals the air conductivity and V equals the Darcy flux rate.

The actual velocities through the backfilled shafts are (Freeze and Cherry, 1979, p. 71)

$$V_a = \frac{V}{n} = \frac{-K'_e(T_o - T_i)\beta}{n} \quad , \quad (E-6)$$

where

V_a = actual velocity and
 n = porosity.

The air conductivity, K'_e , may be expressed as (Freeze and Cherry, 1979, p. 27)

$$K'_e = \frac{\rho g k}{\mu} \quad , \quad (E-7)$$

where

k = intrinsic permeability,
 ρ = mass density,
 g = acceleration constant, and
 μ = absolute viscosity.

Substituting Equation E-8 into Equation E-7, the following relationship is obtained:

$$V_a = \frac{-\rho g k \beta (T_o - T_i)}{n \mu} \quad . \quad (E-8)$$

This relationship is the same as the relationship for flow through a porous media presented by Bear (1972).

APPENDIX F

**ESTIMATED CONSTRUCTION SCHEDULE AND COSTS FOR LINER REMOVAL
AND SEAL INSTALLATION**

TABLES

	<u>Page</u>
F-1 Overall Site Cost Estimate	242

FIGURES

F-1 Estimated Schedule for Liner Removal and Seal Installation	241
--	-----

APPENDIX F

ESTIMATED CONSTRUCTION SCHEDULE AND COSTS FOR LINER REMOVAL AND SEAL INSTALLATION

This appendix presents the estimated construction costs and schedule for completely removing the liner from the exploratory shaft and for constructing a single anchor-to-bedrock plug/seal. The estimated schedule of 44 weeks is presented in Figure F-1 for the case where the liner is assumed to be broken by a nonexplosive expansive demolition agent. As discussed in Section 8.1.1, it is estimated that the use of hydraulic splitters or drilling and blasting would require a similar amount of time, while the use of handheld pneumatic splitters would require more time. The estimated overall site costs are presented in Table F-1 and assume no existing shaft services at the time the liner is removed. It is estimated that \$3.5 million is required for all activities, with approximately 60% of the costs incurred for removing the liner and backfilling the shaft. The estimated costs for pregrouting and constructing the plug are \$134,000 and \$380,000, respectively.

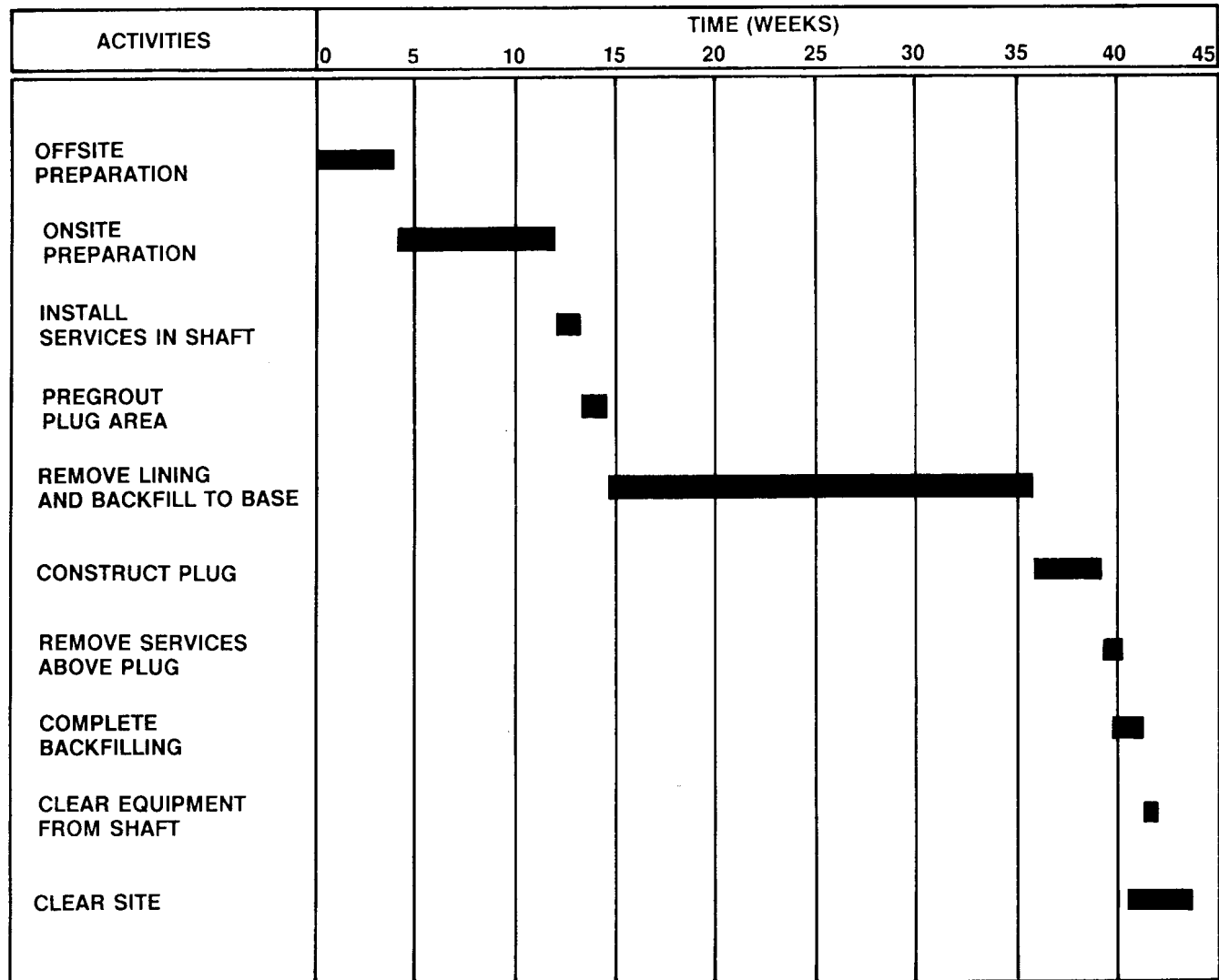


Figure F-1. Estimated Schedule for Liner Removal and Seal Installation

Table F-1. Overall Site Cost Estimate

	Offsite ^(a)	Onsite ^(b)	Shaft Services	PregROUT Plug	Removal of Lining and Backfill	Construct Plug	Shaft Services	Clear Shaft Top	Clear Site	Follow-up Reports	Total
WEEKS	4.0	8.0	1.0	1.5	22.5	3.5	0.5	1.0	2.5	6.0	
LABOR	56,800	223,600	52,500	78,800	1,437,000	241,800	14,600	29,100	82,800	46,200	2,263,200
EQUIPMENT											
Common ^(c)	1,000	177,200	48,600	13,600	57,000	30,500	5,100	7,900	16,200		357,100
Grouting				23,400		10,700					34,100
Drilling				1,900	8,700	4,400					15,000
Mucking					6,500	3,500					10,000
Subtotal	1,000	177,200	48,600	38,900	72,200	49,100	5,100	7,900	16,200		416,200
MATERIALS											
Concrete		10,600				32,500					43,100
Grout				2,200		300					2,500
Subtotal		10,600		2,200		32,800					45,600
CONSUMABLES											
Common ^(d)	7,400	26,200	6,600	9,900	182,900	30,400	1,800	3,600	9,000	6,000	283,800
Grouting											
Drilling				900	87,200	4,900					93,000
Mucking					8,400	400					8,800
Subtotal	7,400	26,200	6,600	10,800	278,500	35,700	1,800	3,600	9,000	6,000	385,600

Table F-1. Overall Site Cost Estimate (Concluded)

	Offsite(a)	Onsite(b)	Shaft Services	PregROUT Plug	Remove Lining and Backfill	Construct Plug	Shaft Services	Clear Shaft Top	Clear Site	Follow-up Reports	Total
WEEKS	4.0	8.0	1.0	1.5	22.5	3.5	0.5	1.0	2.5	6.0	
POWER											
Diesel		3,200	400	600	8,400	1,400	200	400	1,000		15,600
Electrical											
Bristar					306,000	12,000					318,000
Explosives											
Hydraulic Breaker											
Subtotal		3,200	400	600	314,400	13,400	200	400	1,000		333,600
OTHER											
Office	1,700	6,100	1,500	2,300	14,100	7,100	400	800	2,100	1,400	37,400
Freight		35,000							25,000		60,000
Subtotal	1,700	41,100	1,500	2,300	14,100	7,100	400	800	27,100	1,400	97,500
TOTAL	66,900	481,900	109,600	133,600	2,116,200	379,900	22,100	41,800	136,100	53,600	3,541,700(e)

(a) Offsite costs include necessary administrative costs for procurement and the mobilization costs associated with loading equipment onto trucks.

(b) Onsite costs include placement of trailers, establishment of a power supply, and erection of the shaft headframe.

(c) Common costs for equipment include a trailer at the site, vehicles used by field personnel, and large equipment such as a front-end loader.

(d) Common costs for consumables include such items as protective clothing, general oil and greases, diesel fuel, pipe fittings, safety equipment necessary for construction activities, and tools.

(e) Assumes the length of the shaft is 420 m, and secondary grouting costs are not included.

APPENDIX G

CALCULATION OF THE TEMPERATURE OF WATER REACHING THE BASE
OF THE EXPLORATORY SHAFTS

TABLES

	<u>Page</u>
G-1 Values of Parameters Used to Estimate the Dimensionless Thermal Diffusivity and the Resulting Average Dimensionless Temperatures	253

FIGURES

G-1 Thermal Profiles at the ES as Computed by Blanford and Linearized for this Calculation	247
G-2 Dimensionless Temperature (θ) Versus Dimensionless Radius (r) for Different Dimensionless Thermal Diffusivities (K)	251
G-3 Average Dimensionless Temperature (θ_{AVG}) Versus Dimensionless Thermal Diffusivity (K).....	252

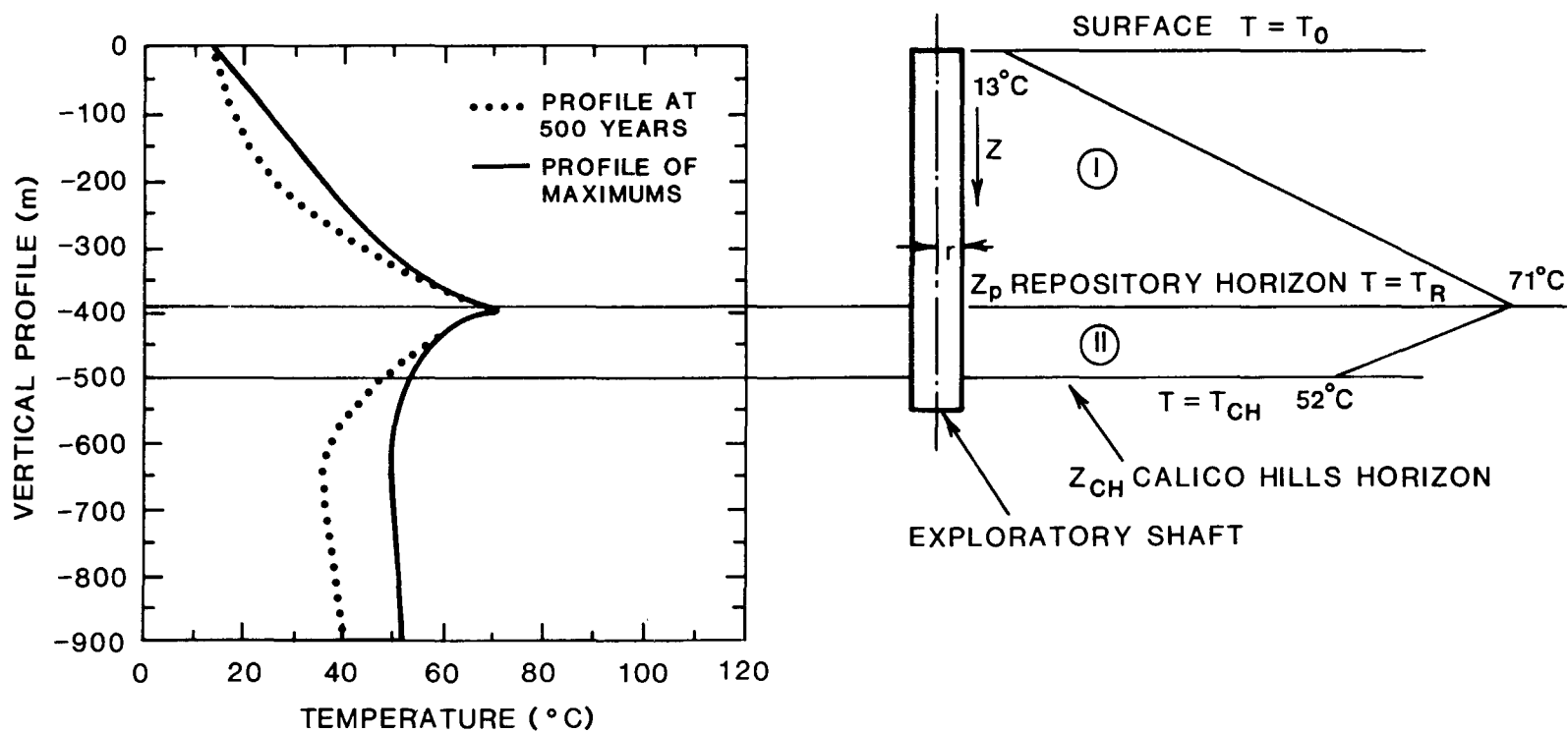
APPENDIX G

CALCULATION OF THE TEMPERATURE OF WATER REACHING THE BASE OF THE EXPLORATORY SHAFTS

In Chapter 7 changes in the sorptive capacity of the Calico Hills unit as a result of elevated ground-water temperature were addressed. The prevalent zeolites in the Calico Hills unit are known to be stable at temperatures <95°C. Hence, the purpose of this appendix is to show that the expected temperature of the water entering the Calico Hills unit through the exploratory shaft (ES) is <95°C.

To predict the temperature of water passing through the ES and its modified permeability zone (MPZ), we modeled the flow of water vertically downward through a cylinder whose surface temperature varied to show the maximum global temperature field as calculated by Blanford (Morales, 1985). Consistent with the bounding nature of these calculations, no local cooling of the cylinder surface, which models the formation, is considered; so that maximum effluent temperatures are obtained. As water passes through this cylinder, the temperature changes caused by the radial conduction of heat to the water moving downward is modeled. For a linear change in formation temperature with depth, an analytical solution to the thermal field has been obtained.

Two separate water flow scenarios that are based on the maximum water entry scenario presented in Appendix C have been considered. These two scenarios have yearly influxes of 44.2 m³/year and a probable maximum flood (PMF) of 20,000 m³/year. Because the unsaturated fracture flow scenarios considered in Chapter 3 have maximum ES influxes, which approximate 44.2 m³/year, the following calculations for 44.2 m³/year will approximate the actual temperature rise resulting from downward movement of water. For these calculations, we assume that the rock mass temperature near the ES and hence the cylinder surface temperature increases in a linear fashion from 13°C (average ground-water temperature) to 71°C (average formation temperature at the repository horizon). Below the repository, we assume that the temperature decreases linearly to 52°C at the top of the Calico Hills unit. This model is illustrated in Figure G-1. As seen in Figure G-1, the linear approximation to the profile of maximums is



(FROM BLANFORD IN MORALES, 1985, PP. 36-39)

Figure G-1. Thermal Profiles at the ES as Computed by Blanford and Linearized for this Calculation

always greater than the maximum temperature so that the model assumptions are again conservative.

The thermal response of water flowing through the ES is described by the conservation-of-energy equation, which takes the form

$$U_Z \frac{\partial T}{\partial Z} = \alpha \frac{1}{r} \frac{\partial}{\partial r} \left(r \frac{\partial T}{\partial r} \right), \quad (G-1)$$

where α = the thermal diffusivity of the combination of water and rock within the ES and the MPZ;
 U_Z = the average flow velocity;
 T = the temperature;
 r = the radial distance from the shaft centerline; and
 Z = vertical distance downward as shown in Figure G-1.

This equation is solved in two regions, I and II, where Region I is the zone above the repository and Region II is the zone below the repository. The boundary conditions for Region I are

$$\begin{aligned} Z_I = 0 & & T_I = T_o \\ r_I = R_o, \quad Z_I > 0 & & T_I = T_o + (T_R - T_o) \frac{Z_I}{Z_R} \end{aligned} \quad (G-2)$$

and for Region II are

$$\begin{aligned} Z_{II} = Z_R & & T_{II} = T_R \\ \text{and } r_{II} = R_o, \quad Z_{II} > Z_R & & T_{II} = T_R + (T_{CH} - T_R) \frac{(Z_{II} - Z_R)}{(Z_{CH} - Z_R)} \end{aligned} \quad (G-3)$$

These equations may be nondimensionalized, where $\theta_I = \frac{T_I - T_o}{T_R - T_o}$,

$r_I = r'_I R_o$, $Z_I = Z'_I Z_R$, and $K_I = \frac{\alpha}{U_Z} \frac{Z_R}{R_o^2}$ in Region I to give

$$\frac{\partial \theta_I}{\partial Z'_I} = \frac{K_I}{r'_I} \frac{\partial}{\partial r'_I} \left(r'_I \frac{\partial \theta_I}{\partial r'_I} \right), \quad (G-4)$$

$$\begin{aligned} Z'_I &= 0 & \theta_I &= 0 \\ r'_I &= 1 & \theta_I &= Z'_I \end{aligned} .$$

In Region II, we similarly nondimensionalize, where $\theta_{II} = \frac{T_{II} - T_R}{T_{CH} - T_R}$,

$$r_{II} = r'_{II} R_o, \quad Z_{II} = Z'_{II} (Z_{CH} - Z_R) + Z_R, \quad \text{and } K_{II} = \frac{\alpha}{U_Z} \frac{(Z_{CH} - Z_R)}{R_o^2}, \quad \text{to give}$$

$$\frac{\partial \theta_{II}}{\partial Z'_{II}} = \frac{K_{II}}{r_{II}} \frac{\partial}{\partial r'_{II}} \left(r'_{II} \frac{\partial \theta_{II}}{\partial r'_{II}} \right), \quad (G-5)$$

$$\begin{aligned} Z'_{II} &= 0 & \theta_{II} &= 0 \\ r'_{II} &= 1 & \theta_{II} &= Z'_{II} \end{aligned} .$$

Equations G-4 and G-5 are identical except that the nondimensional diffusivities are slightly different. Equations G-4 and G-5 are solved analytically in Carslaw and Jaeger (1959, p. 201) and involve a series of Bessel functions that converge very rapidly on their solution.

The solution is

$$\theta = \left(Z' - \frac{1 - r'^2}{4K} \right) + \frac{2}{K} \sum_{n=1}^{\infty} e^{\left(-K\alpha_n^2 Z' \right)} \frac{J_0(r'\alpha_n)}{\alpha_n^3 J_1(\alpha_n)}, \quad (G-6)$$

where the terms, α_n , are the nonzero roots of $J_0(\alpha) = 0$.

To solve this equation for the average fluid temperature entering Calico Hills, we should apply Equation G-6 in both Regions I and II. The solution obtained in Region I would then be used as a starting temperature for Region II. However, because our problem is to estimate the maximum fluid temperature of water entering Calico Hills, a convenient simplification is to assume that the fluid temperature exiting Region I and entering Region II is in thermal equilibrium with the formation at the repository horizon. If water with a lower temperature were to enter Region II, then the water temperature exiting Region II would be correspondingly reduced. Hence, we now consider the solution in Region II with the assumption that

T_R is the rock temperature computed by Blanford. Hence, T_R is taken to be 71°C and T_{CH} is 52°C.

The solution to Equation G-6 for Region II is a function of r' , Z' , and K . At the entrance to the Calico Hills unit, where Z'_{II} is 1, the variation in dimensionless fluid temperature with dimensionless radius is computed and presented in Figure G-2 for K varying between 0.5 and 10. The fluid temperature profile more closely approaches the formation temperature, $\theta = 1$, as the dimensionless thermal diffusivity increases.

The average fluid temperature at the entrance to the Calico Hills unit is

$$\theta_{AVG} = \frac{\int_0^1 \theta(r') 2\pi r' dr'}{\int_0^1 2\pi r' dr'} = 2 \int_0^1 \theta(r') r' dr' \quad (G-7)$$

This average at the upper margin of the Calico Hills unit may be presented as a function of K (Figure G-3). In this figure, the average dimensionless fluid temperature increases as the dimensionless thermal diffusivity increases, and the average dimensionless fluid temperature is >0.9 for values of K exceeding 1. When θ_{AVG} is equal to 0.9, the actual fluid temperature is 53.9°C.

In the estimation of the dimensionless thermal diffusivity,

$$K = \frac{\alpha}{U_Z} \frac{(Z_{CH} - Z_R)}{R_o^2} \quad (G-8)$$

a range of values is considered for α and U_Z , while R_o and $Z_{CH} - Z_R$ are defined by the design of the ES. The values of these parameters for two extreme conditions are presented in Table G-1.

For both of these cases, the shaft radius is assumed to encompass the MPZ. By selecting this larger radius, the value of K assumes a conservatively smaller value. In addition, the permeability of the MPZ is assumed to be 60 times the conductivity of the Tiva Canyon. The fluid

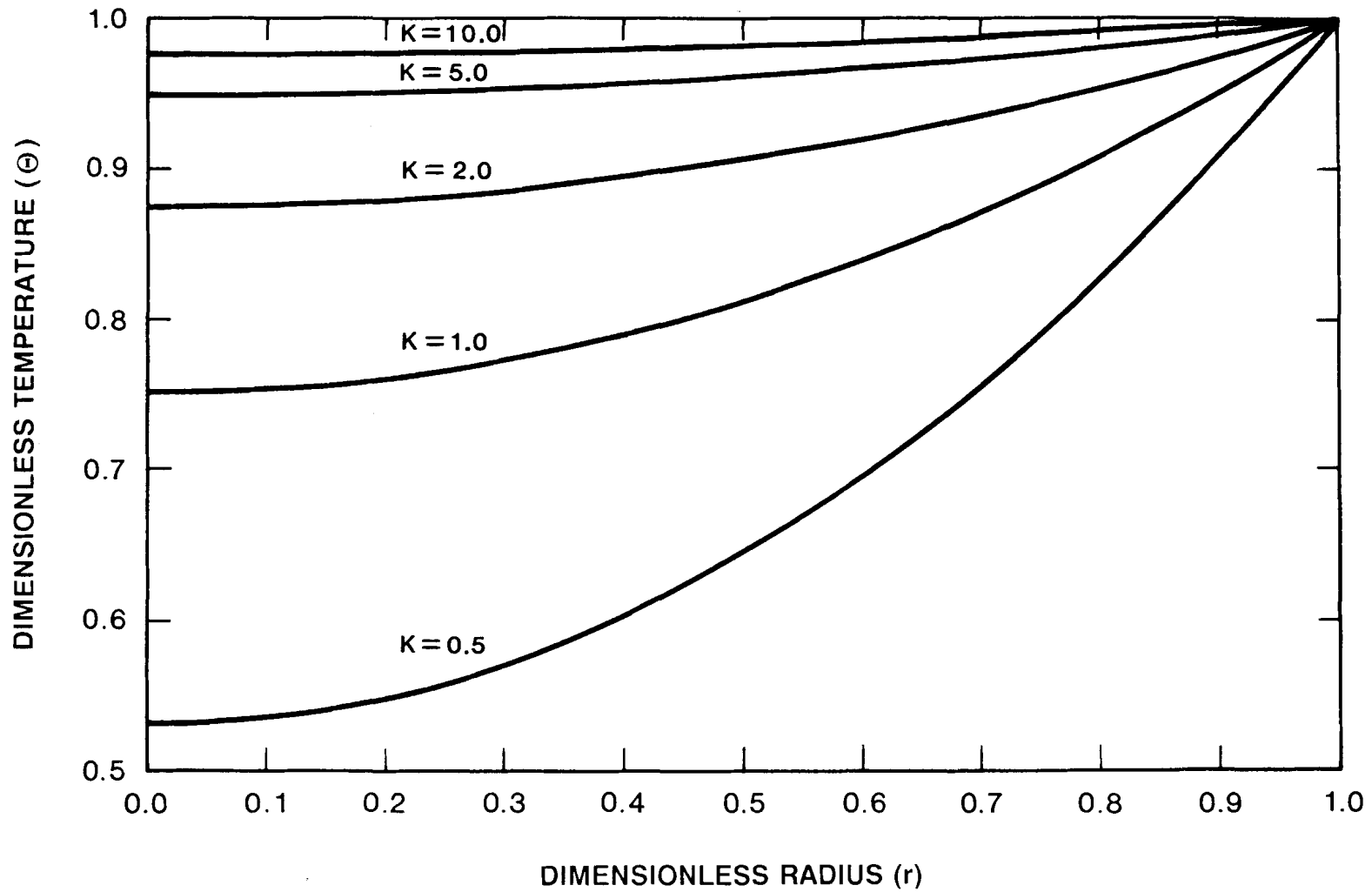


Figure G-2. Dimensionless Temperature (θ) Versus Dimensionless Radius (r) for Different Dimensionless Thermal Diffusivities (K)

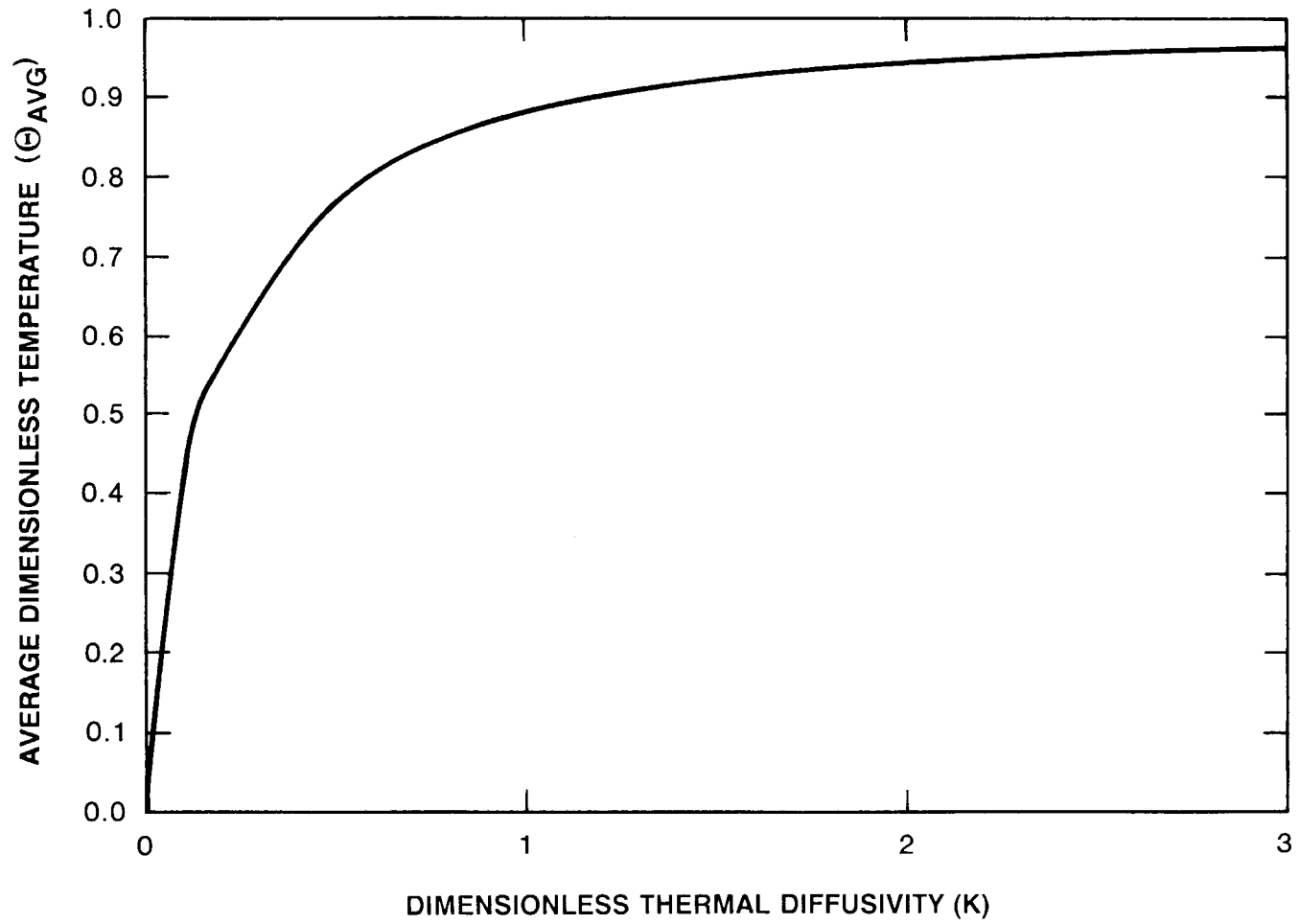


Figure G-3. Average Dimensionless Temperature (θ_{AVG}) Versus Dimensionless Thermal Diffusivity (K)

Table G-1. Values of Parameters Used to Estimate the Dimensionless Thermal Diffusivity and the Resulting Average Dimensionless Temperatures

Annual Inflow (m ³ /yr)	Z _{CH} - Z _R [m (ft)]	R _o [m (ft)]	U _Z (cm/s)	α (cm ² /s)	K	θ _{AVG}
44.2	116.7(383)	4.42(14.5)	2.3 x 10 ⁻⁶	.0078	200	1.00
20,000	116.7(383)	4.42(14.5)	6 x 10 ⁻¹	30	3	.96

velocity for the 44.2 m³/year flow condition is computed by dividing the flow by the area of the shaft and MPZ, while the maximum fluid velocity is equivalent to the worst-case hydraulic conductivity assumed for the MPZ. The thermal diffusivity is computed by one of two possible methods. When the fluid velocity is very low, as in the lower flow case, a volumetric average of the thermal diffusivity of the rock and of the intergranular water is computed. At the larger fluid velocity, the thermal diffusivity equivalent to the mass diffusivity is determined by convection processes and is computed by

$$\alpha = \frac{2U_Z d_p}{\epsilon} \quad [\text{Levenspiel, 1972, p. 282}] \quad (\text{G-9})$$

where d_p is the effective distance between fractures, and other terms are as defined previously. We assume 16 fractures/m to give the smallest possible d_p within the MPZ.

As may be seen in Table G-1, the value of K for the 20,000 m³/year case is large enough so that the average dimensionless temperature is 0.96. In actual temperature units, the maximum fluid temperature is expected to be 52.8°C.

For the 44.2 m³/year influx, the value of K is 200 so that the dimensionless average temperature is approximately one and the actual fluid temperature will be elevated by 0.01 to 52.01°C. For the PMF scenarios of Section 3-2, the total inflow of water will be 47.4 m³ so that a similar temperature rise is expected for this case.

APPENDIX H

COMPARISON OF DATA USED IN THIS REPORT WITH THE REFERENCE INFORMATION BASE*

The following notes are used throughout this appendix:

- (A) No section in the RIB applies to these parameters.
- (B) Section was identified in the RIB, but values were not found.

*Version 02.002 of the RIB, dated August 1987, was used in this appendix.

Table M-1. Comparison of Data Used in This Report with the Reference Information Base (RIB)

Parameter	Section	Report Value	RIB Value	RIB Section	Explanation
Location of Unsaturated Portion of the Topopah Spring Member	2.0	200 - 400 m	None	1.1.2	(B)
Men-and-Materials Shaft Sump	2.0	24 m	None	2.2.5, 2.2.6	(B)
Emplacement Exhaust Shaft Sump	2.0	3 m	None	2.2.5, 2.2.6	(B)
Exploratory Shaft 1 (ES-1) Sump	2.0	15 m	None	2.2.5, 2.2.6	(B)
Exploratory Shaft 2 (ES-2) Sump	2.0	31 m	None	2.2.5, 2.2.6	(B)
Location of ES-1	2.1	See Fig 2-2.	N 766,255 E 563,630	2.2.8	Figure depicts RIB location.
Location of ES-2	2.1	See Fig 2-2.	N 766,337 E 563,918	2.2.8	Figure depicts RIB location.
Excavated Diameter of ES-1 and ES-2	2.2	4.3 m	4.3 m (14 ft)	2.2.8	---
Finished Diameter of ES-1 and ES-2	2.2	3.7 m	3.7 m (12 ft)	2.2.8	---
Thickness of ES-1 and ES-2 Liners	2.2	0.3 m	0.3 m (1 ft)	2.2.8	---
Maximum Temperature at Station Plug	2.4	40°C	None	-----	(A)
Probable Maximum Precipitation	3.1.1				
- Thunderstorm event		13.9 in./6 hr	14.1 in./6 hr	1.17.1.2.3	Values consistent with Bullard (1986).
- General storm event		8.1 in./14 hr	None	1.17.1.2.3	

(A) No section in the RIB applies to these parameters.

(B) Section was identified in the RIB, but values were not found.

Table H-1. Comparison of Data Used in This Report with the Reference Information Base (RIB) (Continued)

Parameter	Section	Report Value	RIB Value	RIB Section	Explanation
Manning's Roughness Coefficient	3.1.2	0.06	None	-----	(A)
Peak PMF Discharges--Clearwater Flow	3.1.2				
- Thunderstorm event		95 m ³ /s (3,350 cfs)		1.17.1.2.1	(B)
- General storm event		8.6 m ³ /s	None	1.17.1.2.1	
Horizontal Distance from	3.1.2				
- ES-1 to thunderstorm PMF + debris		91 m	None	-----	(A)
- ES-2 to thunderstorm PMF + debris		83 m	None	-----	(A)
- ES-1 to general storm PMF + debris		95 m	None	-----	(A)
- ES-2 to general storm PMF + debris		88 m	None	-----	(A)
Vertical Distance from	3.1.3				
- ES-1 to thunderstorm PMF + debris		5 m	None	-----	(A)
- ES-2 to thunderstorm PMF + debris		11 m	None	-----	(A)
- ES-1 to general storm PMF + debris		6 m	None	-----	(A)
- ES-2 to general storm PMF + debris		13 m	None	-----	(A)
Drainage Area of Coyote Wash	3.1.3	0.2 mi ²	None	-----	(A)
Surface Erosion Rate (Yucca Mtn)	3.1.5	0.5 m/10,000 yr	None	1.5.1	(B)

(A) No section in the RIB applies to these parameters.

(B) Section was identified in the RIB, but values were not found.

Table H-1. Comparison of Data Used in This Report with the Reference Information Base (RIB) (Continued)

Parameter	Section	Report Value	RIB Value	RIB Section	Explanation
Tiva Canyon Van Genuchten Curve Fit Parameters	3.2.2				
- α		0.0231 m ⁻¹	1.285	1.1.4.3	RIB values are generic.
- β		1.693	4.23	1.1.4.3	RIB values are generic.
Residual Saturation (Tiva Canyon)	3.2.2	0.0355	0.355	1.1.3.2	(B)
Saturation of Tiva Canyon Member	3.2.3	67 ± 23%	67 ± 23%	1.1.3.1	---
Porosity of Tiva Canyon Member	3.2.3	11 ± 4%	11 ± 4%	1.3.1.2	---
Fracture Aperture (Tiva Canyon)	3.2.3	89 μm	89 μm	1.1.4.3	Values selected after Sinnock et al., 1984
Fracture Frequency (Tiva Canyon)	3.2.3	20/m ³	20/m ³	1.1.4.3	Values selected after Sinnock et al., 1984
Bulk Saturated Hydraulic Conductivity (Tiva Canyon Member)	3.2.3	1.2 x 10 ⁻³ cm/s	1.2 x 10 ⁻³ cm/s or (3.65 x 10 ⁴ mm/yr)	1.1.4.3	Values selected after Sinnock et al., 1984
Porosity of Shaft Backfill	3.2.6	30%	None	2.3	(B)
Storage Capacity of ES-1 and ES-2 Sumps	3.2.6	200 m ³	None	-----	(A)
Storage Capacity of ES Facility Drifts	3.2.6	630 m ³	None	-----	(A)
Bulk Saturated Hydraulic Conductivity (Topopah Spring Member)	3.2.6	1.2 x 10 ⁻³ cm/s	1.2 x 10 ⁻³ cm/s or (3.65 x 10 ⁴ mm/yr)	1.1.4.3	---

(A) No section in the RIB applies to these parameters.

(B) Section was identified in the RIB, but values were not found.

Table H-1. Comparison of Data Used in This Report with the Reference Information Base (RIB) (Continued)

Parameter	Section	Report Value	RIB Value	RIB Section	Explanation
Time to Reach Maximum Temperature Increase in Rock	4.0	2,500 yr	None	3.1.1	(B)
Hydraulic Conductivity of Shaft Backfill	4.1	10 ⁻² cm/s	None	2.3	(B)
Shaft Temperature at Surface	4.3.1	13°C	13°C (54.9°F)	1.11.1	---
Initial Shaft Temperature at Repository Level	4.3.1	23°C	None	3.1.1.2	Computed from repository thermal gradient in RIB.
Peak Temperature at Repository Level	4.3.1	115°C	115°C	3.1.1.2	---
Extent of MPZ Around Shafts	4.3.2	+1 RADIUS	None	2.3	(B)
Total Cross-Sectional Roof Area of Repository	4.3.2				
- Vertical emplacement		983,700 m ²	None	-----	(A)
- Horizontal emplacement		486,000 m ²	None	-----	(A)
Total Thickness of Welded Units Above the Repository	4.3.2	260 m	260 m	1.3.1.1.1	Scaled from stratigraphic column.
Total Thickness of Nonwelded Units Above the Repository	4.3.2	40 m	40 m	1.3.1.1.1	Scaled from stratigraphic column.

(A) No section in the RIB applies to these parameters.
 (B) Section was identified in the RIB, but values were not found.

Table H-1. Comparison of Data Used in This Report with the Reference Information Base (RIB) (Continued)

Parameter	Section	Report Value	RIB Value	RIB Section	Explanation
Air Conductivity of Welded Units (Topopah Spring and Tiva Canyon Members)	4.3.2	3×10^{-7} to 3×10^{-4} m/min	4×10^{-5} m/min	1.1.4.3	Calculated from saturated hydraulic conductivity values which bound the RIB value.
Air Conductivity of Nonwelded Paintbrush Tuff Unit	4.3.2	3×10^{-7} to 3×10^{-5} m/min	7×10^{-6} m/min	1.1.4.3	Calculated from saturated hydraulic conductivity values which bound the RIB value.
Length of Ramps/Shafts to Repository Horizon	4.3.2				
- Waste ramp		2,012 m	2,012 m (6,603 ft)	2.2.8	---
- Tuff ramp		1,410 m	1,410 m (4,627 ft)	2.2.8	---
- Men-and-materials shaft		314 m	314 m (1,030 ft)	2.2.8	---
- Emplacement exhaust shaft		314 m	314 m (1,030 ft)	2.2.8	---
- ES-1		311 m	311 m (1,020 ft)	2.2.8	---
- ES-2		311 m	311 m (1,020 ft)	2.2.8	---
Internal Cross-Sectional Area of Ramps/Shafts	4.3.2				
- Waste ramp					
Vertical emplacement		34.2 m ²	21-ft diam	2.2.2.7	Cross-sectional areas calculated from ramp dimensions given in the RIB. Also assumes that part of liner at floor will be removed.
Horizontal emplacement		28.3 m ²	19-ft diam	2.2.1.7	
- Tuff ramp					
Vertical emplacement		42.8 m ²	24-ft diam	2.2.2.7	Cross-sectional areas calculated from ramp dimensions given in the RIB. Also assumes that part of liner at floor will be removed.
Horizontal emplacement		30.1 m ²	20-ft diam	2.2.1.7	
- Men-and-materials shaft		29.2 m ²	20-ft diam	2.2.8	Calculated from shaft dimensions given in the RIB.
- Emplacement exhaust shaft		29.2 m ²	20-ft diam	2.2.8	
- ES-1		10.5 m ²	12-ft diam	2.2.8	
- ES-2		10.5 m ²	12-ft diam	2.2.8	

(A) No section in the RIB applies to these parameters.

(B) Section was identified in the RIB, but values were not found.

Table H-1. Comparison of Data Used in This Report with the Reference Information Base (RIB) (Continued)

Parameter	Section	Report Value	RIB Value	RIB Section	Explanation
Air Conductivity Factor for MPZ	4.3.2	20 to 60 times undisturbed rock	None	2.3	(B)
Saturated Hydraulic Conductivity of Shaft Backfill	4.3.2	10^{-4} to 100 cm/s	None	2.3	(B)
Air Conductivity of Shaft Backfill	4.3.2	3.0×10^{-6} to 3.0 m/min	None	2.3	(B) Calculated from saturated hydraulic conductivity value.
Effective Unsaturated Porosity of MPZ	5.1.2	4.2%	None	2.3	(B)
Variation in Barometric Pressure Thunderstorm Event --	5.2				
- Amplitude		19.0 mbars	19.0 mbars (max)	1.11.4	Value obtained from data presented in the RIB.
- Period		5 days	None	-----	(A)
Tornado					
- Amplitude		132.0 mbars	None	-----	(A)
- Period		1 min	None	-----	(A)
Seasonal Fluctuation					
- Amplitude		3 mbars	3 mbars	1.11.4	---
- Period		365 days	365 days	1.11.4	---
Hydraulic Conductivity of Ordinary Concrete	6.1	10^{-8} to 10^{-6} cm/s	None	2.3	(B)
Hydraulic Conductivity of Grout, Mortar, and Concrete for YMP Sealing Program	6.1	1.6×10^{-10} to 9.5×10^{-10} cm/s	None	2.3	(B)
Alkali Content of Portland Cement	6.2.1	0.05 to 0.15%	None	2.3	(B)
pH of Portland Cement Pore Fluid	6.2.1	13.88	None	2.3	(B)

(A) No section in the RIB applies to these parameters.

(B) Section was identified in the RIB, but values were not found.

Table H-1. Comparison of Data Used in This Report with the Reference Information Base (RIB) (Continued)

Parameter	Section	Report Value	RIB Value	RIB Section	Explanation
J-13 Water Composition	6.2.1	See Table 6-1	None	1.2.3	(B)
Shaft Liner Surface Area	6.2.1	4.17 x 10 ⁷ cm ²	None	2.2.8	Calculated from data in the RIB--Section 2.2.8.
Concrete Liner Void Fraction	6.2.1	0.28	None	-----	(A)
pH of J-13 Water (Base case)	6.2.2	6.9	None	1.2.3	(B)
Temperature of J-13 Water (Base case)	6.2.2	25°C	None	1.2.3	(B)
Fracture or Pore Aperture in MPZ	6.2.2.1	50 μm	None	2.3	(B)
Ground-water Fluid Diffusivity	6.2.2.1	10 ⁻⁵ cm ² /s	None	1.2.3	(B)
MPZ Fracture Porosity	6.2.4	.001 to .0001	None	2.3	(B)
Minimum Average Fracture Aperture Around Sumps	6.3	6 μm	None	-----	Value from Section 8.4.3.2.1.2 of SCP
Thermal Load of the Repository	7.1.1	57 kW/acre	57 kW/acre	3.1.1.1	---
Temperature at Edge of Repository After 500 Years (Calico Hills Unit)	7.1.1	47°C	57°C	3.1.1.2	Figure in the RIB represents the temperature at an average repository depth as opposed to the depths at the ESs.
Maximum Temperature at Edge of Repository (Calico Hills Unit)	7.1.1	52°C	59°C	3.1.1.2	Figure in the RIB represents the temperature at an average repository depth as opposed to the depths at the ESs.

(A) No section in the RIB applies to these parameters.
 (B) Section was identified in the RIB, but values were not found.

Table H-1. Comparison of Data Used in This Report with the Reference Information Base (RIB) (Continued)

Parameter	Section	Report Value	RIB Value	RIB Section	Explanation
Maximum Temperature at Top of Calico Hills Unit--with Barrier Pillar	7.1.1	40°C	None	3.1.1.2	Report value reflects calculations which include a barrier pillar.
Transition Temperature of Clinoptilolite to Mordenite and Analcime	7.1.2	95° to 105°C	None	-----	(A)
Effective Thickness of Calico Hills Unit	7.2				
- At ES-1		100 m	100 m	1.3.1.1.2	---
- Minimum over repository		70 m	70 m	1.3.1.1.2	---
Ratio of Crack Aperture to Grout Particle Size	8.2.1	1.7 to 3.0	None	-----	(A)
Maximum Particle Size for Ordinary Cement	8.2.1	100 μm	None	-----	(A)
Particle Size for Ultrafine Cement	8.2.1	10 μm	None	-----	(A)
Saturated Hydraulic Conductivity of Welded Tuff (Tiva Canyon and Topopah Spring)	8.2.1	10 ⁻² to 10 ⁻⁵ cm/s	1.2 x 10 ⁻³ cm/s or 3.65 x 10 ⁵ mm/yr	1.1.4.3	Saturated hydraulic conductivity values bound the RIB value.
Anticipated Volume of Concrete Shaft Plug	8.2.2	250 m ³	None	2.3	(B)
Maximum Depth of Cut for ES Pad Construction	8.3.1	17 m	None	-----	(A)

(A) No section in the RIB applies to these parameters.
 (B) Section was identified in the RIB, but values were not found.

Table H-1. Comparison of Data Used in This Report with the Reference Information Base (RIB) (Continued)

Parameter	Section	Report Value	RIB Value	RIB Section	Explanation
Maximum Depth of Fill for ES Pad Construction	8.3.1	11 m	None	-----	(A)
Depth of Shaft Backfill	A.1	300 m	None	2.3	(B) Assumes shaft is back-filled from repository level to near the surface.
Distance From ESs to Waste Disposal Areas	A.2	140 m			
Dip of Majority of Fractures (Topopah Spring Member)	A.2	≤13°	"Steeply Dipping"	1.3.2.4.2	The RIB indicates "most" fractures are >70°.
Molecular Diffusion Coefficient of Uranium Through Welded Tuff (Solid-Solid Diffusion)	A.4	10 ⁻¹⁵ to 10 ⁻³⁰ cm ² /s	None	-----	(A)
Binary Gas Diffusion Coefficient for	A.5				
- Air-iodine system		0.081 cm ² /s	None	-----	(A)
- Air-carbon dioxide system		0.156 cm ² /s	None	-----	(A)
Knudsen Diffusion Coefficient for	A.5				
- Air-iodine system		10.6 cm ² /s	None	-----	(A)
- Air-carbon dioxide system		25.3 cm ² /s	None	-----	(A)
Porosity of Shaft Backfill		.3	None	-----	(B)
Tortuosity of Shaft Backfill	A.5	3	None	-----	(A)
Depth to Topopah Spring Unit (MPZ Analysis)	B.1	100 m	75 to 125 m	1.3.1.1.3	RIB values bound the selected value.
Depth to Intersection of ES-1 and Repository Horizon (MPZ Analysis)	B.1	310 m	311 m	2.2.8	

(A) No section in the RIB applies to these parameters.

(B) Section was identified in the RIB, but values were not found.

Table H-1. Comparison of Data Used in This Report with the Reference Information Base (RIB) (Continued)

Parameter	Section	Report Value	RIB Value	RIB Section	Explanation
Intact Rock Compressive Strength (Topopah Spring Member)	B.1				
- Range		110 to 230 MPa	166 ± 65 MPa	1.3.1.4.1	Report values reflect previous strength values--the RIB has been updated.
- Expected value		171 MPa	166 MPa	1.3.1.4.1	
Rock Mass Quality (RMR System) (Topopah Spring Unit)	B.1				
- Range		48 to 84	None	-----	(A)
- Expected value		65	None	-----	(A)
In situ Stress Factor (Multiple of Overburden Stress)	B.1				
- Range		0.25 to 1.0	0.3 to 1.0	1.3.1.6.1	---
- Expected value		0.6	0.6	1.3.1.6.1	---
Extent of Blast Damage Around Shaft (MPZ Analysis)	B.1				
- Range		0.3 to 2.0 m	None	2.3	(B)
- Expected values					
• Controlled blasting		0.5 m	None	2.3	(B)
• Uncontrolled blasting		1.0 m	None	2.3	(B)
Relative Permeability Factor	B.2				
- At 100-m depth					
• Expected case		20	None	2.3	(B)
• Upper bound		40	None	2.3	(B)
- At 310-m depth					
• Expected case		20	None	2.3	(B)
• Upper bound		80	None	2.3	(B)

(A) No section in the RIB applies to these parameters.

(B) Section was identified in the RIB, but values were not found.

Table H-1. Comparison of Data Used in This Report with the Reference Information Base (RIB) (Continued)

Parameter	Section	Report Value	RIB Value	RIB Section	Explanation
Probable Maximum Flood Clear-Water Volume	C.1	159,000 m ³	None	1.17.1	(B)
Relative Permeability Factor (Water Flow into Shaft Model)	C.2.1	20 to 60	None	2.3	(B)
Slope of Wash in Area of Old ES-1 Location	C.2.1	0.16	None	-----	(A)
Suction Head for Backfill	C.2.1	-1.0 m	None	-----	(A)
Excavated Diameter of ES-1 and ES-2 (MPZ Analysis)	C.2.2	4.4 m	4.3 m	2.2.8	Slight overbreak assumed in MPZ model.
Saturated Hydraulic Conductivity of Alluvium	C.2.2	10 ⁻⁵ to 100 cm/s	None	-----	(A)
Radius of Influence for Flow into ES-1 Shaft (Old ES-1 Location)	C.2.2	76.2 m	None	-----	(A)
Depth of Alluvium at Old ES-1 Location	C.2.2	9.1 m	None	-----	(A)
Porosity of Alluvium	C.2.2	30%	None	-----	(A)
ES-1 Sump Depth (Old ES-1 Location and Design)	C.3.1	140 m	15 m	2.2.5, 2.2.6	Value reflects old ES-1 location and design.
Suction Head of Backfill Material	C.3.1	0 to -1.6 m	None	-----	(A)

(A) No section in the RIB applies to these parameters.

(B) Section was identified in the RIB, but values were not found.

Table H-1. Comparison of Data Used in This Report with the Reference Information Base (RIB) (Concluded)

Parameter	Section	Report Value	RIB Value	RIB Section	Explanation
Suction Head of Tuff Matrix	C.3.1	0 to -1,000 m	None	-----	(A)
Saturated Hydraulic Conductivity of Calico Hills Unit	C.3.2	2.4×10^{-4} or 1×10^{-3} cm/s	2.4×10^{-4} cm/s or 7.5×10^4 mm/yr	1.1.4.3	Saturated hydraulic conductivity values bound the RIB value.
Temperature Profile with Depth	G	See Fig G-1	RIB Fig 2	3.1.1.2	The figures are identical.
Thermal Diffusivity (Average of Water, Rock, and Fill Material)	G	0.0078 to 30.0	None	-----	(A)

(A) No section in the RIB applies to these parameters.

(B) Section was identified in the RIB, but values were not found.

APPENDIX I

**DATA RECOMMENDED FOR INCLUSION INTO THE SITE AND
ENGINEERING PROPERTIES DATA BASE (SEPDB)
AND INFORMATION PROPOSED FOR THE INCLUSION INTO THE
REFERENCE INFORMATION BASE (RIB)**

No data or information contained in this report is recommended for inclusion into the SEPDB or the RIB.

REFERENCES

- Abrams, A., 1977, "Mud Design to Minimize Rock Impairment Due to Particle Invasion," Journal of Petroleum Technology, 29, p. 586-592.
- Auld, F. A., 1983, "Design of Underground Plugs," International Journal of Mining Engineering, Chapman and Hall Ltd., London, Vol. 1, pp. 189-228.
- Barnes, P., ed., 1983, Structure and Performance of Cements, Applied Science Publishers, London.
- Bear, J., 1972, Dynamics of Fluids in Porous Media, Elsevier, New York, 763 pp.
- Berner, R. A., 1980, Early Diagenesis, a Theoretical Approach, Princeton University Press, Princeton, NJ, pp. 118-124.
- Bird, R. B., W. E. Stewart, and E. N. Lightfoot, 1960, Transport Phenomena, John Wiley & Sons, Inc., New York, NY.
- Bullard, K. L., 1986, PMF (Probable Maximum Flood) Study for Nevada Nuclear Waste Storage Investigation Project, GR-87-8, U.S. Department of the Interior, Bureau of Reclamation, Denver, CO.
- Carslaw, H. S., and J. C. Jaeger, 1959, Conduction of Heat in Solids, Clarendon Press, Oxford.
- Case, J. B., and P. C. Kelsall, 1987, Modification of Rock Mass Permeability in the Zone Surrounding a Shaft in Fractured, Welded Tuff, SAND86-7001, Sandia National Laboratories, Albuquerque, NM, 79 pp.
- Case, J. B., P. C. Kelsall, and J. W. Holland, 1984, "The Development of Interface Stress in a Concrete Plug During Cement Hydration," presented at the Symposium on Concrete and Cementitious Materials for Radioactive Waste Management, November 1, 1984, American Concrete Institute, New York, NY.
- Cording, E. J., A. J. Hendron, and D. U. Deere, 1971, "Rock Engineering for Underground Caverns," Proceedings of Underground Rock Chambers, Amer. Soc. of Civil Engineers, New York, NY.
- Costin, L. S., and S. J. Bauer, 1988, Preliminary Analyses of the Excavation Investigation Experiments Proposed for the Exploratory Shaft at Yucca Mountain, Nevada Test Site, SAND87-1575, Sandia National Laboratories, Albuquerque, NM.
- Cummins, A. B., and I. A. Given, 1973, SME Mining Engineering Handbook, Port City Press, Baltimore, MD.

- Daniels, W. R., K. Wolfsberg, R. S. Rundberg, A. E. Ogard, J. F. Kerrisk, C. J. Duffy, T. W. Newton, J. L. Thompson, B. P. Bayhurst, D. L. Bish, J. D. Blacic, B. M. Crowe, B. R. Erdal, J. F. Griffith, S. D. Knight, F. O. Lawrence, V. L. Rundberg, M. L. Skyes, G. M. Thompson, B. J. Travis, E. N. Treher, R. J. Vidale, G. R. Walter, R. D. Aguilar, M. R. Cisneros, S. Masetas, A. J. Mitchell, P. Q. Oliver, N. A. Raybold, and P. L. Wanik, 1982, Summary Report on the Geochemistry of Yucca Mountain and Environs, LA-9328-MS, Los Alamos National Laboratory, Los Alamos, NM.
- D'Appolonia, 1976, Preliminary State-of-the-Art Survey: Mining Techniques for Salt & Other Rock Types, Project No. 76-292, Office of Waste Isolation, Union Carbide Corporation, Nuclear Division, Oak Ridge, TN.
- Davis, S. N., and R. J. M. DeWiest, 1966, Hydrogeology, John Wiley & Sons, Inc., NY.
- Dial, B. W., D. E. Maxwell, E. G. McNulty, and M. Reeves, 1988, "Near-Field Shaft Response Analysis Using the CAVS Jointed Rock Model," Key Questions in Rock Mechanics: Proceedings of the 29th U. S. Symposium, University of Minnesota, Minneapolis, 13-15 June 1988, P. A. Cundall, R. L. Sterling, and A. M. Starfield, eds., pp. 421-428.
- Dietz, H. K. O., 1982, "Grouting Technique Used in Deep South African Mines," Proceedings of the Conference on Grouting in Geotechnical Engineering, American Society of Civil Engineers, New York, NY, pp. 606-620.
- DOE (U.S. Department of Energy), 1986, "Environmental Assessment, Yucca Mountain Site, Nevada Research and Development Area, Nevada," DOE/RW-0073, Office of Civilian Radioactive Waste Management, Washington, D.C.
- DOE (U.S. Department of Energy), 1987a, Exploratory Shaft Facility, Subsystem Design Requirements Document, NVO-309, Nevada Operations Office, Las Vegas, NV.
- DOE (U.S. Department of Energy), 1987b, The Nevada Nuclear Waste Storage Investigations Project Reference Information Base, Version 03.001.
- DOE (U.S. Department of Energy), 1988, Consultation Draft, Site Characterization Plan, Yucca Mountain Site, Nevada Research and Development Area, Nevada, Office of Civilian Radioactive Waste Management, Washington, D.C.
- Dowding, C. H., and J. F. Labuz, 1982, "Fracturing of Rock with Expansive Cement," Journal of the Geotechnical Engineering Division, Vol. 108, No. GT10, American Society of Civil Engineers, New York, NY, pp. 1288-1299.
- Erickson, J. R., and R. K. Waddell, 1985, Identification and Characterization of Hydrologic Properties of Fractured Tuff Using Hydraulic and Tracer Tests--Test Well USW H-4, Yucca Mountain, Nye County, Nevada, USGS-WRI-85-4066, U.S. Geological Survey, Denver, CO.

- Fernandez, J. A., P. C. Kelsall, J. B. Case, and D. Meyer, 1987, Technical Basis for Performance Goals, Design Requirements, and Material Recommendations for the NNWSI Repository Sealing Program, SAND84-1895, Sandia National Laboratories, Albuquerque, NM.
- Finley, J. B., M. D. Harvey, and C. C. Watson, 1985, "Experimental Study: Erosion of Overburden Cap Material Protected by Rock Mulch," in Management of Uranium Mill Tailings. Low-Level Waste and Hazardous Waste. Proceedings of the 7th Symposium, Vol. II, Colorado State University, Fort Collins, CO.
- Freeze, R. A., and J. A. Cherry, 1979, Groundwater, Prentice-Hall, Inc., Englewood Cliffs, NJ.
- Froment, G. F., and K. B. Bischoff, 1979, Chemical Reactor Analysis and Design, John Wiley & Sons, Inc., New York, NY.
- Glasser, F. P., M. J. Angus, C. E. McCulloch, D. MacPhee, and A. A. Rahman, 1985, "The Chemical Environment in Cements," Proceedings of the Materials Research Society Symposium, Vol. 44, p. 849.
- Hartman, H. L., 1982, Mine Ventilation and Air Conditioning, John Wiley & Sons, Inc., New York, NY.
- Herzig, J. P., D. M. LeClerc, and P. LeGaff, 1970, "Flow of Suspensions Through Porous Media, Application to Deep Filtration," Industrial and Engineering Chemistry, Vol 62, No. 5, pp. 8-35.
- Herzog, B. L., K. Cartwright, T. M. Johnson, and H. J. H. Harris, 1982, A Study of Trench Covers to Minimize Infiltration at Waste Disposal Sites, NUREG/CR-2478, U.S. Nuclear Regulatory Commission, Washington, D.C.
- Hillel, D., 1971, Soil and Water, Academic Press, Inc., New York, NY, 288 pp.
- Hoek, E., and E. T. Brown, 1980, Underground Excavations in Rock, Institution of Mining and Metallurgy, London, England, 527 pp.
- Ingraffea, A. R., and J. F. Beech, 1983, "Fracturing of Rock with Expansive Cement," Journal of Geotechnical Engineering, Vol. 109, No. 9, American Society of Civil Engineers, New York, NY, pp. 1205-1209.
- Jaeger, J. C., and N. G. W. Cook, 1976, Fundamentals of Rock Mechanics, John Wiley & Sons, Inc., New York, NY.
- Kelsall, P. C., J. B. Case, and C. R. Chabannes, 1982, A Preliminary Evaluation of the Rock Mass Disturbance Resulting from Shaft, Tunnel, or Borehole Excavation, ONWI-411, Office of Nuclear Waste Isolation, Battelle Memorial Institute, Columbus, OH.
- Kelsall, P. C., J. B. Case, and C. R. Chabannes, 1984, "Evaluation of Excavation-induced Changes in Rock Permeability," Int. J. Rock Mech. Min. Sci. and Geomech. Abst., Vol. 21, No. 3, pp. 123-135.

- Keshian, B., M. Bone, and T. Schruben, 1985, "Design of Erosion Protection for Long-Term Stability," in Management of Uranium Mill Tailings, Low-Level Waste and Hazardous Waste, Proceedings of the 7th Symposium, Vol. II, Colorado State University, Fort Collins, CO.
- Khilar, D. C., H. S. Fogler, D. H. Gray, 1985, "Model for Piping-Plugging in Earthen Structure," Journal of Geotechnical Engineering, Vol. III, No. 7, American Society of Civil Engineers, pp. 833-846.
- Klavetter, E. A., and R. R. Peters, 1986, Fluid Flow in a Fractured Rock Mass, SAND85-0855, Sandia National Laboratories, Albuquerque, NM.
- Klavetter, E. A., and R. R. Peters, 1987, An Evaluation of the Use of Mercury Posimetry in Calculating Hydrologic Properties of Tuffs from Yucca Mountain, Nevada, SAND86-0286, Sandia National Laboratories, Albuquerque, NM.
- Langkopf, B. S., and P. R. Gnirk, 1986, Rock-Mass Classification of Candidate Repository Units at Yucca Mountain, Nye County, Nevada, SAND82-2034, Sandia National Laboratories, Albuquerque, NM.
- Lea, F. M., 1971, The Chemistry of Cement and Concrete, Chemical Publishing Company, Inc., New York, NY.
- Levenspiel, O., 1972, Chemical Reaction Engineering, John Wiley & Sons, Inc., New York, NY.
- Licastro, P. H., J. A. Fernandez, and D. M. Roy, in preparation, Mechanical Compatibility Between Selected Cementitious Materials and Topopah Spring Member Tuff, SAND86-0558, Sandia National Laboratories, Albuquerque, NM.
- Lohman, S. W., ed., 1972, Definitions of Selected Ground-Water Terms: Revisions and Conceptual Refinements, U.S. Geol. Surv., Water-Supply Paper 1988, 21 pp.
- Maestas, E., M. Barainca, and J. Smiley, 1985, "An Overview of the Department of Energy's Program for Low-Level Radioactive Waste Disposal," in Management of Uranium Mill Tailings, Low-Level Waste and Hazardous Waste, Proceedings of the 7th Symposium, Vol. II, Colorado State University, Fort Collins, CO.
- Martinez, M. J., 1988, Capillary-Driven Flow in a Fracture Located in a Porous Medium, SAND84-1697, Sandia National Laboratories, Albuquerque, NM.
- Mason, E. A., and R. B. Evans III, 1969, "Graham's Laws: Simple Demonstrations of Gases in Motion," J. of Chemical Education, Vol. 46, No. 4, pp. 358-364.
- Mather, B., 1967, Cement Performance in Concrete, US-CE-C No. 6-787, U.S. Army Engineer Waterways Experiment Station, Corps of Engineers, Vicksburg, MS, 34 pp.
- Miller, C. H., D. R. Cunningham, and M. J. Cunningham, 1974, "An Air-Injection Technique to Study Intensity of Fracturing Around a Tunnel in Volcanic Rocks," Bulletin of the Association of Engineering Geologists, Vol. XI, No. 3, pp. 203-217.

- Mitchell, D. L., 1984, Evaluation of Habitat Restoration Needs at Yucca Mountain, Nevada Test Site, Nye County, Nevada, EGG 10282-2030, EG&G, Goleta, CA.
- Montazer, P. M., and W. A. Hustrulid, 1983, An Investigation of Fracture Permeability Around An Underground Opening in Metamorphic Rocks, BMI/OCRD-4(5), Battelle Memorial Institute, Columbus, OH.
- Morales, A. R., compiler, 1986, Technical Correspondence in Support of the Final Environmental Assessment, SAND85-2509, Sandia National Laboratories, Albuquerque, NM.
- National Research Council, 1985, Safety of Dams, Flood and Earthquake Criteria, National Academy Press, Washington, D.C.
- Ogard, A. E., K. Wolfsberg, D. T. Vaniman, compilers, 1983, Research and Development Related to the Nevada Nuclear Waste Storage Investigations, April 1 - June 30, 1983, LA-9846-PR, Los Alamos National Laboratory, Los Alamos, NM.
- Ogard, A. E., and J. F. Kerrisk, 1984 Groundwater Chemistry Along Flow Paths Between a Proposed Repository Site and the Accessible Environment, LA-10188-MS, Los Alamos National Laboratory, Los Alamos, NM.
- Peters, R. R., 1988, YMP Hydrologic Technical Correspondence in Support of Site Characterization Plan, SAND88-2784, Sandia National Laboratories, Albuquerque, NM.
- Peters, R. R., E. A. Klavetter, I. J. Hall, S. C. Blair, P. R. Heller, G. W. Gee, 1984, Fracture and Matrix Hydrologic Characteristics of Tuffaceous Materials from Yucca Mountain, Nye County, Nevada, SAND84-1471, Sandia National Laboratories, Albuquerque, NM.
- Reid, R. C., J. M. Prausnitz, and T. K. Sherwood, 1977, The Properties of Gases and Liquids, McGraw-Hill Book Company, New York, NY.
- Richardson, A. R., in preparation, Preliminary Shaft Liner Design Criteria and Methodology Guide (Working-Draft: Revision B), SAND88-7060, Sandia National Laboratories, Albuquerque, NM.
- Scott, R. B., R. W. Spengler, S. Diehl, A. R. Lappin, and M. P. Chornack, 1983, "Geologic Character of Tuffs in the Unsaturated Zone at Yucca Mountain, Southern Nevada," Role of the Unsaturated Zone in Radioactive and Hazardous Waste Disposal, J. Mercer, P. S. C. Rao, I. W. Marine, eds., Butterworth Publishing Co., Ann Arbor, MI, pp. 285-335.
- Sheetz, B. E., and D. M. Roy, in preparation, Preliminary Survey of the Stability of Silica-Rich Cementitious Mortars [82-22 and 84-12] with Tuff, Materials Research Laboratory, Pennsylvania State University, prepared for Los Alamos National Laboratory, Los Alamos, NM.
- Sinnock, S., Y. T. Lin, and J. P. Brannen, 1984, Preliminary Bounds on the Expected Postclosure Performance of the Yucca Mountain Repository Site, Southern Nevada, SAND84-1492, Sandia National Laboratories, Albuquerque, NM.

- Siskind, D. E., R. C. Steckley, and J. J. Olson, 1973, "Fracturing in the Zone Around a Blasthole, White Pine, Michigan," BuMines Report of Investigations 7753, 20 p.
- Smith, J. M., 1970, Chemical Engineering Kinetics, McGraw-Hill Book Company, New York, NY.
- Smyth, J. R., 1982, "Zeolite Stability Constraints on Radioactive Waste Isolation in Zeolite-Bearing Volcanic Rocks," Journal of Geol., Vol. 90, pp. 195-201.
- Smyth, J. R., and F. A. Caporuscio, 1981, Review of the Thermal Stability and Cation Exchange Properties of the Zeolite Minerals Clinoptilolite, Mordenite, and Analcime: Applications to Radioactive Waste Isolation in Silicic Tuff, LA-8841-MS, Los Alamos National Laboratory, Los Alamos, NM.
- SNL (Sandia National Laboratories), 1987, Site Characterization Plan Conceptual Design Report, SAND84-2641, H. R. MacDougall, L. W. Scully, and J. R. Tillerson (compilers), Sandia National Laboratories, Albuquerque, NM.
- Squires, R. R., and R. L. Young, 1984, Flood Potential of Fortymile Wash and Its Principal Southwestern Tributaries, Nevada Test Site, Southern Nevada, USGS-WRI-83-4001, U. S. Geological Survey, Carson City, NV.
- Stephens, D. B., and S. P. Neuman, 1982, "Vadose Zone Permeability Tests: Steady State Results," Journal of the Hydraulics Division, Proceedings of the American Society of Civil Engineers, Vol. 108, No. HY5, pp. 640-659.
- Terzaghi, K., and R. B. Peck, 1967, Soil Mechanics in Engineering Practice, John Wiley & Sons, Inc., New York, NY.
- Trefethen, J. M., 1959, Geology for Engineers, D. Van Nostrand Company, Inc., Princeton, NJ.
- Truesdell, A. H., and B. F. Jones, 1974, WATEQ, A Computer Program for Calculating Chemical Equilibria of Natural Waters, Jour. Research U.S. Geol. Survey, Vol. 2, No. 2, p. 233.
- Valley, S. L., ed., 1965, Handbook of Geophysics and Space Environments, McGraw-Hill Book Company, New York, NY.
- Van Koynenburg, R. A., C. F. Smith, H. W. Culham, and C. H. Otto, Jr., 1984, "Behavior of Carbon-14 in Waste Packages for Spent Fuel in a Repository in Tuff," UCRL-90855, prepared for submittal to the Materials Research Society Symposium on the Scientific Basis for Nuclear Waste Management, Boston, MA, Vol. 44, Materials Research Society, Pittsburgh, PA, pp. 405-412.
- Wallace, A., and E. M. Romney, 1972, Radioecology and Ecophysiology of Desert Plants at the Nevada Test Site, TID-25954, University of California, Los Angeles, CA.

- Wang, J. S. Y., and T. N. Narasimhan, 1984, Hydrologic Mechanisms Governing Fluid Flow in Partially Saturated, Fractured, Porous Tuff at Yucca Mountain, LBL-18473, Lawrence Berkeley Laboratory, University of California, Berkeley, CA.
- Wilson, C. R., P. A. Witherspoon, J. C. S. Long, R. M. Galbraith, A. O. DuBois, and M. J. McPherson, 1983, "Large-scale Hydraulic Conductivity Measurements in Fractured Granite," Int. J. Rock Mech. Min. Sci. and Geomech. Abstr., Vol. 20, No. 6, pp. 269-276.
- Winterkorn, H. F., and H. Y. Fang, eds., 1979, Foundation Engineering Handbook, Van Nostrand Reinhold Company, NY.
- Wolery, T. J., 1979, Calculation of Chemical Equilibrium Between Aqueous Solution and Minerals: The EQ3/6 Software Package, UCRL-52658, Lawrence Livermore Laboratory, Livermore, CA.
- Wolfsberg, K., B. P. Bayhurst, B. M. Crowe, W. R. Daniels, B. R. Erdal, F. O. Lawrence, A. E. Norris, and J. R. Smyth, 1979, Sorption-Desorption Studies on Tuff. I. Initial Studies with Samples from the J-13 Drill Site, Jackass Flats, Nevada, LA-7480-MS, Los Alamos National Laboratory, Los Alamos, NM.
- Worsey, P. N., 1985, "Insitu Measurement of Blast Damage Underground by Seismic Refraction Surveys," Proceedings of the 26th U.S. Symposium on Rock Mechanics, E. Ashworth, ed., A. A. Balkema, Boston, MS, pp. 1133-1140.
- Zienkiewicz, O. C., 1977, The Finite Element Method, McGraw-Hill Book Company, (UK) Limited, New York, NY, 787 pp.
- Zimmerman, R. M., M. L. Wilson, M. P. Board, M. E. Hall, and R. L. Schuch, 1985, "Thermal Cycle Testing of the G-Tunnel Heated Block," Proceedings of the 26th U.S. Symposium on Rock Mechanics, Rapid City, SD, E. Ashworth, ed., A. A. Balkema, Boston, MS, pp. 749-758.

DISTRIBUTION LIST

Samuel Rousso, Acting Director (RW-1)
Office of Civilian Radioactive
Waste Management
U.S. Department of Energy
Forrestal Bldg.
Washington, D.C. 20585

V. J. Cassella (RW-123)
Office of Civilian Radioactive
Waste Management
U.S. Department of Energy
Forrestal Bldg.
Washington, D.C. 20585

Ralph Stein (RW-30)
Office of Civilian Radioactive
Waste Management
U.S. Department of Energy
Forrestal Bldg.
Washington, D.C. 20585

S. H. Kale (RW-20)
Office of Civilian Radioactive
Waste Management
U.S. Department of Energy
Forrestal Bldg.
Washington, D.C. 20585

M. W. Frei (RW-22)
Office of Civilian Radioactive
Waste Management
U.S. Department of Energy
Forrestal Bldg.
Washington, D.C. 20585

T. H. Isaacs (RW-40)
Office of Civilian Radioactive
Waste Management
U.S. Department of Energy
Forrestal Bldg.
Washington, D.C. 20585

B. G. Gale (RW-23)
Office of Civilian Radioactive
Waste Management
U.S. Department of Energy
Forrestal Bldg.
Washington, D.C. 20585

D. H. Alexander (RW-332)
Office of Civilian Radioactive
Waste Management
U.S. Department of Energy
Forrestal Bldg.
Washington, D.C. 20585

F. G. Peters (RW-10)
Office of Civilian Radioactive
Waste Management
U.S. Department of Energy
Forrestal Bldg.
Washington, D.C. 20585

C. Bresee (RW-10)
Office of Civilian Radioactive
Waste Management
U.S. Department of Energy
Forrestal Bldg.
Washington, D.C. 20585

J. D. Saltzman (RW-20)
Office of Civilian Radioactive
Waste Management
U.S. Department of Energy
Forrestal Bldg.
Washington, D.C. 20585

Gerald Parker (RW-333)
Office of Civilian Radioactive
Waste Management
U.S. Department of Energy
Forrestal Bldg.
Washington, D.C. 20585

S. J. Brocoum (RW-221)
Office of Civilian Radioactive
Waste Management
U.S. Department of Energy
Forrestal Building
Washington, D.C. 20585

Chief, Repository Projects Branch
Division of Waste Management
U.S. Nuclear Regulatory Commission
Washington, D.C. 20555

NTS Section Leader
Repository Project Branch
Division of Waste Management
U.S. Nuclear Regulatory Commission
Washington, D.C. 20555

Document Control Center
Division of Waste Management
U.S. Nuclear Regulatory Commission
Washington, D.C. 20555

Carl P. Gertz, Project Manager (5)
Yucca Mountain Project Office
Nevada Operations Office
U.S. Department of Energy
Mail Stop 523
P.O. Box 98518
Las Vegas, NV 89193-8518

T. H. Beall (12)
Technical Information office
Nevada Operations Office
U. S. Department of Energy
P.O. Box 98518
Las Vegas, NV 89193-8518

C. L. West, Director
Office of External Affairs
U.S. Department of Energy
Nevada Operations Office
P.O. Box 98518
Las Vegas, NV 89193-8518

W. M. Hewitt, Program Manager
Roy F. Weston, Inc.
955 L'Enfant Plaza, Southwest
Suite 800
Washington, D.C. 20024

Technical Information Center
Roy F. Weston, Inc.
955 L'Enfant Plaza, Southwest
Suite 800
Washington, D.C. 20024

L. B. Ballou (3)
Actg. Technical Project Officer for
YMP
Lawrence Livermore National
Laboratory
Mail Stop L-204
P.O. Box 808
Livermore, CA 94550

N. E. Carter
Actg. Technical Project Officer for
YMP
Science Applications International
Corp.
101 Convention Center Dr.
Suite 407
Las Vegas, NV 89109

H. N. Kalia
Exploratory Shaft Test Manager
Los Alamos National Laboratory
Mail Stop 527
101 Convention Center Dr.
Suite P230
Las Vegas, NV 89109

D. T. Oakley (4)
Technical Project Officer for YMP
Los Alamos National Laboratory
N-5, Mail Stop J521
P.O. Box 1663
Los Alamos, NM 87545

L. R. Hayes (6)
Technical Project Officer for YMP
U.S. Geological Survey
P.O. Box 25046
421 Federal Center
Denver, CO 80225

K. W. Causseaux
NHP Reports Chief
U.S. Geological Survey
P.O. Box 25046
421 Federal Center
Denver, CO 80225

R. V. Watkins, Chief
Project Planning and Management
U.S. Geological Survey
P.O. Box 25046
421 Federal Center
Denver, CO 80225

Center for Nuclear Waste
Regulatory Analyses
6220 Culebra Road
Drawer 28510
San Antonio, TX 78284

R. L. Bullock
Technical Project Officer for YMP
Fenix & Scisson, Inc.
Mail Stop 403
101 Convention Center Dr.
Suite P250
Las Vegas, NV 89193-3265

James C. Calovini
Technical Project Officer for YMP
Holmes & Narver, Inc.
101 Convention Center Dr.
Suite 860
Las Vegas, NV 89109

Dr. David W. Harris
YMP Technical Project Officer
Bureau of Reclamation
P.O. Box 25007 Bldg. 67
Denver Federal Center
Denver, CO 80225-0007

M. D. Voegele
Science Applications International
Corp.
101 Convention Center Dr.
Suite 407
Las Vegas, NV 89109

J. A. Cross, Manager
Las Vegas Branch
Fenix & Scisson, Inc.
P.O. Box 93265
Mail Stop 514
Las Vegas, NV 89193-3265

P. T. Prestholt
NRC Site Representative
1050 East Flamingo Road
Suite 319
Las Vegas, NV 89119

A. E. Gurrola, General Manager
Energy Support Division
Holmes & Narver, Inc.
P.O. Box 93838
Mail Stop 580
Las Vegas, NV 89193-3838

A. M. Sastry
Technical Project Officer for YMP
MAC Technical Services
Valley Bank Center
101 Convention Center Drive
Suite P-113
Las Vegas, NV 89109

B. L. Fraser, General Manager
Reynolds Electrical & Engineering Co.
P.O. Box 98521
Mail Stop 555
Las Vegas, NV 89193-8521

P. K. Fitzsimmons, Director
Health Physics & Environmental
Division
Nevada Operations Office
U.S. Department of Energy
P.O. Box 98518
Las Vegas, NV 89193-8518

Robert F. Pritchett
Technical Project Officer for YMP
Reynolds Electrical & Engineering Co.
Mail Stop 615
P.O. Box 98521
Las Vegas, NV 89193-8521

Elaine Ezra
YMP GIS Project Manager
EG&G Energy Measurements, Inc.
P.O. Box 1912
Mail Stop H-02
Las Vegas, NV 89125

SAIC-T&MSS Library (2)
Science Applications International
Corp.
101 Convention Center Dr.
Suite 407
Las Vegas, NV 89109

Dr. Martin Mifflin
Desert Research Institute
Water Resources Center
2505 Chandler Avenue
Suite 1
Las Vegas, NV 89120

John Fordham
Desert Research Institute
Water Resources Center
P.O. Box 60220
Reno, NV 89506

E. P. Binnall
Field Systems Group Leader
Building 50B/4235
Lawrence Berkeley Laboratory
Berkeley, CA 94720

Prof. S. W. Dickson
Department of Geological Sciences
Mackay School of Mines
University of Nevada
Reno, NV 89557

J. F. Divine
Assistant Director for
Engineering Geology
U.S. Geological Survey
106 National Center
12201 Sunrise Valley Dr.
Reston, VA 22092

J. R. Rollo
Deputy Assistant Director for
Engineering Geology
U.S. Geological Survey
106 National Center
12201 Sunrise Valley Dr.
Reston, VA 22092

V. M. Glanzman
U.S. Geological Survey
P.O. Box 25046
913 Federal Center
Denver, CO 80225

Eric Anderson
Mountain West Research-Southwest
Inc.
Phoenix Gateway Center
432 North 44 Street
Suite 400
Phoenix, AZ 85008-6572

C. H. Johnson
Technical Program Manager
Nuclear Waste Project Office
State of Nevada
Evergreen Center, Suite 252
1802 North Carson Street
Carson City, NV 89710

Judy Foremaster (5)
City of Caliente
P.O. Box 158
Caliente, NV 89008

T. Hay, Executive Assistant
Office of the Governor
State of Nevada
Capitol Complex
Carson City, NV 89710

A. T. Tamura
Science and Technology Division
Office of Scientific and Technical
Information
U.S. Department of Energy
P.O. Box 62
Oak Ridge, TN 37831

R. R. Loux, Jr., (3)
Executive Director
Nuclear Waste Project Office
State of Nevada
Evergreen Center, Suite 252
1802 North Carson Street
Carson City, NV 89710

L. Jardine
Project Manager
Bechtel National Inc.
P.O. Box 3965
San Francisco, CA 94119

R. Harig
Parsons Brinckerhoff Quade &
Douglas
1625 Van Ness Ave.
San Francisco, CA 94109-3679

Dr. Roger Kasperson
CENTED
Clark University
950 Main Street
Worcester, MA 01610

Robert E. Cummings
Engineers International, Inc.
P.O. Box 43817
Tucson, AZ 85733-3817

Dr. Jaak Daemen
Department of Mining and
Geotechnical Engineering
University of Arizona
Tucson, AZ 85721

Department of Comprehensive Planning
Clark County
225 Bridger Avenue, 7th Floor
Las Vegas, NV 89155

Economic Development Department
City of Las Vegas
400 East Stewart Avenue
Las Vegas, NV 89109

Planning Department
Nye County
P.O. Box 153
Tonopah, NV 89049

Director of Community Planning
City of Boulder City
P.O. Box 367
Boulder City, NV 89005

Commission of the European
Communities
200 Rue de la Loi
B-1049 Brussels
Belgium

Lincoln County Commission
Lincoln County
P.O. Box 90
Pioche, NV 89043

Community Planning & Development
City of North Las Vegas
P.O. Box 4086
North Las Vegas, NV 89030

City Manager
City of Henderson
Henderson, NV 89015

ONWI Library
Battelle Columbus Laboratory
Office of Nuclear Waste Isolation
505 King Avenue
Columbus, OH 43201

Librarian
Los Alamos Technical
Associates, Inc.
P.O. Box 410
Los Alamos, NM 87544

John B. Case (5)
International Technology
5301 Central Avenue NE
Suite 700
Albuquerque, NM 87108

6300 R. W. Lynch
6310 T. O. Hunter
6310 100/12471/SAND85-0598/Q2
6310 YMP CRF
6311 A. L. Stevens
6311 C. Mora
6312 F. W. Bingham
6312 P. G. Kaplan
6312 R. D. Klett
6312 A. C. Peterson
6312 M. S. Tierney
6313 T. E. Blejwas
6314 J. R. Tillerson (10)
6314 J. A. Fernandez (10)
6314 T. E. Hinkebein (5)
6314 R. E. Stinebaugh
6315 L. E. Shephard
6316 R. P. Sandoval
6317 S. Sinnock

6332 WMT Library (20)
6410 N. R. Ortiz, Actg.
3141 S. A. Landenberger (5)
3151 W. I. Klein (3)
8524 J. A. Wackerly
3154-1 C. L. Ward (8)
for DOE/OSTI

☆ U.S. GOVERNMENT PRINTING OFFICE: 1989-673-049/81029